# Atmosferik Aerosollerde $PM_{2.5}$ ve Saatlik Yarı Uçucu Organik Bileşiklerin Araştırılması

**Program Kodu:** 1001

**Proje No:** 115Y625

**Proje Yürütücüsü:**

**Dr. Öğr. Üyesi Rosa Maria FLORES RANGEL**

Araştırmacılar:
Dr. Hüseyin ÖZDEMİR
Doç. Dr. Bülent O. AKKOYUNLU
Prof. Dr. Mete TAYANÇ

NISAN 2019
ISTANBUL

## PREFACE

This project with title “Atmosferik Aerosollerde PM2.5 ve Saatlik Yarı Uçucu Organik Bileşiklerin Araştırılması” and TUBITAK project number: 115Y625 originated as a personal interest from R. Flores as the study of SVOCs was part of her PhD dissertation. Organic aerosols are highly abundant and variable in the atmosphere as they constitute 20-90% the PM2.5 mass. The semi-volatile fraction of organic aerosol is composed of various compounds with properties that allow them to be actively partitioning into the particle- and gas phases. Semi-volatile organic compounds include PAHs, n-alkanes, hopanes, steranes, and low-volatility oxygenated nalkanoic acids, n-alkenoic acids, alkane dicarboxylic acids, aromatic carboxylic acids, resin acids, polyols and sugars, and other multi- and poly-functionalized species. Their variations in the atmosphere are commonly not well understood as they vary both temporally and geographically. Organic aerosols have important influence of human health, climate change, and ecosystems and therefore, understanding their composition and diurnal and seasonal variations is essential. Istanbul is a Megacity with over 15 million inhabitants and due to its strategic location, sources of organic aerosols include ship emissions, plane emissions, industries, and various point and non-point area sources. In addition, Istanbul has been identified as the 10th city in the World with worst traffic and during the winter fuel burning for residential heating has been identified as a very important factor that contributes to air pollution. In addition to high emission sources, dominant high-pressure systems during the winter contributes to low dispersion of pollutants and high concentrations. This project allowed the establishment and development of methods for characterization of PAH and n-alkanes in high-time resolved PM2.5 samples. In addition to these selected SVOCs, average daily PM2.5, OC, and EC concentrations were also investigated for the first time in Istanbul and Turkey. The impact of this project has both local and global implications in order to understand effects on human health and climate change.

**Table of contents**

**List of tables**

## List of figures

**Ozet**

Yapılan çalışmada, seçili yarı uçucu organik bileşiklerin (n-alkanlar ve PAH gibi) mevsimsel ve günlük değişimlerini anlayabilmek için bir sene içinde altı hafta boyunca geceleri 12 saatte bir, gün boyu ise her iki saatte bir olmak üzere toplam 295 yüksek hacim örneği toplanmıştır. Mevsimsel değişimlerin incelenmesinde, ortalama günlük PM2.5, OC ve EC konsantrasyon değerleri kullanılmıştır. Toplanan numunelerde 15 PAH ve 28 n-alkan bileşeninin belirlenmesi ve ölçülmesi İstanbul ve Türkiye'de ilk defa yapılmıştır. Meteorolojik ve trafik verileri kullanılarak bu faktörlerin yüksek çözünürlüklü SVOC konsantrasyonlarına etkisi anlaşılmaya çalışılmıştır. Genel olarak bakıldığında, en yüksek PM2.5, OC, EC, PAH ve n-alkan konsantrasyonlarına güz ve kış döneminde rastlanılmıştır. Bunun nedeni, düşük karışma yüksekliği ve ışıma nedeniyle oluşan yetersiz atmosfer yayılımı ile evsel ısınma kaynaklı gaz salınımlarındaki artış olarak belirlenmiştir. Elde edilen OC/EC, PAH ve n-alkan konsantrasyonlarının dünya genelindeki diğer büyük şehirler ve kentsel alanlar ile karşılaştırılması da bu çalışma kapsamında yapılmıştır. Yapılan analizler sonucunda, İstanbul için elde edilen konsantrasyonların Avrupa, Amerika ve dünyadaki diğer büyük şehirlerden daha fazla olduğu gözlemlenmiştir. Buradaki iki istisna büyük şehir ise Çin'de bulunan Guanzhou ve Almanya'da bulunan Augsburg şehirleridir. Bu sonuçlar, İstanbul için özellikle kış ve güz dönemlerinde sıkı önlemlerin alınması ve uygulanmasının önemini göstermektedir. Bu önlemlerden bazıları; özel amaç için kullanılan dizel araç sayısının kısıtlanması, transatlantik ve yerel gemilerde kullanılan yakıtların kontrolü, evsel ısınmada kullanılan yakıtların kalitesinin kontrol edilmesi veya bazı yakıtların yasaklanması ve bir hafta boyunca trafikte bulunan araç sayısının kontrol edilmesi olarak verilebilir.

**Anahtar Kelimeler: GC-MS, yüksek zaman çözünürlüklü örnekleme, mega şehir İstanbul, organik aerosol, yarı-uçucu organik bileşikler**

**Abstract**

In this work, 295 high-volume samples were collected at high-time resolution for 2h during the day and 12h during the night for six weeks during one year in order to understand diurnal and seasonal variations of selected semi-volatile organic compounds (i.e., n-alkanes and PAH). Average daily PM2.5, OC and EC concentrations were also studied in order to understand the seasonal variations. A total of 15 PAH and 28 n-alkanes were identified and quantified in the samples for the first time in Istanbul and Turkey. Various meteorological conditions and traffic were used to understand their influence on high-time resolved SVOC concentrations. Overall, the highest PM2.5, OC, EC, PAH, and n-alkane concentrations were observed during the fall and winter due to a combination of increased emission sources from residential heating and poor atmospheric dispersion due to low radiation and mixing heights. Comparison of OC/EC, PAH, and n-alkane concentrations found in this work with other megacities and urban areas in the world was performed. The analysis of these results showed that concentrations in Istanbul are higher than those found in Europe, USA, and other Megacities in the world, except the Megacity of Guanzhou in China, and Augsburg, Germany. This shows the importance of implementation and enforcement of stringent control measures in Istanbul, particularly during the fall and winter. Some of these measures may include limiting the number of diesel vehicles for private use, control of fuel used in transatlantic ships and local ferries, controlling the quality or banning of fuels used for residential heating, or controlling the number of vehicles that circulate during the week.

**Keywords: GC-MS, highly time-resolved sampling, Istanbul Megacity, organic aerosol, semi-volatile organic compounds**

# 1. INTRODUCTION

## 1.1 Air pollution in megacities

According to the World Health Organization, air pollution is the world's largest environmental health risk, with seven million premature deaths due to exposure of indoor and outdoor air pollutants (Im et al., 2015). Megacities are urban agglomerations with over 10 million inhabitants. The increase in urbanization affects air quality and ecosystems on both local and regional levels, mainly due to motor traffic increase. Istanbul is the second largest Megacity in the Eastern basin of the Mediterranean. With over 15 million inhabitants, its population constitutes approximately 20% of Turkey's population. In addition, it welcomes 11.6 million tourists from around the world (Kanakidou et al., 2011). According to (Im and Kanakidou, 2012), the Megacity of Istanbul often exceeds $O_3$ and PM air quality standard limits. The population in Istanbul is often exposed to high levels of contaminants, mainly due to domestic heating, industrial, and road traffic activities, especially during the heating season in the Winter (Tayanç, 2000). Available information on volatile organic compound (VOC) concentrations, reactivity, and chemical speciation is limited, thus studies of PM chemical characterization in Istanbul are recommended to elucidate sources and impact of PM pollution (Kanakidou et al., 2011). On the other hand, Megacities have a massive impact on greenhouse gas emissions. Particularly, the East Mediterranean region is expected to have increased concentrations of pollutants in the future due to climate change. Istanbul has experienced rapid growth due to development of roads, skyscrapers, housing, business centers, airports, railways, and metro lines. In addition, a total of 3,230,908 vehicles circulated in Istanbul in 2013 (Sevimoglu, 2015). The carbon footprint in Istanbul was estimated for the year of 2010. Approximately the following contributions were observed: consumption of residential electricity, natural gas, coal, and vehicles (58%), energy consumption in industry (15%), and industrial and waste emissions (6.7%). It is crucial that a stringent emission control is developed in Megacities for climate change mitigation (Sevimoglu, 2015).

## 1.2 Aerosols and their organic fraction. Effects on ecosystems, health, and climate change

Aerosols are small liquid or solid particles suspended in the atmosphere. Although they represent a small fraction of the atmospheric mass, they have important effects on climate, biogeochemistry, and health. Because of these impacts, they have been of research interest for many years, however, many uncertainties remain. The purpose of this proposal is to study organic fraction speciation of atmospheric aerosols.

Atmospheric carbonaceous aerosol (black carbon BC, and organic aerosol, OA) is highly abundant and complex. It constitutes 20-90% of the $PM_{2.5}$ mass and its sources vary both temporally and

geographically. It has been found that organic material contributes to 20-50% of the total fine aerosol mass at continental mid-latitudes and as much as 90% in the tropical forested areas (Jimenez et al., 2009). The composition of organic aerosols varies in time and space due to equilibrium partitioning between the gas and particle phases, irreversible partitioning from the gas to the aerosol phase, and reactions occurring in the liquid and gas phases and on the surface of the particles (Mahowald et al., 2011). Reactions on the particle phase have been found to impact aerosol physicochemical properties. For example hygroscopicity, which influences interactions of particles with water in the atmosphere, is intensified by addition of organic functionalities. Furthermore, their chemical composition is complex and typically not well understood. Characteristics of number, color, size, hygroscopicity, and chemical composition strongly determine the impacts of aerosols on ecosystems, health, climate, and the hydrological cycle (Mahowald et al., 2011).

Black carbon and organic aerosol (i.e., brown carbon) affect Earth's radiation balance (i.e., direct radiative effect) by absorbing light in the UV-Vis and near-UV, respectively. In addition organic aerosol scatters light and affects cloud formation and lifetime (i.e., indirect radiative effect) by acting as cloud condensation nuclei, thereby altering the water cycle. Both, the size and composition of organic aerosol are important in calculating radiative balance. For example, small particles with diameters 0.1-1 μm, likely to be of anthropogenic origin, influence short-wave aerosol optical depth (i.e., the amount of light that is absorbed or scattered at a particular wavelength). The speciation of organic aerosol composition is important because organic species determine the color of the particle (i.e., the amount of light absorbed) and amount of water that will be taken up by the molecule, which in turn determines particle growth (Mahowald et al., 2011).

People started being aware of air pollution during the industrial revolution due to the use of coal in industries and residences. The effects of particulate matter (PM) in human health have been of scientific interest since 1952 due to a severe air pollution episode in London that caused the death of thousands of people in one week. The government has since then established threshold limits to protect human health from exposure to hazardous air pollutants (HAP) that are mostly organic in nature (Mauderly and Chow, 2008). Particulate matter has been linked to short-term acute respiratory effects. Long-term effects could be associated to decreased lung function, increased chronic respiratory and cardiovascular diseases, and premature death (Incecik and Im, 2012). Lately there have been more efforts to correlating epidemiological studies and PM speciation. (Kim et al., 2012) studied $PM_{2.5}$ constituents ($PM_{2.5}$, organic carbon OC, elemental carbon EC, sulfate, and nitrate) daily at a residential site 2003-2007 and correlated the concentrations to daily admissions to hospitals in the area. Strong

associations between $PM_{2.5}$ concentrations, its constituents, and cardiovascular hospital admissions were observed on the same day. On the other hand, effects of $PM_{2.5}$ and their constituents on respiratory illnesses where developed and observed a few days later. It was also found that OC and EC had larger effects than sulfate and nitrate (Kim et al., 2012). Vedal et al., (2009) studied the adverse effects that specific $PM_{2.5}$ sources such as meat cooking, diesel vehicle exhaust, and wood combustion, among others, have on human health. Daily counts of mortality, hospitalizations, and measures of asthma control were simultaneously investigated (Vedal et al., 2009). The clearest associations were observed between OC, EC, and total mortality, especially for people with terminal cancer. Combustion sources, specifically EC emissions from diesel exhaust, are more likely associated to these effects than secondary inorganic aerosol (Kim et al., 2015). Volatile organic compounds are known carcinogenic toxics that have a wide range of effects on human health. Exposure to VOCs can cause irritation in eyes, nose, and throat, nausea, and damage to kidneys, liver, or central nervous system (Yalçın et al., 2015). McDonald et al., (2004) used multivariate statistical methods to separate semi-volatile organic compounds (SVOCs) emitted by gasoline and diesel exhaust by chemical class and thus understand their toxicity effects. Functionalized polycyclic aromatic hydrocarbons (PAHs) (i.e., nitro- and oxy-) were most closely associated with pulmonary toxicity, and hopanes and steranes showed the strongest association with toxicity (McDonald et al., 2004).

Interdisciplinary work between scientists, government, industry, and the public is necessary for air quality monitoring, source apportionment, epidemiological studies, and implementation of regulations for understanding the air quality-health relationship and successful air quality management (McDonald et al., 2004). Future work should focus on assessment of individual species or mixtures and finding specific linkage between $PM_{2.5}$ sources and impacts on human health. For this reason, receptor-based models are very useful tools for $PM_{2.5}$ source apportionment (Mauderly and Chow, 2008; Vedal et al., 2009; Xie et al., 2013). Identification of diurnal and seasonal cycles of organic aerosol chemical composition is essential for tracing sources, elucidating formation and transformation processes, evaluating effects on human health, and assessing climate change effects.

### 1.3 SVOCs and fast time-resolved sample collection

It has been estimated that organic aerosol is composed of 10,000 to 100,000 different organic compounds (Goldstein and Galbally, 2007). Semi-volatile organic compounds include PAHs, *n*-alkanes, hopanes, steranes, and low-volatility oxygenated *n*-alkanoic acids, *n*-alkenoic acids, alkane dicarboxylic acids, aromatic carboxylic acids, resin acids, polyols and sugars, and other multi- and poly-functionalized species. Semi-volatile organic compounds (saturation concentration $C^*$ $10^{-1}$ to $10^3$ μg $m^-$

$^{3}$) have been identified as a substantial source for secondary organic aerosol since the products of their oxidation reactions form secondary organic aerosol (SOA) effectively. Despite their importance, this fraction is usually not accounted for. Furthermore, it has been observed that inclusion of SVOC emissions in SOA production models result in a better agreement between models and measurements than previous modeling efforts. Models, however, still fail to reproduce SOA mass and oxygen to carbon ratios, which indicates that to better predict SOA formation, more work is necessary to understand speciation, sources, emissions, oxidation mechanisms and gas-to-particle reaction pathways (Zhao et al., 2012).

One of the reasons for the disagreement between models and measurements is the fundamental mechanism used to simplify input to the model which lumps SOA precursors into bins according to volatility. It has been reported that molecular structure and functionality are better representations for SOA formation. For example, oxidation of alkane isomers with OH radicals have the following order: (1) branched, (2) linear, and (3) cyclic (Zhao et al., 2012). In addition to their reactivity, partitioning of SVOCs between the gas and particle phases varies diurnally and seasonally according to temperature. This partitioning variation has implications in the potential of SVOCs for SOA formation since specific reaction mechanisms may be enhanced by the presence of acidic compounds. The variation in the concentration of SVOCs during the day requires sampling, extraction, and analytical techniques that are capable of resolving these fluctuations (Yalçın et al., 2015). On the other hand, brown carbon is a fraction of organic aerosol that is complex in composition and composes a large group of organic compounds. It has been found that inclusion of its contribution in climate and chemical transport models improves the simulations of aerosol light absorption (Lu et al., 2015). Brown carbon is responsible for 20% to more than 50% of the light absorption in UV region.

Organic aerosol composition experiences both diurnal and seasonal variation due to multiple sources and transformation during transport. High time resolved aerosol sampling provides insight into SVOCs sources, reactivity, and transformation pathways that can improve models of organic aerosol formation and growth. In addition, studying the diurnal and seasonal variation in the composition of organic aerosol is essential to the understanding and modeling of their effect in radiative balance and tropospheric chemistry.

### 1.4 Thermal desorption of SVOCs associated to PM2.5

Thermal desorption is the only method that allows extraction for direct gas chromatographic analysis of fast time resolved samples since a small sample of a few $m^3$ of collected air is required for analysis. Only non-thermally labile and volatile or semi-volatile organic compounds in the aerosol or gas phases are amenable for thermal desorption. Due to its versatility, thermal desorption can be used for a number of applications in air quality, food, flavor, and fragrance, and other interdisciplinary areas in environmental engineering, healthcare, materials emissions, and work exposure. The need for high-time resolved collection and fast analysis has led to the development of hybrid instruments with powerful analytical techniques for stand-alone automatic sample and analysis of aerosol and gas phases. These instruments include thermal desorption-gas chromatograph (TD-GC-FID), thermal desorption-gas chromatograph with mass spectrometer detector (TD-GC-MS), thermal desorption-two dimensional gas chromatograph with mass spectrometer (TD-GC×GC-MS), and more recently thermal desorption-aerosol mass spectrometer (TD-GC-AMS) (Isaacman et al., 2014; Lambe et al., 2010; Schnelle-Kreis et al., 2005; Williams et al., 2006; Williams et al., 2014; Worton et al., 2011). These analytical instruments have been designed for in-situ simultaneous collection and analysis. Method development has been also performed for analysis of less volatile non-polar and polar organic compounds using online derivatization-thermal desorption- gas chromatography mass spectrometry (Isaacman et al., 2014; Orasche et al., 2011). High recoveries are typically obtained with thermal desorption, in addition its performance is comparable to traditional solvent extraction techniques (Graham et al., 2010). The proposed work will serve to develop methods and collect preliminary data that will potentially serve as basis for future instrument development. In addition, hourly samples collected in this project will be helpful for more accurate analysis of mass and source apportionment

# 2. LİTERATURE REVİEW

## 2.1 Pollution levels in Istanbul

Istanbul (5400 $km^2$) is the most populated (~15 million inhabitants) city in Turkey. Its population has grown since 1970s, following a rapid urbanization growth due to the movement of national and foreign immigrants. The municipality has accomplished the improvement of the public transportation system, which currently operates 8, 7, and 3 different road, railway, and sea transportation services, respectively (Sevimoglu, 2015). Despite this great effort, traffic is still a large source of air pollutant emissions, with over 3 million cars circulating in 2013 (Sevimoglu, 2015). In addition to traffic, domestic heating and ships are also important black carbon, nitrogen oxides, sulfur oxides, and particulate matter emitters (Viana et al., 2015). Despite recent efforts to use natural gas, residences in some parts of the city still use coal as source of domestic heating during the winter, causing a 30% increase in $PM_{10}$ concentrations (Unal et al., 2011). Istanbul also has high ship traffic through the Bosporus strait (~30 km long) with nearly circulating 60,000 ships yearly. The Istanbul Greater Metropolitan Environment Department, the Ministry of Environment and Forestry of Turkey, and the Turkish State meteorological Service operate ten continuous sampling and 72 meteorological stations in Istanbul. This continuous monitoring allows the retrieval of data in real time for evaluation of pollutant emissions in both spatial and temporal resolutions. It has been observed, for example, that in Istanbul, traffic emissions are constant throughout the year but air quality diminishes during the Winter because of domestic heating emissions (Erdun et al., 2015). Industrial emissions in the city are from cement plants, oil refinery, petrochemicals, and two international airports. In addition to emissions, meteorology in Istanbul plays a big role on the dispersion and stagnation of air pollutants.

Meteorological conditions that influence a clean atmosphere in Istanbul are dominant winds from the SW due to the Marmara sea breeze and total rainfall of 774 mm during rainy season in the Winter (344 mm) and Fall (309 mm). On the other hand, stagnation episodes are caused by emissions, temperature inversions, atmospheric stability, light wind speed, and topography (Toros et al., 2014). Overall, it has been found that PM indoor and outdoor concentrations in Istanbul repeatedly exceed the air quality standards (Onat and Şahin, 2012; Onat and Stakeeva, 2014; Unal et al., 2011). In addition to local emissions, air quality in Istanbul is worsened during stable atmospheric conditions (Tanriover et al., 2014; Toros et al., 2014) and the influence of long-range transport (Karaca et al., 2009; Karaca and Camci, 2010; Kindap et al., 2006). The region of Kartal, showed the highest concentrations of $PM_{10}$ with average monthly concentrations of 31.8-63.5 μg $m^{-3}$ (Summer) and 42.9-86.9 μg $m^{-3}$ (Winter). These concentrations exceeded the EU limit of 50 μg $m^{-3}$ 1208 days in five years (~ 75%) and were the result of combined emissions from traffic, industry, and domestic heating (Unal et al., 2011). Unal et al.,

(2011) showed that this limit was exceeded in all 10 monitoring stations during 2005-2009, mostly during the Winter season. In addition to local emissions and meteorological stagnant conditions, it has been observed that long range transport could be responsible for as much as 50 % of the background $PM_{10}$ concentrations in Istanbul (Karaca et al., 2010, Kindap et al., 2006). The effects of pollutants on human health and cultural heritage have been investigated in Istanbul. Positive correlations between $SO_2$, NO, CO, $PM_{10}$ concentrations and the number of emergency admissions for obstructive pulmonary disease were found (Hapçioğlu et al., 2006). In addition, corrosion risks for copper, cast bronze, and carbon steel materials were found in two locations in the historical peninsula of Istanbul (Karaca, 2013). Identification of sources is essential for development of emission inventories and air quality management.

**2.2 Daily and seasonal variation**

Time-resolved concentration of air pollutants is necessary for evaluation of air quality impacts on human health and ecosystems, evaluation of sources, implementation of air pollution control strategies, and understanding of atmospheric chemistry (Chuersuwan et al., 2000). The study of diurnal, spatial, and air quality during pollution episodes is useful for human health exposure and public notification (Chuersuwan et al., 2000). Typical national and international standard methods for $PM_{10}$ and $PM_{2.5}$ concentrations and chemical speciation includes the off-line collection of coarse time-resolved samples (i.e, 24 h) once every third day or sixth day (EPA, 2015b) for subsequent chemical analysis (see e.g., EPA methods IO-2.1, IO-3.1, 8270D, SVOC/PAH SOP) (EPA, 1999, 2007; Mycock et al., 1995). However, it has long been realized that integrated daily sampling misses substantial information between sampling days, diurnal variation, the complexity of source contribution, and impacts on atmospheric chemistry (Wexler and Johnston, 2008). In addition, positive and negative artifacts in filters collected on a daily basis (e.g., 24 h), that would be avoided in high-time resolved samples, have been reported (Cabada et al., 2004; Miyazaki et al., 2006a; Xu et al., 2015). The continuous real-time measurement of PM concentrations has been extensively studied with automatic samplers see e.g., (Chuersuwan et al., 2000). Automatic samplers measure the oscillation frequency every 2 seconds and calculate the amount of PM added to the filter. Detailed PM speciation, however, requires the use of rapid and sensitive high-resolution methods. Recent efforts for high-time resolution studies involve collecting integrated 12 h samples (Crippa et al., 2014; Li et al., 2014; Ma et al., 2014; Miyazaki et al., 2006b). On the other hand, the aerosol mass spectrometer (AMS) is a state-of-the art instrument that allows high resolution studies but chemical speciation of the organic fraction is not possible (Crippa et al., 2013, Lambe et al., 2010, Williams et al., 2014). The AMS measures quantitative, size-resolved PM components and has been extensively used to characterize detailed sources, processes, and

mechanisms of severe air pollution episodes. For example, sulfate, nitrate, ammonium, chloride, and organics in $PM_1$ were analyzed every 5 min in Beijing during 9-21 July 2006 and July 24-September 20 2008 to understand physical and chemical processes leading to air pollution (Huang et al., 2010; Sun et al., 2011). The AMS has also been used for some specific purposes, such as identifying organic markers and signature from wood combustion emissions in real-time (Elsasser et al., 2012).

The importance of using high-time resolved data collection and analysis in source apportionment studies has been acknowledged. In addition, advanced multilinear models that account for the variation in composition of the source emissions in different size ranges have been developed (Peré-Trepat et al., 2007; Perrino et al., 2010; Zhao et al., 2004). High-time resolved data is necessary to more accurately apportion sources to account for dynamic emission patterns and temporal and spatial changes due to chemical reactivity and physico-chemical properties (Xie et al., 2013). For example variations during weekends and weekdays are expected for some sources since some industries do not operate and fewer people commute to their work over the weekends. Diurnal variations may be due to changes in biogenic emissions, leaks from storage tanks in chemical plants, vehicle and ship emissions during peak traffic hours, degradation due to photochemical reactions, changes in emission rates from anthropogenic sources, dilution effect caused by wind speed (i.e., atmospheric mixing), and vaporization due to increased temperature (Zhao et al., 2004). Discussion regarding findings in source apportionment studies using high-time resolved data can be found in section 3.6.

In addition to source apportionment and understanding of diurnal and seasonal variation, high-time resolved data has been useful for evaluation of impacts to human health in indoor environments and resolving long-range transport of pollutants from local phenomena (Long et al., 2001; Perrino et al., 2010). Detailed chemical speciation of particulate matter in high-time resolved data requires compromise, sensitive methods, and is expensive (Karaca et al., 2008, Perrino et al., 2010). For this reason, typically short field campaigns in the order of a few days to a few weeks are carried out for high-time resolution studies (Elsasser et al., 2012; Huang et al., 2013; Huang et al., 2012; Miyazaki et al., 2006a; Peré-Trepat et al., 2007; Williams et al., 2010). In addition, numerous instruments have been developed, constructed, and used for in-situ unattended high-time resolved sampling, extraction, and analysis of PM chemical speciation in various types of environments (Isaacman et al., 2014, Lambe et al., 2010, Schnelle-Kreis et al., 2005, Williams et al., 2006, Williams et al., 2014, Worton et al., 2011). In Turkey continuous measurement of $PM_{10}$ and $PM_{2.5}$ concentrations are available through the Ministry of Environment and Urbanization (http://havaizleme.gov.tr/Default.htm). However, detailed

chemical speciation studies are limited (Karaca et al., 2008), and specially, those collected at high-time resolved intervals are not available.

### 2.3 PM2.5 levels in Istanbul

Particulate matter suspended in the atmosphere is regulated by numerous national and international governmental units. In the United States, the PM national ambient air quality standards (NAQQS) have evolved over the time because research has helped understand the different effects that PM has on human health. The 24-h average limit for total suspended matter (TSP) was established in 1971 to 260 $\mu g/m^3$, not to be exceeded once per year. Subsequently, limits for $PM_{10}$ and $PM_{2.5}$ were established in 1987 and 1997 with average 24-h of 150 and 65 $\mu g/m^3$, respectively. Currently, average annual limits are 50 and 12 $\mu g/m^3$ for $PM_{10}$ and $PM_{2.5}$, respectively. In Europe, the 24-h and annual $PM_{10}$ limit are considerable lower than in the USA, with 50 and 40 $\mu g/m^3$, respectively (EPA, 2015; EU, 2004). There are a total of five Conventions and Frameworks related to air quality that Turkey has become part of. For example, the Convention of Long Range Transboundary Air Pollution was signed in 1983. In addition, Turkey is a European Union (EU) candidate and its air quality needs to satisfy their established regulations, which encourages chemical speciation of $PM_{2.5}$ (Aydin Coskun et al., 2011; Karaca et al., 2008). Regulations are continuously being updated. The US-EPA is currently performing studies to make PM standards more rigorous (EPA, 2015).

The air quality in Istanbul considerably improved in 1996 due to the establishment of natural gas pipelines across the country and a regulation to use coal with less than 1.5% sulfur content (Tayanç, 2000). However, it has been reported multiple times that average concentrations of $PM_{10}$ continuously exceed the established limits (Erdun et al., 2015; Karaca et al., 2005; Unal et al., 2011). In Turkey, continuous measurements of $PM_{10}$ and $PM_{2.5}$ (in selected stations) are available through the Ministry of Environment and Urbanization since late 90's, and 2013, respectively (http://havaizleme.gov.tr/Default.htm). However, concentrations and chemical speciation of $PM_{10}$ and $PM_{2.5}$ have been scarcely reported (Karaca et al., 2008). High and variable average $PM_{10}$ concentrations ranged 47–115 $\mu g/m^3$ in 10 sampling stations in Istanbul 1998-2008 (Ozdemir et al., 2009). More recently, average annual concentrations of 48–58 $\mu g/m^3$ were reported in Istanbul between 2008-2012 (Erdun et al., 2015). However, some regions in Istanbul experience even higher concentrations. For example, Unal et al., (2011) reported that $PM_{10}$ concentrations in Kartal exceeded the EU limit of 50 $\mu g/m^3$ 75 % of the time in 2005-2009, mostly during the Winter season. Annual average $PM_{2.5}$ concentrations also exceed US-EPA standard of 15 $\mu g/m^3$. Annual $PM_{2.5}$ concentrations were 20.8 $\mu g/m^3$ in 2002-2003 and 36 $\mu g/m^3$ in 2010, whereas a lower average 24-h $PM_{2.5}$

concentration of approximately 3.2 μg/$m^3$ was predicted by models on March 3, 2015 (Çavuş et al., 2015, Karaca et al., 2005, Ozdemir et al., 2014). Erdun et al., (2015) provide recommendations to accomplish sustainable and healthy development in urban areas (like Istanbul) such as reducing emissions from vehicles and encouraging the use of natural gas in residences.

**2.4 Organic carbon (OC) and elemental carbon (EC) studies**

The abundant organic fraction constitutes 10-90 % of fine particulate matter. Carbonaceous aerosol is typically classified in organic carbon (OC) and elemental carbon (EC). Organic carbon exists in both primary (emitted directly) and secondary (formed in the atmosphere) forms. Whereas, EC is strictly emitted by primary sources, and thus can be used as a tracer for combustion sources (Cabada et al., 2004). Because OC is also produced by gas-to-particle conversion reactions in the atmosphere, high ratios of OC to EC can be used as indicator for these types of processes. High-time resolved samples have been used for temporal and seasonal variation of OC and EC studies. Samples were collected for 45 min at 8 l $min^{-1}$ during 12, 16, and 15 days during the winter, summer, and fall, respectively (Miyazaki et al., 2006). Average OC/EC ratios were 1.46, 1.36, and 1.33 during the winter, summer, and fall, respectively. High OC/EC ratios during the winter were associated to transport of pollutants from local sources, followed by stagnation in a lower mixed layer. On the other hand, high OC/EC ratios during the summer (August) were associated to high photochemical activity (Miyazaki et al., 2006). Although Istanbul is a Megacity with high PM concentrations that often exceed standard limits, carbonaceous aerosol has been scarcely investigated.

In Istanbul, OC and EC concentrations in daily $PM_{10}$ were studied for approximately 10 days in July 2008- June 2009 (Theodosi et al., 2010). Annual average concentrations of OC (6.65 μg $m^{-3}$) and EC (2.92 μg $m^{-3}$) in $PM_{10}$ In Istanbul were three times lower than those observed in Beijing, and comparable to other megacities, such as Paris. High EC concentrations in $PM_{10}$ in Istanbul were tracer for uncontrolled vehicle and industrial emissions, whereas higher concentrations of OC and EC during the winter were attributed to domestic heating emissions. Concentrations of black carbon (BC) have been also investigated in Istanbul in the spring seasons of 2009 and 2010 (Ozdemir et al., 2014). Annual average concentrations of BC were found to contribute to approximately 38 $\pm$ 14 % the total $PM_{2.5}$ concentration. Air pollution from traffic-related sources is expected to worsen in the near future in Istanbul, where approximately 3 million cars will be circulating (Ozdemir et al., 2014). (Öztürk and Keleş, 2016) studied OC/EC concentrations in Bolu (winter 2014). Concentrations of OC and EC have strong seasonality with highest concentrations in winter and lowest concentrations in summer. This reflects the importance of residential heating and poor atmospheric ventilation during the winter, which

was observed by Ozturk and Keleş. OC and EC concentrations observed by Theodosi et al. are comparable to other Megacities in Belgium, Italy, and France. However, EC concentrations observed by Ozdemir et al., are significantly higher than those reported by Theodosi et al. This shows the importance of a heavily influenced traffic site chosen by Ozdemir et al. on the continuous monitoring OC/EC concentrations.

The EU directive on ambient air and cleaner air for Europe 2008/50/EC (article 6.2 and Annex IV) (EU, 2008) requires measurements of organic carbon and elemental carbon (OC/EC) in $PM_{2.5}$ in all urban and rural areas. The study of OC and EC in high-time resolved samples will give additional information about daily variations due to sources and meteorology. In this work, OC/EC concentrations will be studied in high-time resolved samples (~2h) with thermal-optical methods. EC concentrations will be compared to BC concentrations as explained in section 7.2.

Although source apportionment of carbonaceous aerosol with OC, EC, and BC has been investigated in Istanbul, the study of species and organic markers is necessary for a more accurate source apportionment of organic aerosol that can be potentially used for the development of mitigation strategies (Lambe et al., 2010, Xu et al., 2015). In this work, OC and EC associated to high-time resolved $PM_{2.5}$ samples will be investigated for the first time in Istanbul.

**2.5 Speciation of SVOCs associated to PM2.5 by thermal desorption**

Thermal desorption gas chromatography mass spectrometry (TD-GC-MS) is a cost-, effort-, and time-effective alternative method for qualitative and quantitative analysis of non-polar organic compounds in the aerosol and gas phases. Thermal desorption does not require the use of sample pretreatment and organic solvents for extraction, minimizes sample contamination, reduces uncertainties from extraction, and most importantly, improves analytical sensitivities. In addition, similar accuracies, better precision, and low method detection limits (0.01-0.03 ng $m^{-3}$) have been obtained by thermal desorption compared to solvent extraction methods (Chow et al., 2008; Chow and Watson, 2012). Thermal desorption coupled to gas chromatography mass spectrometry (TD-GC-MS) instruments have been developed and used for in-situ unattended high-time resolved studies of SVOCs. High-time resolution sampling has also been combined to thermal desorption and multidimensional gas chromatography mass spectrometry (TD-GC×GC-ToFMS) for greater resolution and sensitivity power of over one order of magnitude higher than conventional GC-MS. In addition, more recently, a thermal desorption aerosol mass spectrometer (TD-AMS) has been developed and used to determine hourly speciation and quantification of semi-volatile organic compounds and selected non-volatile organic compounds

(Isaacman et al., 2014, Lambe et al., 2010, Schnelle-Kreis et al., 2005, Welthagen et al., 2003, Williams et al., 2006, Williams et al., 2014, Worton et al., 2011). Efforts in advancing thermal desorption techniques is often related to achieving source apportionment of organic carbon using species as source markers (Hays and Lavrich, 2007).

Organic carbon is composed of thousands of individual species. Approximately 100-130 semi-volatile organic compounds can be identified and quantified simultaneously in organic aerosol (~ 4-30 % of the total mass) using thermal desorption techniques (Chow et al., 2008, Chow et al., 2012). Several studies have focused on studying diurnal, temporal variation and contribution of SVOCs to specific sources (Schnelle-Kreis et al., 2007, Xie et al., 2013a, Zhang et al., 2009). Schnelle et al., (2007) performed quantitative studies of *n*-alkanes, alkanones, alkanoic acid methylesters, long chain linear alkyl benzenes and toluenes, hopanes, PAH and oxidized PAH. Variable seasonal concentrations were observed for all compounds, with highest concentrations during the cold seasons, except for selected alkanones. Sources of organic compounds were also investigated (see section 3.6). Williams et al., (2006) and Williams et al., (2010) were able to identify and quantify 100 and 300 organic compounds in ambient particle samples using a newly developed TD-GC-FID instrument, respectively.

In Turkey, chemical speciation of organic aerosol has been scarcely studied (Hanedar et al., 2014; Karaca et al., 2008; Ozdemir et al., 2014). Hanedar et al., (2014) studied the seasonal variation and sources of 16 PAHs in total suspended particles (TSP). Measured PAH concentrations were mostly associated to diesel vehicle emissions. Observed strong seasonal variations, specially between winter and spring, were associated to residential heating during the winter (Hanedar et al., 2014). (Kuzu et al., 2014) studied the concentration of 84 PCB during the summer and fall in the gas and particle phases. Average PCB concentrations in the particle phase were 49 pg $m^{-3}$, which is comparable to data observed in Bursa (Turkey) and South Korea. However, higher PCB concentrations of 105, 314-3136, and 316-570 pg $m^{-3}$ have been observed in Bolu, Izmir, and Bursa, respectively (Kuzu et al., 2014). Understanding sources, transformation, and fate of organic aerosol in the atmosphere is essential to determining effects on human health and global radiation balance (Williams et al., 2007). The hourly measurements of SVOCs associated to $PM_{2.5}$ provided by this study will be among the first ones carried out in urban environments on a global level.

**2.6 Sources of organic aerosol markers**

Anthropogenic aerosols are complex due to their wide variety of sources. In addition, organic aerosol composition is expected to change as fuel mixtures, industrial emissions, and emission control

technologies continue to evolve (Brook et al., 2009; Scheffe et al., 2011). Marker compounds have been analyzed and used in multi-variate statistical programs to understand sources of PM in urban areas and Megacities (Crippa et al., 2013, Onat et al., 2012, Theodosi et al., 2010, Zheng et al., 2014). The understanding of sources is important to air quality management to reduce impacts to human health. Biogenic sources of PM include trees, plants, and grasses. Biogenic SVOC markers are α-pinene, isoprene, and β-caryophyllene. Anthropogenic sources of PM are motor vehicles and industries which emit alkanes, alkenes, single and multiple ring aromatics, and functionalized hydrocarbons with side chains. Toluene, mono- or di-substituted aromatics, and *n*-alkanes ($C_9$-$C_{12}$) are significant anthropogenic precursors to SOA formation (Derwent et al., 2010). Source apportionment studies show that contributions to PM less than 2.5 μm ($PM_{2.5}$) during the Summer are 85% secondary organic matter (SOM) and 88% water soluble organic matter (WSOM), with approximately 50% from anthropogenic sources (Rutter et al., 2014). Concentrations of SVOCs could be potentially reduced by controlling emissions from anthropogenic sources such as vehicles, industries, and domestic heating. In Istanbul, PM was apportioned to traffic and industry (22%), fuel and oil combustion (16%), sea-salt (16%), crustal (13%), secondary (10%), and ammonium sulphate (7%) (Theodosi et al., 2010). However, organic aerosol semi-volatile species and sources have not been studied before.

## 3. HYPOTHESIS and OBJECTIVES

### 3.1 Hypothesis

1. High-time resolved PM2.5 concentrations are a better metric for evaluation of air quality and impact on human health

2. Correlations between high-time resolved PM2.5 and NO and CO are a better metric than traffic counts

3. High-time resolved PM2.5 and SVOC concentrations are a better metric for identification of the impact of residential heating

4. Due to different physicochemical properties, PAH and n-alkanes will exhibit different diurnal variations according to meteorology and concentrations of oxidants.

5. The concentration of PAH and n-alkanes and their diurnal and seasonal variation is the result of a complex interaction between their physicochemical properties, meteorological variables, and traffic.

### 3.2 Objectives

1. Analysis of hourly PM2.5 concentrations and comparison to average daily air quality standards.

2. Analysis of diurnal variations of PM2.5, NO, and CO concentrations, and traffic counts and calculation of Pearson correlation coefficients.

3. Study diurnal and seasonal variations of PM2.5, PAH, and n-alkanes.

4. Collection of high-time resolved PM2.5 samples during spring, summer, fall, and winter in Istanbul

5. Analysis of n-alkanes and PAH at high-time resolved PM2.5 samples.

6. Study of diurnal and seasonal variations of PAH and n-alkanes and their correlation with meteorological variables and concentrations of O3 and NOx.

7. Quantification of the impact of PM2.5, meteorology, and traffic on high-time resolved PAH and n-alkanes and their seasonal variation with multiple regression analysis and Pearson correlation coefficients.

## 4. METHODS

### 4.1 Collection of $PM_{2.5}$ samples

$PM_{2.5}$ were collected with both, high-volume and low-volume samplers. The high-volume sampler was used to collect samples at high-time resolution of 2h between 7:00 h and 19:00 h, and 12h from 19:00 to 07:00 h continuously during 7 days for 3 weeks during the winter and one week during spring, summer, and fall. Average 24 h $PM_{2.5}$ concentrations were obtained with the low-volume sampler according to the gravimetric method. High-time resolution samples were used for determination of semi-volatile organic compounds while low-volume samples were used for determination of organic carbon and elemental carbon concentrations (OC/EC). The high-volume sampler was calibrated prior to sampling during each sampling period (see e.g., Fig. 1) while the settings of the low-volume sampler were programmed automatically. The volume of air collected for each sample was determined with the calibration curve of the high-volume sampler and read from a counter in the low-volume sampler. Details about the calibration procedure, calculations, and quality control can be found in our first progress report. The sampling station is located in Beşiktaş, near the Bosphorous and approximately 10 m from the road on Barvados Bulevar (Fig. 2).

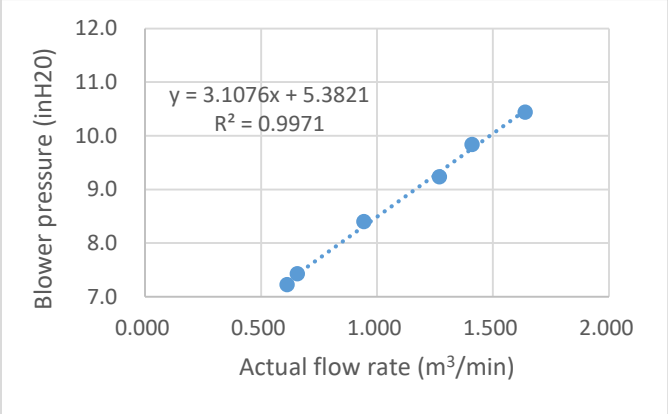


Figure 1. High-volume sampler calibration curve performed on 30 June 2017


Figure 2. Location of sampling and meteorological stations in Beşiktaş.

### 4.1.1 Determination of sampling dates

Sampling dates were determined after careful analysis of weather forecasts. In order to obtain the best sampling conditions with atmospheric stagnation, sampling dates were chosen on days dominated by high-pressure systems, low wind speed, lack of precipitation, and lack of horizontal and vertical transport, dispersion, and dilution. For this purpose, numerical weather predictions of Global Forecast System (GFS, NOAA) model for Europe was investigated for 16 days in advance from models such as ECMWF, GEM, WRF, ARPEGE (.e.g., www.wetterzentrale.de). Analysis of 500 hPa geopotential heights (~ z=5500m), 500 hPa temperature, and sea level pressure maps were recorded daily (See Appendix A). After careful analysis, the sampling dates for each week were determined as follows:

Winter Week 1: January 28 - 4 February 2017
Winter Week 2: February 17-23 2017
Spring Week 3: May 3–9 2017
Summer Week 4: July 6-12 2017
Fall Week5: October 20-26 2017
Winter Week 6: January 4-10 2018

### 4.1.2 Real-time $PM_{2.5}$ concentrations

Real-time $PM_{2.5}$ concentrations were provided by the Turkish Council of Environment and Urbanization for four sampling sites: Çatladıkapı, Kağıthane, Silivri, and Ümraniye. Average hourly and daily concentrations were calculated based on real-time concentrations.

### 4.2. Meteorology and Traffic

#### 4.2.1 Meteorological data

Meteorological data was obtained from Turkish Meteorological Service (Meteoroloji Genel Müdürlüğü") for station No. 17603 (41.0155N, 28.9601E) which is 4000 m SW of the sampling station (Fig. 2 left). Real-time meteorological data was obtained from Enka weather at http://w.enka.com/weather/ and weather underground at https://www.wunderground.com for Balmuncu station (41°3'29"N, 29°1'1"E) which is 1570 m NE of the sampling station (Fig. 2, right). Meteorological data includes temperature (°C), dew Point (°C), humidity (%), wind direction, wind Speed (km/h), pressure (hPa), precipitation rate (mm), and solar radiation (w/m²). Wind roses were created with WRPLOT v.8.0.2 (Lakes Environmental, USA).

#### 4.2.2 Mixing height

For calculation of mixing height, radiosonde data was obtained from Turkish Meteorological Service for sampling collection dates. Alternatively, radiosonde data can be obtained from Atmospheric Science department at University of Wyoming (http://weather.uwyo.edu/upperair/sounding.html) for station 17064 which is located in Kartal (40.911N, 29.155E) approximately 20 km SSE of the sampling station (Fig. 3). Mixing height was located at the point where temperature stops following the adiabatic cooling rate of -9.8 °C/Km. Vertical distribution of temperature can be observed in Appendix B.


Figure 3. Location of the sampling station and radiosonde station.

#### 4.2.3 Air mass backward trajectories

Air mass backward trajectories were obtained with the web version of HYSPLIT model (NOAA, USA) at 100 m AGL at the sampling site location (41.045N, 29.007 E) for all sampling dates during each sampling week. The starting time and duration of the backward trajectories were similar to each 2h sample during the day and 12h during the night. Backward trajectories can be found in Appendix C.

#### 4.2.4 Traffic density

Traffic density collected every minute was provided by the department of transportation in Istanbul for sensor 263, which is located approximately 90 N of the sampler. Total vehicle counts were calculated for all six lanes of Barbaros Bulvari according to each sampling time (ie., 2h and 12h) for winter 2017 (sampling weeks 1 and 2), Fall (sampling week 5) and winter 2018 (sampling week 6). Due to technical difficulties, traffic data was not available for spring (sampling week 3) and summer (sampling week 4).

### 4.3. Determination of Organic Carbon (OC) and Elemental Carbon (EC) concentrations

Organic carbon (OC) and elemental carbon (EC) concentrations were determined in daily $PM_{2.5}$ samples with a Sunset thermo-optical carbon analyzer according to the recommended method NIOSH 870 as follows: (1) Organic carbon temperature ramps at 310, 475, 615, and 870°C in a 100% helium atmosphere and (2) Elemental carbon temperature ramps at 550, 625, 700, 775, 850, and 870°C in a 2% oxygen atmosphere (Andreae and Gelencsér, 2006a). Organic compounds and soot carbon are oxidized to $CO_2$ during combustion and converted to $CH_4$. The total area under the ramp curves of OC and EC are calculated and converted to concentrations using a calibration standard of sucrose solution (Yavuzsoy et al., 2018). The standard deviation of these analysis in triplicate ranged 1.1-7.5% with average of 4.0%. Standard deviations of 20% have been reported in the literature.

### 4.4. Method development for determination of semi-volatile organic compound concentrations

#### 4.4.1. Analytes of interest

Semi-volatile organic compounds were obtained in the highest purity available as follows: (1) light aromatic compounds benzene, ethylbenzene, xylenes, naphthtalene, toluene, (2) PAH Acenaphthene, Acenaphthylene, Anthracene, Benz[a]anthracene, Benzo[a]pyrene, Benzo[b]fluoranthene, Benzo[ghi]perylene, Benzo[k]fluoranthene, Chrysene, Dibenz[a,h]anthracene, Fluoranthene, Fluorene,

Indeno[1,2,3-cd]pyrene, Naphthalene, Phenanthrene, Pyrene, and (3) C8-C40 n-alkanes. The neat solutions had the following concentrations: (1) PVOC Mixture 3 (Wisconsin) 1000 µg/ml in Methanol, (2) PAH Calibration Mix TraceCERT 10 µg/ml in acetonitrile, and (3) 3C7-C40 Saturated Alkane Mixture 1000 µg/ml in hexane. In order to choose the correct organic solvent for our target analytes, solubilities of organic compounds in dichloromethane, iso-octane, and methanol were predicted according to the method below:

$$P_s = \frac{S_s}{S_w} \quad (1)$$

Where, Ps is the Abraham partition coefficient of the SVOC in water and an organic solvent. Ss and Sw are the solubilities of the SVOC in water and the organic solvent, respectively.

Abraham partition coefficients, Ps, are predicted with equation (2):

$$\log P = vV + sS + aA + eE + bB \quad (2)$$

Where v, s, a, e, and b are coefficients that depend on molecular structure of the organic solvent and V, S, A, E, and B are coefficients that depend on molecular structure of SVOC. Coefficients in equation 1 are referred as solvation parameters and represent the following: v, V are the molecular volume ( cm3/M)/100; a, A and b, B are the hydrogen bonding in a basic and acidic solvent, respectively; s, S are dipolarizability parameters which measure the ability of the molecule to stabilize a charge (i.e., dipole); e, E are the excess molar refractivity and measure the ability of the molecule to interact with a solvent through n- and $\pi$- electron pairs. Abraham solvation parameters were predicted with the ACD/Percepta Absolv module. Predicted solubilities are given in Appendix D. According to the predictions, dichloromethane is a suitable organic solvent for a mixture of target SVOCs.

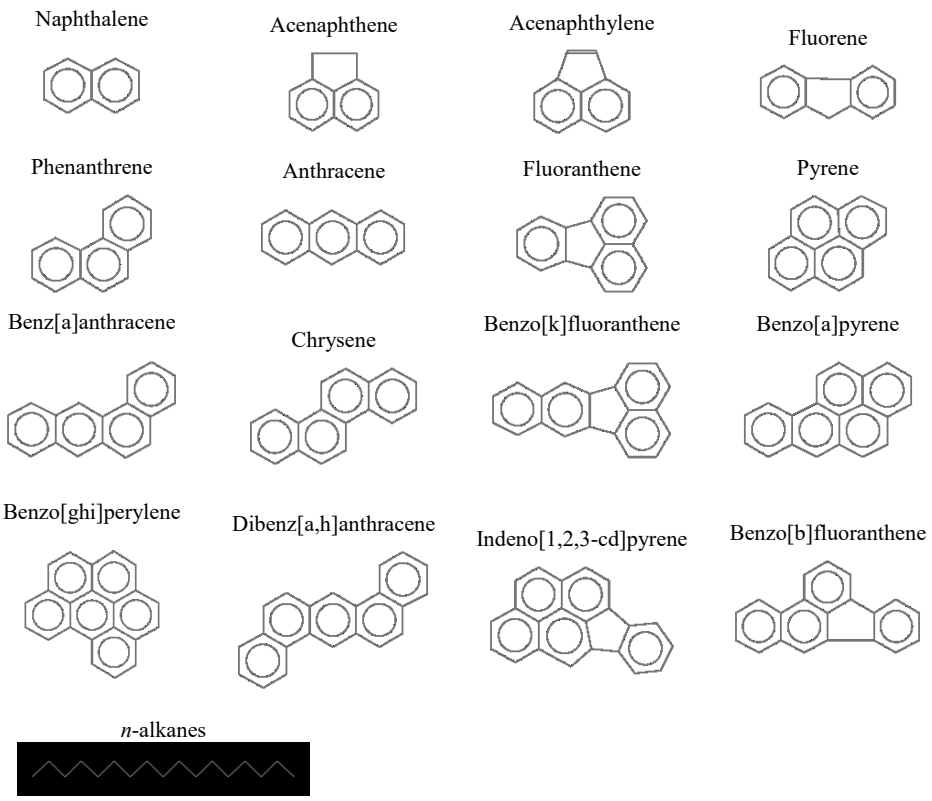


Figure 4. Chemical structures of PAH and n-alkanes.

Table 1. Physical properties of SVOCs in Figure 4.

| Target compound name | Functional group | Formula | Molecular weight | BP (°C) |
|---|---|---|---|---|
| Naphthalene | PAH | $C_{10}H_8$ | 128,17 | 217 |
| Acenaphthene | PAH | $C_{12}H_{10}$ | 154,21 | 279,2 |
| Acenaphthylene | PAH | $C_{12}H_8$ | 152,19 | 280,2 |
| Fluorene | PAH | $C_{13}H_{10}$ | 166,22 | 298,2 |
| Phenanthrene | PAH | $C_{14}H_{10}$ | 178,23 | 336,2 |
| Anthracene | PAH | $C_{14}H_{10}$ | 178,23 | 340,2 |
| Fluoranthene | PAH | $C_{16}H_{10}$ | 202,25 | 375 |
| Pyrene | PAH | $C_{16}H_{10}$ | 202,25 | 393 |
| Benz[a]anthracene | PAH | $C_{18}H_{12}$ | 228,29 | 437,8 |
| Chrysene | PAH | $C_{18}H_{12}$ | 228,29 | 448,2 |
| Benzo[k]fluoranthene | PAH | $C_{20}H_{12}$ | 252,31 | 480,2 |
| Benzo[a]pyrene | PAH | $C_{20}H_{12}$ | 252,31 | 495,2 |
| Benzo[ghi]perylene | PAH | $C_{22}H_{12}$ | 276,33 | 500 |
| Dibenz[a,h]anthracene | PAH | $C_{22}H_{14}$ | 278,35 | 524,2 |
| Indeno[1,2,3-cd]pyrene | PAH | $C_{22}H_{12}$ | 276,33 | 164 (Melting ℃) |
| Benzo[b]fluoranthene | PAH | $C_{20}H_{12}$ | 252,31 | 166 (Melting ℃) |

| Target compound name | Functional group | Formula | Molecular weight | BP (°C) |
|---|---|---|---|---|
| Tridecane | n-alkane | $C_{13}H_{28}$ | 184,36 | 234 |
| Tetradecane | n-alkane | $C_{14}H_{30}$ | 198,39 | 250 |
| Pentadecane | n-alkane | $C_{15}H_{32}$ | 212,41 | 267 |
| Hexadecane | n-alkane | $C_{16}H_{34}$ | 226,44 | 281 |
| Heptadecane | n-alkane | $C_{17}H_{36}$ | 240,47 | 302 |
| Heneicosane | n-alkane | $C_{21}H_{44}$ | 296,57 | 306 |
| Octadecane | n-alkane | $C_{18}H_{38}$ | 254,49 | 316,3 |
| Nonadecane | n-alkane | $C_{19}H_{40}$ | 268,52 | 330 |
| Eicosane | n-alkane | $C_{20}H_{42}$ | 282,55 | 343,2 |
| Docosane | n-alkane | $C_{22}H_{46}$ | 310,6 | 368,8 |
| Tricosane | n-alkane | $C_{23}H_{48}$ | 324,63 | 380,2 |
| Tetracosane | n-alkane | $C_{24}H_{50}$ | 338,65 | 391 |
| Pentacosane | n-alkane | $C_{25}H_{52}$ | 352,68 | 402,1 |
| Hexacosane | n-alkane | $C_{26}H_{54}$ | 366,71 | 412 |
| Heptacosane | n-alkane | $C_{27}H_{56}$ | 380,73 | 422 |
| Octacosane | n-alkane | $C_{28}H_{58}$ | 394,76 | 431,8 |
| Nonacosane | n-alkane | $C_{29}H_{60}$ | 408,79 | 441 |
| Triacontane | n-alkane | $C_{30}H_{62}$ | 422,81 | 450 |
| Hentriacontane | n-alkane | $C_{31}H_{64}$ | 436,84 | 458 |
| Dotriacontane | n-alkane | $C_{32}H_{66}$ | 450,87 | 467,2 |
| Tritriacontane | n-alkane | $C_{33}H_{68}$ | 464,89 | 474 |
| Tetratriacontane | n-alkane | $C_{34}H_{70}$ | 478,92 | 483 |
| Pentatriacontane | n-alkane | $C_{35}H_{72}$ | 492,95 | 490,2 |
| Hexatriacontane | n-alkane | $C_{36}H_{74}$ | 506,97 | 497 |
| Nonatriacontane | n-alkane | $C_{39}H_{80}$ | 549,05 | 517,5 |
| Heptatriacontane | n-alkane | $C_{37}H_{76}$ | 521,00 | 77 (Melting ℃) |
| Octatriacontane | n-alkane | $C_{38}H_{78}$ | 535,03 | 79 (Melting ℃) |
| Nonatriacontane | n-alkane | $C_{39}H_{80}$ | 549,05 | 517,5 |

### 4.4.2. Thermal desorption system

The Markes Unity-xr thermal desorption unit (TDU) is connected to an Agilent 7890B gas chromatograph and an Agilent 5877E mass spectrometer (TD-GC-MS, Fig. 5) through a deactivated silica column. The GC-MS contains an Agilent DB5ms column with the following dimensions: 30m×0.25μm×0.25mm. The sample is inserted into a glass tube that is inserted in the tube oven section of the TDU. The TD-GC-MS process is as follows: (1) the tube oven heats at chosen temperature and time, (2) the volatile compounds are collected into a carbon trap at a chosen temperature, and (3) the compounds of interest are desorbed from the carbon trap at given temperature and time and transported to the GC-MS for speciation and quantification.

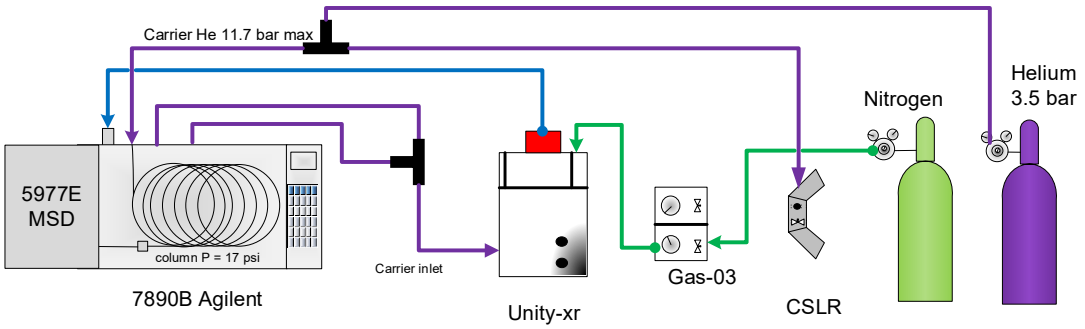


Figure 5. TD-GC-MS system.

In order to determine the best method conditions that provide the maximum recoveries of SVOCs, various parameters in the TDU and GC-MS were varied as follows: tube desorption temperature, tube desorption time, trap desorption temperature, trap desorption time, trap sorption temperature, trap flow rate, and GC program at 17psi and 23 psi, and at 23 psi with GC temperature ramps. The effects of each parameter on the recoveries of SVOCs are explained below. Additional VOCs were initially considered in the method development section as explained in our first and second progress reports and in our paper by Gok et al (2017), however, they were not considered in the final method development due to their high volatilities they are not present in the particle phase.

*Tube desorption temperature*

Figure 6 shows the instrument response of 10 ng of PAH and n-alkanes with various tube desorption temperatures of 330℃ (blue bars), 340℃ (red bars), and 350℃ (green bars) compared to 320℃ that had been chosen in the previous method. Average improvement in recoveries of PAH and n-alkanes were 11.4% and 14% when 350°C were used compared to 330°C. Small differences of 0.5% and -2% can be observed between 340 and 350℃. In order to preserve the materials in the sample area, we chose 340°C.

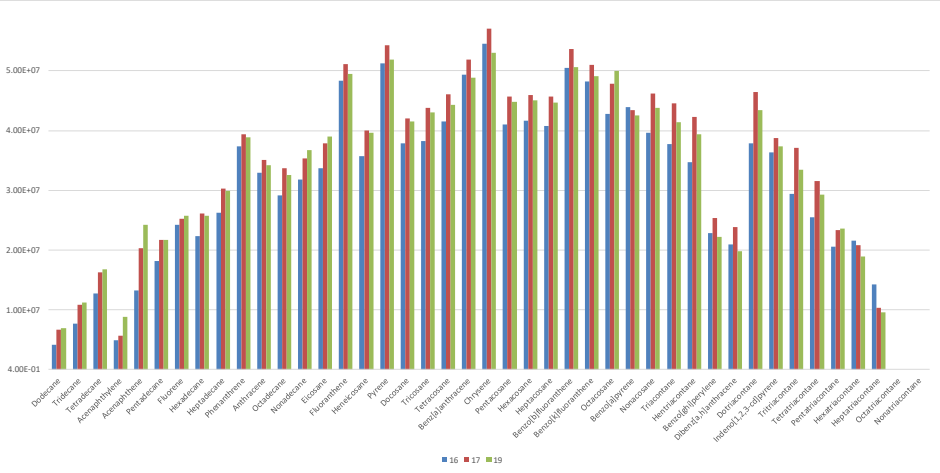


Figure 6. Effect of tube desorption temperature at 330°C (SVOC16), 340°C (SVOC17), and 350°C (SVOC19) for 10 min. Trap is 350°C for 10 min.

*Tube desorption time*

Various tube desorption times between 5 and 10 minutes were investigated. Figure 7 shows the instrument response for 10 ng of PAH and n-alkanes at 340°C for 5 min (blue columns), 7 min (red columns), and 10 min (green columns). The objective was to make the method a little slower, however, there is an improvement in recoveries when the sample is extracted for 10 min compared to 5 min and 7 min, particularly for n-alkanes. The average improvement in recoveries of PAH and *n*-alkanes was 4% and 17.4%, respectively. In our work we chose 10 min.

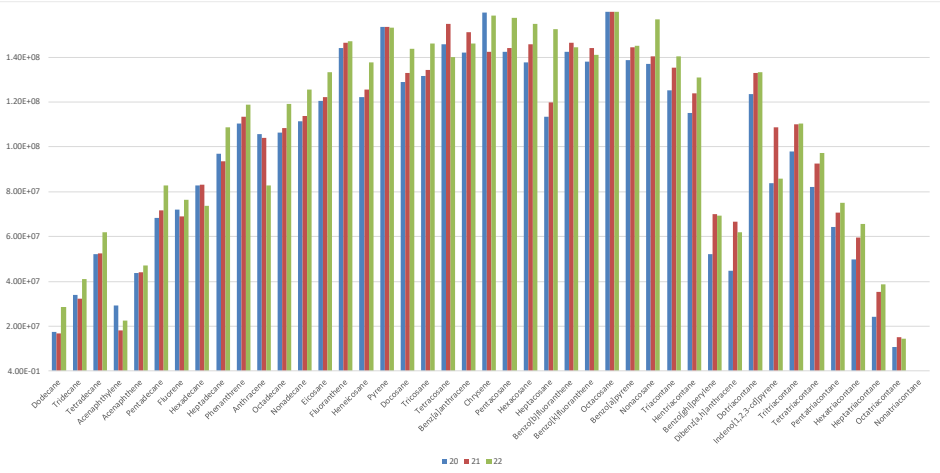


Figure 7. Effect of tube desorption time at 340°C for 5 (SVOC20), 7 (SVOC21), and 10 min (SVOC22). Trap is 350°C for 10 min.

*Trap desorption temperature*

Figure 8 shows the instrument response of 10 ng n-alkanes, and 10 ng PAH at general conditions of 23 psi and desorption temperatures of 330C *(blue column), 340C (red columns), and 350°C (green columns) for 5 min at sample desorption flow rates of 50 ml/min. As expected, recoveries increased with temperature. In our previous method, the maximum operating temperature of the carbon trap was 320°C and we chose 310°C during method development to preserve its lifetime. Average recoveries of PAH and n-alkanes increased 22% and 48% when 340°C was chosen compared to 330°C. No considerable improvement was observed between 350°C and 340°C. Therefore, in order to preserve the lifetime of the trap, 340°C was chosen.

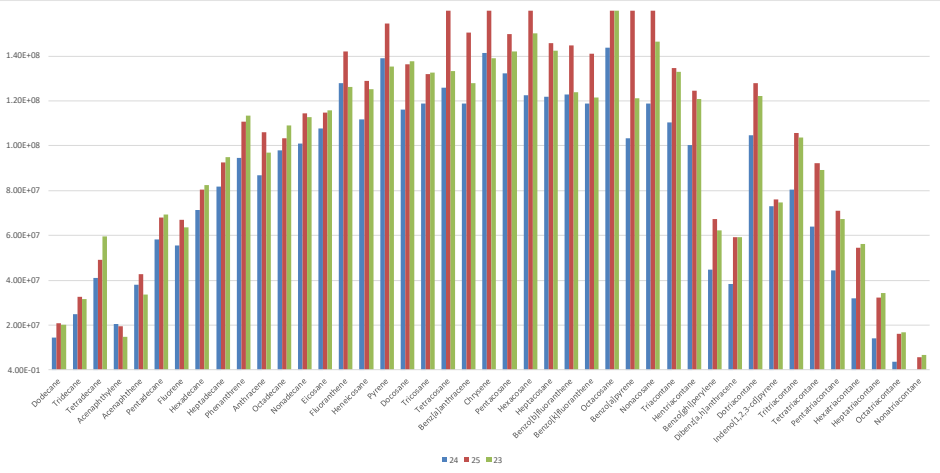


Figure 8. Effect of trap desorption temperature at 330°C (SVOC24), 340°C (SVOC25), and 350°C (SVOC 23) for 10 min. Tube is 340°C for 5 min

*Trap desorption time*

The effect of desorption time in extraction efficiencies was investigated at 3-10 min. Normally, desorption times of 3 minutes are recommended, however, this time depends on user applications. In our work, we focus on a wide range of organic compounds with various volatilities. We observed that desorption time influences the recoveries of the organic compounds. From dodecane to heptadecane, recoveries slightly decrease with desorption time, this may be due to breakthrough. For various organic compounds from fluoranthene to chrysene, 5 minutes provides the highest recovery. Finally, as expected, for dotriacontrane and compounds with greater molecular weight, 10 minutes provides the highest recoveries. In order to improve the recoveries of the compounds with highest molecular weight, 10 minutes was chosen.

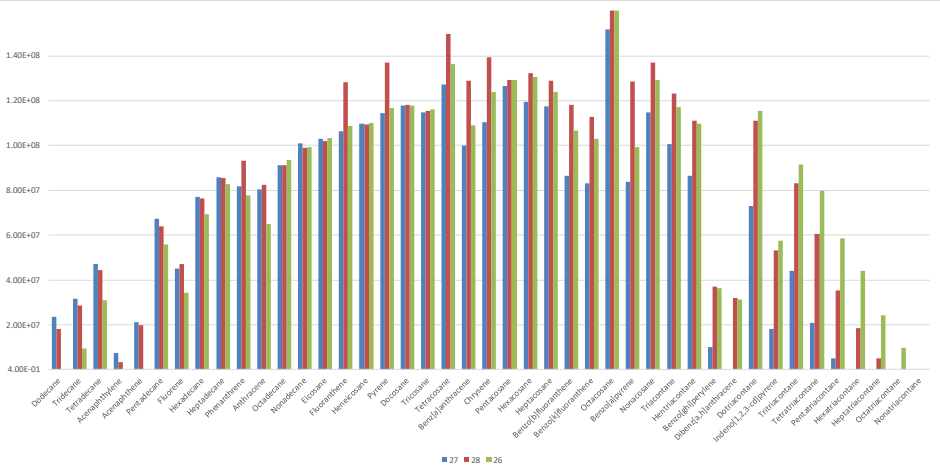


Figure 9. Effect of trap desorption time at 340°C for 3 min (SVOC27), 5 min (SVOC28), and 10 min (SVOC26).

*Trap sorption temperature*

The effect of trap sorption temperature was investigated at temperatures of -15°C (blue columns), 0°C (red columns), and 20°C (green columns). Trap sorption temperature also influences the recoveries of compounds due to their various volatilities. Better recoveries of ~7-15% were observed for *n*-alkanes $C_{12}$-$C_{23}$. On the other hand, better recoveries were observed at 0°C for compounds with molecular weight greater than $C_{24}$ n-alkane. Overall, average recoveries of PAH and n-alkanes were 11% and 6% better with 0°C compared to -15°C. Therefore, we chose 0°C.

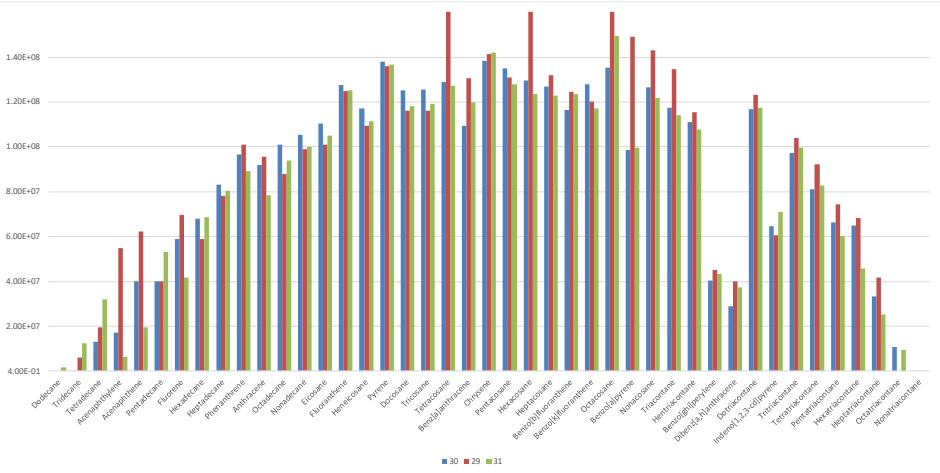


Figure 10. Effect of trap sorption temperature at -15°C (SVOC30), 0°C (SVOC29), and 20°C (SVOC31).

*Trap flow rate*

Trap flow rate determines the flow during sample desorption and the flow during sample sorption onto the trap. Therefore, there should be a balance between both flows. We evaluate three flow rates at 30, 50, and 70 ml/min. We observed that the intermediate flow of 50 ml/min provides the best recoveries of both PAH and n-alkanes. Average recoveries of PAH and n-alkanes improved 31% and 10% when 50 ml/min was used compared to 30 ml/min. On the other hand, average recoveries of PAH and n-alkanes improved 18% and 3% when 50 ml/min was used compared to 70 ml/min. For our application we chose 50 ml/min.

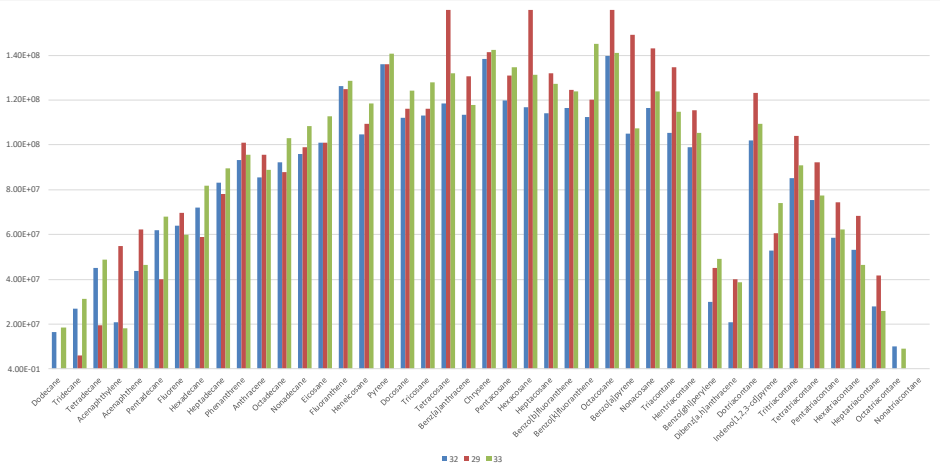


Figure 11. Effect of trap flow rate at 30 ml/min (SVOC32), 50 ml/min (SVOC29), and 70 ml/min (SVOC33).

*GC program*

Figure 12 shows the response of the instruments at various GC conditions of 17 psi (blue bars), 23 psi (red bars), and a GC program that includes two temperature ramps (green bars). Originally we determined that the best separation was obtained at a slow temperature rate of 5°C/min. However, the GC-MS analysis time was 68 minutes. In this work we tried to reduce the analysis time by adding two temperature ramps (i.e., 40°C for 7 minutes, increase to 115°C at 25°C/min, increase to 325°C at 5°C/min, then hold at 325°C for 5 min). The total analysis time with the temperature ramps decreased 13 min (55 min). In our previous report we mentioned pressure is one of the parameters that more clearly determines selectivity. As can be observed in Fig. 12, 17 psi gives better recoveries for compounds with molecular weight lower than tetracosane (blue bar). On the other hand, 23 psi gives better recoveries for compounds with molecular weight greater than tetracosane. In this work we chose 23 psi due to the lower volatility compounds present in the particle phase. The average recoveries of

PAH and n-alkanes decreased 4% and 14% when a GC program with temperature ramps were used. However, the total analysis time of four samples was reduced approximately one hour per working day which is necessary due to the tight operating hours in the laboratory.

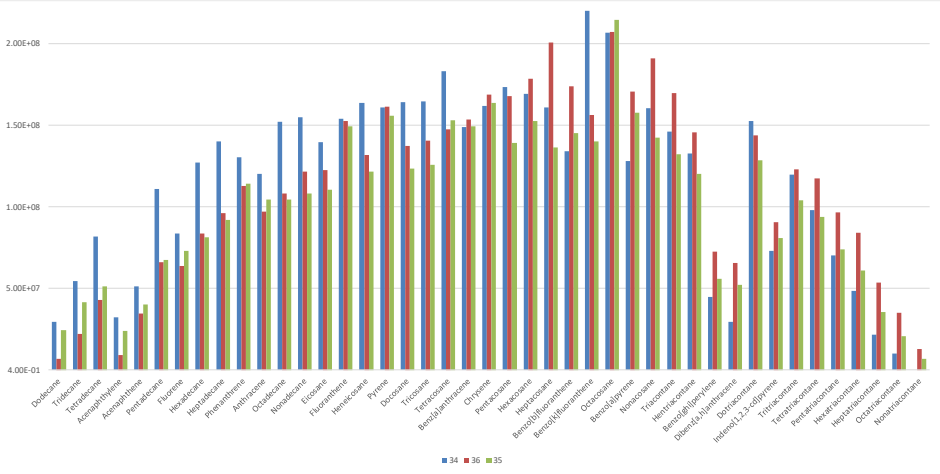


Figure 12. Effect of GC program at 17 psi (SVOC34), 23 psi (SVOC36), and 23 psi with ramps (SVOC35)

### 4.4.3. GC calibration curves and detection limits

Detection limits of PAH and *n*-alkanes were calculated according to the following equation (Flores et al., 2014):

$$LOD\ (ng\ m^{-3}) = \frac{3\times(\frac{SD}{m})}{V} \quad (3)$$

Where *LOD* is limit of detection, *SD* is the standard deviation of five replicate injections of the lowest mass in the calibration curve, *m* is the slope of the calibration curve obtained from regression analysis, and *V* is the average volume of air collected in all samples ($m^3$). The LOD are shown in Table 2 below. 137 $m^3$ were considered as the volume collected in 2 h samples. Calibration curves are shown in Appendix E.

Table 2. Quantitative data obtained from calibration curves

| Compound | LOD ($pg/m^3$) | $R^2$ | Std. error (%) |
|---|---|---|---|
| acenapthylene | 1.76 | 0.9996 | 5.06 |
| acenapthene | 2.29 | 0.9995 | 5.67 |
| fluorene | 1.41 | 0.9972 | 3.99 |
| phenanthrene | 0.95 | 0.9999 | 2.89 |
| anthracene | 0.93 | 0.9999 | 4.48 |
| fluoranthene | 0.77 | 1.000 | 3.90 |
| pyrene | 0.97 | 1.000 | 3.49 |
| benz(a)anthracene | 0.84 | 0.9993 | 4.03 |
| chrysene | 0.69 | 0.9993 | 5.11 |
| benzo(b)fluoranthene | 0.81 | 0.9982 | 3.47 |
| benzo(k)fluoranthene | 0.77 | 0.9975 | 5.06 |
| benzo(a)pyrene | 0.85 | 0.9957 | 4.79 |
| benzo(ghi)perylene | 0.56 | 0.9846 | 8.47 |
| indeno(1,2,3-cd)pyrene | 0.72 | 0.9805 | 8.72 |
| dibenz(a,h)anthracene | 0.79 | 0.9881 | 7.52 |
| dodecane | 5.18 | 0.996 | 10.83 |
| tridecane | 3.17 | 0.9973 | 5.92 |
| tetradecane | 3.01 | 0.9942 | 4.17 |
| pentadecane | 2.02 | 0.9947 | 3.52 |
| hexadecane | 1.71 | 0.9933 | 3.48 |
| heptadecane | 1.11 | 0.998 | 3.43 |
| octadecane | 1.89 | 0.9983 | 2.41 |
| nonadecane | 1.2 | 0.9986 | 3.16 |
| eicosane | 2.0 | 0.9989 | 1.73 |
| heneicosane | 1.17 | 0.9991 | 3.08 |
| docosane | 1.13 | 0.9991 | 2.99 |
| tricosane | 1.12 | 0.9993 | 3.19 |
| tetracosane | 1.28 | 0.9995 | 4.07 |
| pentacosane | 1.27 | 0.9997 | 3.39 |
| hexacosane | 1.14 | 0.9998 | 3.32 |
| heptacosane | 1.03 | 0.9998 | 3.41 |
| octacosane | 1.91 | 0.9992 | 5.38 |
| nonacosane | 1.18 | 0.9997 | 3.91 |
| triacontane | 0.88 | 0.9993 | 3.86 |
| hentriacontane | 0.74 | 0.999 | 3.85 |
| dotriacontane | 0.7 | 0.995 | 4.08 |
| titriacontane | 0.56 | 0.9966 | 4.22 |
| tetratriacontane | 0.54 | 0.9931 | 3.51 |
| pentatriacontane | 0.41 | 0.9866 | 4.19 |
| hexatriacontane | 0.5 | 0.9776 | 4.52 |
| heptatriacontane | 0.66 | 0.9646 | 6.28 |
| octatriacontane | 0.43 | 0.9427 | 11.26 |
| nonatriacontane | 1.33 | 0.9076 | 15.42 |

### 4.4.4. Preliminary analysis of ambient air samples

Figures 13 and 14 show the chromatograms of ambient aerosol samples collected for 1h (1 m3) and 2h (2 m3). The chromatogram in Figure 13 shows an usual high baseline due to two reasons (a) at time 1-23 min due to inconsistent carrier gas flow during trap desorption that was identified as inadequate carrier gas line connections during installation of TD system, and (b) after 23 min due to the presence of nitrogen and oxygen levels due to MS method. Overall, the 1h sample (Figure 13) shows low levels of a few identified n-alkanes and PAH compared to a 2h sample (Figure 14). For this reason, it was decided that collection of 1h sample was not enough for quantification of SVOCs in the aerosol phase, especially during periods of high radiation such as middle of the day and summer time.

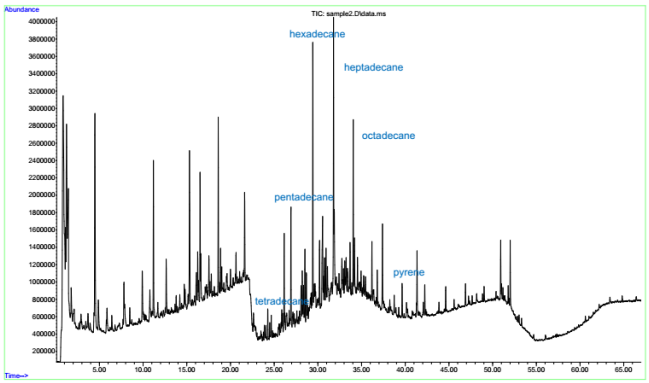


Figure 13. TD-GC-MS analysis of a 1h ambient air sample.

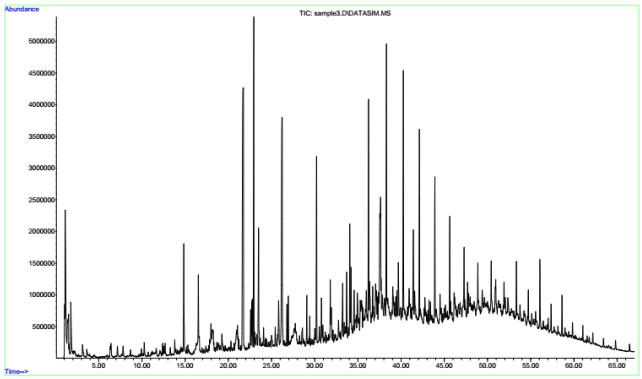


Figure 14 Selected ion chromatogram of TD-GC-MS analysis of a 2h ambient air sample

### 4.5 Cluster analysis

The clustering algorithm of the PC-based version of HYSPLIT v4 was used to create mean cluster trajectories during the day and during the night in separate runs. The number of cluster means is determined according to the value that is able to resolve the highest amount of variance of the data. In this work, 75% is chosen in order to limit the complexity of the resultant clusters. Concentrations of SVOCs were organized according to the resultant cluster means into box plots and histograms in order to determine the air mass trajectories associated to high and low concentrations.

### 4.6 Multiple regression analysis

Multiple regression analysis was performed to understand the individual influence and cumulative influence to the total and individual concentrations of PAH, n-alkanes, and all SVOCs according to the equation below:

$$y = m_1 x_1 + m_2 x_2 + \ldots m_n x_n + b \quad (4)$$

Where *y* is the total concentration of PAH, *n*-alkanes, and SVOCs, *x* are the meteorological variables and traffic, and *m* are the slopes that correspond to each variable. Regression analysis was done according to PAH and n-alkanes, during the day and night.

In polynomial regression, for N number of data points, the maximum number of independent variables that can be used to minimize the variance of the dependent variable is N-1. However, meaningful analysis requires to use a number of independent variables lower than N-1. For this reason, due to the limited dataset at night (n=7), multiple regression analysis done with 3 variables.

# 5. RESULTS AND DISCUSSION

## 5.1 Meteorological data

Figures 13-18 show temperature, wind speed, solar radiation, dew point, pressure, traffic, humidity, precipitation rate, and $PM_{2.5}$ concentrations observed during each 2-hour sample on Week 1: January 28 - 4 February 2017; Week 2: February 17 - February 23 2017; Week 3: May 3 – May 9 2017; Week 4: July 6 – July 12 2017; Week 5: October 20-26 2017; and Week 6: January 5-11 2018, respectively. Statistical analysis that shows the influence on these parameters on SVOC concentrations can be found in section 4.10. The axes of Figures 13-18 have been fixed to be comparable among weeks. A version of these figures with flexible axes that allow observation of oscillations week to week can be found in Appendix F. Due to technical issues with the count sensor, traffic data was not available in spring (Fig. 17k) and summer (Fig. 18k). Additionally, precipitation was not observed during sampling days in winter 1 (Fig. 15i), summer (Fig. 18i), and winter 3 (Fig. 20i).

Temperature gradually increased according to seasonal variations during this sampling campaign from winter week 1 to summer week 4 and decreased from fall week 5 to winter week 6. Significant variations can be observed between sampling weeks 1 (-2-14°C) and 2 (0-16°C) in 2017 and winter week 3 (6-14°C) in 2018. The lowest temperature can be observed in winter week 1 (~-2°C). Typical diurnal oscillations can be observed in spring (12-22°C), summer (20-32°C), fall (12-24°C). Dew point depends on temperature and relative humidity and could influence the condensation of SVOCs on $PM_{2.5}$. During this sampling campaign, dew point followed very similar trends as temperature and relative humidity with high positive correlations (e.g, $R^2 = 0.99$ for week 1). Relative humidity showed high diurnal variations and from week to week during this sampling campaign. No specific trend can be observed with large variations from 40 – 95%.

For this project, sampling days where chosen as weeks with high pressure system as was explained in section 1. High pressure systems are associated with light winds that hinder dispersion of pollutants. During these 6 sampling weeks, most of the days showed pressures higher than 1013 hPa. In addition, light winds below 6 m/s can be observed in most of the weeks, with exception of the first sampling day on summer week with wind speed of 9 m/s. The lowest wind speeds with nearly calm conditions were observed during winter week 6 which also showed the highest pressure.

Low pressure systems are associated to vertical motion and therefore precipitation. During this sampling campaign, low pressure was observed only during the second half of the spring and fall sampling weeks, which coincides with precipitation events. Total precipitation of 172, 212, and 74 mm was observed in winter week 2, spring, and fall. Rainfall events ranged as 1.5-25 mm/h (light-intense)

during winter, 1.5-60 mm/h (light-torrential) during the spring, and 1.5-9 mm/h (light-heavy) during the Fall.

Solar radiation increases reactivity of SVOCs during the day and therefore determines concentrations of SVOCs in the particle phase. Solar radiation follows a similar trend as temperature with diurnal and seasonal oscillations. As expected, the minimum values are observed during the winter with approximately 100 W/m$^2$. These values gradually increased from Winter to spring and reached maximum values of 850-950 W/m$^2$ during the summer. Radiation considerably decreased during the Fall and reached minimum values during winter week 3. Significant variations were observed during winter 2017 and winter 2018. Similar radiation was observed during sampling week 1 and 2, however radiation significantly decreased during winter week 3.

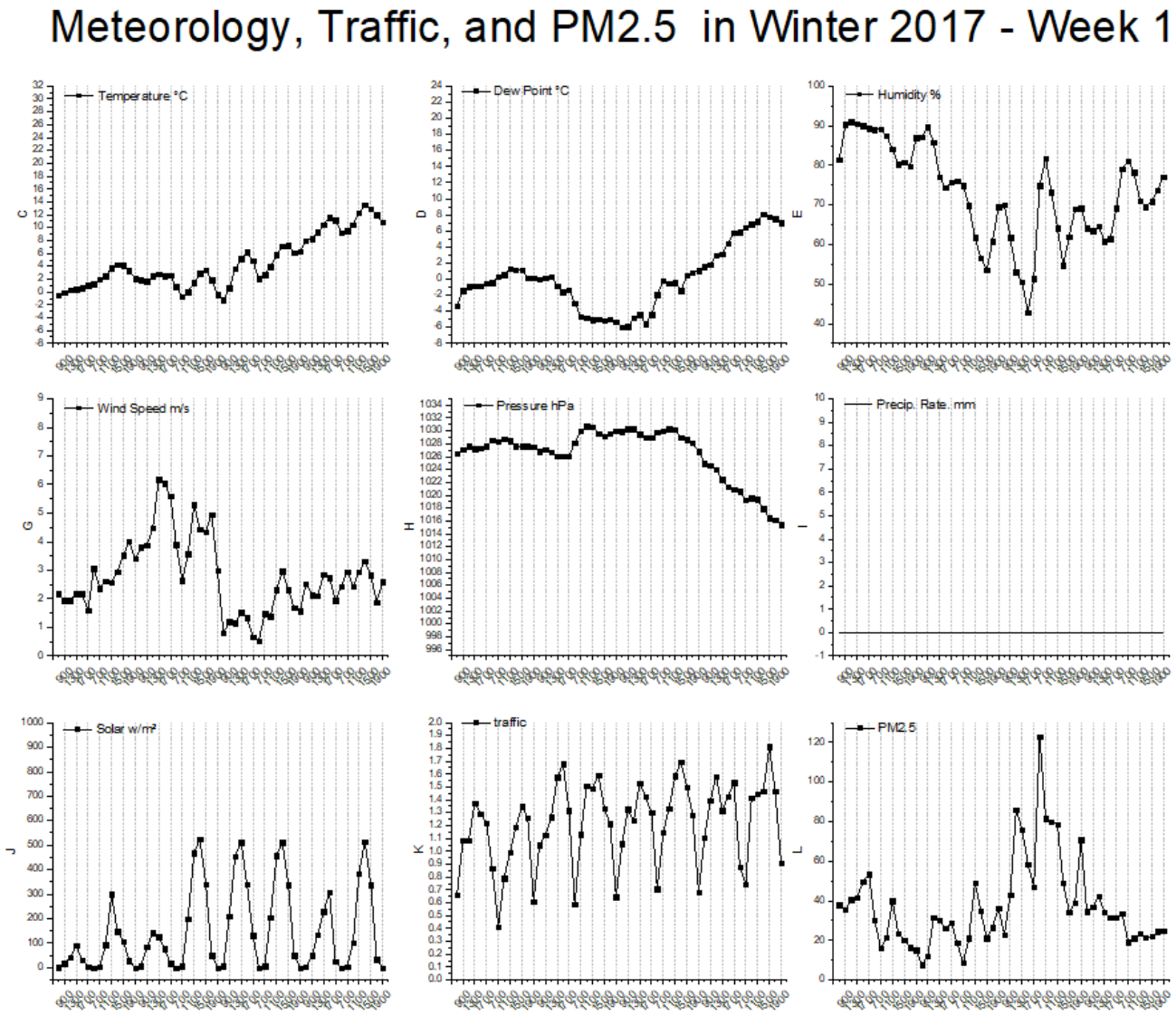


Figure 15. Meteorological conditions observed during sampling week 1

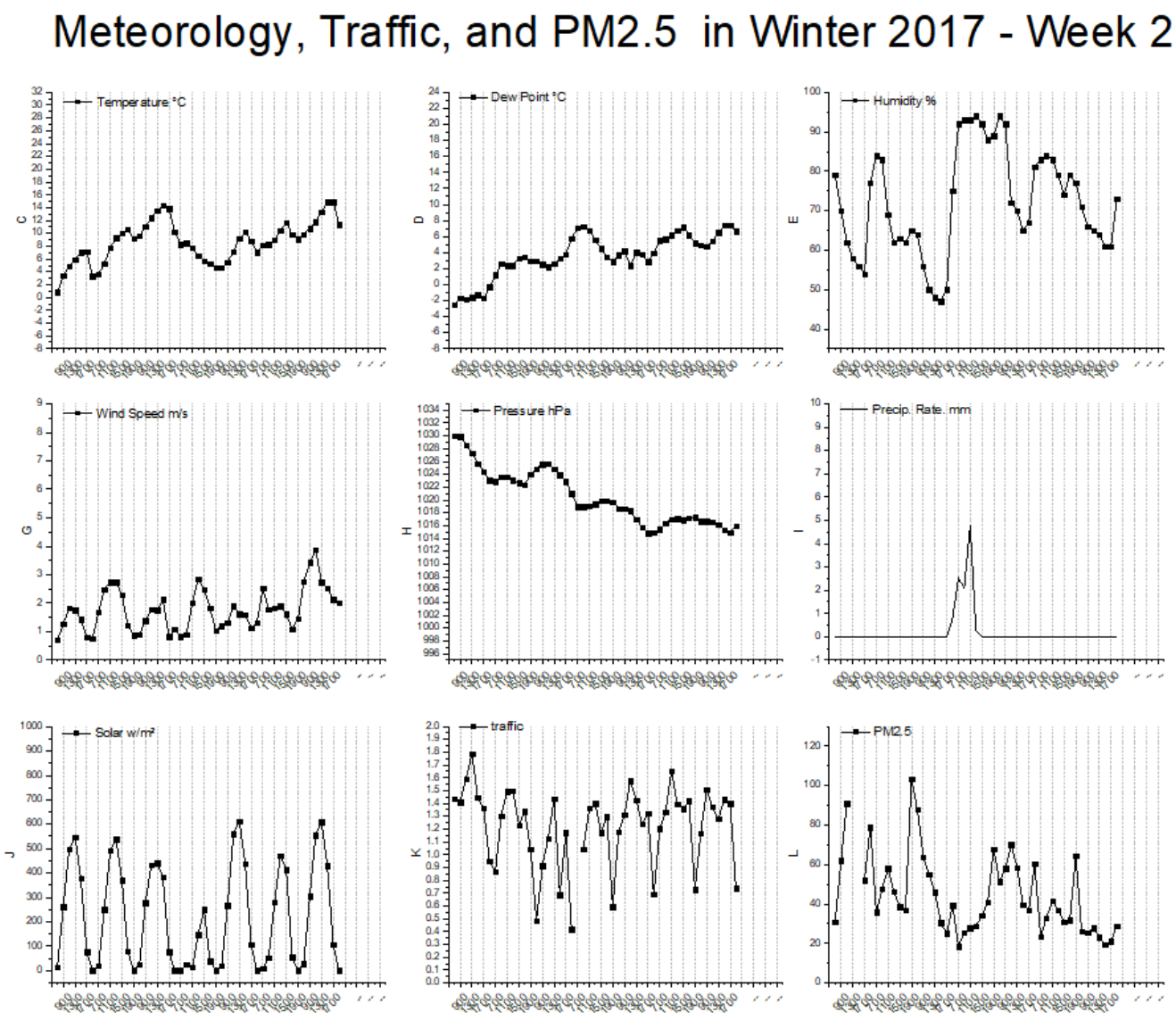


Figure 16. Meteorological conditions observed during sampling week 2

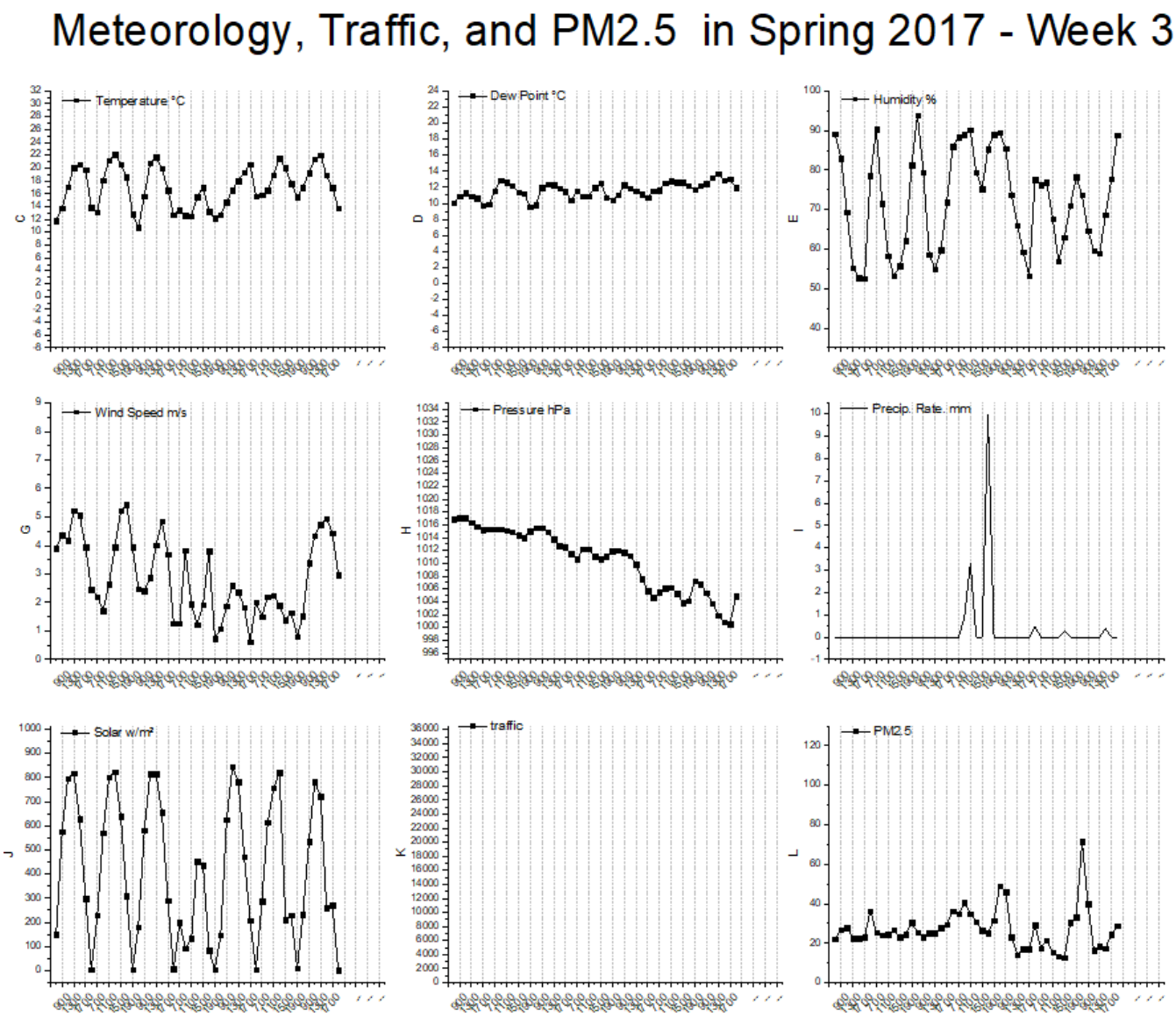


Figure 17. Meteorological conditions observed during sampling week 3

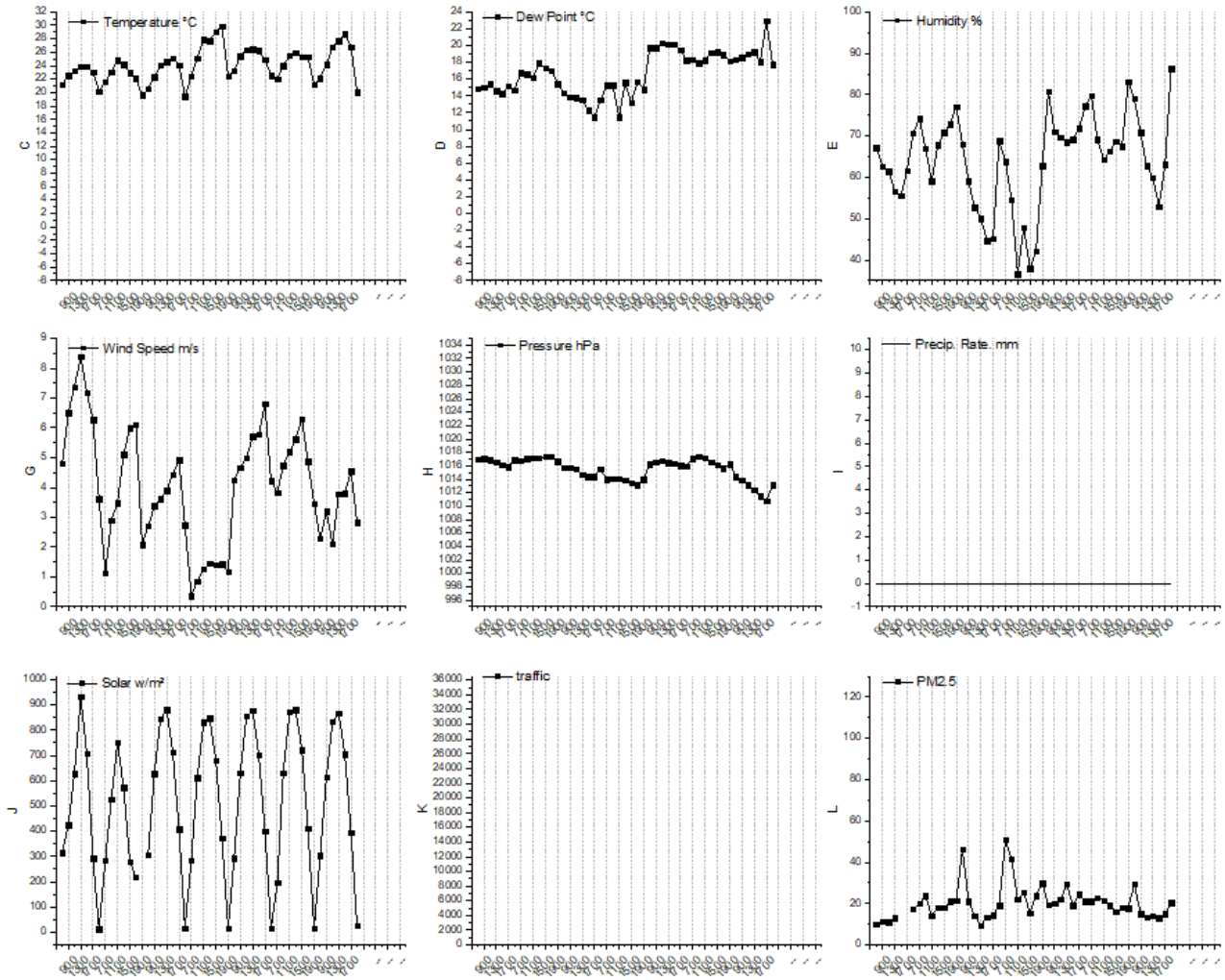


Figure 18. Meteorological conditions observed during sampling week 4

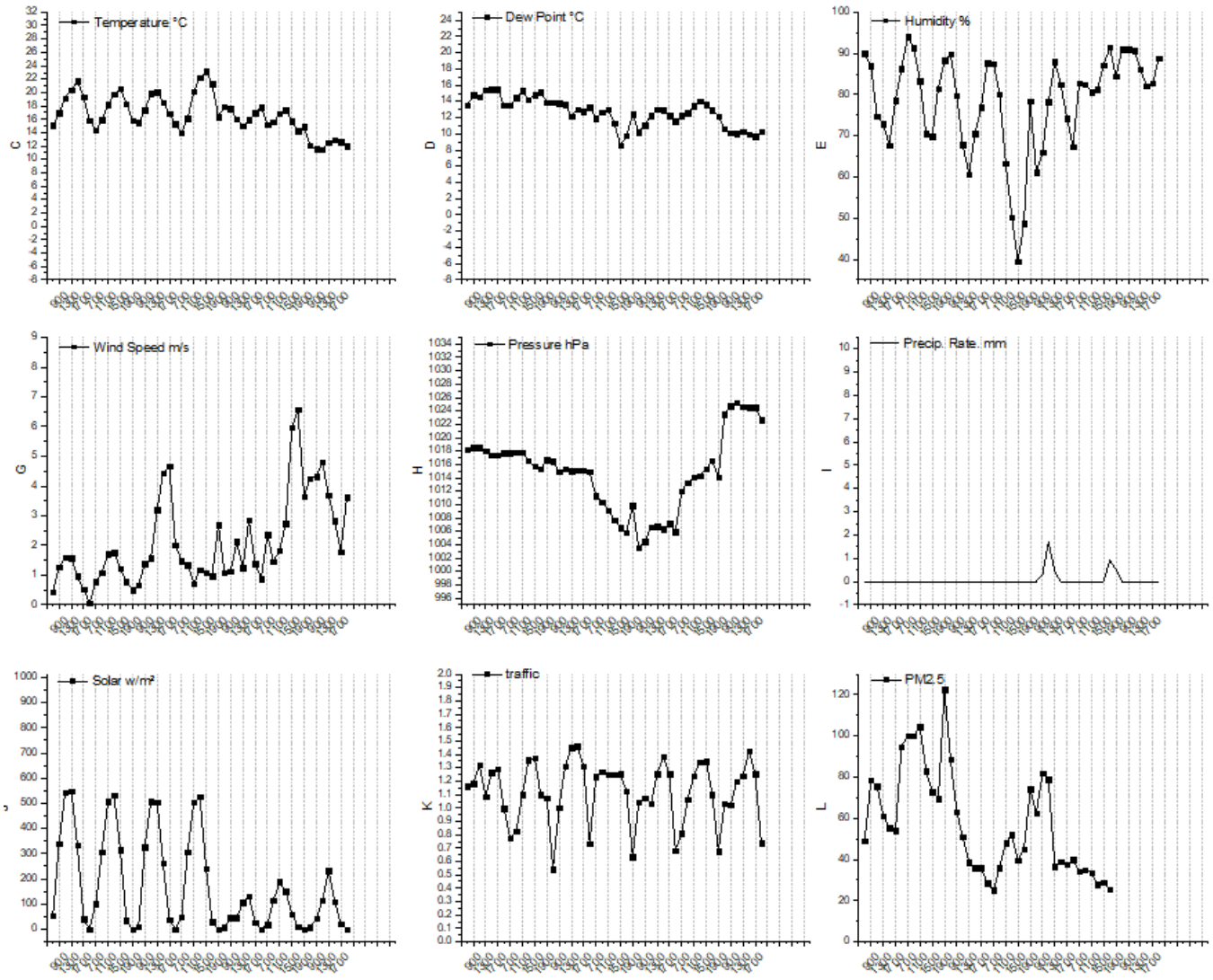


Figure 19. Meteorological conditions observed during sampling week 5

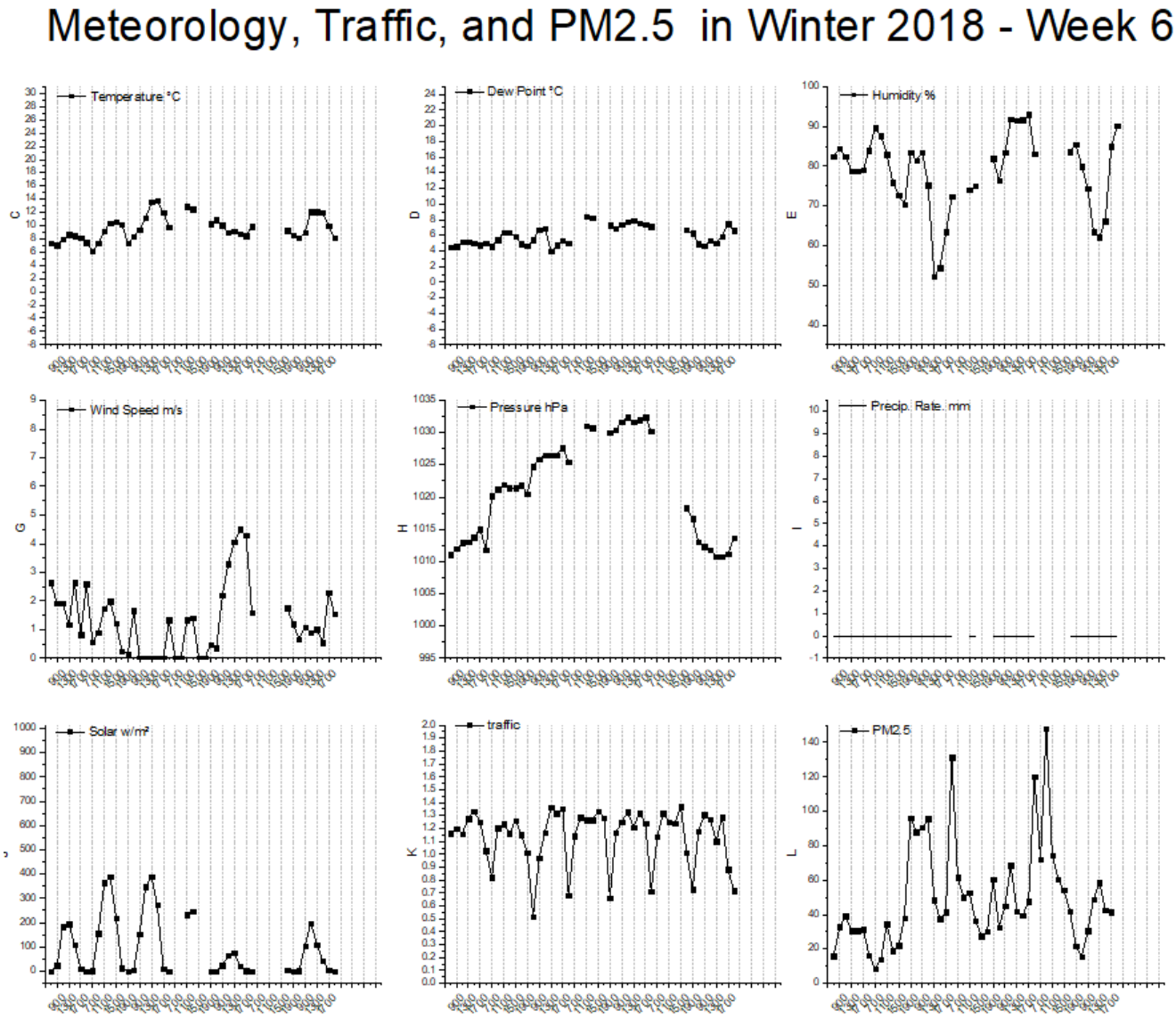


Figure 20. Meteorological conditions observed during sampling week 6.

Statistical analysis of meteorological and traffic data corresponding to each high-time resolved sample are shown in table 3. Ventilation coefficients ($m^2$ $s^{-1}$) indicate the potential of vertical and horizontal air pollutant dispersion in the boundary layer and were calculated as the product of PBLH and horizontal wind speed. Ventilation indices are derived from ventilation coefficients and organized into categories that represent pollution dispersion as follows: bad (0-2000 $m^2$ $s^{-1}$), fair (2001-4000 $m^2$ $s^{-1}$), good (4001-6000 $m^2$ $s^{-1}$), and excellent (6000 $m^2$ $s^{-1}$ or more) (Zakey et al., 2006).

During this sampling campaign, average daily temperature varied among seasons as follows winter 1: -1.2-13.5°C, winter 2: 0.8-14.9°C, spring: 10.8-22.2°C, summer: 19.5-29.9°C, fall 11.6-23.2°C, and winter 3: 6.1-13.8°C with averages of 4.6, 8.3, 15.6, 22.7, 16.2, and 9.4°C, respectively. Relative humidity decreased with temperature with lowest values at 15:00h. Very low relative humidity was observed in all seasons and particularly lowest values were observed during the summer (36.7%) and fall (39.5%). Similarly, very high relative humidity was observed in all seasons with maximum ranges of 86% (summer) to 93.8% (winter 2 and spring). Ventilation coefficients showed wide variations among seasons with highest average values during the summer (i.e., 2720$\pm$1700 $m^2$ $s^{-1}$) and lowest values during winter 3 (i.e., 419$\pm$370 $m^2$ $s^{-1}$) and winter 2 (447$\pm$191 $m^2$ $s^{-1}$). Average ventilation coefficients during all sampling days in the winter were 855$\pm$1012 $m^2$ $s^{-1}$, mainly due to higher ventilation coefficients observed in winter 1 (i.e., 1700$\pm$1423 $m^2$ $s^{-1}$). Hourly ventilation coefficients were used as air pollution dispersion indicators during sampling days. The analysis showed poor air pollution dispersion in winter 2 and 3, spring, and fall with 100, 97.6, and 83.3% of the ventilation coefficients below 2000 $m^2$ $s^{-1}$. Good and excellent air pollution dispersion was observed only during the summer and winter 3, with 33.3 % and 16.6 % of the data above 4000 $m^2$ $s^{-1}$, respectively. Fair air pollution dispersion was observed in summer=fall, and winter 1 with 16.7 and 14.3% of the ventilation coefficients between 2001 and 4000 $m^2$ $s^{-1}$. With exception of summer, sampling days in winter 3 showed better air pollution dispersion with 31% of the ventilation coefficients above 2001 $m^2$ $s^{-1}$

Table 3. Statistical analysis of meteorological variables and traffic with high-time resolved data

| Date | Temperature °C | Dew Point °C | Humidity % | Pressure hPa | Solar (day range) w/m² | wind speed (m/s) | Traffic | NOAA Boundary Layer (m) | ventilation coeff (m2/s) |
|---|---|---|---|---|---|---|---|---|---|
| Winter1 | -1.2 - 13.5 | -6.0 - 8.1 | 42.8 - 91.1 | 1015.4 - 1030.7 | 0.0 - 524.5 | 0.5 - 6.2 | 2353.0 - 30800.0 | 130.0 - 1230.0 | 204.1 - 7427.6 |
| | 4.6 ± 4.1 | 0.2 ± 4.0 | 75.0 ± 8.9 | 1026.2 ± 4.6 | 86.0 ± 48.3 | 2.7 ± 1.1 | 16156.8 ± 2312.3 | 377.1 ± 319.8 | 1700.6 ± 1423.6 |
| Winter2 | 0.8 - 14.9 | -2.5 - 7.4 | 47.2 - 93.8 | 1014.8 - 1030.0 | 0.0 - 611.5 | 0.7 - 3.9 | 0.0 - 35483.0 | 50.0 - 585.0 | 53.9 - 1608.0 |
| | 8.7 ± 3.3 | 3.7 ± 2.4 | 74.0 ± 9.1 | 1020.0 ± 3.9 | 130.6 ± 45.1 | 1.5 ± 0.5 | 16136.0 ± 3998.6 | 216.7 ± 104.0 | 447.6 ± 191.0 |
| Spring | 10.8 - 22.2 | 9.6 - 13.7 | 52.6 - 93.9 | 1000.5 - 1017.1 | 3.0 - 843.6 | 0.6 - 5.4 | * | 110.0 - 840.0 | 153.4 - 4257.1 |
| | 15.6 ± 1.3 | 11.3 ± 0.8 | 76.6 ± 5.0 | 1010.4 ± 4.6 | 243.3 ± 57.4 | 2.5 ± 1.0 | * | 228.6 ± 114.3 | 759.1 ± 238.4 |
| Summer | 19.5 - 29.9 | 11.5 - 22.9 | 36.7 - 86.3 | 1010.8 - 1017.4 | 11.6 - 932.5 | 0.4 - 8.4 | * | 5.0 - 1245.0 | 4.3 - 9643.9 |
| | 22.7 ± 1.3 | 16.4 ± 2.3 | 68.7 ± 8.3 | 1015.5 ± 1.5 | 299.5 ± 38.3 | 3.6 ± 1.4 | * | 557.7 ± 359.4 | 2720.4 ± 1700.8 |
| Fall | 11.6 - 23.2 | 8.6 - 15.5 | 39.5 - 94.0 | 1003.6 - 1025.2 | 0.0 - 548.0 | 0.1 - 6.6 | 3085.0 - 36503.0 | 55.0 - 750.0 | 5.8 - 3416.8 |
| | 16.2 ± 2.0 | 12.6 ± 1.5 | 80.3 ± 7.0 | 1014.6 ± 5.8 | 99.8 ± 56.8 | 2.0 ± 1.2 | 16773.7 ± 2855.4 | 264.4 ± 206.6 | 790.1 ± 856.3 |
| winter3 | 6.1 - 13.8 | 4.0 - 8.4 | 52.3 - 93.0 | 1010.7 - 1032.4 | 0.0 - 389.9 | 0.0 - 4.5 | 2935.0 - 34950.0 | 60.0 - 670.0 | 11.2 - 1927.8 |
| | 9.4 ± 1.3 | 6.1 ± 1.1 | 80.5 ± 5.1 | 1021.5 ± 7.8 | 58.8 ± 45.3 | 1.2 ± 0.8 | 16838.1 ± 2671.9 | 204.6 ± 151.9 | 419.2 ± 370.3 |

*Traffic data was not available during spring and summer

Table 4. Percent of data during sampling days indicating air pollution dispersion categories

| | N | Poor (0-2000 $m^2$ $s^{-1}$) | fair (2001-4000 $m^2$ $s^{-1}$) | good (4001-6000 $m^2$ $s^{-1}$) | excellent (>6000 $m^2$ $s^{-1}$) |
|---|---|---|---|---|---|
| Winter1 | 42 | 69.0 | 14.3 | 9.5 | 7.1 |
| Winter2 | 42 | 100.0 | 0.0 | 0.0 | 0.0 |
| Spring | 42 | 97.6 | 0.0 | 2.4 | 0.0 |
| Summer | 42 | 50.0 | 16.7 | 14.3 | 19.0 |
| Fall | 42 | 83.3 | 16.7 | 0.0 | 0.0 |
| Winter3 | 25 | 100.0 | 0.0 | 0.0 | 0.0 |

Figures 21-26 show diurnal variation of meteorological parameters and traffic observed in our sampling campaign. After pollutants have been emitted to the atmosphere or transported from nearby locations, meteorological conditions are a very important factor that determines PM2.5 mass concentrations due to diffusion, dilution, and accumulation of pollutants. In addition, understanding daily distributions of SVOCs is a complex task due to dispersion, gas-particle partitioning, and reactivity. Solar radiation is the most important parameter that determines diurnal and seasonal temperature and pressure changes which ultimately determine relative humidity, dew point, wind speed, and boundary layer height. Regarding individual effects of meteorological parameters on pollutant concentrations, important positive correlations have been found between temperature and PM2.5 due to two reasons: increased

temperature promotes the formation of PM2.5 from combustion sources and secondary particles due to photochemical reactions.

Relative humidity is an important factor that determines particle mass in terms of particle growth. Both positive and negative correlations can exist due to two simultaneous processes in which particles absorb water first, then they grow in size, followed by dry deposition and a decrease in PM2.5 number and mass concentrations. Wind speed and ventilation coefficients have been determined as a very important contributor to accumulation or dispersion of pollutants. It has been observed that wind speed lower than 2 m/s contributes to accumulation of pollutants (Xu et al 2018). On the other hand, wind speed higher than 3 m/s may either contribute to dispersion of pollutants (i.e., negative correlation) or transport of pollutants (positive correlation).

Precipitation is often considered as means for cleaning the atmosphere due to wet deposition. However, collection efficiency is determined by size of particle, water droplets, and amount of precipitation. For example, for a 1 μm particle, collection efficiency by water droplets is 20% and a high amount of water droplets in a rainfall is required to further decrease PM concentration by 60%. This process is further complicated by the fact that sizes of particles, water droplets, and amount of rain are variable. For this reason, low correlations between PM and rainfall are often found, however, negative correlation coefficients indicate some degree of correlation of a decrease in concentration with precipitation.

Wind direction is used as means to understand local and regional sources of pollutants which is particular for each sampling location and varies according to the type of station (i.e., urban, rural, traffic) and geography. HYSPLIT model is widely used as it provides air mass trajectory and height at high time resolution. For this reason, the influence of air pollutants by local and regional sources is also determined by loading, stability of the atmosphere, and terrain patterns during transport.

Due to the complex interaction of air pollutants with meteorological parameters and oxidant concentrations, low correlation coefficients are often found in the literature. It is understood that the total variance of the datasets is due to a combination of variables. For this reason, in our work, multiple regression analysis is performed on section 4.10 in which the total contribution of meteorology and

traffic are considered in an optimized model that considers variations per season rather than the use of a limited number of variables as is often used in the literature.

During our sampling campaign, diurnal variations of meteorological parameters and traffic follow similar trends throughout the various seasons (Fig. 21-26), with important differences in their magnitude that ultimately determine the PM2.5 concentrations and distribution of SVOCs in the particle and gas-phases by affecting dispersion, accumulation, and gas-particle partitioning. Variations of PM2.5 and SVOCs with meteorology and traffic are discussed in sections 5.6 and 5.8.

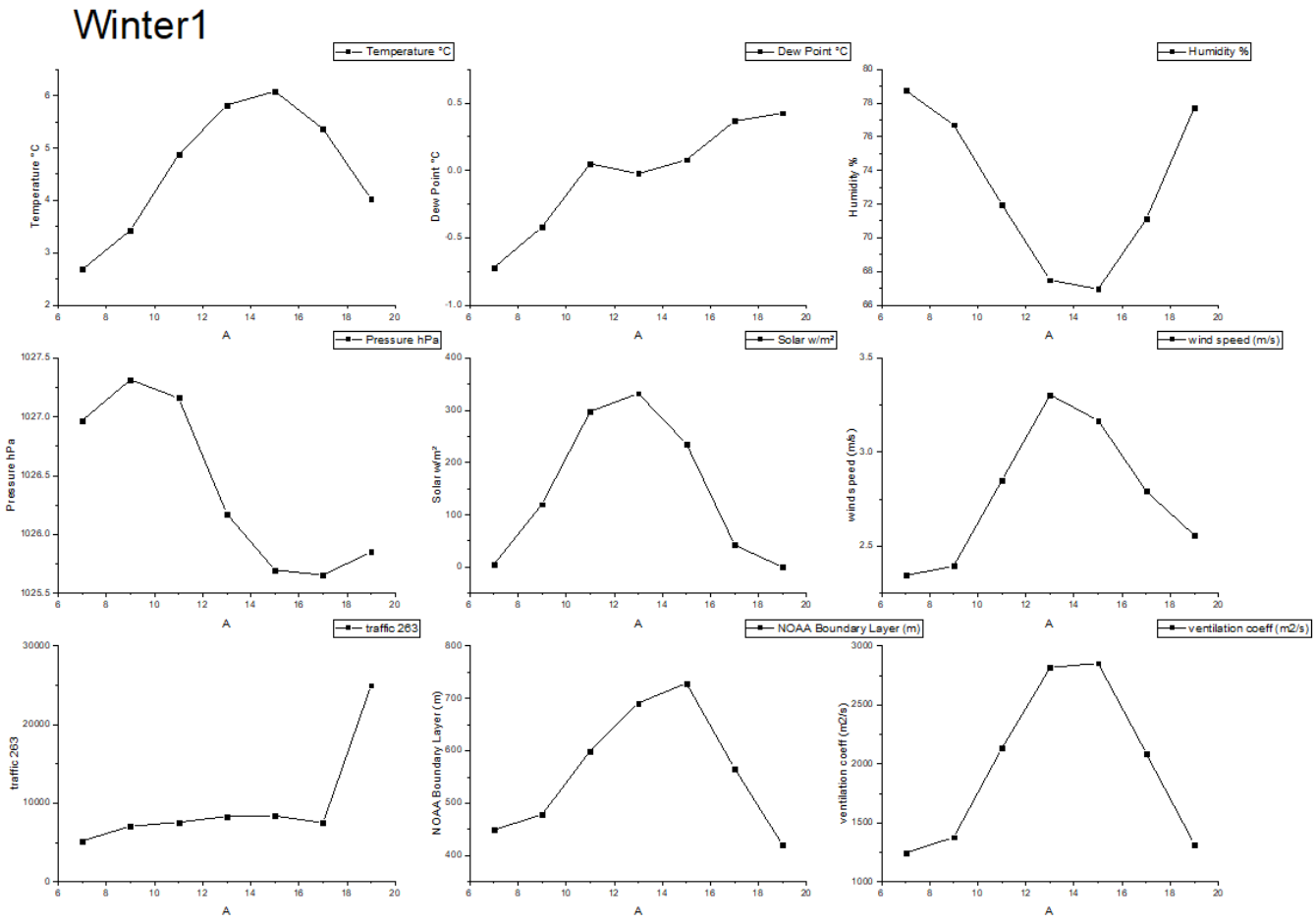


Figure 21. Diurnal variations of meteorological variables during sampling week 1

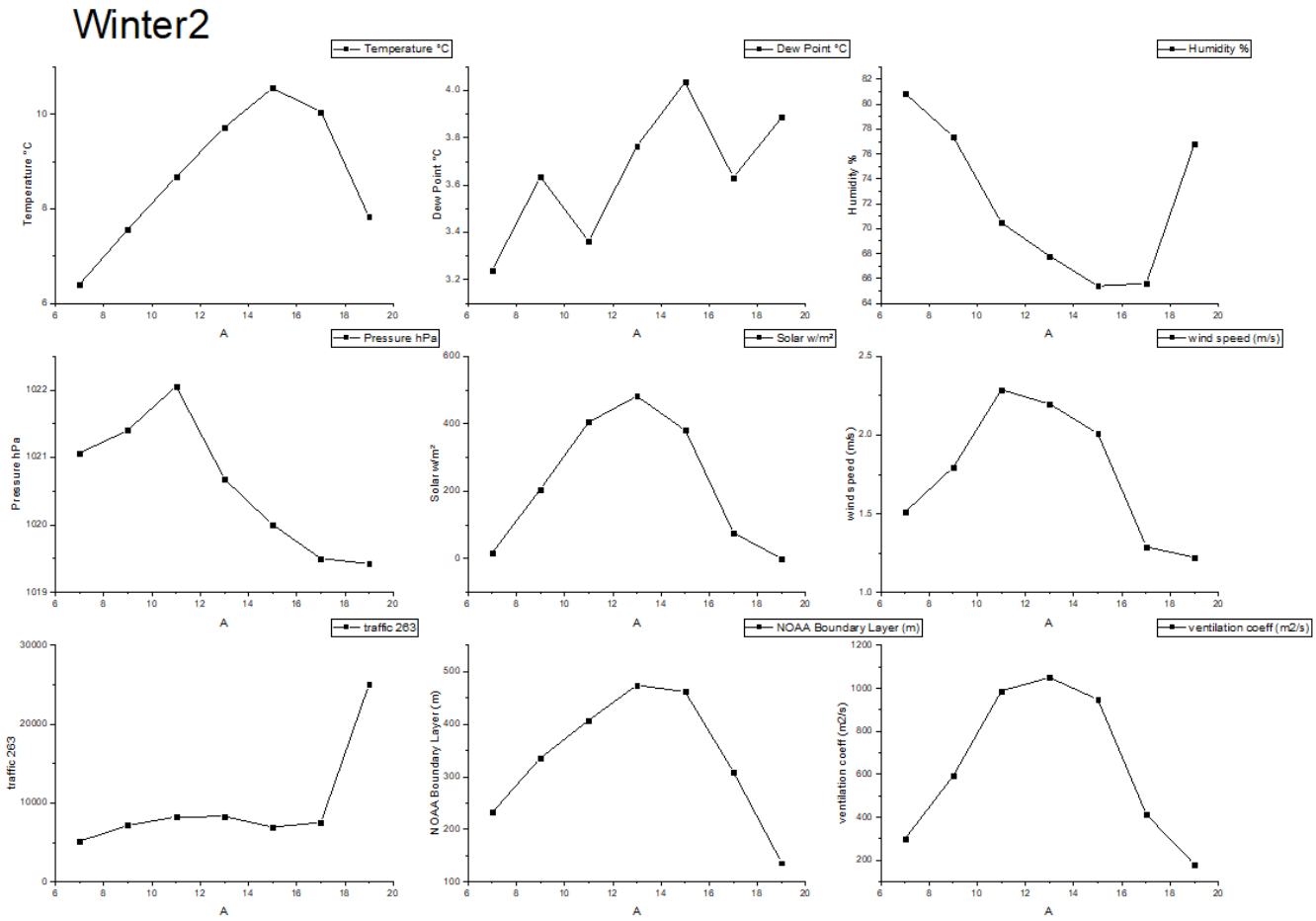


Figure 22. Diurnal variations of meteorological variables during sampling week 2

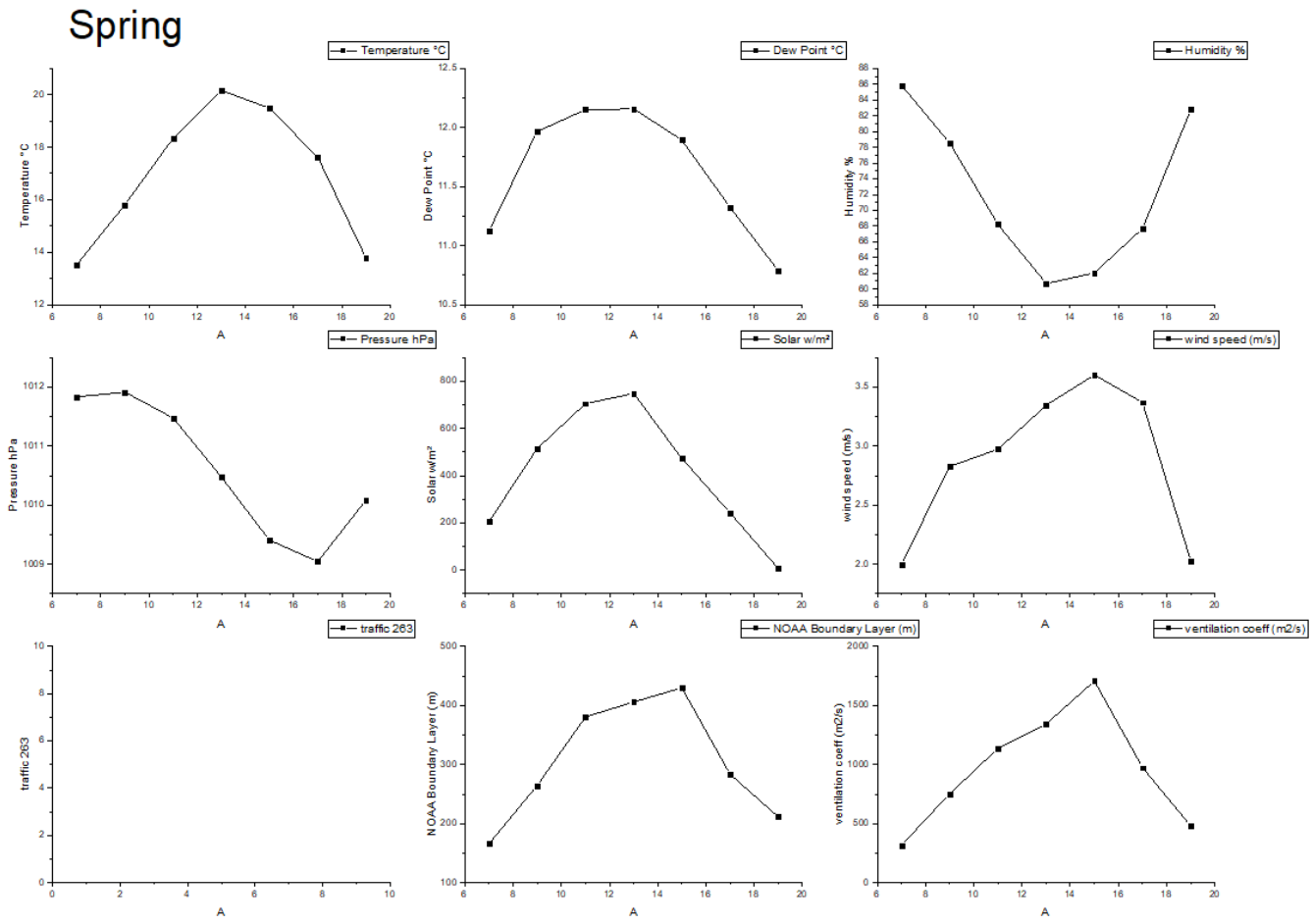


Figure 23. Diurnal variations of meteorological variables during sampling week 3

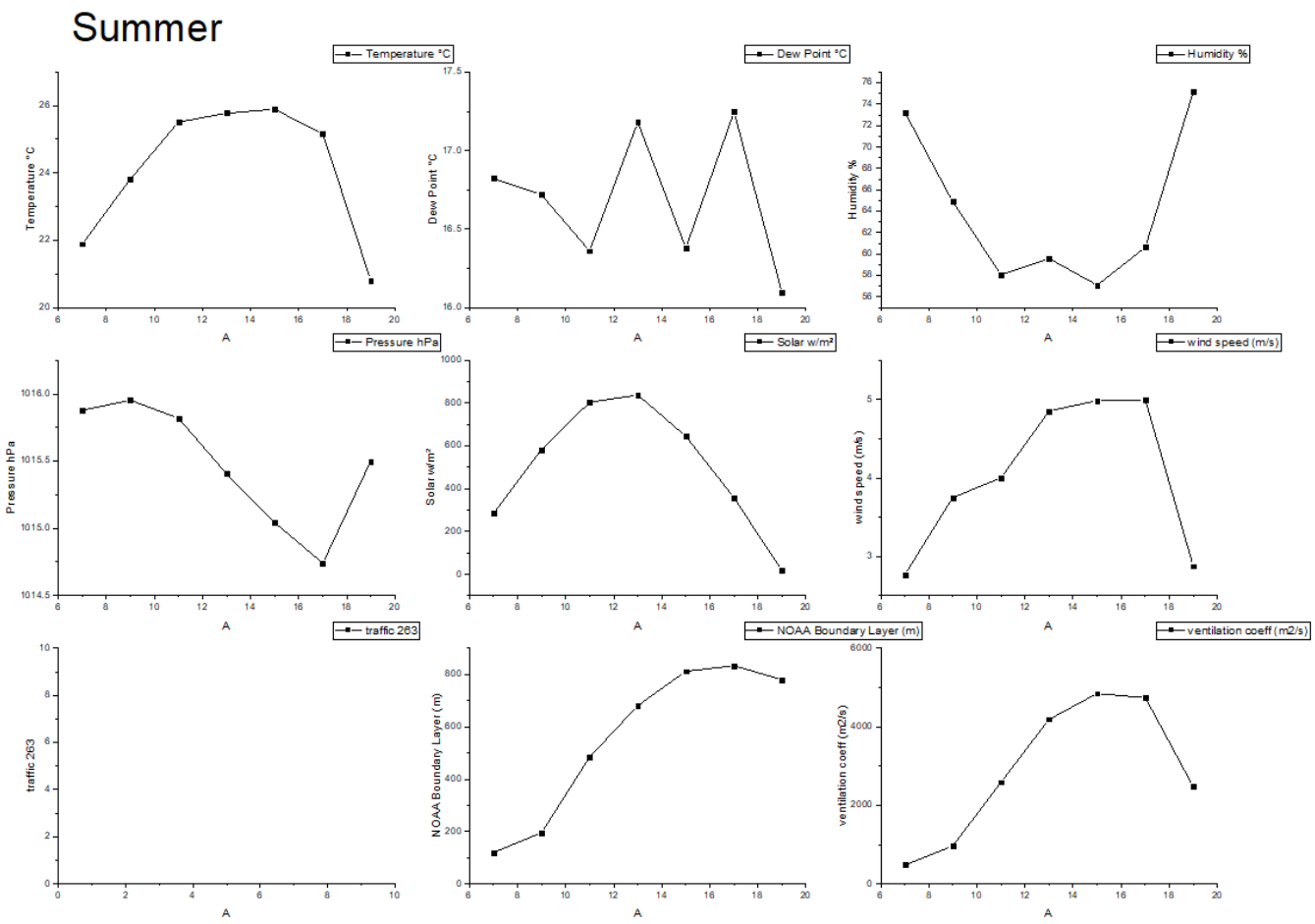


Figure 24. Diurnal variations of meteorological variables during sampling week 4

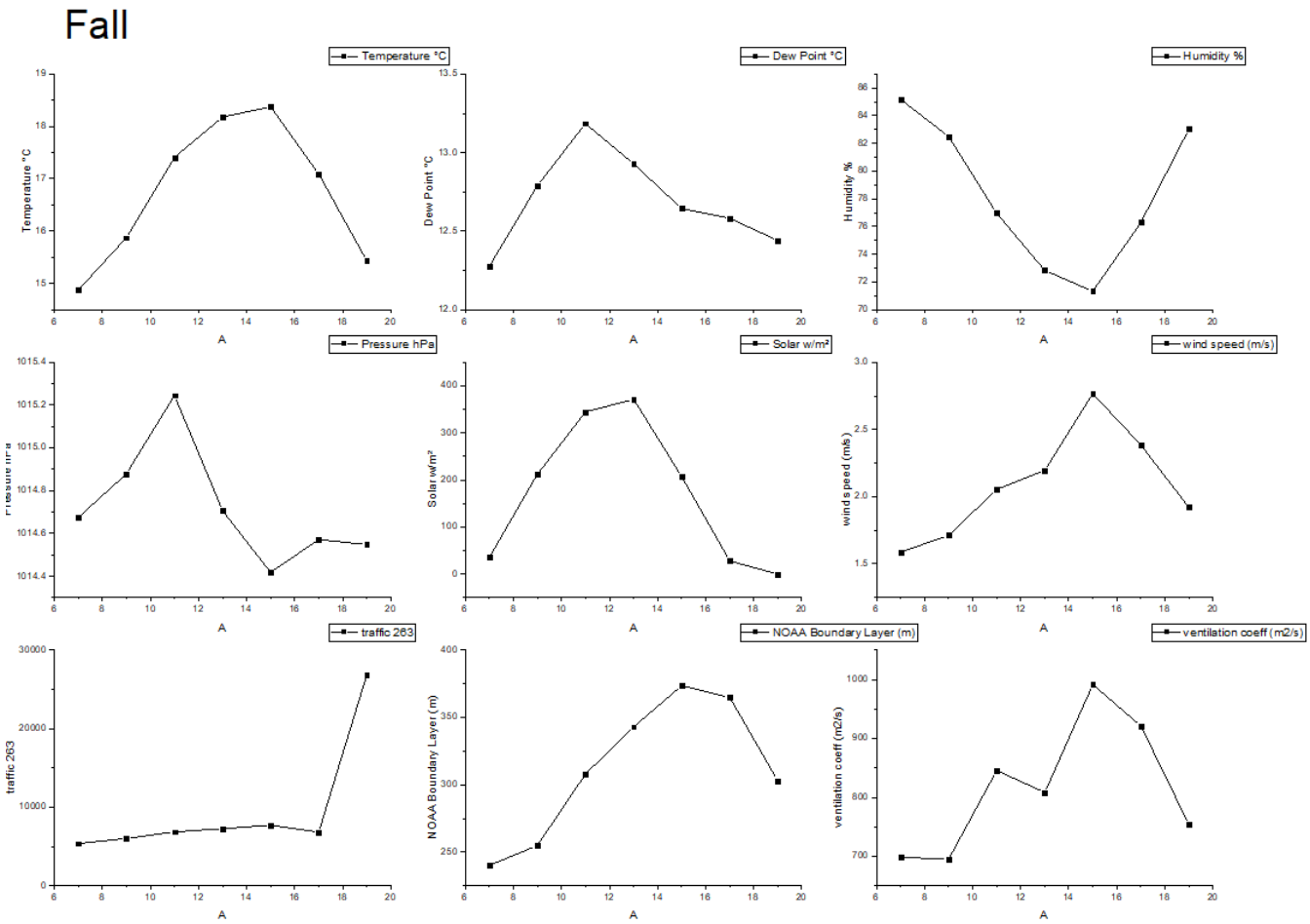


Figure 25. Diurnal variations of meteorological variables during sampling week 5

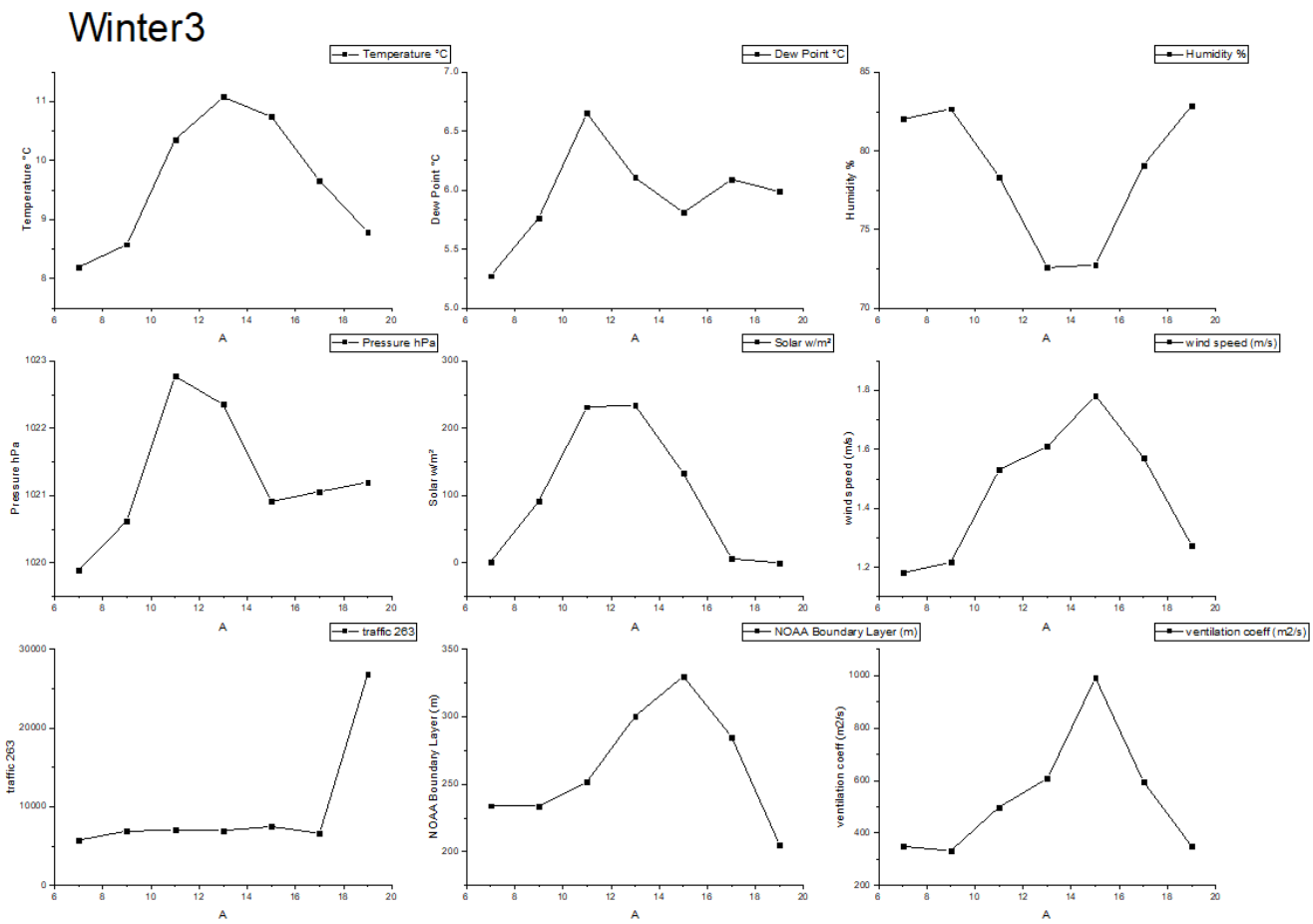


Figure 26. Diurnal variations of meteorological variables during sampling week 6

### 5.2 Mixing height

For calculation of mixing height (Table 3), radiosonde data was obtained from Atmospheric Science department at University of Wyoming (http://weather.uwyo.edu/upperair/sounding.html) for station 17064 which is located in Kartal (40.911N, 29.155E) approximately 20 km SSE of the sampling station. Mixing height was located at the point where temperature stops following the adiabatic cooling rate of -9.8 °C/Km. Vertical distribution of temperature can be observed in Appendix B.

Radiosonde data is collected twice a day at 0300 h and 1500 h, local time. The change of temperature with height determines stability of the atmosphere and dispersion of pollutants. As can be observed in Table 2, temperature inversion conditions with very low mixing heights varying from 0 to less than 100 m can be observed in most of the days during the first three sampling weeks that correspond to winter and spring seasons at 0300 h. This indicates poor dispersion of contaminants particularly during the night and before sunrise due to the lack of solar radiation. On the other hand, during collection of temperature data with radiosonde measurements, it is possible that some temperature measurements will be missed due to the lack of precise measurements at specific height points. It is possible that these temperature measurements were missing on 28, 29, and 31 of January 2017 and 10 January 2018 where mixing height layers of 956-2260 m are reported.

Normal boundary layer heights are considered as 1000 m. During these six sampling weeks, temperature inversions where observed at night during most of the sampling days which is an indicator of a very stable atmosphere particularly during the winter, spring, fall, and some days in the summer seasons. Mixing heights during the summer showed a variation of 430-1273 m. Temperature changes with height are determined by solar radiation and temperature, cloud cover, and wind speed. The probability of the occurrence of greater mixing heights is higher during the Spring and Summer, which is expected owing to higher ambient air temperatures and mixing coefficient ($m^2/s$). Mixing heights at midday showed variations during sampling days and during different seasons with no particular trend observed.

Table 5. Mixing height (m) as obtained from radiosonde data.

| Date | 00Z (3am local time) | 12Z (3pm local time) |
|---|---|---|
| **Week 1 - Winter** | | |
| 28/01/2017 | 2260 | 1953 |
| 29/01/2017 | 956 | 1378 |
| 30/01/2017 | 0 | 1567 |
| 31/01/2017 | 1501 | 1308 |
| 1/2/2017 | 0 | 241 |
| 2/2/2017 | 0 | 504 |
| 3/02/2017 | 0 | 25 |
| 4/02/2017 | 0 | 49 |
| **Week 2- Winter** | | |
| 17/2/2017 | 0 | 775 |
| 18/2/2017 | 0 | 1254 |
| 19/2/2017 | 0 | 2884 |
| 20/2/2017 | 0 | 113 |
| 21/2/2017 | 0 | 140 |
| 22/2/2017 | 76 | 121 |
| 23/2/2017 | 0 | 93 |
| | | |
| **Week 3 – Spring** | | |
| 03/05/17 | 98 | 68 |
| 04/05/17 | 25 | 113 |
| 05/05/17 | 0 | 153 |
| 06/05/17 | 0 | 1446 |
| 07/05/17 | 0 | 1398 |
| 08/05/17 | 0 | No inversion |
| 09/05/17 | 0 | 715 |
| **Week 4 - Summer** | | |
| 6/7/2017 | 1273 | 1345 |
| 7/7/2017 | 0 | 1907 |
| 8/7/2017 | 1043 | 126 |
| 9/7/2017 | 0 | 117 |
| 10/7/2017 | 0 | 2548 |
| 11/7/2017 | 430 | 1254 |
| 12/7/2017 | 602 | 342 |
| **Week 5 - Fall** | | |
| 20/10/2017 | 0 | 151 |
| 21/10/2017 | 0 | 136 |
| 22/10/2017 | 0 | 123 |
| 23/10/2017 | 0 | 137 |
| 24/10/2017 | 0 | 0 |
| 25/10/2017 | 0 | 0 |
| 26/10/2017 | 596 | 0 |
| **Week 6 - Winter** | | |
| 5/01/2018 | 59 | 59 |
| 6/01/2018 | 0 | 0 |
| 7/01/2018 | 0 | 115 |
| 8/01/2018 | 0 | 1116 |
| 9/01/2018 | 0 | 300 |
| 10/01/2018 | 1139 | 0 |
| 11/01/2018 | 0 | 87 |

### 5.3 Wind rose elaboration and analysis

Meteorological wind roses were created with hourly meteorological data provided by the Turkish Meteorological Service for station No. 17603 (41.0155N, 28.9601E) which is 4000 m SW of the sampling station (Fig. 2). Figures 19a-f show weekly wind roses corresponding to all sampling weeks of this Project.

Average weekly wind direction and speeds are observed in Fig. 19 for (a) winter week 1, (b) winter week 2, (c) spring, (d) summer, (e) fall, and (f) winter week 3. Overall, during the winter, dominant direction is easy to observe as winds coming from S and SSW. However, variable winds with no apparent dominant wind direction are observed during Spring and Summer (Fig. 19c, d). Dominant wind directions varied from NW to SSW on each sampling day during week 1 (Appendix G) and overall 30% of the winds arrived from SSW direction. During week 2, variable wind directions were observed during each sampling day, however, dominant wind directions were from southerly directions (SSW-SSE) as follows: SSE-14%, S-29%, and SSW-30% (Fig. 19b). Variable winds were observed during Spring sampling week, with variable northerly winds during the first two sampling dates, mixed northerly and easterly the following two days, variable southerly winds during the next two sampling days, and mixed northerly and westerly the last sampling day. Dominant wind directions during the week are NNW-14%, N-18%, and NNE-11% (Fig. 19c). Mixed variable winds were also observed during sampling week 4 that corresponds to summer season as follows: NNW- 8%, N-18%, NNE- 16%, ENE-15%, and E-10% (Fig. 19d). Similarly to spring and summer, variable winds were observed during the fall and winter sampling weeks. A higher frequency of variable winds was observed during fall and winter week 3 than any other sampling week. During the fall, 52.4% of the wind had northerly direction, 32% had southerly direction, and 7% had easterly direction. During the winter week 3, variable winds were observed throughout the sampling week, with approximately 45% and 34% of the winds having southerly and northerly directions and small frequencies from easterly locations. Westerly winds were not frequently observed in any of the sampling weeks, NNW direction had 6% and 12% frequencies during winter week 1 and spring. Westerly winds may be associated to cleaner air masses from the forest and least populated areas however, they were not commonly observed during this project. Variable winds complicate the understanding of sources and transport of air pollutants, therefore, it is expected that HYSPLIT simulations of 2h air mass trajectories will provide better insight into specific air mass direction and height during the collection of each sample.

The dominant wind speed category for all sampling weeks, except during the fall, was light breeze (1.6-3.4 $ms^{-1}$) with 46%, 48%, 51%, 44, and 54% for winter weeks 1 and 2, spring, summer, and winter week 3 respectively. The second most dominant wind category was light air (0.3-1.6 $ms^{-1}$) with 19%,

43%, 20%, 25, and 32% for winter weeks 1 and 2, spring, and summer, respectively. During the fall, the dominant wind category was light air followed by light breeze with 45 and 30% frequency, respectively. Gentle breeze winds (3.4-5.5%) winds were also observed with 18% frequency. Only during the summer sampling week, moderate breeze winds (>5.5 $ms^{-1}$) were observed with 2.2% occurrence (Fig. 19d). Daily wind roses for all weeks can be found in Appendix G. Overall, the dominant wind speeds observed during this project, except during summer, are considered as light and gentle winds that may not contribute to the dispersion of pollutants, although may contribute to horizontal transport to the sampling location.

Overall, during all sampling weeks in 2017, there is a clear distinction with dominant wind direction. Northerly winds (NNW, N, NNW, NE) had frequencies of 9, 12, 13, and 16%, while southerly winds (SSW, S, SSW) had frequencies of 8, 13, and 7%. In general, southerly winds were observed during the winter, while northerly winds were observed during the spring, summer, and fall. The dominant wind speed category during sampling weeks in 2017 was light air (45%), followed by light breeze (30%), and gentle breeze (18%). Very high winds between 5.5 and 8 m/s were observed during the summer, possibly due to a greater mixing height due to increased solar radiation. During the winter of 2018 (sampling week 6), the dominant wind speed category

a) week 1: 28/01- 04/02 2017

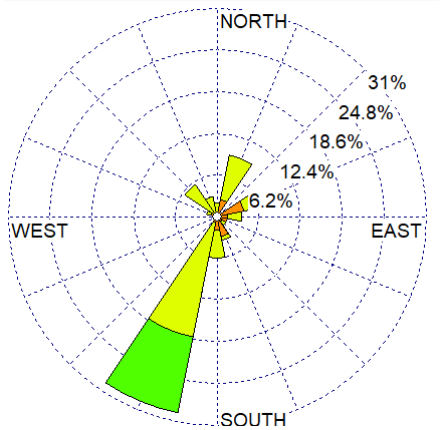


b) week 2: 17/02 – 23/02 2017

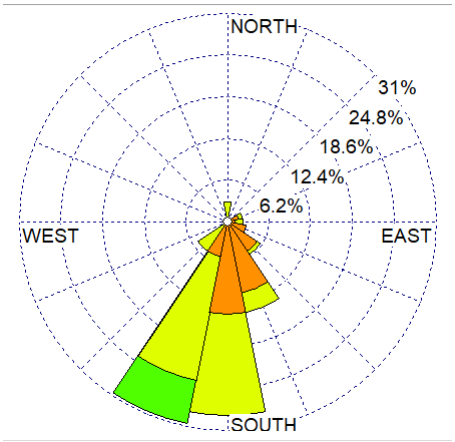


g) wind categories

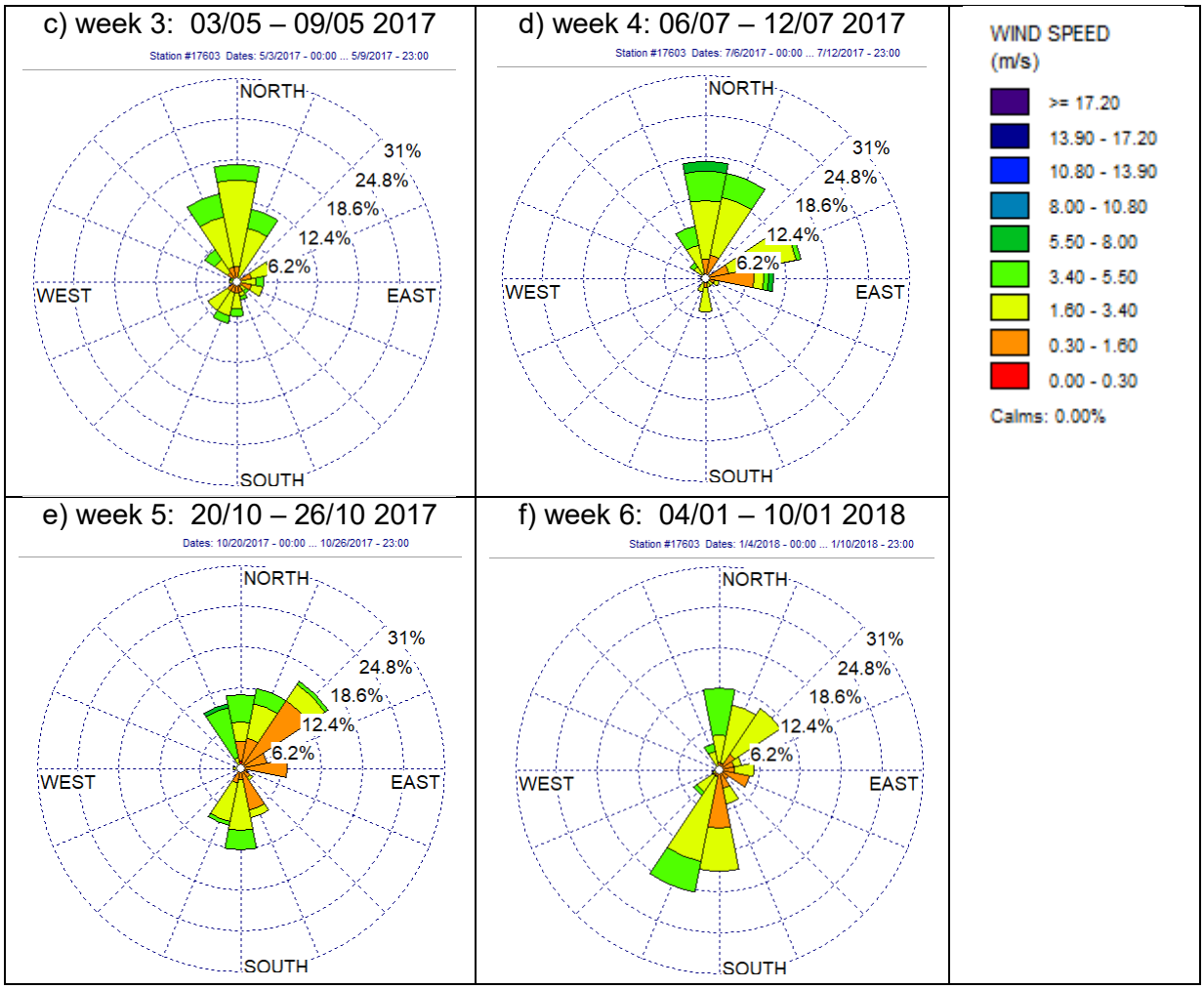


Figure 27. Wind roses observed for all weeks during sampling collection for (a) winter week 1, (b) winter week 2, (c) spring, (d) summer, (e) fall, and (f) winter week 3.

### 5.4 Hysplit trajectory modeling and analysis.

Two-hour air mass trajectories were obtained during the day and 12-h during the night according to the time resolution of high-volume air samples for the sampling dates below.

Winter Week 1: January 28 - 4 February 2017

Winter Week 2: February 17-23 2017

Spring Week 3: May 3–9 2017

Summer Week 4: July 6-12 2017

Fall Week5: October 20-26 2017

Winter Week 6: January 4-10 2018

As mentioned before, wind roses provide an overview of occurrence of wind speed and direction during the day or week, however, air mass trajectories are better indicators of local or regional transport according to wind speed and stability of the atmosphere. During our first four sampling weeks, variable winds were observed, particularly during spring and summer (Fig. 19c,d). HYSPLIT simulations provide greater resolution to understand source of air masses and their trajectories at chosen heights for each sample. This can be observed in all HYSPLIT backward trajectories. Air mass trajectories for spring and summer sampling weeks can be found in our second progress report, Appendix C.

Air masses may follow complex trajectories in the horizontal and vertical direction that are determined by local or regional topography and meteorological conditions such as the presence of high or low pressure systems, temperature of air masses, and local temperature inversions that affect mixing height.

A detailed analysis to evaluate each air mass trajectory will be necessary to understand how they affect concentrations of $PM_{2.5}$ and SVOCs. Istanbul is located in an area sensitive to air pollution from various sources, particularly from local light and heavy vehicles, ships, airplanes, etc. The topography as well differs from various directions. For example, air masses may freely travel through the Black Sea located North of Istanbul and transport air pollutants from Asia and Russia (see e.g., Fig. 20, left). On the other hand, trajectories arriving from southern locations such as the Aegian region (i.e., Çanakkale, Izmir) will encounter 1200 m mountains that will change their trajectory and height (see e.g., Fig. 20, right).

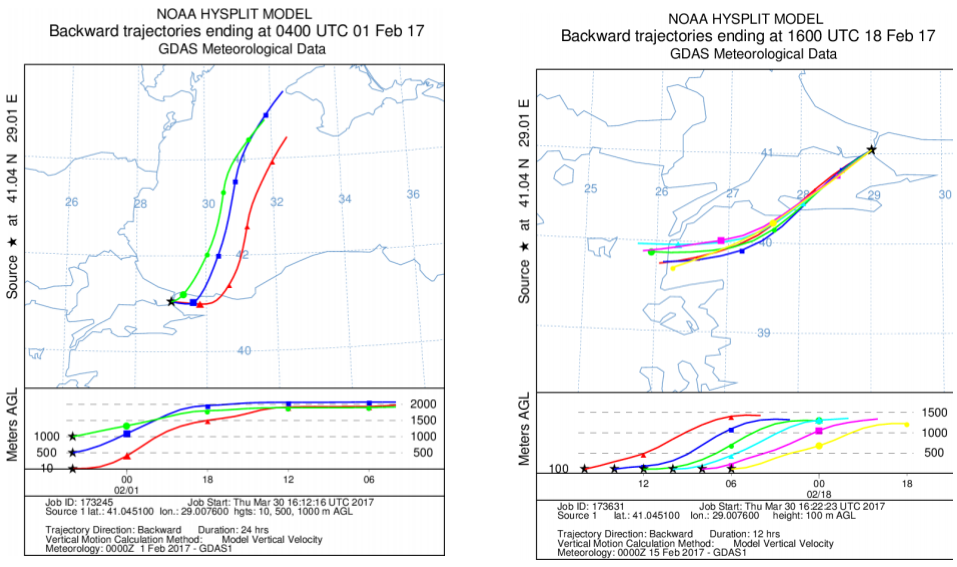


Figure 28. Examples of backward air mass trajectories

During the winter (sampling weeks 1 and 2), most of the air masses originated at 1000-1500 meters above ground level (m.a.g.l) from various specific northern and southern directions identified for each sampling day. However, a few hours before they arrive to Istanbul, the air masses follow trajectories at very low heights, from 100-300 m a.g.l. During the day, the air masses have short trajectories that originate in the coast of the Black Sea (28-31 Jan, 01 Feb, 17 Feb), the coast of the Marmara Sea (02 Feb, 18 Feb, 21 Feb) or the Coast of the Aegean Sea (03-04 Feb, 18 Feb, 19 Feb, 20 Feb, 22 Feb, and 23 Feb). Stable conditions in the atmosphere were observed on various days during week 1 and week 2 due to very low radiation and low temperatures. This is shown in Figs. 18, 20, 22, 23, 29, and 31 (Appendix D, first progress report) due to the lack of vertical motion in air mass trajectories. Similar behavior is observed on 30-Jan with air mass trajectories arriving from maximum a couple hundred meters above ground level (m.a.g.l). Greater vertical motion, and possible dispersion of pollutants, can be observed on other days with air masses arriving from approximately 500-1000 m.a.g.l. Similar behavior of limited vertical motion can be observed during sampling days in spring and summer, where most of the trajectories during the day showed heights below 500 m, except on 7 and 8 May with air masses originating at 2000 m and 1500 m, respectively (Appendix C). Most of the air masses during spring and summer are short and originated N-NE of the sampling station.

During fall and winter season, most of the trajectories originate at low heights close to ground level, both during the day and during the night. This is an indicator of stability of the atmosphere, lack of vertical motion and dispersion of pollutants in Istanbul. Vertical motion is only observed on 23-24 october 2017 in the Fall and 10-11 Jan 2018 during the winter, with trajectories originating at 1000-1500 m.a.g.l. Most of the trajectories were short with southern trajectories originating at Marmara Sea during the day however, northern trajectories originating in the Black Sea were also observed. Samples collected at night had duration of 12h therefore, trajectories may be longer. Some of the nighttime air masses originated at Agean Sea and Ukraine. In order to simplify the frequency, length, and origin of air masses, the clustering algorithm of HYSPLIT model will be used to organize trajectories according to mean clusters. This will be useful to determine the influence of high-time resolved wind direction on total SVOC concentrations as will be explain in Section 4.8.

### 5.5 Traffic density

Traffic density collected every minute was provided by the department of transportation in Istanbul. Total vehicle counts were calculated for all six lanes of Barbaros Bulvari for every 2-h sample during winter

and fall sampling weeks. Data for spring and summer is not available. This data is organized consecutively for weeks 1-2 and 5-6 (Fig. 21). Barbaros Bulvari is a very busy road due to its location in a touristic/business area and connection to the first bridge that joins the European to the Asian side.

As can be observed on Fig. 21, traffic counts follow an interesting behavior according to people activities for specific time, day of the week, and season. The oscillations during the day 0700-1900 are approximately between 2,500 and 10,000 vehicles per 2 h period. On the other hand, oscillations at night 1900-0700 range between 20,000 and 35,000 vehicles per 12 h period. Normalized traffic per hour and yearly average (day and night) can be observed in Figures 13-18. In these normalized figures, oscillations between day and night can be more clearly observed.

Overall, it can be observed that the highest traffic in Beşiktaş is on Friday night and Saturday night as expected, due to the presence of business and tourist attractions. Traffic during the weekdays is lowest on Sunday and slightly increases from Monday to Saturday. During the day, the general trend is lowest traffic at 0700-0900h that progressively increases until 13:00h or 15:00h.

Figures 22 and 23 show total daily traffic counts and average variations of traffic per sample, respectively. Overall, it can be observed that traffic was higher during winter weeks 1-2 than in Fall and winter week 3. The total vehicle counts registered during weeks 1-2 and 5-6 varied according sampling day as follows: Monday: 55,740-68,781; Tuesday: 63,083-69,024; Wednesday: 62,136-72,119; Thursday: 64,070-77,080; Friday: 67,581-83,511; Saturday: 54,635-79,254; and Sunday: 47,112-65,208.

Average values in Fig. 23 give an idea about variations during various seasons in order to simply the data. However, in order to understand variations in traffic, Figures 24 and 25 are more useful. Fig. 23 shows that although there are some variations, traffic is similar during weeks 1-2 and 5-6. Small variations among various weeks are observed at 0700-0900h, 1500-1700h, and 1700-1900. It is clear that traffic during the day is higher at weeks 1-2 than 5-6 as was observed in Fig. 22. On the other hand, traffic during the night is slightly higher at weeks 5-6 than 1-2. Finally, it can be observed in Fig. 23 that traffic is lowest at 0700 and gradually increases until 1300h or 1500h. Fig. 24 and 25 show variations according to sampling time during the day and night. Two main observations are obtained from these figures: higher traffic counts and variations during weeks 1-2 compared to weeks 5-6. In weeks 5-6 higher variations are observed at 0700 and traffic becomes relatively constant with less dispersion among sampling days after 0900h.

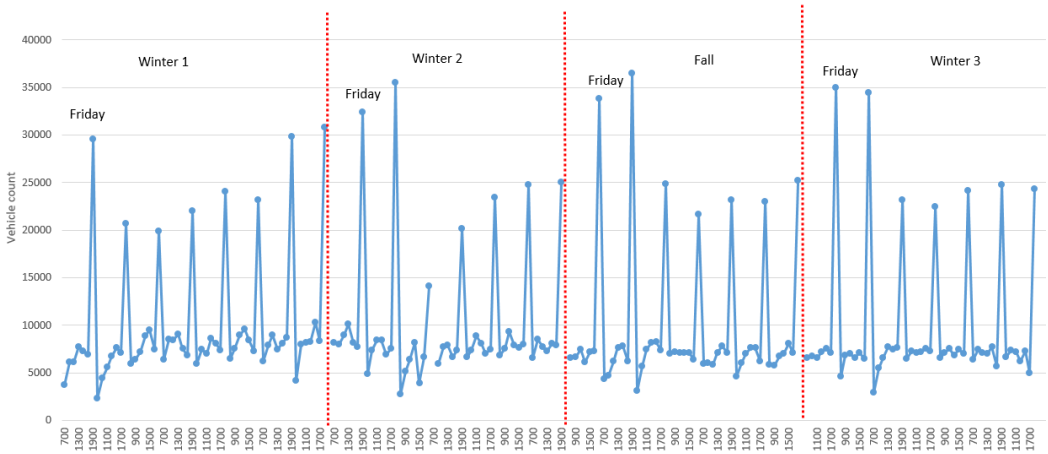


Figure 29. Daily variations in total traffic count during this sampling campaign

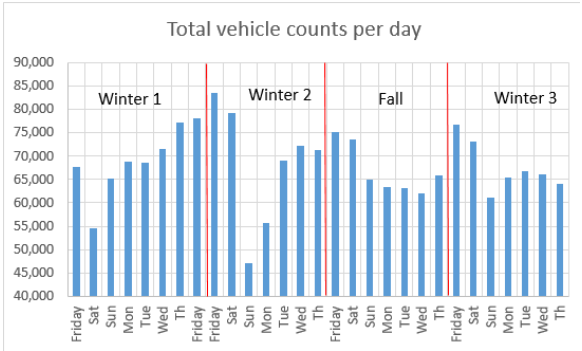


Figure 30. Total vehicle counts per day

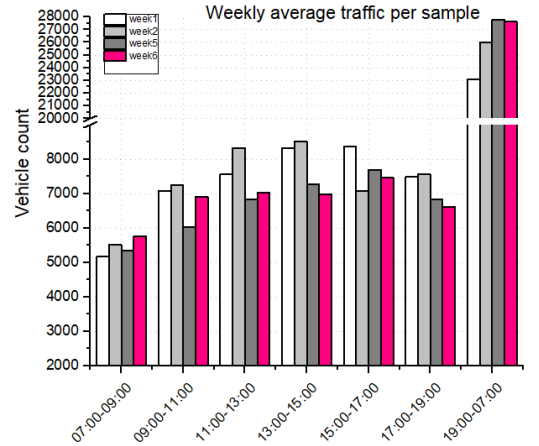


Figure 31. Average vehicle count per sample

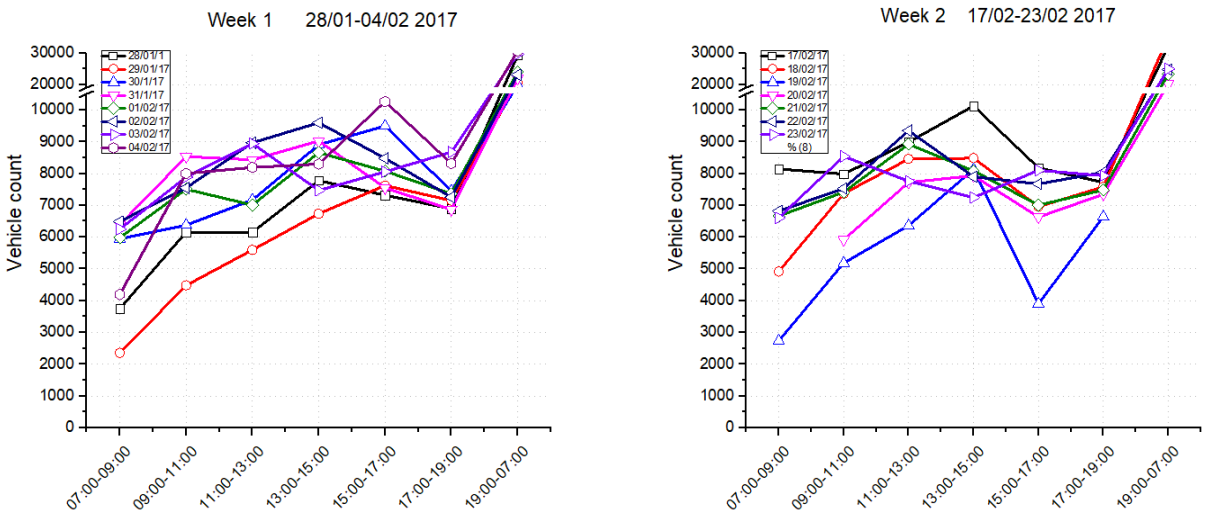


Figure 32. Traffic density per 2-h and 12-h sample during winter week 1 (left) and winter week 2 (right)

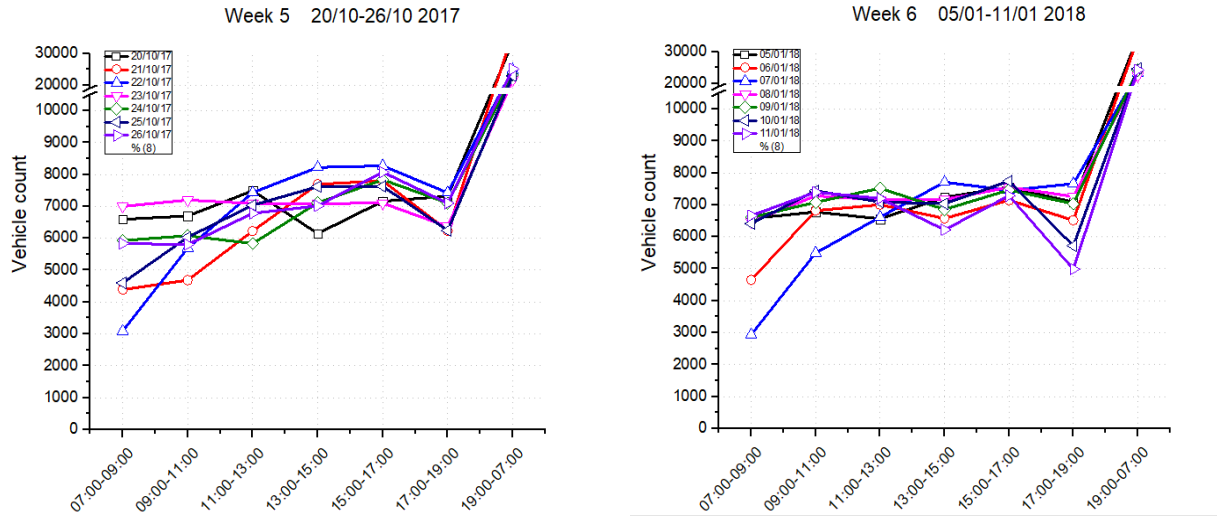


Figure 33. Traffic density per 2-h and 12-h sample during Fall (left) and winter week 3 (right)

### 5.6 $PM_{2.5}$ concentrations

$PM_{2.5}$ concentrations were obtained from the Turkish Council of Environment and Urbanization. Hourly concentrations are shown in Figs. 27-32 for winter sampling weeks 1 and 2, spring, summer, fall, and winter week 3, respectively for Catladikapi, Kagithane, Silivri, and Umraniye. Average daily concentrations are shown in Table 4. Additionally, in our sampling station we collected 24h $PM_{2.5}$ samples and calculated $PM_{2.5}$ concentrations with the gravimetric method. $PM_{2.5}$ concentrations for weeks 3-6 for our sampling station in Besiktas are observed in Table 4.

Data for Catladikapi was only available for weeks 3 and 4. Similarly, data for Umraniye station is also missing during week 2 and some data is missing during week 1. However, during week 1, Umraniye station appears to follow similar concentrations and behavior as Kagithane. Both Kagithane and Umraniye have a population of approximately 400,000 and 700,000, respectively. Lower population of 150,000 live in Silivri, thus lower concentrations of $PM_{2.5}$ are expected during the winter. The 24-h air quality standards established by World Health Organization (WHO) and United States Environmental Protection agency (US-EPA) are 25 and 35 μg $m^{-3}$, respectively. Daily averages have not been established in the European Union and Turkey. Yearly averages are 10, 12, and 25 μg $m^{-3}$ according to WHO, EPA, and EU, respectively. During the study period, the 24-h WHO air quality standard of 25 μg $m^{-3}$ was exceeded 71, 33, 80, 55 and 51% of the time in Catladikapi, Kagithane, Silivri, and Umraniye, respectively. However, these estimations are underestimated in Catladikapi and Umraniye due to missing data during the winter. Therefore, these amounts represent approximately 28, 64, 39, and 28% of the available data in Besiktas, Catladikapi, Kagithane, Silivri, and Umraniye, respectively (Table 4). On the other hand, the 24-h US-EPA air quality standard of 35 μg $m^{-3}$ was exceeded 54, 13, 51, 33, and 41% the available data in Besiktas, Catladikapi, Kagithane, Silivri, and Umraniye, respectively. These exceedances on the EPA air quality standard occur during the Fall and winter and are possibly due to the absence of vertical atmospheric motion and low mixing heights (Table 3). Higher daily $PM_{2.5}$ concentrations have been observed in our sampling station in Besiktas during the spring and summer seasons (Table 3). During the spring, concentrations in Besiktas are approximately 17-56% greater than those recorded in Kagithane. On the other hand, during Fall and Winter, concentrations in Besiktas are approximately 2-3 times less than those recorded in Kagithane. During summer concentrations in Besiktas and Kagithane are comparable. In Besiktas, the WHO and EPA air quality standards were exceeded 71 and 54% of the time during the complete sampling campaign, respectively (Table 3). Although lower concentrations are observed during Spring and Summer, the WHO and EPA air quality standards are still exceeded 71 and 43 % of the time.

During the complete year, there is a clear difference in hourly $PM_{2.5}$ concentrations observed in fall-winter compared to spring and summer in all sampling stations (Fig. 27-32). Maximum hourly concentrations of 100-200 μg $m^{-3}$ can be observed during the fall and winter weeks. On the contrary, all hourly concentrations recorded during the spring and summer are below 50 μg $m^{-3}$ (Fig. 29-30). This is consistent with observed low temperatures during the winter (Fig. 13-18) and the use of low quality of fuels for residential heating combined with poor dispersion of air pollutants due to low mixing heights (Table 3), lack of vertical dispersion of contaminants (Appendix C), and low wind speeds during the winter (Fig. 13-18) compared to spring and summer. Although low correlations between PM2.5 measured in this

work and other criteria pollutants were obtained ($R^2$ = 0.38-0.55), concentrations follow similar trend during the sampling campaign as can be observed in the figure below.

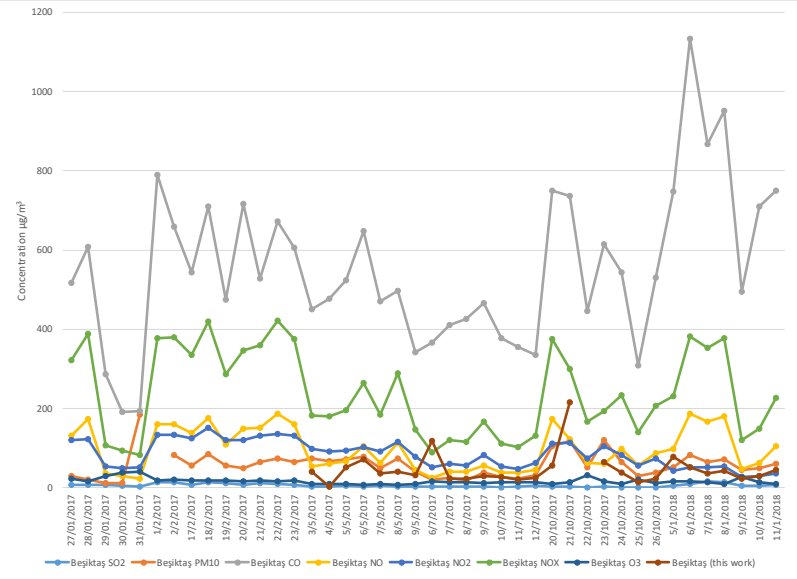


Figure 34. Concentrations of criteria pollutants in Beşiktaş during the sampling campaign

Table 6. Daily average PM2.5 concentrations in µg/m$^3$.

| Date | Beşiktaş (this work) | Çatladıkapı | Kağıthane | Silivri | Ümraniye |
|---|---|---|---|---|---|
| **Week 1** | | | | | |
| 27/01/2017 | - | - | 47.29 | 38.25 | 65.00 |
| 28/01/2017 | - | - | 21.00 | 18.71 | 21.14 |
| 29/01/2017 | - | - | 20.29 | 12.78 | 26.29 |
| 30/01/2017 | - | - | 27.13 | 17.00 | 19.09 |
| 31/01/2017 | - | - | 55.88 | 35.96 | 39.50 |
| 1/2/2017 | - | - | **87.96** | 53.87 | 35.83 |
| 2/2/2017 | - | - | 46.00 | 39.88 | 29.18 |
| **Week 2** | | | | | |
| 17/2/2017 | - | - | 49.95 | 27.29 | 24.64 |
| 18/2/2017 | - | - | 69.46 | 47.96 | - |
| 19/2/2017 | - | - | 68.79 | 38.42 | - |
| 20/2/2017 | - | - | 34.17 | 24.04 | - |
| 21/2/2017 | - | - | 65.63 | 43.25 | 44.67 |
| 22/2/2017 | - | - | 45.04 | 34.04 | 31.17 |
| 23/2/2017 | - | - | 36.29 | 29.13 | 24.94 |
| **Week 3** | | | | | |
| 03/05/17 | 40.31 | 30.56 | 27.58 | 18.04 | 20.92 |
| 04/05/17 | 2.57 | 38.35 | 29.29 | 22.00 | 23.88 |
| 05/05/17 | 50.07 | 33.60 | 28.83 | 23.23 | 22.33 |
| 06/05/17 | 71.97 | 30.29 | 31.63 | 28.35 | 24.88 |
| 07/05/17 | 36.56 | 20.60 | 30.46 | 18.87 | 17.04 |
| 08/05/17 | 40.42 | 23.06 | 22.79 | 12.86 | 15.21 |

| Date | Beşiktaş (this work) | Çatladıkapı | Kağıthane | Silivri | Ümraniye |
|---|---|---|---|---|---|
| 09/05/17 | 31.37 | 20.53 | 32.58 | 16.92 | 16.92 |
| **Week 4** | | | | | |
| 6/7/2017 | 116.59 | 9.44 | 12.85 | 11.30 | 10.21 |
| 7/7/2017 | 22.71 | 15.31 | 18.83 | 14.58 | 12.13 |
| 8/7/2017 | 21.32 | 8.13 | 20.08 | 12.78 | 9.25 |
| 9/7/2017 | 28.31 | 22.00 | 27.04 | 18.75 | 11.79 |
| 10/7/2017 | 27.17* | 16.14 | 25.04 | 14.64 | 15.21 |
| 11/7/2017 | 20.53 | 12.86 | 19.92 | 10.15 | 11.25 |
| 12/7/2017 | 25.14 | 18.62 | 18.42 | 17.75 | 10.79 |
| **Week 5** | | | | | |
| 20/10/2017 | 55.16 | 42.95 | 62.50 | 45.17 | 51.42 |
| 21/10/2017 | 215.87 | -- | 94.88 | 82.33 | 75.76 |
| 22/10/2017 | * | -- | 72.63 | 62.09 | 54.15 |
| 23/10/2017 | 63.53* | -- | 42.58 | 32.91 | 36.77 |
| 24/10/2017 | 37.91 | -- | 59.42 | 25.88 | 52.09 |
| 25/10/2017 | 13.18 | -- | 30.00 | 30.00 | |
| 26/10/2017 | 22.27 | -- | | 18.30 | |
| **Week 6** | | | | | |
| 5/01/2018 | 76.60 | -- | 29.50 | 27.11 | 30.53 |
| 6/01/2018 | 50.00 | -- | 97.42 | 47.57 | 53.83 |
| 7/01/2018 | 35.66 | -- | 71.29 | 49.83 | 44.08 |
| 8/01/2018 | 42.01 | -- | 60.67 | 60.95 | 45.60 |
| 9/01/2018 | 23.03 | -- | 79.79 | 47.58 | 59.50 |
| 10/01/2018 | 29.00 | -- | 35.83 | 24.42 | 36.08 |
| 11/01/2018 | 43.51 | -- | 56.00 | 34.00 | 62.00 |

Note 1. WHO 24-h air quality guideline is 25 μg/$m^3$

Note 2. USA-EPA daily air quality standard is 65 μg/$m^3$

*Due to technical issues, the sample was collected for only 19, 2, and 14 hours

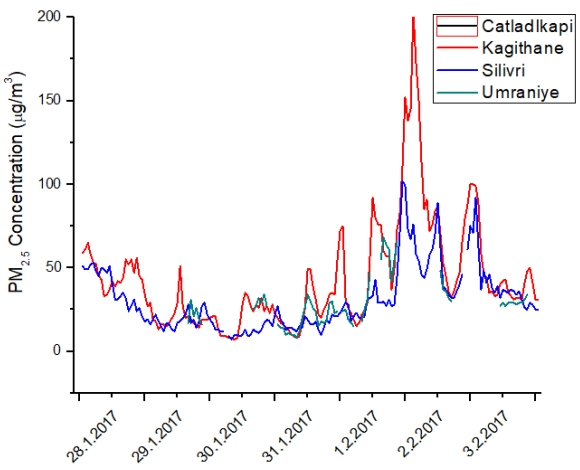


Figure 35. Hourly PM2.5 during sampling week 1

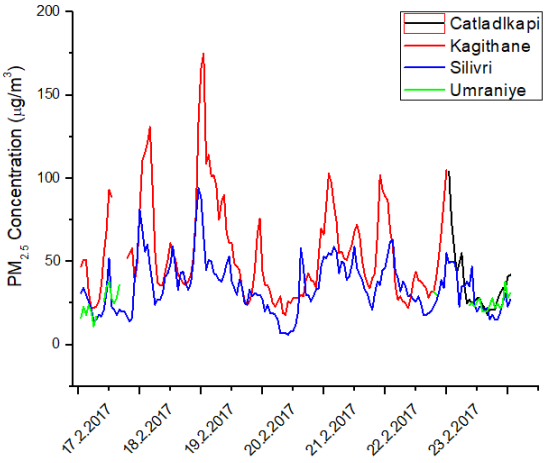


Figure 36. Hourly PM2.5 during sampling week 2

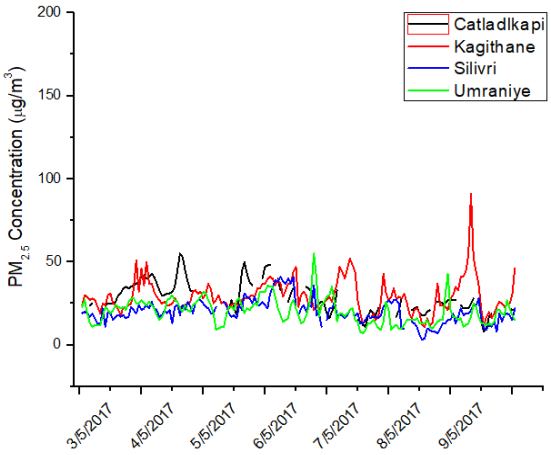


Figure 37. Hourly PM2.5 during sampling week 3

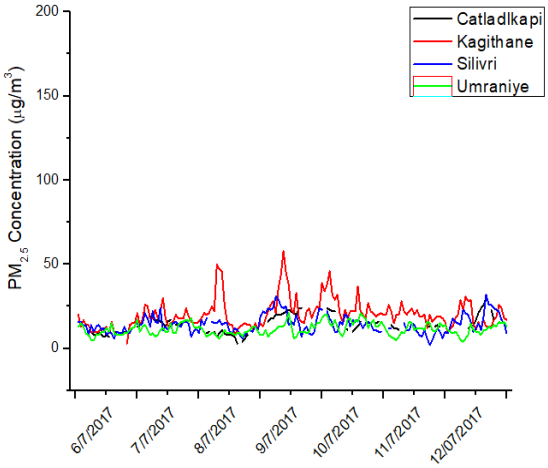


Figure 38. Hourly PM2.5 during sampling week 4

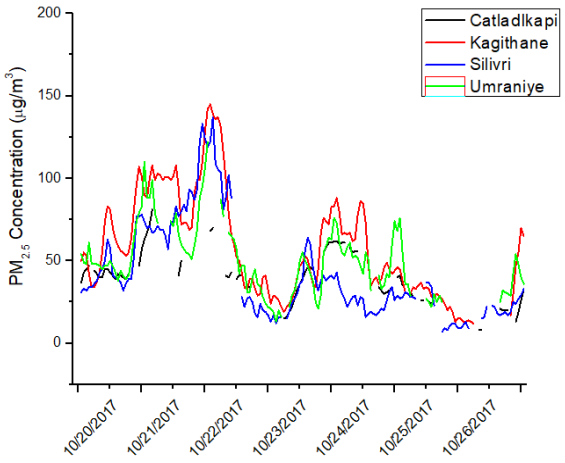


Figure 39. Hourly PM2.5 during sampling week 5

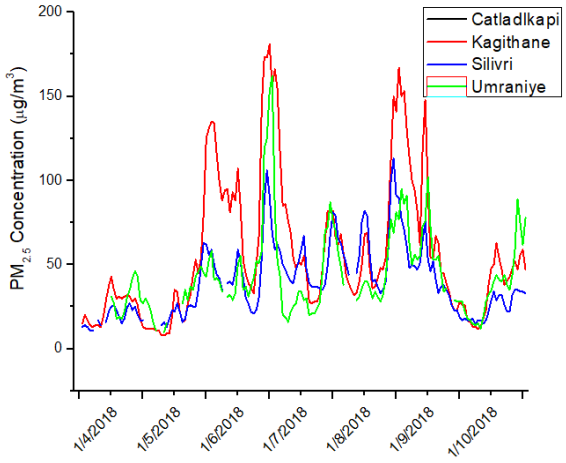


Figure 40. Hourly PM2.5 during sampling week 6

In addition to data observed in Table 6 for selected days in 2017-2018, hourly PM2.5 concentrations were obtained from the Turkish ministry of Environment and Urbanization for the period Jan 2017-Jan 2018 for Kagithane station in order to understand potential impacts of hourly concentration on air quality and human health and their comparison with the daily average air quality standard. Average values were calculated as follows: (1) 2h and 12h averages on days high-time resolved PM2.5 samples were collected and (2) daily averages on all days from 15 Jan 2017 – 14 Jan 2018. Diurnal (i.e., 2h and 12h averages) variations of PM2.5 concentrations and basic statistics (i.e, minimum, maximum, average, and standard deviations) of daily average PM2.5 concentrations observed during our sampling campaign can be observed in Figures 56-60 and Table 7, respectively. The European Union Directive 2008/50/EC establishes 25 µg m-3 as maximum average yearly air quality standard, with no standard established for daily average PM2.5 (EU, 2008). The US Environmental Protection Agency (US-EPA) establishes 35 and 12 µg m-3 as maximum daily and yearly average, respectively, in revised primary PM2.5 standards (EPA, 2013). Table 7 shows seasonal variations of average daily PM2.5 concentrations in Kağıthane district in Istanbul. The yearly average of PM2.5 was 30 µg m-3, hence both the US-EPA and EU air quality standards of 12 and 25 µg m-3 were violated in the period 15 Jan 2017-14 Jan, 2018. Average PM2.5 concentrations during spring, fall, and winter ranged 31-35 µg m-3, whereas during summer, the average concentration was 20.7 µg m-3. Minimum and maximum concentrations during all seasons ranged 3.2-11.4 µg m-3 and 44.8-97.4 µg m-3, respectively. On average, the US-EPA daily average limit of 35 µg m-3 was exceeded 29% of the days during the whole year, with minimum of 4% during the summer and maximum of 46% during the fall. Similarly to the European Commission, the National Environment Protection Council (NEPC) of Australia has

established the air quality standard of 25 μg m-3 as 24h average(NEPC, 2015). In addition, the Environment Protection Authority Victoria (EPA Victoria) has developed a system to group daily average PM2.5 concentrations into categories according to their effects on human health. In this system, a recommended value of 40 μg m-3 is an indicator of poor air quality that is unhealthy for everybody (EPA, 2018). In addition, one hour averages have been grouped into categories to represent air quality as follows: very good (<13.1 μg m-3), good (13.2-26.3 μg m-3), fair (26.4-39.9 μg m-3), poor (40-59.9 μg m-3), and very poor (>60 μg m-3). Table 8 shows the percent distribution of hourly PM2.5 concentrations and the air quality in Istanbul between 15 Jan 2017 and 14 Jan 2018. Overall during the whole year, the majority of the hourly averaged PM2.5 concentrations are in the categories of good (44.1%) and fair (22.5%), followed by very good (13.3%) and poor (12.1). Very poor air quality was observed 8% of the year, particularly during the fall and winter seasons. Poor and very poor air quality were observed as follows: fall>winter>spring with 21.1-29.6% and summer with 4.8% of the hourly PM2.5 concentrations exceeding 40 μg m-3. The best air quality was observed as follows: summer>spring>winter>fall with 77.3, 53.8, 52.6, and 46.1% of the hourly PM2.5 concentrations below 26.3 μg m-3.

In our hypothesis we propose that high time resolved PM2.5 concentrations can be used as a better metric for identification of air quality based on their effects on human health. As discussed before, only the USA-EPA establishes air quality regulations from USA for 24h average PM2.5 concentrations. However, due to the adverse effects of fine particulate matter on human health, particularly in areas where people spend more time outdoors, hourly standards should be established. For this reason, we considered recommendations by EPA Victoria with hourly PM2.5 concentrations organized in categories according to their effects on human health and air quality (Table 8). By comparing both standards at low resolution (24h) and high resolution (1h), it is clear that hourly standards are a better indicator for air quality. According to the daily average standard, 3.6% and 31-46% and of the days in summer and winter-spring-fall exceeded the regulation, respectively (Table 7). However, according to the hourly recommendation, approximately 50% of the days in the winter-spring-fall, and 33% of the days in the summer had fair, poor, and very poor air quality. In addition, a better idea about the magnitude of the exceedances is obtained with the hourly system, in which is it understood that between 20-30% in the winter, spring, and fall, and 5% of the days in the summer had air quality with potential effects on human health. This suggested metric can be an alternative for comparison of air quality among urban areas and implementation of control strategies.

Table 7. Descriptive statistics of daily $PM_{2.5}$ concentrations μg $m^{-3}$ in Kağıthane district in Istanbul

| Season | Mean | Min | Max | N total | N>35 μg $m^{-3}$ | Exceedance (%) |
|---|---|---|---|---|---|---|
| Winter | 33.0 | 6.9 | 97.4 | 85 | 29 | 34.1 |
| Spring | 31.3 | 8.8 | 91.1 | 86 | 27 | 31.4 |
| Summer | 20.7 | 3.2 | 44.8 | 84 | 3 | 3.6 |
| Fall | 34.9 | 11.4 | 94.9 | 87 | 40 | 46.0 |
| Annual | 30.0 | 3.2 | 97.4 | 342 | 99 | 28.9 |

Table 8. Percent distributions of hourly $PM_{2.5}$ concentrations used as indicators of air quality

| Season | N | Range (μg $m^{-3}$) | Very good (<13.1 μg $m^{-3}$) | Good (13.2-26.3 μg $m^{-3}$) | Fair (26.4-39.9 μg $m^{-3}$) | Poor (40-59.9 μg $m^{-3}$) | Very poor (>60 μg $m^{-3}$) |
|---|---|---|---|---|---|---|---|
| Winter | 2070 | 3.4-203.1 | 15.6 | 37.0 | 22.5 | 13.9 | 11.0 |
| Spring | 2117 | 5.4-247.6 | 8.9 | 44.9 | 25.1 | 13.5 | 7.6 |
| Summer | 2054 | 0.6-121.1 | 19.8 | 57.5 | 18.0 | 3.9 | 0.9 |
| Fall | 2105 | 4.7-145.6 | 9.1 | 37.0 | 24.2 | 17.1 | 12.6 |
| Annual | 8346 | 0.6-247.6 | 13.3 | 44.1 | 22.5 | 12.1 | 8.0 |

Diurnal variations of PM2.5 concentrations can be observed on Figures 55-60 for all seasons. As can be observed in all seasons, diurnal variation follows a similar trend with highest concentrations early in the morning that decrease until reaching minimum values at 15:00 h followed by increasing concentrations later in the afternoon. This diurnal variation is a common signature found in traffic sites with high values at rush hours and low values due to atmospheric dilution in the middle of the day. As expected, slightly higher concentrations are found early in the morning which is when accumulated pollutants due to low boundary layers are mixed with fresh emissions. During winter 2 and winter 3 weeks, higher concentrations are observed at night due to poor air quality with lowest ventilation coefficients of only 200-300 m2/s. As has been found in the literature, the highest concentrations during the whole year are found during the winter due to increased emissions from residential heating and low dispersion conditions due to stability of the atmosphere. On the contrary, low concentrations are found during the spring and summer due to the lack of important residential heating emissions and helped by dispersion due to increased mixing layer heights. In our sampling campaign we found important variations during the winter seasons due to variations in ventilation coefficients. At night, PM2.5 concentrations were 44% and 67% higher during winter 2 and 3 compared to winter 1 which is very likely due to ventilation coefficients. In winter 1, the ventilation coefficients at night were 1250 m2/s, whereas in winter week 2 and 3 only 200-300 m2/s. Although these ventilation coefficients at night during the winter weeks are still in the category that indicates poor air pollution, the impact of having ventilation coefficients 5 times greater has great impacts on PM2.5 concentrations at night. During spring and summer, maximum concentrations observed early in the morning and at night are less than half the concentrations observed during the winter weeks. Although poor air quality conditions are

found in spring (97.6%) and summer (50%) due to low ventilation coefficients (Table 4), lower PM2.5 concentrations are observed with 70% and 76% hourly averaged PM2.5 concentrations in the category of good and fair (Table 8) in spring and summer, respectively. This shows that although poor ventilation coefficients can be found at all seasons, the use of high quality of fuel for residential heating is the most important management strategy for the decrease of PM2.5 concentrations during the winter.

High time resolved PM2.5 concentrations are useful for more accurate understanding of their correlation with air pollutants in the gas phase and fast-changing meteorological conditions. Pearson correlation coefficients calculated with high-time resolved concentrations showed very high correlations between $PM_{2.5}$ concentrations and primary gas pollutants associated to vehicle emissions (i.e., NO, CO). During all seasons, except fall, Pearson correlations between high-time resolved PM2.5 concentrations and NO varied as R=0.70-0.80. Only during the fall, the correlation coefficient was 0.45. Similarly, high correlations were found with CO during winter weeks 1, 3, and fall with R=0.55-0.63. Better correlations found with NO may be due to the fast response of NO due to being continuously emitted and destroyed to conversion to NO2. On the contrary, CO tends to follow more complex patterns due to lack of photochemical reactions, its concentration tends to show accumulation and dispersion. The lack of correlation during spring and summer is likely due to higher mixing heights and ventilation coefficients affecting CO concentrations that do not follow similar transport patterns as PM2.5. Negative correlations with O3 explain the differences in the sources, PM2.5 being primarily emitted and decrease in concentration shown in the middle of the day, which is when O3 is produced due to photochemical reactions.

Similarly, high-time resolved PM2.5 concentrations were used to calculate correlations with traffic (i.e., vehicle counts). Fast variations in PM2.5 and traffic can yield better estimations for source identification. In our sampling location, low correlation coefficients were found in all seasons, being the most important 0.49 during winter week 2. Better correlation coefficients are expected during the winter and fall due to the fact that low dispersion conditions do not affect the correlations. However, high correlations were not observed. This is likely due to the fact that in Barvaros bulevar high traffic congestion of stationary traffic is when highest emissions occur. On the contrary, at high congestion low traffic counts are observed. At this situation, low correlations are expected and it can be concluded that traffic counts at this particular location may not be the best indicator for correlations between traffic and PM2.5 at high time resolution or real time measurements. However, because real-time CO and NO are emitted by traffic and high correlations with PM2.5 were observed, this correlation can be better used as indicators of sources of PM2.5.

### 5.7 OC/EC concentrations

Organic carbon (OC) can be both emitted directly and be a tracer for primary organic carbon (POC) or formed in the atmosphere and be a tracer for secondary organic carbon (SOC). Elemental carbon (EC) is a tracer for carbon fuel-based combustion processes, particularly for diesel emissions. POC can show atmospheric aging processes of organic aerosol and can be a good parameters used for development of air quality control policies. OC/EC ratios are helpful for estimating sources of organic aerosol. OC/EC ratios lower than 1 indicate high EC concentrations and therefore emissions from diesel vehicles. Increasing OC/EC ratios are indicator for increasing emissions of OC and can be separated into sections.

In Turkey, OC/EC measurements have been scarcely studied. In this work we evaluated the concentration of OC, EC, total carbon (TC), and % contribution to PM2.5 in 4 seasons. Figure 33 shows seasonal variations of OC, EC, TC, and PM2.5. In order to make PM2.5 concentrations comparable to OC, EC, and TC, concentration factor was 0.25. OC/EC ratios of 2.2-5.2 indicate emissions from light duty gasoline vehicles, residential wood combustion, and typical PM2.5 concentrations. OC/EC ratios ranging 12.7-14.5 are indicators of emissions from natural gas home appliances, paved road dust, and forest fires. A very high OC/EC ratio such as 67.6 indicates emissions from meat charbroiling (Table 5).

In this work, the average ratio during the four seasons was 3.95. The lowest average ratios were observed during spring and summer with 3.6 and 2.21, respectively. The highest average ratios were observed during the fall and winter with average ratios of 4.56 and 5.42, respectively. The highest OC/EC ratios during the complete sampling dates ranged 7.81-10.34. These high ratios were due to low EC concentrations rather than high OC concentrations. This could be due to low traffic emissions. According to table 5, the OC/EC ratios observed in Beşiktaş appear to be a combination of light-duty gasoline and diesel vehicles and possibly shipping emissions during the summer and residential burning during the winter. The lowest OC/EC ratios of 1.34-1.56 were mostly due to a decrease in OC concentrations, however, EC concentrations were also slightly increased. The lowest OC/EC ratios also coincide with precipitation events.

Average OC concentrations ranged 6.62-7.32 ug/m3 during spring and summer, respectively and 13.76-14.1 ug/m3 during the fall and winter, respectively (Table 6). The OC concentrations observed in this work during the summer and winter are 46% and 3.5x higher than concentrations observed in USA and Europe and comparable to China (Table 7). The EC concentrations on the other hand, do not show considerable diurnal variation with values between 2.16-3.26. These concentrations are 6.5x and 1.6x higher than USA and Europe, respectively. Higher EC concentrations observed in Europe than in USA could reflect the higher use of diesel vehicles. In Beşiktaş, the traffic is mainly light-duty vehicles that could use both gasoline or diesel. High average EC concentrations have been reported in Korea and Beijing with 7.3 and 8.7 ug/m3, respectively.

Table 9. Ratios of OC to EC in emissions by different sources (Na et al., 2004)

| Emission source | OC/EC ratio |
|---|---|
| Tunnel | 0.76 |
| Heavy-duty diesel vehicles | 0.8 |
| Light-duty gasoline vehicles | 2.2 |
| Ship emissions | 2-3, 7 |
| Residential wood combustion | 4.15 |
| Ambient PM2.5 | 5.2±2.7 |
| Forest fire | 6, 14.5 |
| Natural gas home appliances | 12.7 |
| Paved road dust | 13.1 |
| Meat charbroiling | 67.6 |

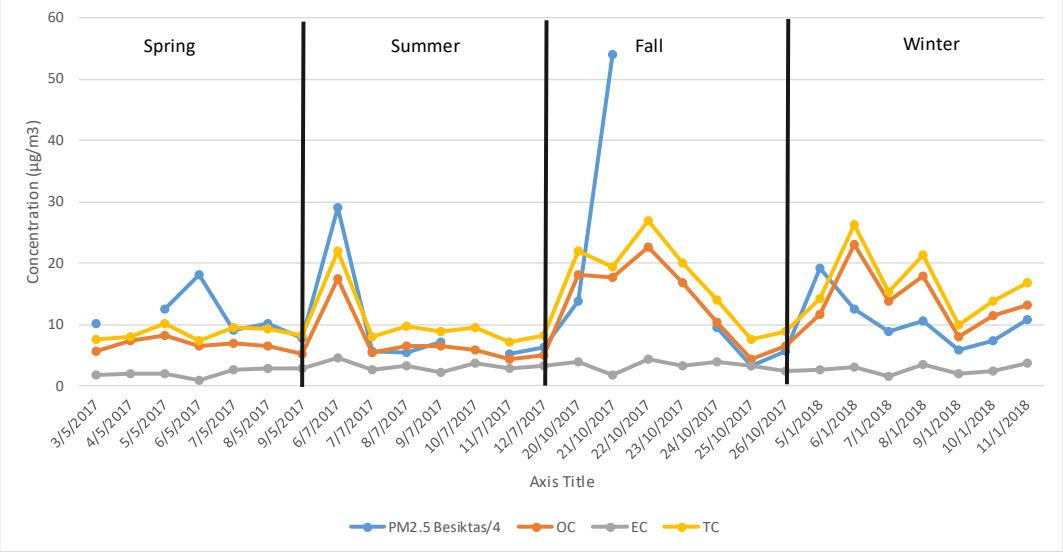


Figure 41. Average daily concentrations of OC, EC, TC, and PM2.5 in PM2.5 (µg/m3)

Table 10. Average daily concentrations of OC, EC, TC, and PM2.5 in PM2.5 (μg/m3)

| Date | OC | EC | TC | OC/EC | %PM2.5 |
|---|---|---|---|---|---|
| **Week 3** | | | | | |
| 3/5/2017 | 5.62 | 1.84 | 7.46 | 3.05 | 18.52 |
| 4/5/2017 | 7.41 | 2.06 | 8.03 | 3.59 | 312.49 |
| 5/5/2017 | 8.18 | 2.05 | 10.22 | 4.00 | 20.42 |
| 6/5/2017 | 6.43 | 0.82 | 7.32 | 7.81 | 10.17 |
| 7/5/2017 | 6.89 | 2.65 | 9.54 | 2.60 | 26.10 |
| 8/5/2017 | 6.55 | 2.76 | 9.32 | 2.37 | 23.05 |
| 9/5/2017 | 5.23 | 2.92 | 8.14 | 1.79 | 25.96 |
| **Week 4** | | | | | |
| 6/7/2017 | 17.42 | 4.64 | 22.05 | 3.76 | 18.91 |
| 7/7/2017 | 5.45 | 2.62 | 8.07 | 2.08 | 35.53 |
| 8/7/2017 | 6.49 | 3.23 | 9.72 | 2.01 | 45.59 |
| 9/7/2017 | 6.57 | 2.25 | 8.82 | 2.92 | 31.16 |
| 10/7/2017 | 5.84 | 3.74 | 9.58 | 1.56 | |
| 11/7/2017 | 4.37 | 2.86 | 7.23 | 1.53 | 35.21 |
| 12/7/2017 | 5.08 | 3.20 | 8.28 | 1.59 | 32.93 |
| **Week 5** | | | | | |
| 20/10/2017 | 18.05 | 3.90 | 21.95 | 4.62 | 39.80 |
| 21/10/2017 | 17.74 | 1.72 | 19.46 | 10.34 | 9.01 |
| 22/10/2017 | 22.59 | 4.39 | 26.98 | 5.14 | |
| 23/10/2017 | 16.81 | 3.28 | 20.08 | 5.13 | |
| 24/10/2017 | 10.25 | 3.82 | 14.07 | 2.68 | 37.11 |
| 25/10/2017 | 4.38 | 3.27 | 7.65 | 1.34 | 58.07 |
| 26/10/2017 | 6.53 | 2.42 | 8.95 | 2.69 | 40.19 |
| **Week 6** | | | | | |
| 5/1/2018 | 11.57 | 2.62 | 14.19 | 4.42 | 18.53 |
| 6/1/2018 | 23.03 | 3.14 | 26.17 | 7.35 | 52.33 |
| 7/1/2018 | 13.70 | 1.61 | 15.31 | 8.49 | 42.94 |
| 8/1/2018 | 17.85 | 3.42 | 21.27 | 5.22 | 50.62 |
| 9/1/2018 | 7.91 | 1.97 | 9.88 | 4.01 | 42.89 |
| 10/1/2018 | 11.48 | 2.41 | 13.89 | 4.76 | 47.91 |
| 11/1/2018 | 13.16 | 3.59 | 16.75 | 3.67 | 38.49 |

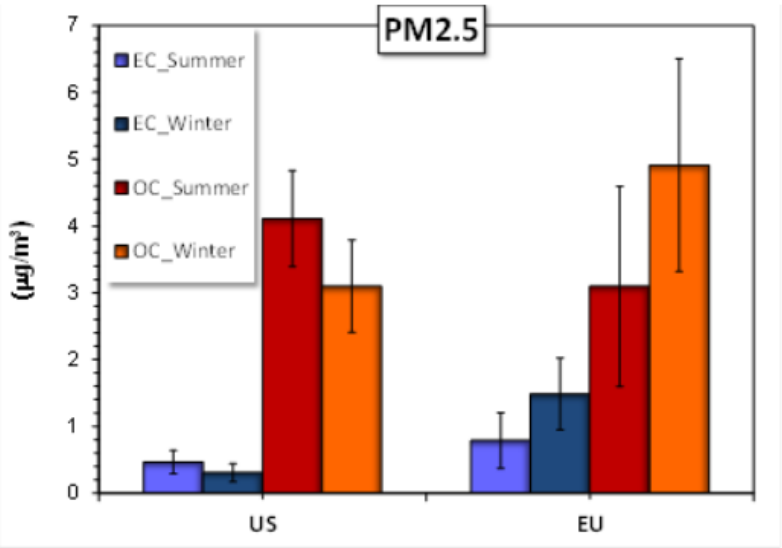


Figure 42. Average OC and EC concentrations during summer and winter in USA and Europe considering 19 and 9-20 sampling sites, respectively (Weijers et al., 2013).

Table 11. Literature values for organic carbon (OC), elemental carbon (EC) in PM2.5 (μg/m3)

| Time-Type of Area | $PM_{2.5}$ | OC | EC | OC/EC | REF. |
|---|---|---|---|---|---|
| Sep to Jan 2001-2002-agricultural area | 41.8±6.4 | 10.8±4.9 | 2.1±1.0 | 5.2±2.7 | (Na et al., 2004) |
| 23 July to 23 August 2016. China –inside university | - | 15.1(day) 13.(night) | 3.2(day) 3.3(night) | 5.2(day) 4.8(night) | (Ye et al. 2017) (Rutter et al., 2014) (Rutter et al., 2014) (Rutter et al., 2014) (Rutter et al., 2014) (Rutter et al., 2014) |
| (day) 1-2/99 USA | 26.7 | 5.7 | 3.3 | 1.7 | (Tolocka et al., 2001) |
| | 14.9 | 7.6 | 3.3 | 2.3 | |
| | 17.4 | 4.3 | 1.5 | 2.9 | |
| 1/95-2/96 USA | 31.32 | 7.74 | 3.81 | 2.03 | (Kim et al., 2000) |
| | 6.82 | 1.49 | 0.19 | 7.84 | |
| 7/99-9/2000 Bejiing | 11.5 | 21.5 | 8.7 | 2.5 | (He et al., 2001) |
| 1/06/2010 to 31/12/2014 Shangai-Commercial Area | | - | - | 28.04(max.annual) 0.46(min.annual) | (Chang et al., 2017) |
| 11/98-4/99 Taiwan | 68 | 10.4 | 4.0 | 2.6 | (Lin and Tai, 2001) |
| December 2014–February 2015 Bolu,Turkey-Urban city | - | 59.9 | 5.92 | 10.1 | (Öztürk and Keleş, 2016) |
| 11/27-12/9/99 Korea | - | 15.2 | 7.3 | 2.1 | (Park et al., 2002) |

### 5.8 Identification and quantification of SVOCs

A total of 41 PAH and n-alkanes were analyzed in 295 $PM_{2.5}$ samples with thermal desorption gas chromatography and mass spectrometry (TD-GC-MS) according to the method developed by Gok et al., (2017). The analyzed $PM_{2.5}$ samples were collected every two hours from 0700 h to 1900 h and for 12 h from 19:00 to 07:00 h for a total of six weeks that represent all seasons. n-alkanes and PAH were quantified with calibration curves in Appendix E. The boxplot with statistical information for each week can be found in Fig. 35-40. The limits of the bars represent the minimum and maximum values, while the limits of the boxes represent the lower 25 and higher 75% of the data. The median and average values are observed inside the boxes. A total of 15 PAH and 28 *n*-alkanes ($C_{14}$-$C_{38}$) were identified and quantified in the samples. Due to higher volatility of naphthalene, and tetradecane, they were not normally found in the particle phase.

Among all sampling weeks, during the day the total PAH concentration ranged as 9.6-73.5, 7.2-56.9, 5.0-56.0, 5.6-11.1, 10.3-187.9, and 11.8-111.6 ng $m^{-3}$ during winter weeks 1 and 2, spring, summer, fall, and winter week 3, respectively. During the night, PAH ranged as 9.4-111.7, 9.0-41.9, 6.3-11.9, 5.6-7.2, 12.2-21.9, and 13.6-118.3 during winter weeks 1 and 2, spring, summer, fall, and winter respectively. Overall, PAH concentrations are higher during the winter and fall than during spring and summer, both during the day and night, as expected, due to a decrease in residential heating emissions and increased mixing layer height (Table 3). During the day, n-alkanes ranged as 73.2-240.0, 74.0-274.0, 34.4-141.1, 33.5-149.8, 39.5-166.3, and 75.6-368.5 ng $m^{-3}$ during winter weeks 1 and 2, spring, summer, fall, and winter respectively. During the night, n-alkanes ranged as 105.4-243.8, 159.5-273.9, 37.7-90.4, and 33.5-117.8, 16.7-24.3, and 54.0-221.9 ng $m^{-3}$ during winter weeks 1 and 2, spring, summer, fall, and winter, respectively. Similarly to PAH, n-alkanes showed higher concentrations during winter and fall, than spring and summer with a decrease of approximately 50%.

Overall, winter week 1 showed the highest concentrations during winter, spring, and summer both during the day and night, except for n-alkanes during the night, which showed highest concentrations during winter week 2. During winter weeks, average concentrations of total SVOCs were 10-40% lower during the day. On the contrary, during the spring and summer, total SVOC concentrations were 20-80% higher during the day. PAH represented an average of 16, 10, 7, 8, 17, and 16 % the total SVOC concentrations during winter weeks 1 and 2, spring, summer, fall, and winter respectively. However, During the night, the contributions of PAH to total SVOCs increased to 11, 11, 21 and 28%, for spring, summer, fall, and winter week 3, respectively. Higher contributions of PAH to total SVOCs are night are expected due to increased emissions and lower temperature at night favoring partitioning into the particle phase. The average contributions of PAH to total SVOCs during the night in winter weeks 1 and

2 were similar to day and night with 12% and 10%, respectively. Maximum concentrations during the night are similar than during the day in the winter weeks 1 and 2. This could be related to a much higher traffic counts observed in winter weeks 1 and 2 compared to winter week 3.

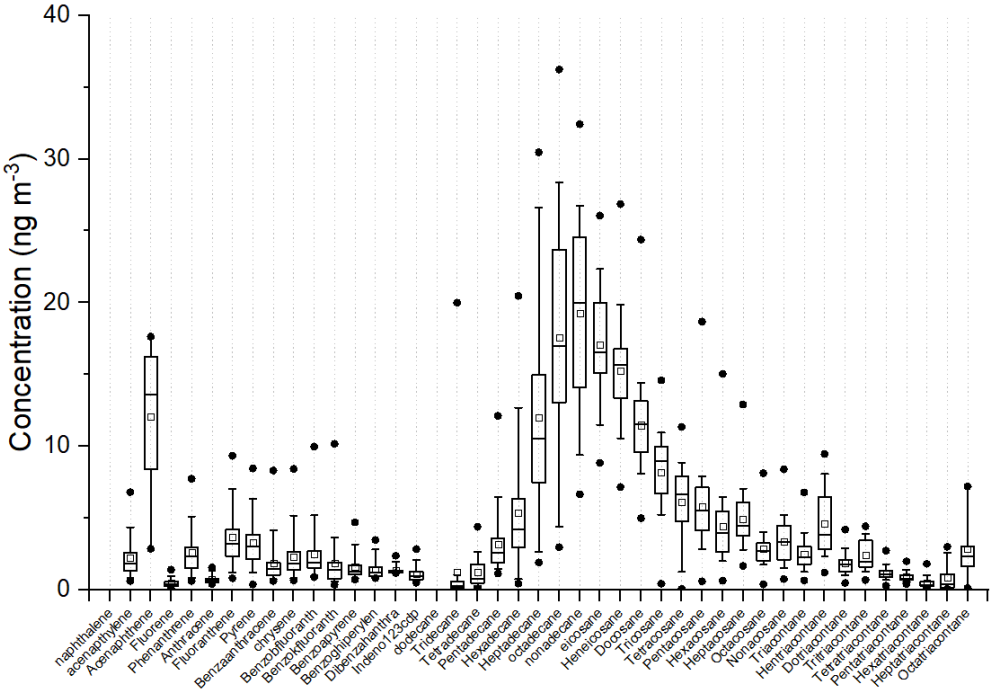


Figure 43. Variation of PAH and n-alkanes during first week of winter

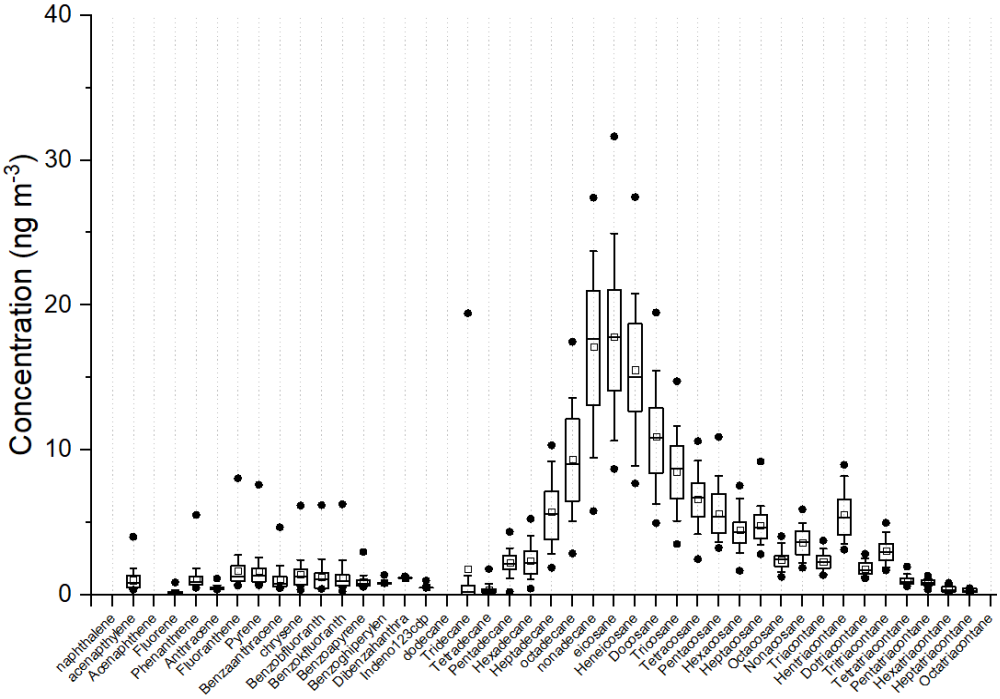


Figure 44. Variation of PAH and n-alkanes during second week of winter

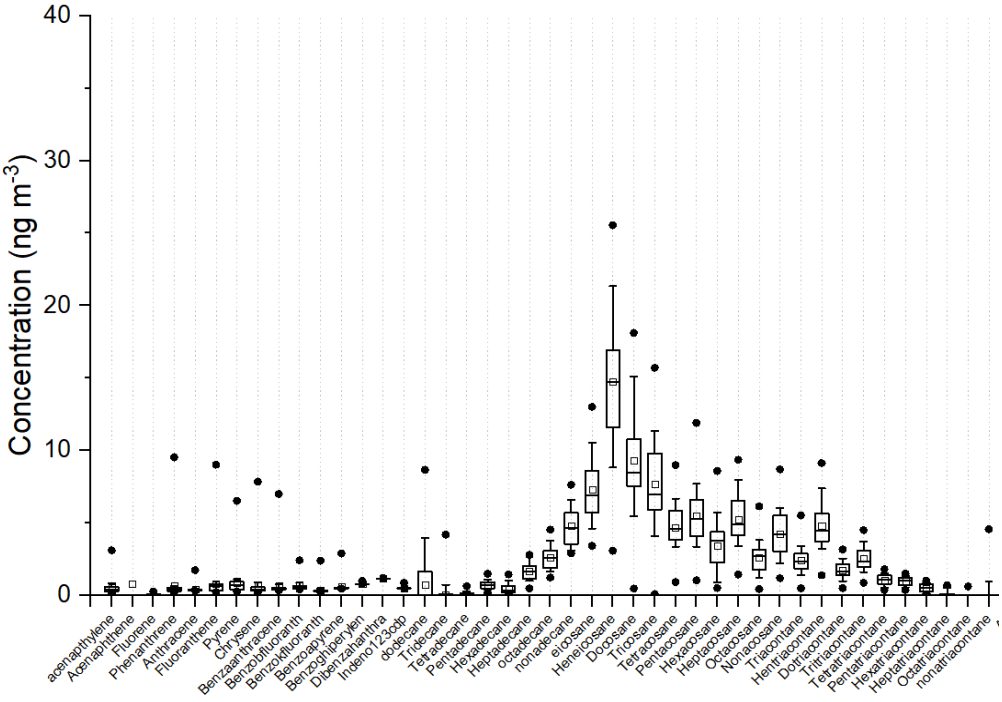


Figure 45. Variation of PAH and n-alkanes during third sampling week of Spring

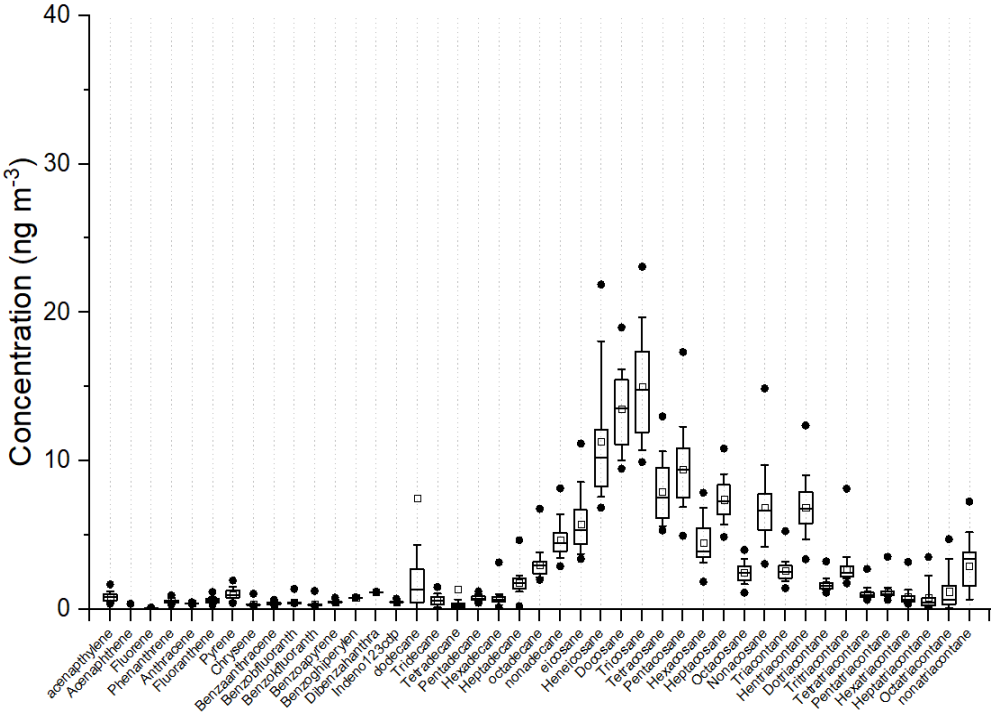


Figure 46. Variation of PAH and n-alkanes during fourth sampling week of summer

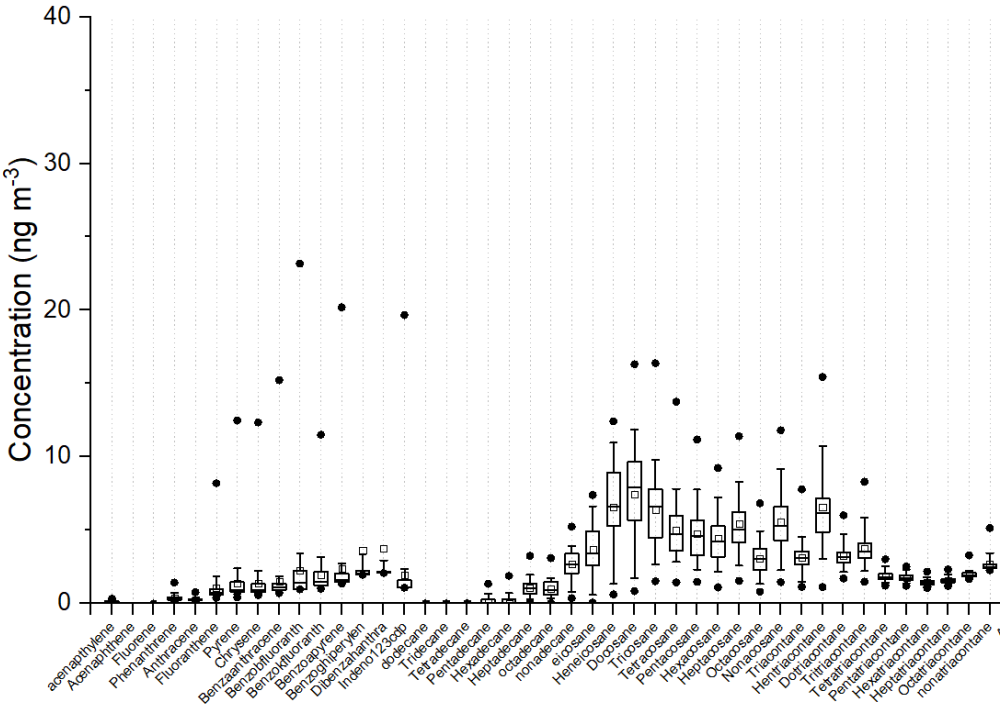

Figure 47. Variation of PAH and n-alkanes during fifth sampling week of Fall

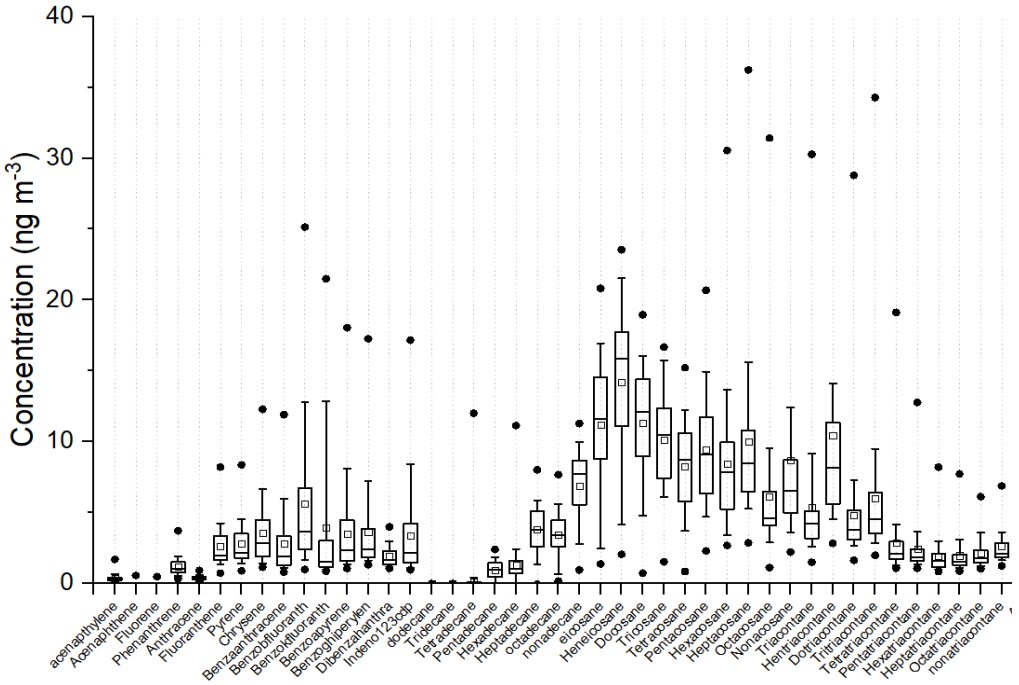


Figure 48. Variation of PAH and n-alkanes during sixth sampling week of Winter

Figures 41-46 show the diurnal variation and distribution of PAH and n-alkanes in 2-h samples collected in the traffic-influenced area of Beşiktaş during the winter weeks 1 and 2, spring, and summer. The total concentrations showed considerable diurnal variations during all sampling weeks. Variations in concentrations during winter week 1 are approximately 50% to approximately 4x with highest variations at 0700 and 1900. Variations during winter week 2 are approximately 44% to 2x with highest variations at 1300 h and 1500 h. Variations in spring are 80% to 3.4x with highest variations at 1700h. During the summer, variations in diurnal concentrations during the day were 26% to 84% with maximum variations at night 3x. During the fall, variations of average minimum and maximum concentrations were 39% to 5x, while during the winter, there were higher variations with 79% to 5x. Average concentrations of SVOCs per sample ranged as follows 161-201, 131-239, 83-112, 66-130, 84.8-161.6, and 154.5-236.7 ng/m$^3$ during winter weeks 1 and 2, spring, summer, fall, and winter week 3, respectively.

The study of organic compounds in high-time resolved samples presented here is reported for the first time in Turkey and has been scarcely reported in the world see e.g., (Isaacman et al., 2014; Williams et al., 2006; Zhao et al., 2013). Concentrations of organic compounds in the atmosphere depend on physicochemical properties that determine reactivity and volatility, sources, and transport or dispersion

through the atmosphere. Therefore, traffic density and meteorological conditions such as temperature, solar radiation, wind speed, wind direction, and stability of the atmosphere play a very big role on their diurnal variations. The main sources of organic compounds in the atmosphere have been identified as coal combustion mostly for residential heating (20-29%), vehicle emissions (13-15%), and secondary organic carbon (15-17%). The distribution of these sources varies during the winter and summer and includes additional contributions from cooking (11-13%) and biomass burning (3-8%) (Wang et al., 2016). According to OC/EC analysis, sources of organic carbon in Beşiktaş could be a mixture between light vehicle and diesel traffic, shipping emissions during the summer and an additional source of residential heating during the winter. In the next section, statistical analysis will be used to try to understand the reason for diurnal variations of SVOCs during different seasons.

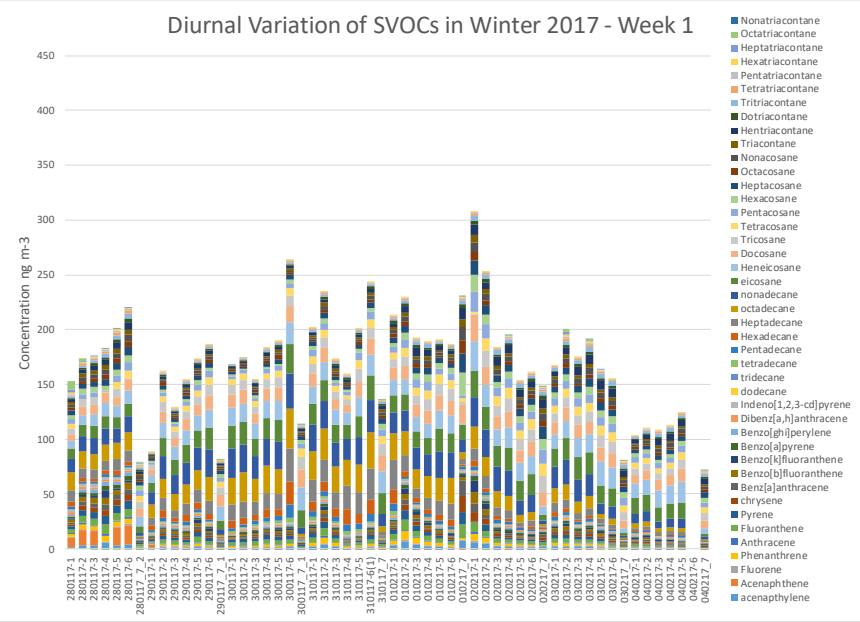


Figure 49. Total concentration of n-alkanes and PAH in 2-h samples collected during 1st Week of Winter

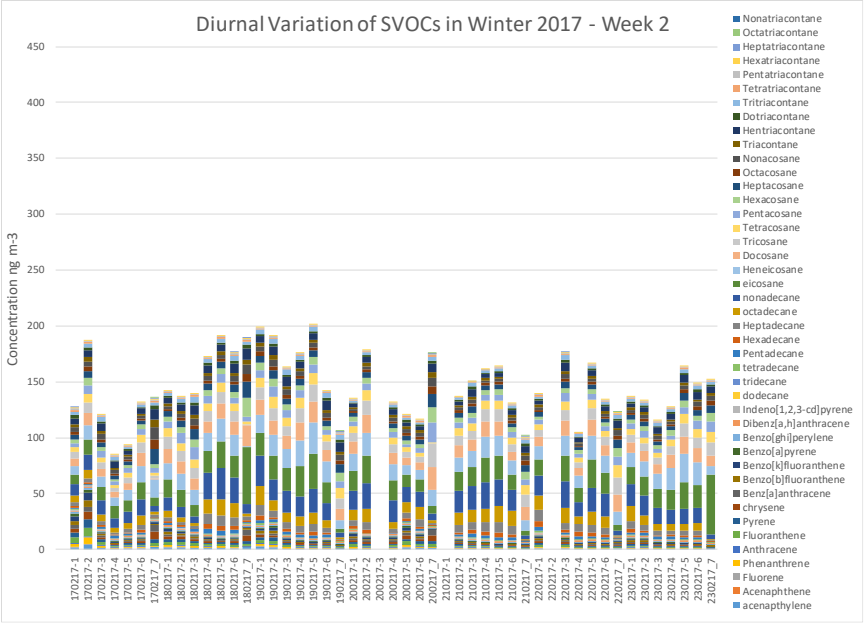


Figure 50. Total concentration of n-alkanes and PAH in 2-h samples collected during 2nd Week of Winter

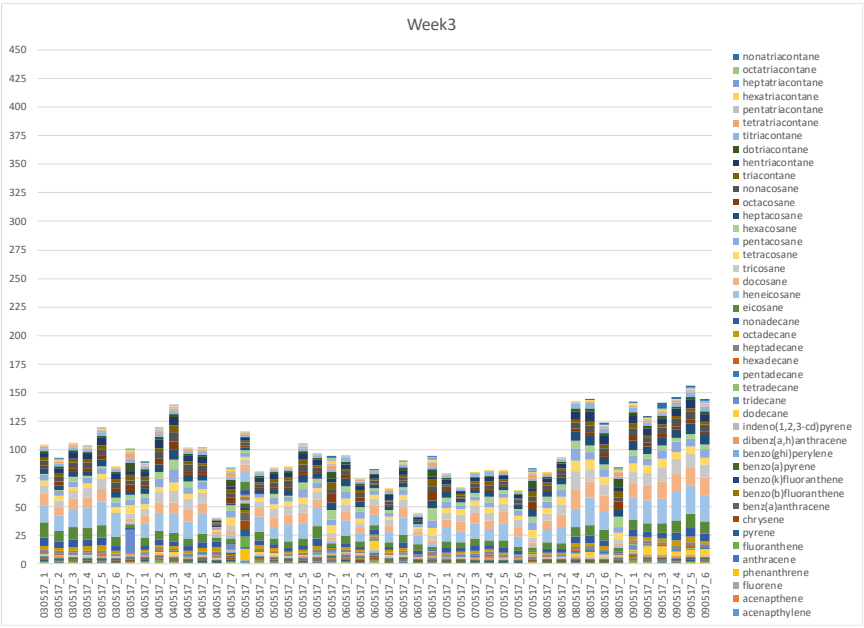


Figure 51. Total concentration of n-alkanes and PAH in 2-h samples collected during third sampling week of Spring

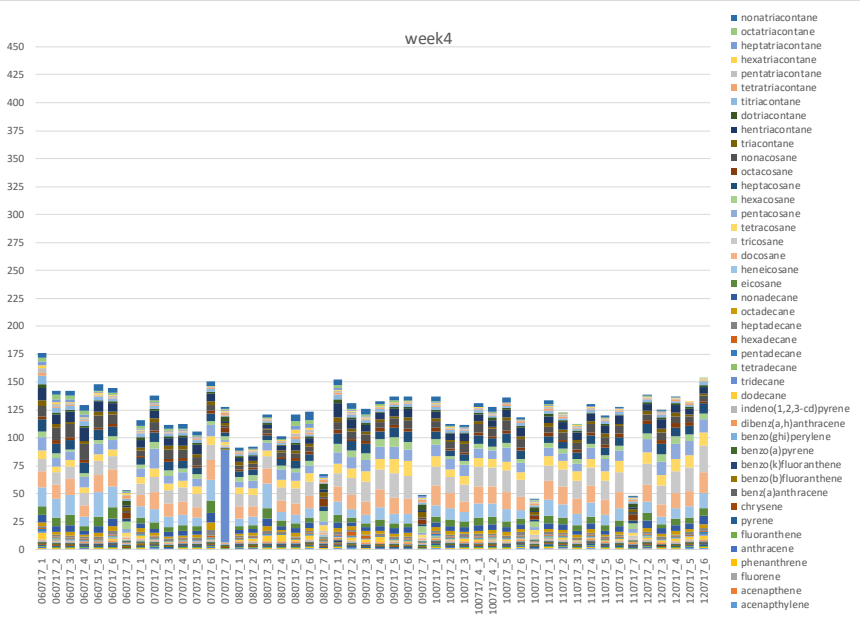


Figure 52. Total concentration of n-alkanes and PAH in 2-h samples collected during fourth sampling week of summer

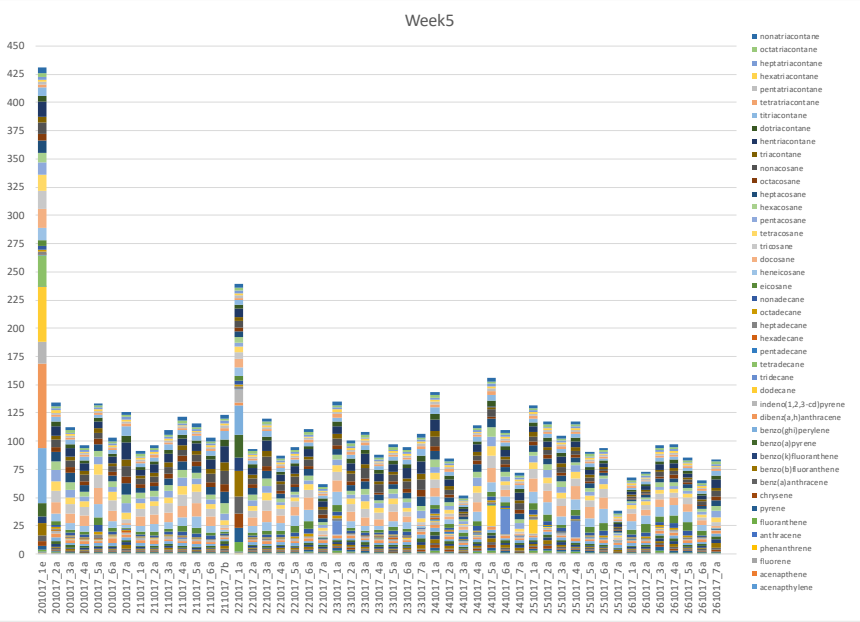


Figure 53. Total concentration of n-alkanes and PAH in 2-h samples collected during fifth sampling week of fall

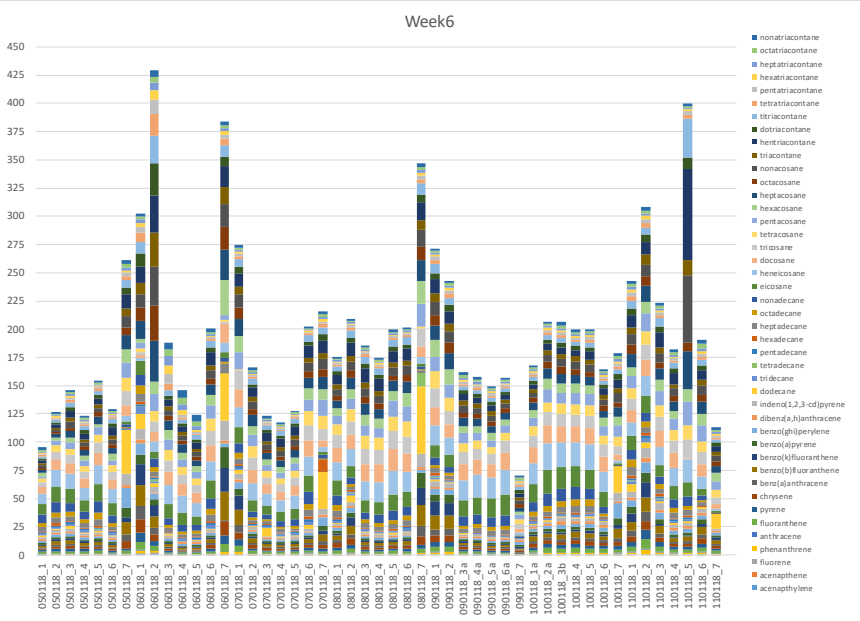


Figure 54. Total concentration of n-alkanes and PAH in 2-h samples collected during sixth sampling week of winter

Table 12. Descriptive statistics of PM2.5 and gas pollutant concentrations

| Date | | PM2.5 | O3 ppb | NO ppb | CO ppb | Ox ppb |
|---|---|---|---|---|---|---|
| **Winter1** | Min-Max | 19.0 - 89.3 | 5.8 - 19.3 | 20.0 - 101.5 | 153.9 - 637.2 | 40.5 - 123.2 |
| | Mean ± std dev | 40.1 ± 24.7 | 13.5 ± 4.7 | 42.3 ± 36.1 | 386.9 ± 183.4 | 67.7 ± 34.1 |
| **Winter2** | Min-Max | 26.5 - 73.8 | 7.9 - 17.4 | 29.2 - 72.3 | 395.5 - 587.3 | 58.9 - 95.6 |
| | Mean ± std dev | 52.6 ± 15.8 | 11.2 ± 3.3 | 54.2 ± 16.3 | 501.2 ± 78.4 | 78.4 ± 15.8 |
| **Spring** | Min-Max | 25.8 - 31.8 | 15.0 - 35.1 | 13.3 - 49.0 | 290.1 - 543.4 | 60.8 - 98.5 |
| | Mean ± std dev | 28.9 ± 2.2 | 24.2 ± 7.3 | 30.8 ± 15.5 | 411.9 ± 75.6 | 79.6 ± 16.2 |
| **Summer** | Min-Max | 14.4 - 29.8 | 25.2 - 38.7 | 11.6 - 26.3 | 292.5 - 405.9 | 55.9 - 77.2 |
| | Mean ± std dev | 20.5 ± 4.7 | 28.9 ± 4.7 | 19.1 ± 5.5 | 339.5 ± 39.3 | 64.8 ± 7.0 |
| **Fall** | Min-Max | 23.1 - 105.5 | 2.8 - 24.2 | 18.2 - 188.0 | 260.5 - 637.2 | 65.3 - 241.1 |
| | Mean ± std dev | 50.4 ± 34.8 | 9.9 ± 7.4 | 83.9 ± 55.3 | 475.9 ± 134.0 | 126.6 ± 63.5 |
| **winter3** | Min-Max | 42.9 - 99.2 | 0.0 - 7.3 | 48.1 - 185.5 | 409.8 - 933.4 | 69.1 - 221.4 |
| | Mean ± std dev | 62.6 ± 20.7 | 2.9 ± 2.8 | 100.6 ± 50.8 | 666.2 ± 166.1 | 131.7 ± 56.7 |
| **all winter** | Min-Max | 19.0 - 89.3 | 0.0 - 19.3 | 20.0 - 101.5 | 153.9 - 637.2 | 40.5 - 123.2 |
| | Mean ± std dev | 51.2 ± 22.1 | 9.4 ± 5.9 | 64.6 ± 43.6 | 512.1 ± 186.5 | 91.4 ± 46.8 |

Figures 55-60 show diurnal variations of PAH, n-alkanes, and PM2.5, and gas-phase pollutants CO, O3, NO, NO2, Ox (O3+NO2), and SO2 during winter weeks 1-2, spring, summer, fall, and winter week 3, respectively.

During winter week 1, PAH concentrations ranged 15-40 ng/m3 with maximum values observed early in the morning at 9am and minimum values at night 19:00-07:00h. This diurnal behavior in PAH concentrations is due to a combination of factors. The highest concentrations of PAH observed at 9am are possibly related to highest traffic counts of 7000 vehicles at 9:00-11:00h (Fig. 21). Less traffic counts of 5000 vehicles are observed from 7:00-9:00h. Although vehicle counts steadily increase until 17:00h and reach a maximum of 8500 counts, concentrations of PAH decrease due to an increase in high ventilation coefficients from 1300 m2/s (9:00h) to 2800 m2/s (17:00h). In addition to high mixing conditions observed during week 1, PAH concentrations decrease during the day due to reactions with OH, O3, and NOx as shown by high correlation between PAH and O3 (R = -0.62). During the night, lower concentrations are observed possibly due to a lack of constant vehicle emissions and PAH emitted during the day have been partially oxidized.

During winter week 1, n-alkanes ranged 100-155 ng/m3 with maximum values observed at rush hours (i.e., 9am and 17h). A slight decrease in concentration from 155 ng/m3 to 130 ng/m3 is observed from 9am to 11am followed by an increase to 150 ng/m3. The lowest concentrations of 100 ng/m3 are observed at night as an average value between 19:00-07:00h. The change in n-alkane concentrations in this particular traffic urban station is closely related to traffic emissions. The differences between diurnal variation of PAH and n-alkanes are explained by their photochemistry. Lifetimes of n-alkanes vary on the order of 0.5-1.8 days against OH concentrations. The slow photochemistry is shown by the slight decrease in concentrations at 11:00-13:00h, followed by an increase due to accumulation with fresh traffic emissions. Low average concentrations at night are due to a decrease in traffic as can be observed in the normalized traffic plot in Fig. 15k.

During winter week 2, PAH concentrations ranged 10-23 ng/m3 with maximum values observed early in the morning at 9am and minimum values in the middle of the day at 13:00-15:00h. Concentrations slightly increased at night to 14 ng/m3. Lower concentrations of PAH during winter week 2 compared to week 1 can be explained by wind direction predominantly from southern direction (Fig. 62), compared to week 1 in which variable wind directions were observed. A steeper decrease in PAH concentration can be observed from 11:00-13:00h in which concentrations decrease from 23-10 ng/m3. This could be due to a mixture of increased temperature and radiation and a decreased boundary layer that promote higher effective concentrations of oxidants (Ox) when week 2 is compared to week1. These conditions

are ideal for photochemical degradation of PAH. The increased PAH concentrations at night (14 ng/m3) are due to a very low ventilation coefficient of 200 m2/s.

During winter week 2, n-alkanes ranged 125-142 ng/m3 with maximum values observed at rush hours (i.e., 9am and 17h). Low concentrations between 125-127 ng/m3 were observed at 7am, 13h, and during the night. High concentrations of 135 ng/m3 and 142 ng/m3 are only observed during rush hours. Similarly to week 1, a decrease in concentration was observed from 9am to 11am followed by an increase to 142 ng/m3. This decrease however, was steeper during week 2 than during week 1. Higher amounts of radiation may be responsible for producing more OH and O3 during week 2 compared to week 1. Although OH concentrations are produced only during the day, ozone may be accumulated at night and may be responsible for oxidation of n-alkanes. Low concentrations of n-alkanes at night may be also due to lack of traffic and transport to nearby areas.

During spring, PAH concentrations ranged 15-35 ng/m3 with maximum values observed early in the morning at 7am and minimum values in the middle of the day at 13:00-15:00h and 19:00-07:00. Concentrations slightly increased to 18 ng/m3 at 15:00-19:00h. Due to technical difficulties with the sensor, traffic data is not available during this time. However, this slight increase in concentrations at 15:00-19:00h coincides with maximum traffic in week 1 and week 2, combined with a decrease in solar radiation and wind speed. Lower PAH concentrations were observed on two days that coincide with a heavy precipitation event during spring.

During spring, n-alkanes ranged 70-105 ng/m3 with maximum values observed at 15:00h. Low concentrations of 82 and 70 ng/m3 are observed early in the morning at 7:00h and during the night 19:00-07:00h, respectively. Although concentrations of O3 are slightly higher during the spring, a decrease in concentration due to photochemical reactions, can’t be observed. Since the rate of photochemical reactions increases with concentration of reactants, and these are nearly half of those observed during winter week 1, it is possible that n-alkanes tend to accumulate rather than react during this week.

During summer, PAH concentrations ranged 11.5-17.5 ng/m3 with maximum values observed early in the morning at 7am and minimum values at night 19:00-07:00h. Concentrations remained relatively

constant during the day at approximately 13.5 ng/m3. Diurnal PAH variations during the summer coincide with steep increase in Ox concentrations from 7:00h to 17:00h for improved photochemical reactions. During the summer PAH concentrations show good correlations with O3 (R=-0.57) that indicates photochemical degradation, and with NO (R=0.61) that indicates possible traffic source. PAH Concentrations remain relatively constant during the day until 17:00 h due to an increased boundary layer that causes mixing and dispersion. Although traffic data is also not available during summer season, it is possible that a decrease in concentrations at night is due to low vehicle counts as has been observed in previous weeks.

During summer, n-alkanes ranged 40-130 ng/m3 with nearly constant values of 110-130 ng/m3 observed during the day and minimum values of 40 ng/m3 observed during the night at 19:00-07:00h. During this particular sampling week, the decrease in concentration due to photochemistry is slightly observed at 11am with an increase in concentrations at rush hour at 17:00h. It is possible that increased boundary layer and very high ventilation coefficients of 5000 m2/s diluted OH concentrations and promoted sampling in the particle phase rather than favor photochemical reactions. Although traffic data is not available during the summer, according to observations in previous weeks, the continuous increase in traffic observed during the morning until 15:00 may be responsible for accumulation of n-alkanes. The very low concentrations of 40 ng/m3 observed at night are due to a decrease in traffic counts and lack of residential heating during the summer compared to spring (70 ngm3), winter 2 (127 ng/m3), and winter 1 (100 ng/m3).

During fall, PAH concentrations ranged 15-45 ng/m3 with maximum values observed early in the morning at 7am and minimum values at night 19:00-07:00h. Concentrations showed a decreasing trend during the day with a slight increase to 25 ng/m3 at 17:00-19:00h. The concentrations observed in fall are similar to winter week 1, however, the diurnal variation is similar to spring with the variation of the slight increase in concentrations at 17:00 during the fall occurs at 15:00h during the spring. In the fall, this increase in concentration coincides with a maximum traffic counts of 8000 vehicles (Fig. 25). The higher concentrations can be due to lower wind speeds of 1.5-2.7 m/s.

During the fall, n-alkanes ranged 70-100 ng/m3 with maximum values observed early in the morning at 07:00h and lowest values observed at night 19:00-07:00h. Concentrations of n-alkanes decreased from 100 to 82 ng/m3 at 9:00h and further increase at 15:00h. A similar behavior was observed during winter week 1 and 2. The increased concentrations early in the morning are due to combined emissions from residential heating and traffic during rush hour. Traffic steadily increases from 5200 to 7500 vehicles

from 7:00 to 15:00 which is when maximum traffic counts are observed. The decreased concentrations are mainly due to a decrease in boundary layer that hinders dispersion of oxidants and promotes photochemical reactions. The lower peak in concentration of 92 ng/m3 observed at 15:00 is due to slight dilution in an increased boundary layer (370 m) compared to the maximum concentration of 100 ng/m3 observed early in the morning with a lower boundary layer of nearly 250 m. At night, a lower concentration of 70 ng/m3 is due to decreased vehicle counts and background emissions from residential heating.

During winter week 3, PAH concentrations are high at both early in the morning 7:000-9:00h and during the night with 50 and 60 ng/m3 respectively. Minimum values are reached between 11:00-13:00h and remain relatively constant until 17:00-19:00 h. Overall, the highest PAH concentrations are observed during winter week 3. This can be a combination of factors. During the day, lower photochemical degradation due to solar radiation below 200 W/m2, which is the lowest of all seasons, and ozone concentrations below 6 ppb which are also the lowest of all season. During the night, high PAH concentrations show high correlation coefficient (R= 0.54) with PM2.5 concentrations of 75 ug/m3 which are the highest during both day and night of all seasons, which indicate that PAH are emitted in the particle phase and also condensed on suspended particles at night due to high relative humidity and lower temperature. In addition, low dispersion is due to the lowest wind speed of all seasons was observed during winter week 3 (1.2-1.8 m/s).

During winter week 3, n-alkanes ranged 130-190 ng/m3 with maximum values observed at 09:00h and lowest values observed in the middle of the day 13:00h and at night 19:00-07:00h. These are overall the highest concentrations observed during our complete sampling campaign and are approximately 20% higher than during winter week 1. A steeper decrease in concentrations from 190 to 135 ng/m3 is observed from 9:00h to 13:00h. This decrease may be due to faster photochemical reactions due to increased concentrations of reactants and a very low boundary layer that pushes the pollutants to the ground therefore hindering dispersion. The second peak observed at 15:00 with lower concentrations of 170 ng/m3 is consistent with maximum vehicle counts of 7500 vehicles and maximum ventilation coefficients of 1000 m2/s. Overall, the lowest ventilation coefficients are observed during winter week 3.

In conclusion, PAH are able to react with OH, NO3, and O3 and their lifetimes vary on the order of 2.1-12 hours when they react with OH (EC, 2001). n-alkanes have a wide range of volatility and react with OH and NO3 radicals at different rates. They are more stable than PAH and since they have longer lifetimes, they can be transported. For example, from octane to hexadecane lifetime against reactions with OH vary from 1.4 to 0.5 days (Loza et al., 2014). In this work, diurnal variations of PAH are due to variations in traffic, photochemical reactions, and ventilation conditions. In our work, diurnal variations of n-alkanes followed two diurnal variations: (1) during the fall and winter sampling weeks with marked behavior with respect to traffic and photochemistry and possibly enhanced due to lower boundary layer height, and (2) during spring and summer slight variations with photochemistry and traffic, possibly due to dilution and lack of residential heating.

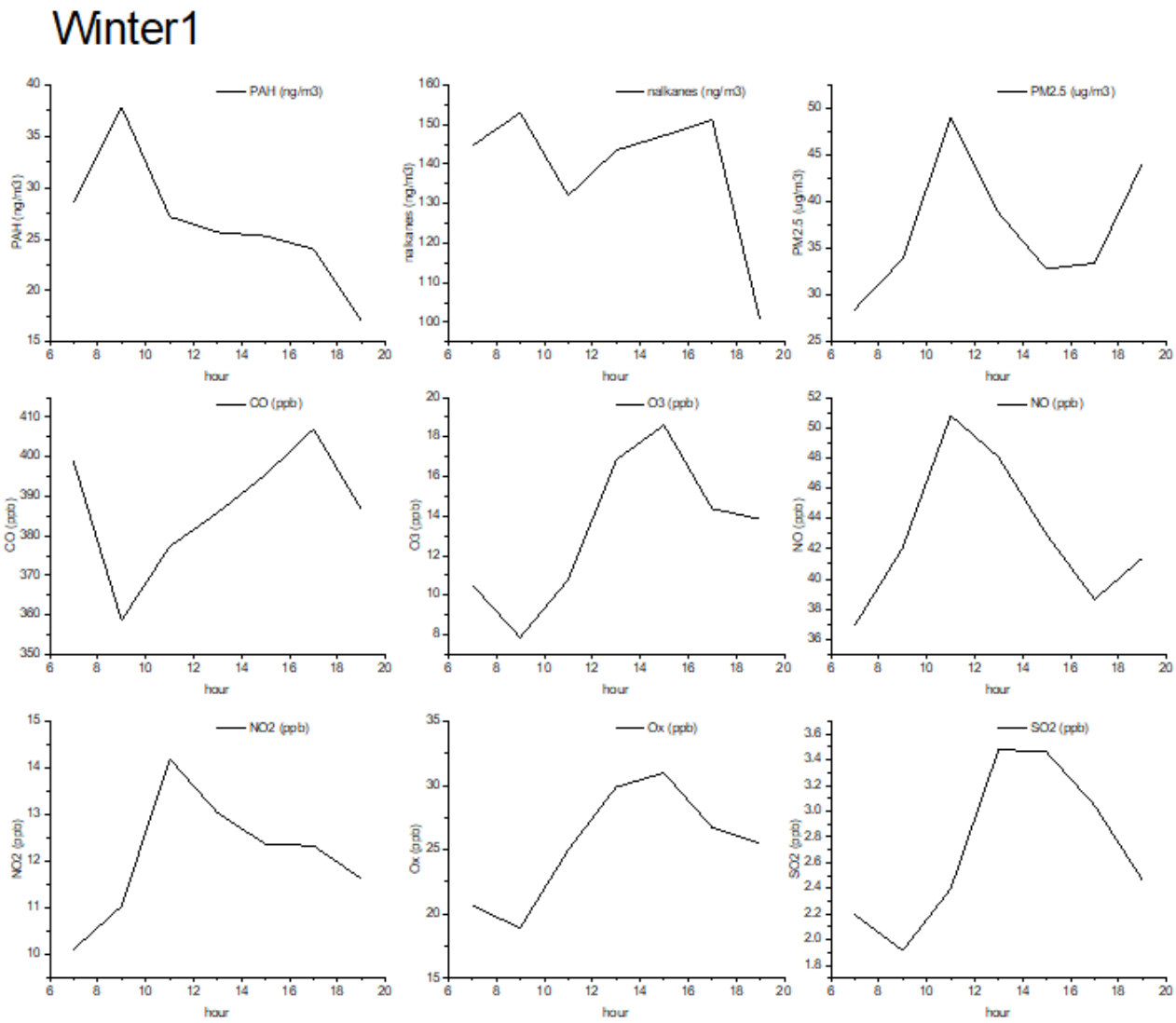


Figure 55. Diurnal variations of chemical components in PM2.5 and gas-phase during sampling week 1

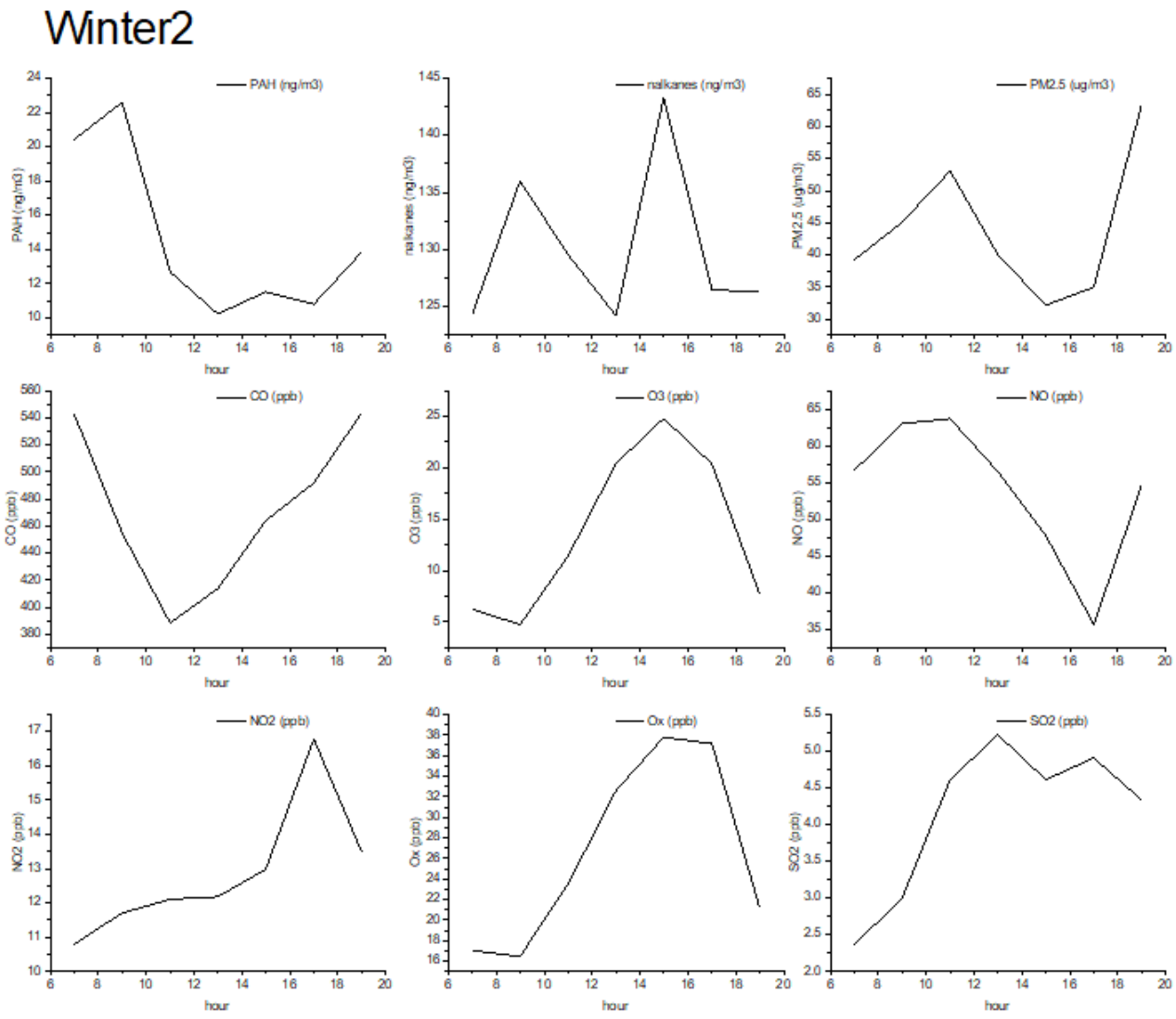


Figure 56. Diurnal variations of chemical components in PM2.5 and gas-phase during sampling week 2

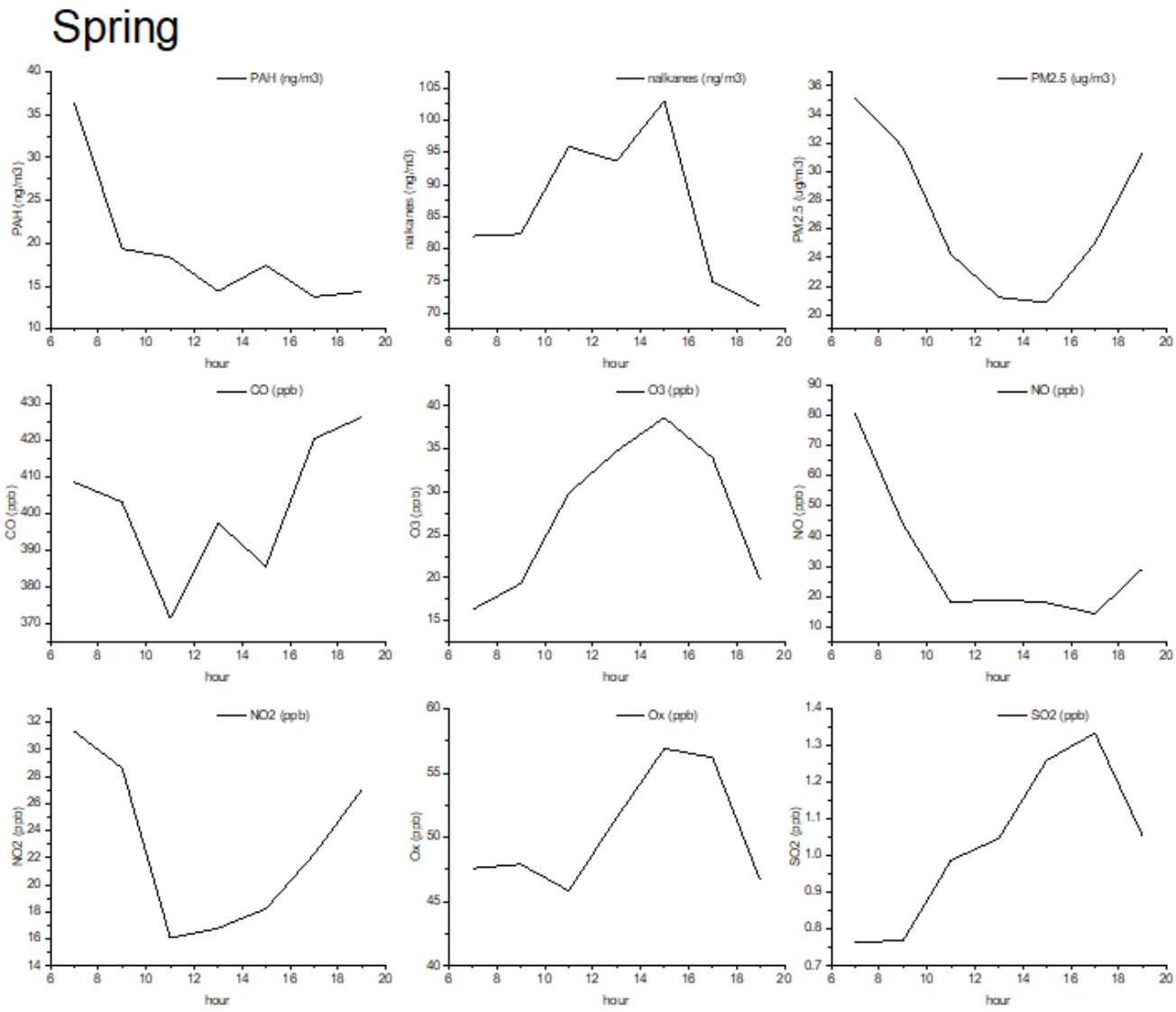


Figure 57. Diurnal variations of chemical components in PM2.5 and gas-phase during sampling week 3

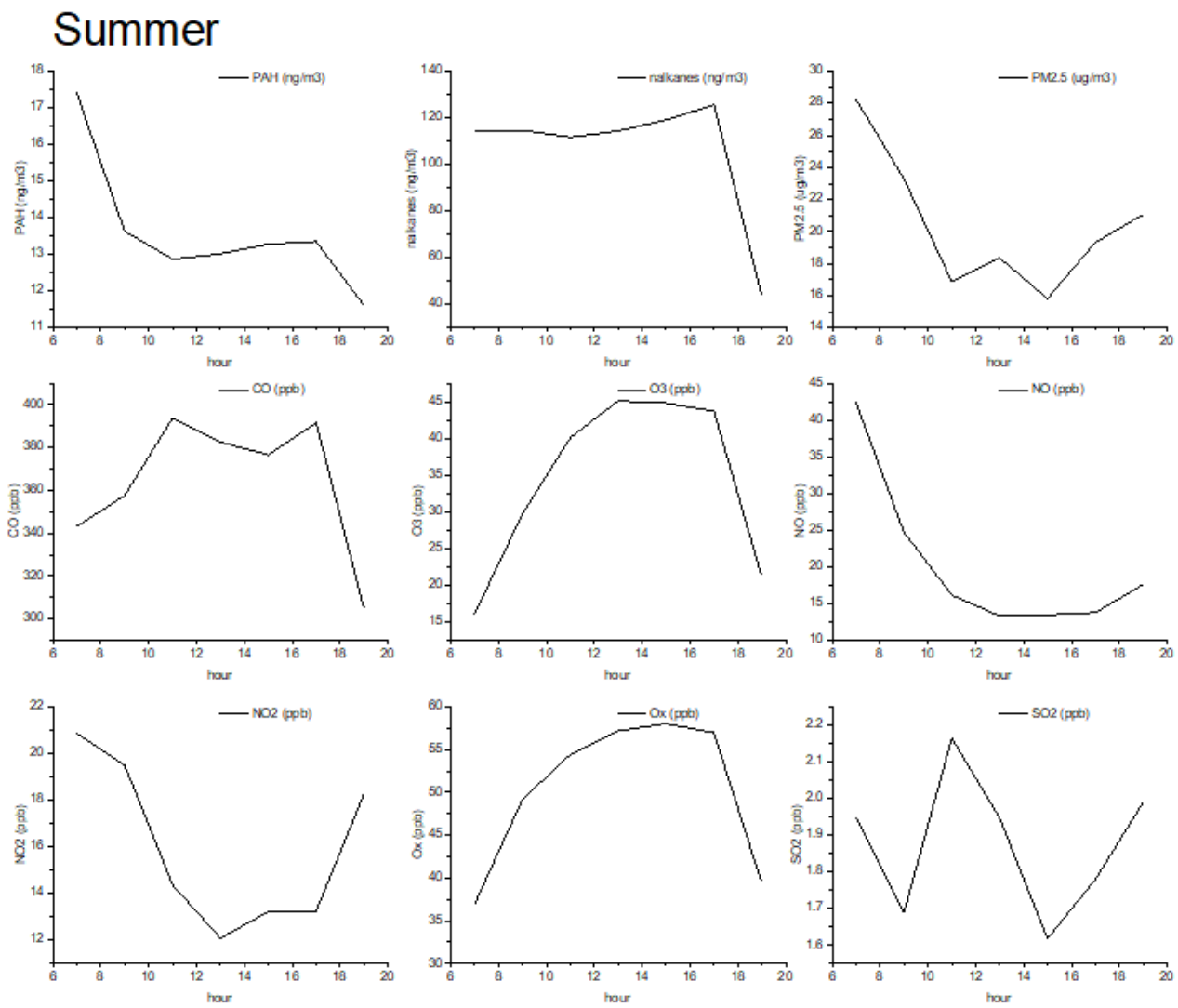


Figure 58. Diurnal variations of chemical components in PM2.5 and gas-phase during sampling week 4

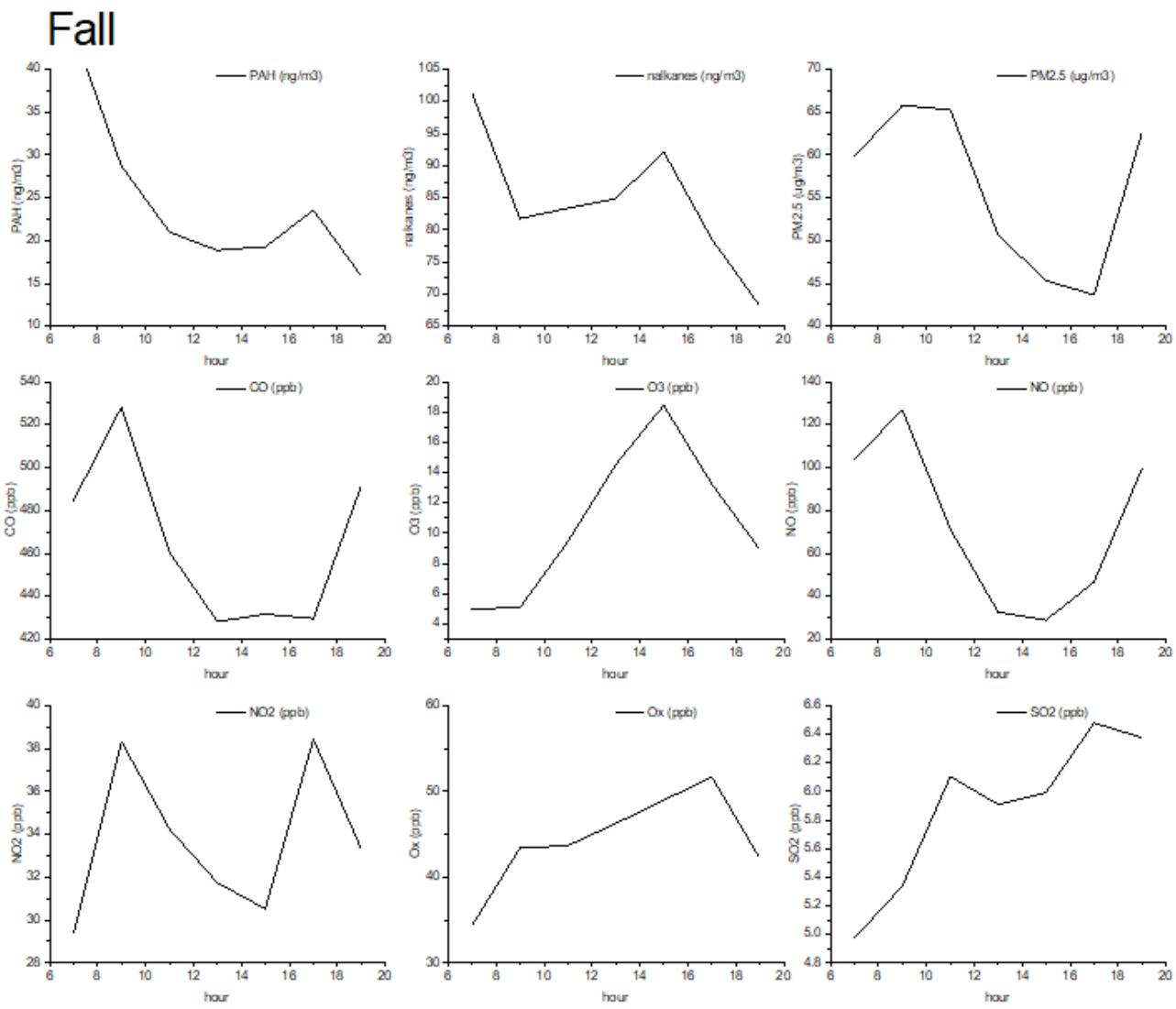


Figure 59. Diurnal variations of chemical components in PM2.5 and gas-phase during sampling week 5

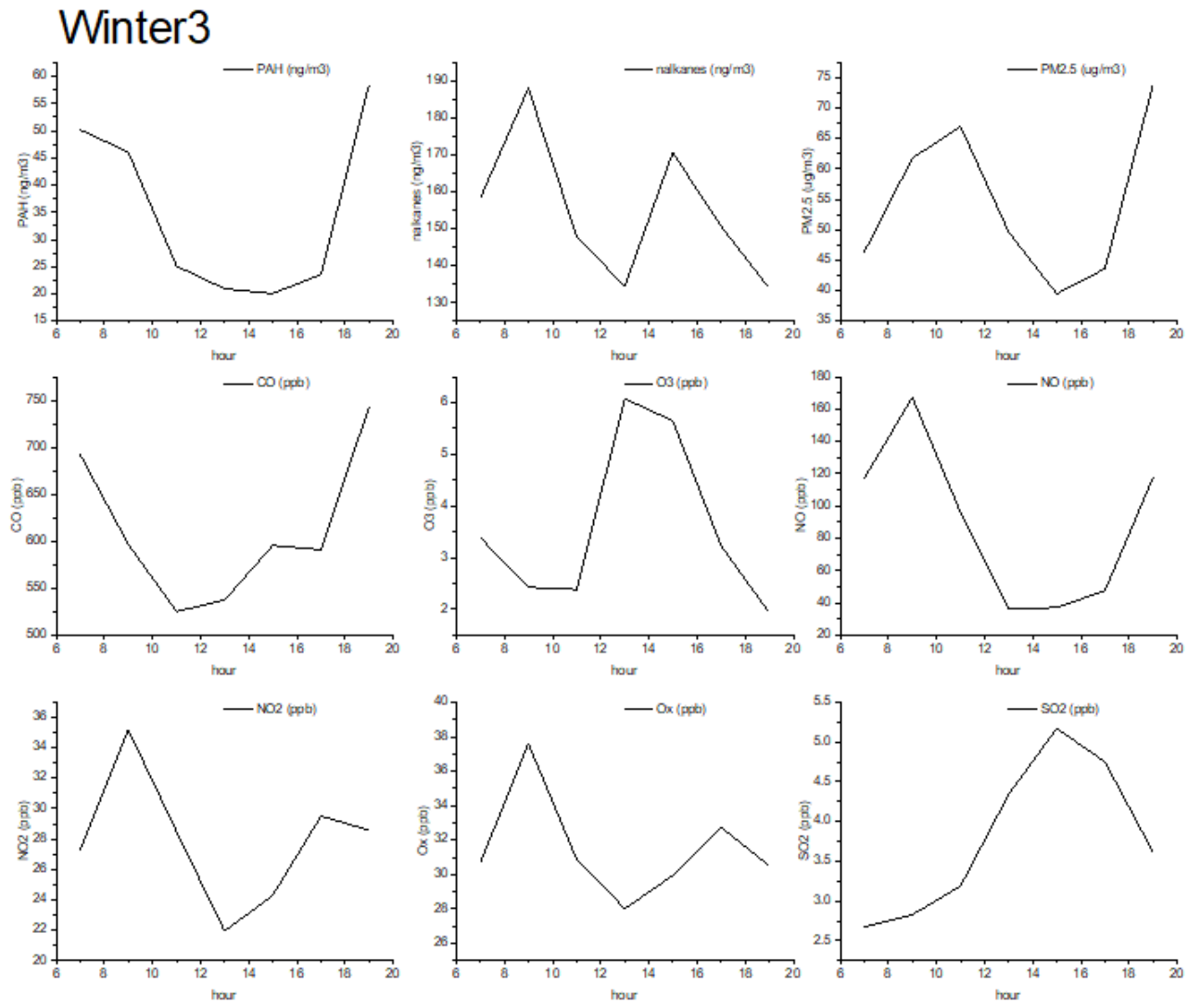


Figure 60. Diurnal variations of chemical components in PM2.5 and gas-phase during sampling week 6

Table 14 shows the seasonal variations of SVOCs and their comparison with other megacities (i.e., Guangzhou, China, Mexico City, and Sao Paulo), urban areas (Bilbao, Spain, Germany, Chicago, USA), and rural area (Chicago, USA) in the world. Average concentrations of PAH and n-alkanes were calculated from all samples collected in each sampling week representing all seasons (~ n=50), and for three sampling weeks representing winter (~n=150).

In this work, significant seasonal variations can be observed with high concentrations during the winter and fall, and lower concentrations during the spring and summer. High concentrations during the winter are expected due to increased emission rates and increased atmospheric stability. Although lower concentrations during the summer than spring are expected due to decrease in emissions and increased photochemical reaction rates, meteorology plays an important role on the transport and dispersion of the pollutants. Temperature plays an important role on the partitioning of SVOCs and PAH show higher concentrations during the spring than during the summer, except the lower volatility compounds Benzo(a)pyrene, benzo(ghi)perylene, dibenzo(a,h)anthracene, and indeno(1,2,3-cd)pyrene, that do not show considerable variations during spring and summer.

Among the selected megacities in Table 8, the highest concentrations can be found in China. Low concentrations of PAH are found in Mexico City followed by Sao Paulo. Average PAH concentrations found in Istanbul are 7-74% as high as those found in Guangzhou. Except, Fluoranthene, pyrene, and chrysene, which were similar, and Benzo(a)anthracene, which was 38% higher during the winter. N-alkanes are generally lower during the winter, except the more volatile fraction C17-C24, however, they are lower than the values found by Schnelle-Kreis et al. (2007) in Germany.

Overall, much lower concentrations were found by Elorduy, et al., (2016) in Bilbao, Spain, which is a region with approximately 1.5 million inhabitants. A very important observation is the very high concentrations that were found in Chicago in late 1990’s which underlines the importance of the development and enforcement of stringent air quality regulations.

Table 13. Comparison with other regions in the world.

| | This work | | | | Wang et al. 2016 | | (Elorduy et al. 2016) | | | | | | | | (Cotham and Bidleman 1995) | |
|---|---|---|---|---|---|---|---|---|---|---|---|---|---|---|---|---|
| | winter avg | spring | summer | fall | winter | summer | summer | fall | winter | (Schnelle-Kreis et al. 2007) | (Mugica et al. 2010) | (Bourotte et al. 2005) | (Viana et al. 2008) | (Cincinelli et al. 2007) | chicago center | rural |
| acenapthylene | 1.29 | 0.58 | 0.81 | 0.49 | ND | ND | ND | ND | ND | - | 0.64 | 0.09 | 0.50 | - | - | - |
| Acenaphthene | 0.09 | ND | ND | ND | ND | ND | ND | ND | ND | - | 0.49 | 0.35 | 0.00 | - | - | - |
| Fluorene | 0.16 | 0.06 | 0.07 | ND | 2.25 | 0.63 | 0.10 | 0.07 | 0.12 | - | 0.29 | 0.00 | 0.17 | - | 92.00 | 4.10 |
| Phenanthrene | 1.49 | 0.62 | 0.51 | 0.84 | 3.00 | 0.58 | 0.17 | 0.19 | 0.39 | - | 0.74 | 0.18 | 0.33 | 21.70 | 159.00 | 9.60 |
| Anthracene | 0.50 | 0.42 | 0.41 | 0.74 | 0.79 | 0.46 | 0.03 | 0.06 | 0.09 | - | 0.67 | 0.00 | 0.03 | 4.48 | 15.00 | 0.05 |
| Fluoranthene | 2.65 | 0.78 | 0.57 | 1.60 | 2.60 | 0.66 | 0.17 | 0.24 | 0.74 | - | 0.86 | 0.68 | 0.37 | 5.85 | 56.00 | 1.70 |
| Pyrene | 2.61 | 0.84 | 0.96 | 1.97 | 2.73 | 0.68 | 0.17 | 0.25 | 0.76 | - | 0.96 | 0.52 | 0.23 | 5.49 | 36.00 | 0.76 |
| chrysene | 2.61 | 0.69 | 0.35 | 2.08 | 2.66 | 0.57 | 0.14 | 0.22 | 0.69 | 3.24 | 1.18 | 0.51 | 0.33 | 1.80 | - | - |
| Benz[a]anthracene | 2.15 | 0.70 | 0.42 | 2.18 | 1.56 | 0.12 | 0.06 | 0.14 | 0.64 | 1.26 | 1.08 | 0.46 | 0.29 | 0.93 | 21.00 | 0.16 |
| Benzo[b]fluoranthene | 3.07 | 0.70 | 0.51 | 3.06 | 4.16 | 0.63 | 0.19 | 0.38 | 2.12 | 4.03* | 1.83 | 1.23 | 0.48 | 0.89 | 39.00* | 0.57* |
| Benzo[k]fluoranthene | 2.25 | 0.41 | 0.36 | 2.76 | 3.41 | 0.73 | 0.11 | 0.12 | 0.56 | | 0.81 | 0.76 | 0.27 | 2.10 | | |
| Benzo[a]pyrene | 1.96 | 0.59 | 0.51 | 3.17 | 4.86 | 0.95 | 0.09 | 0.14 | 0.57 | | | | | | | |
| Benzo[ghi]perylene | 1.95 | 0.82 | 0.81 | 4.48 | 1.47 | 0.74 | 0.15 | 0.19 | 0.61 | | | | | | | |
| Dibenz[a,h]anthracene | 1.46 | 1.19 | 1.19 | 4.60 | 3.88 | 0.54 | 0.05 | 0.07 | 0.24 | | | | | | | |
| Indeno[1,2,3-cd]pyrene | 1.68 | 0.51 | 0.51 | 2.87 | 3.24 | 0.92 | 0.11 | 0.13 | 0.67 | | | | | | | |
| tetradecane | 0.56 | 0.05 | 0.26 | 0.37 | 1.72 | 0.64 | | | | | | | | | | |
| Pentadecane | 1.81 | 0.65 | 0.65 | 0.31 | 3.52 | 0.61 | | | | | | | | | | |
| Hexadecane | 2.66 | 0.47 | 0.64 | 0.32 | 3.02 | 1.14 | | | | | | | | | | |
| Heptadecane | 6.30 | 1.50 | 1.55 | 1.40 | 1.89 | 1.03 | | | | | | | | | | |
| octadecane | 8.82 | 2.33 | 2.67 | 1.36 | 1.21 | 0.69 | | | | | | | | | | |
| nonadecane | 12.58 | 4.22 | 4.10 | 3.13 | 2.00 | 0.64 | | | | | | | | | | |
| eicosane | 14.04 | 6.65 | 5.08 | 4.18 | 0.91 | 030 | | | | 4.71 | | | | | | |
| Heneicosane | 15.21 | 12.88 | 9.80 | 7.03 | 1.03 | 0.27 | | | | 8.95 | | | | | | |
| Docosane | 11.33 | 8.39 | 11.80 | 7.95 | 1.68 | 0.42 | | | | 12.24 | | | | | | |
| Tricosane | 9.70 | 7.12 | 13.09 | 6.92 | 2.89 | 0.75 | | | | 13.80 | | | | | | |
| Tetracosane | 7.58 | 4.90 | 7.27 | 5.62 | 5.64 | 1.13 | | | | 12.04 | | | | | | |
| Pentacosane | 7.21 | 5.49 | 8.48 | 5.41 | 8.10 | 1.03 | | | | 10.77 | | | | | | |
| Hexacosane | 6.26 | 3.87 | 4.70 | 5.11 | 8.16 | 1.47 | | | | 13.15 | | | | | | |

| | This work | | | | Wang et al. 2016 | | (Elorduy et al. 2016) | | | | | | | | (Cotham and Bidleman 1995) | |
|---|---|---|---|---|---|---|---|---|---|---|---|---|---|---|---|---|
| | winter avg | spring | summer | fall | winter | summer | summer | fall | winter | (Schnelle-Kreis et al. 2007) | (Mugica et al. 2010) | (Bourotte et al. 2005) | (Viana et al. 2008) | (Cincinelli et al. 2007) | chicago center | rural |
| Heptacosane | 7.16 | 5.15 | 6.81 | 6.14 | 738 | 2.04 | | | | 9.05 | | | | | | |
| Octacosane | 4.68 | 3.19 | 2.81 | 3.85 | 5.59 | 2.18 | | | | 9.35 | | | | | | |
| Nonacosane | 5.49 | 4.17 | 6.15 | 6.30 | 8.82 | 2.49 | | | | 4.71 | | | | | | |
| Triacontane | 3.91 | 2.82 | 2.73 | 3.96 | 5.73 | 1.96 | | | | 8.40 | | | | | | |
| Hentriacontane | 6.74 | 4.52 | 6.14 | 7.34 | 12.8 | 2.89 | | | | 2.30 | | | | | | |
| Dotriacontane | 3.52 | 2.43 | 2.03 | 4.14 | 4.60 | 134 | | | | 2.30 | | | | | | |
| Tritriacontane | 3.81 | 2.50 | 2.56 | 4.68 | 6.28 | 1.60 | | | | 0.48 | | | | | | |
| Tetratriacontane | 1.96 | 1.42 | 1.24 | 2.82 | 3.13 | 0.70 | | | | | | | | | | |
| Pentatriacontane | 1.49 | 1.06 | 1.16 | 2.75 | 2.60 | 0.60 | | | | | | | | | | |
| Hexatriacontane | 1.03 | 0.66 | 0.89 | 2.47 | 1.74 | 0.29 | | | | | | | | | | |
| Heptatriacontane | 0.55 | ND | 0.82 | 2.62 | 1.29 | 0.02 | | | | | | | | | | |
| Octatriacontane | 0.12 | ND | 1.13 | 3.04 | 0.60 | ND | | | | | | | | | | |
| Nonatriacontane | 0.91 | ND | 2.62 | 3.74 | 0.30 | ND | | | | | | | | | | |

### 5.9 Cluster analysis

Air mass trajectories were obtained for each 2h and 12h sample time during the day and during the night. These high-time resolved air mass trajectories provide input about specific sources of air pollutants during that short period of time. In order to simplify air mass trajectories, the clustering option of HYSPLIT model was used to group air masses according to mean trajectories during the day and during the night in separate runs. The model was run with a number of clusters that resolved approximately 75% of the total variance during that specific week. The total number of mean trajectories were 5 for winter week 1 and summer and 4 for the rest of the sampling weeks (winter week 2 and 6, spring, and fall). Figures 47-52 show the cluster means (left), box plot of total SVOC concentrations associated to each trajectory during the day and night (middle), and frequency analysis for each cluster (right). The influence of other meteorological parameters to total and individual SVOC concentrations will be analyzed in the following section.

During week 1 (Fig 47), northern trajectories were predominantly observed with 63% of the total frequency. Concentrations associated to northerly clusters 1, 2, and 3 had similar variations. Cluster 2 had a very short trajectory possibly transporting emissions from ships, industrial region, and residential areas in the Anatolian side, therefore the average concentrations are slightly higher. Cluster 4 is associated to the highest concentrations, since it follows the trajectory of large transatlantic ships moving from the Marmara Sea through the Bosphorous. The lowest concentrations are observed during cluster 5, which is associated to a longer southwestern trajectory possibly carrying cleaner wind from the Marmara Sea. In addition, to southern trajectory, this air mass mean trajectory was observed on 03-04 Feb 2017, which also showed lower concentrations of $PM_{2.5}$, possibly due to decrease in residential heating due to higher temperatures at the end of the week. The box referring to night samples shows mixed trajectories and therefore the effect of wind direction can’t be explained in this section.

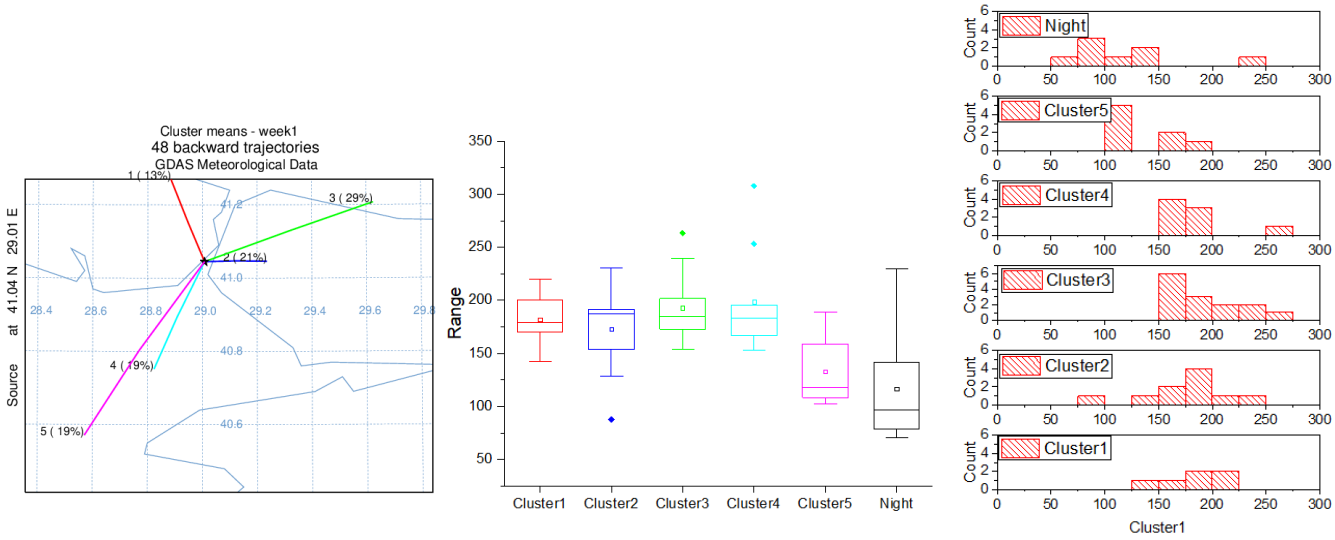


Figure 61. Cluster analysis and box plot of total SVOC concentrations during sampling week 1

During winter week 2 (Fig 48), all of the trajectories during the day showed southern trajectories. Concentrations increased in the following order: short trajectory from Bosphorus (cluster 1, 14%), SW trajectory from Marmara Sea (cluster 2, 33%), downtown (cluster 3, 33%), and trajectory of large trans-Atlantic ships (cluster 4, 19%). The highest concentrations were associated to cluster 4 which could be related to emissions from large transatlantic ships, in addition to emissions, high concentrations are due to a combination of low wind speed, high $PM_{2.5}$ concentrations that provide sorption surface area, and a stable atmosphere and inversion layer due to an increase in the atmospheric pressure, particularly early on 19 February.

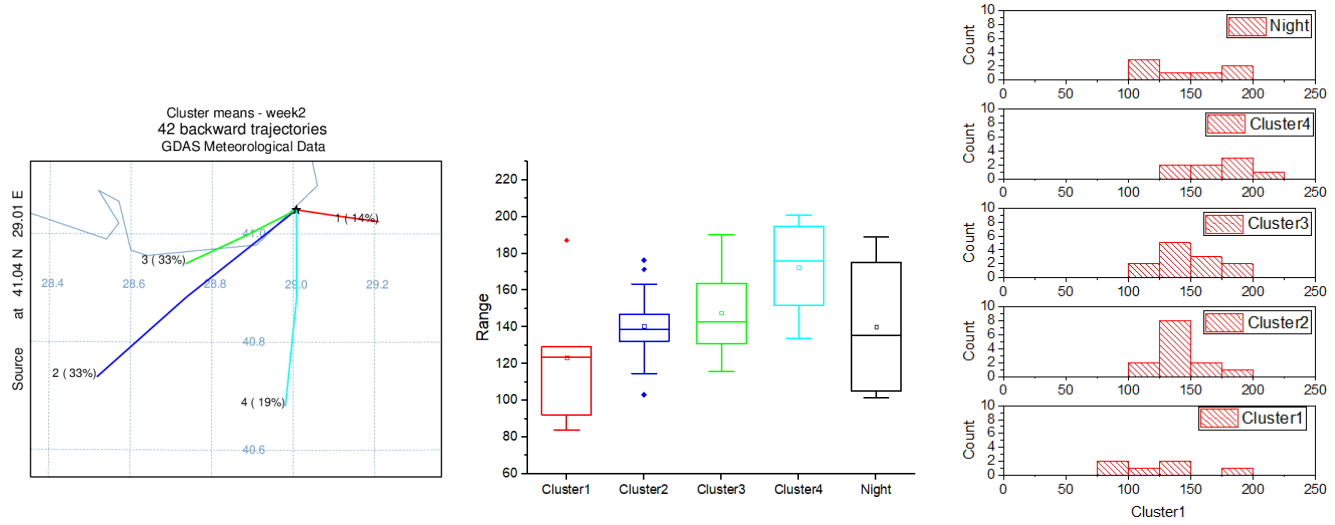


Figure 62. Cluster analysis and box plot of total SVOC concentrations during sampling week 2

In the spring (Fig 49), air masses during the day had two northern trajectories with similar direction and frequency of 57%. Two SW cluster means were divided into a longer trajectory (33%) and a very short trajectory (10%) carrying winds close to the sampling station in Beşiktaş. Contrary to during the winter, the southern trajectory bringing winds from downtown, these southern trajectories during the spring are associated to lower concentrations possibly due to the lack of residential heating emissions. Concentrations observed during the night were also high possibly due to low mixing heights and stable atmosphere that concentrates the air pollutants emitted during the day. The highest concentrations were found during both NE trajectories (clusters 1 and 2) observed on 3-5 and 9 May. A slight high pressure system observed during these 4 days with the lowest mixing heights, in addition to slightly higher wind speeds favoring transport of pollutants from the Black sea may be the reason for increased concentrations.

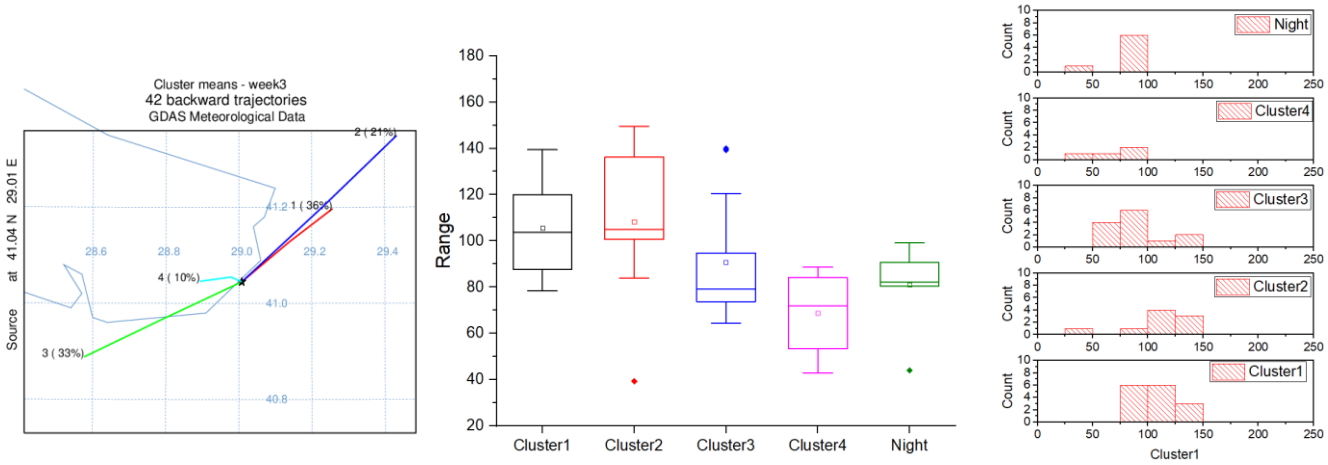


Figure 63. Cluster analysis and box plot of total SVOC concentrations during sampling week 3

During the summer (Fig 50). Air masses were all associated to northern trajectories with similar concentrations as cluster 1 and 2 during the spring (Fig 35). In addition to traffic close to the sampling station, northern trajectories may be transporting ship emissions in the Black Sea region and Bosphorus. Nighttime samples showed the lowest average concentrations with large variations. During the summer, mixed boundary layer heights were observed at night. Wind speed was also relatively higher compared to spring, which may favor transport from the Black sea. These conditions may be the reason for large variations in concentrations at night.

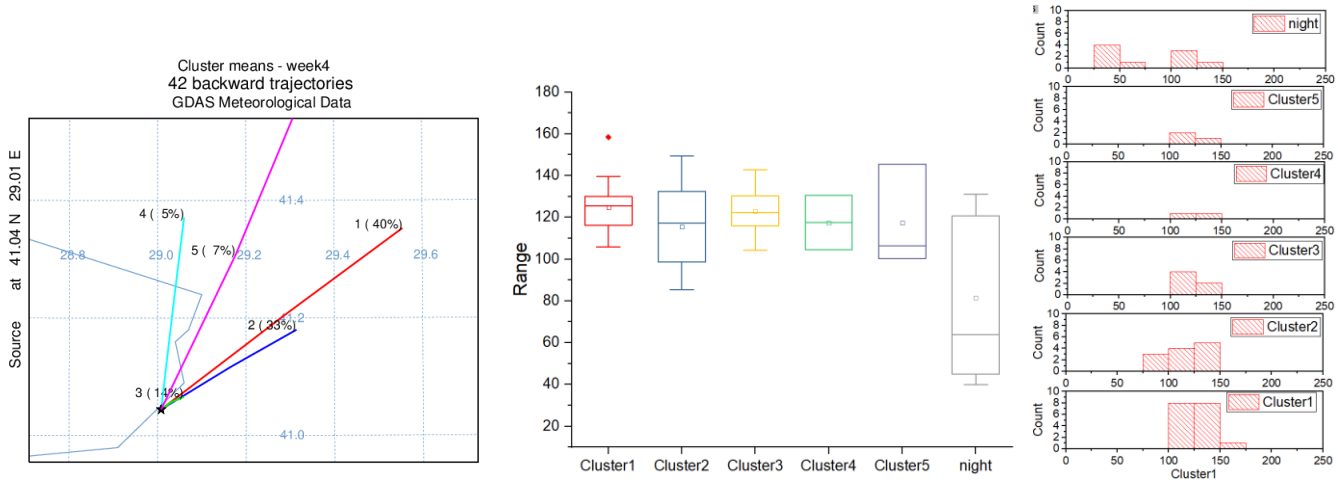


Figure 64. Cluster analysis and box plot of total SVOC concentrations during sampling week 4

During the fall (Fig. 51), 4 cluster means were obtained. Two northerly trajectories had a combined 36% frequency, one trajectory from SE with 29% frequency, and one SSW trajectory had the highest frequency of 36%. Overall, average concentrations from all trajectories show similar values. Higher concentrations are observed during southerly winds, while lower concentrations are observed during northerly winds. Higher concentrations during southerly trajectories (clusters 1 and 3) were found on days with lower wind speed (20-24 october), slightly higher atmospheric pressure, and higher $PM_{2.5}$ concentrations. Although overall, high relative humidity and very mixing heights were observed during the whole week and could also influence partitioning of SVOCs into the particle phase and accumulation of pollutants.

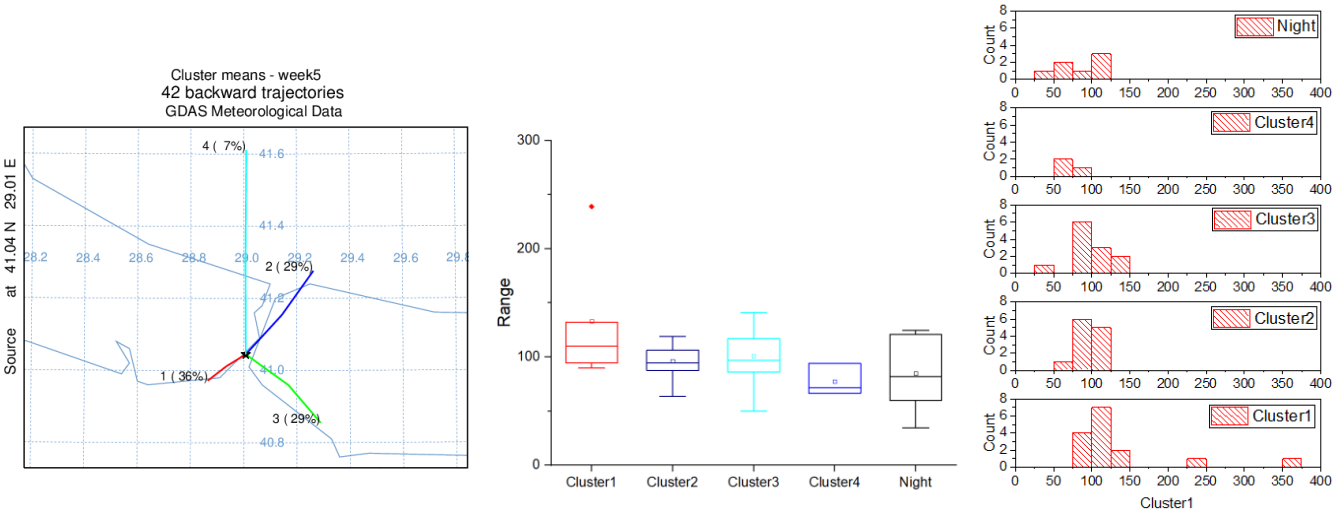


Figure 65. Cluster analysis and box plot of total SVOC concentrations during sampling week 5

Two southerly (SSW, S) and two northerly (NE, NNW) cluster means were obtained during winter week 6 with frequencies of 57% and 43%, respectively (Fig. 52). Average concentrations during winter week varied ~140-200 ng/m3. Low concentrations were observed during northerly trajectories, however very high concentrations were associated to a very short trajectory from the Bosphourus with high frequency of 38%. High concentrations were also observed during the night. Overall, higher average and maximum concentrations were observed in winter week 6 compared to winter weeks 1 and 2. Although temperature was higher in winter week 6, a very high pressure system caused very low mixing heights and wind speed. Contrary to week 1 that showed large mixing height and higher wind speed, particularly during the first 4 days of the sampling week. Overall, the observed concentrations are the results of a complex relationship between emissions and meteorology that determine both transport and dispersion of pollutants.

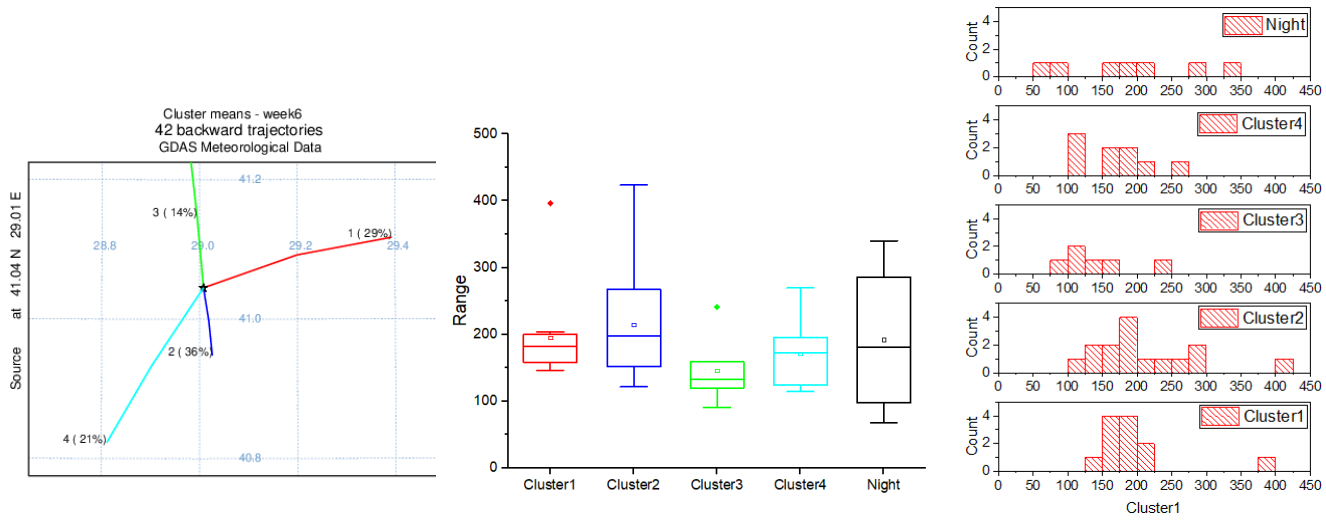


Figure 66. Cluster analysis and box plot of total SVOC concentrations during sampling week 6

### 5.10 Regression analysis

Multiple regression analysis was performed to understand the cumulative influence of meteorological parameters and traffic to the total concentrations of PAH and n-alkanes in datasets obtained for all sampling weeks. Due to differences in meteorology and traffic variations, separate analysis was performed for day and night samples. Table 9 shows the optimized cumulative $R^2$ obtained with multiple regression analysis and the variables that resolve the variance of the data for each sampling week and season.

Overall, it can be observed that the variance of the observed concentrations is due to a complex mixture of meteorological conditions and sources during each season. In this work, only traffic has been considered as emission source. PAH show slightly greater cumulative $R^2$, possibly because n-alkanes show greater variations in vapor pressures. Similarly, better cumulative R2 are usually obtained during night samples due to less variations in meteorology and traffic than during daytime samples. Multiple regression analysis yielded poor results during the summer, spring, and fall for daytime samples. This is due to very different meteorology conditions such as lack of dominant wind direction, variable wind speeds, high solar radiation, etc. Multiple regression analysis yielded the best cumulative R2 during the winter weeks in the following order: Week 1>week 3>week 2 for both PAH and n-alkanes with 0.75, 0.67, and 0.54 for PAH and 0.63, 0.42, and 0.38 for n-alkanes, respectively.

The addition to emission sources such as fuel combustion (i.e., coal, liquid fuel, etc), ship emissions, plane emissions, etc, may be useful in the near future in order to find the variables that are able to resolve the maximum variance in the SVOC concentrations. In this work, different factors were found during different seasons and for PAH and n-alkanes. For example, during week 1, 75% of the total PAH concentrations can be resolved by the various meteorological conditions. According to the results, the most important variables for concentrations during the day are: temperature (32%), wind speed (15%), wind direction (16%), and mixing coefficient (7%). The maximum contribution that could be obtained for n-alkanes was 63%. The most important variables during the day are temperature (14%), traffic (15%), and pressure (26%).

Table 15 shows the results of multiple regression analysis performed with optimized parameters for PAH and n-alkanes during day and night in separate.

### PAH analysis during the day

During winter week 1, PM2.5, temperature, relative humidity, and wind direction are able to resolve 73% of the variance of PAH concentrations. PM2.5 and temperature alone account for 26% and 21% of the variation, respectively. The high correlation with PM2.5 (r=0.46, Table 16) during the day is due to the fact that a high fraction of PAH are emitted in the particle phase. In addition, the high negative correlation with temperature (r=-0.56) indicates that at low temperature partitioning of PAH is preferred onto the fine particles suspended in the air. Relative humidity alone explains 15% of the variance. Positive correlation with relative humidity (r=0.34) may indicate that as PAH are in the particle phase, particles absorb water vapor and precipitate due to dry deposition mechanisms. Wind direction contributes in a less extent (9%) to the variation of the PAH concentrations obtained at high time resolution. Since the location of the station is located next to a busy avenue, traffic emissions are expected to dominate PAH concentrations. However, low radiation observed in winter week 1 may be the reason for low photochemistry and may result in transport from nearby areas. As can be observed in Fig. 61, the highest concentrations are observed during air mass trajectories transporting winds from large transatlantic emissions.

During winter week 2, wind direction, dew point, and traffic were the most important variables that contributed to 57% of PAH concentrations. Wind direction alone was able to resolve 41% of the variation as is also confirmed by high correlation coefficients of -0.65. Week 2 was completely dominated by southern winds as can be observed in Fig. 27b. Figure 62 shows a clear distinction of variation in concentrations with short wind trajectories represented as local sources. Similarly to winter week 1, the highest concentrations are associated to emissions from large transatlantic ships. 10% and 6% of the variation of the data are due to dew point and traffic, respectively. During week 2, a very low boundary layer and wind speed were observed. High photochemical reactivity of PAH was due to lack of dispersion of oxidants as can be observed by marked diurnal changes in Fig. 56. It is possible that dew point and traffic contributed to condensation of PAH and increased emissions, respectively. In addition, high correlation with temperature (r=-0.6, Table 17) provides similar effect as dew point to promote condensation of PAH into the particle phase.

During spring, a greater number of variables contributed to the total variance of PAH concentrations. Overall, temperature, wind direction, wind speed, precipitation, dew point, pressure, and solar radiation contributed to 42% of the variance. The highest contribution was given by temperature (17%) and wind direction (5%). During this sampling week, greater radiation values and temperature were observed. Since temperature determines partitioning into gas- and particle-phases, concentrations of PAH in the particle phase may be determined by both partitioning and photochemical reactions. In addition, an important precipitation event contributed to a decrease in concentrations due to wet deposition mechanisms. Overall, these changes complicate the accurate identification and quantification of the effect of meteorology and traffic.

During the summer, PM2.5, solar radiation, pressure, temperature, and relative humidity contributed to 42% of the variation of the data. PM2.5 concentrations and solar radiation contributed to 20% and 11%, respectively. This is confirmed by high correlation coefficients between PAH and PM2.5 (r=0.46, Table 19) and solar radiation (r=-0.42). The positive correlation with PM2.5 and NO (r=0.61) indicates that PAH are emitted by traffic in the particle phase. The negative correlation with solar radiation and ozone (r=-0.63) indicate a decrease in concentration due to photochemical reactions.

During the fall, the cumulative effect of traffic, boundary layer height, pressure, solar radiation, and wind speed were able to explain 30% of the variation of PAH concentrations. As confirmed by correlation coefficients, high correlation between PAH and traffic was observed with r=-0.56 (Table 20). The negative correlation may be explained in this particular sampling site in which a decrease in vehicle counts during high congestion may result in higher emissions of PAH that are collected immediately. Variations in boundary layer height, pressure, solar radiation, and wind speed contributed each to 4-6% the PAH concentrations.

During winter week 3, a higher variance of 68% was resolved by PM2.5, traffic, solar radiation, wind speed, and relative humidity. Only PM2.5 concentrations and traffic resolved 42% of the variance with 29 and 13% each. Variations in solar radiation, wind speed, humidity, and dew point resolved each 9, 6, 3, and 8% of the variance. In addition, very high correlations between PAH and gases were found. Correlation coefficient between PAH and NO and CO were 0.81 and 0.59, respectively, which indicates emission by traffic. High negative correlations with boundary layer (r=-0.54, Table 21) and ventilation coefficients (r=-0.53) indicate poor dispersion during winter week 3.

### PAH analysis during the night

During the night, due to less variations in meteorological conditions, high correlations are obtained with a less number of variables. Overall, three variables resolved over 94% of the variance. Except summer in which only 37% of the variance of PAH concentrations was resolved.

In winter week 1, PM2.5, temperature, and wind speed resolved 95% of the variance. PM2.5, alone resolved 89% of the variance and 3% due to temperature and wind speed each. Very high correlations with NO (r=0.92, Table 16) and CO (0.89) indicate emissions by traffic. High positive correlation with PM2.5 (r=0.94) and negative correlation with temperature indicate (r=-0.18) that both emission and condensation are responsible for PAH concentration in the particle phase at night. A high negative correlation with wind speed (r=-0.83) and ventilation coefficient (r=-0.52) indicate poor dispersion conditions during winter week 1.

In winter week 2, dew point, pressure, and precipitation resolved 97% of the PAH variance at night. Only dew point resolved 78% of the variance, while pressure and precipitation contributed to 11 and 7%, respectively. Similarly to week 2, high positive correlation coefficients are observed for PM2.5 (r=0.79, Table 17), NO (r= 0.83), and CO (r=0.76) which indicate emissions by traffic. High negative correlation coefficients are found with O3 (r=-0.82), temperature (r=-0.7), dew point (r=-0.88), and wind speed (r=-076).

In spring, solar radiation, boundary layer, and PM2.5, resolved 96% of the variance in PAH concentrations at night. The major contribution was from solar radiation that explains 49% of the variance and boundary layer height that explains 41% of the variance. Variations in PM2.5, concentrations represent 6% of the variance in PAH concentrations. High correlation coefficients with NO (r=0.6, Table 18) and CO (r=0.56) confirm that a fraction of PAH are emitted by traffic during the night.

In summer, relative humidity, wind speed, and pressure resolved 37% of the variance of PAH concentrations. Relative humidity was the most important parameter during the night with 27% of the variance explained. Wind speed and pressure contributed each to 9 and 1% of the variance. High correlations with relative humidity are observed (r=0.52, Table 19) at night. High positive correlation with wind speed

(r=0.52) and lack of correlation with NO and CO may indicate that in the summer, PAH concentrations are transported to the sampling location from nearby areas.

During the fall a combination of precipitation and wind direction are able to resolve 74% of the variance. During the night, the contribution of both precipitation and wind direction are nearly identical with 40% and 34% of the variance explained each. A precipitation event contributed to a decrease in concentrations as can be observed by high negative correlation coefficient between PAH and precipitation (r=-0.63, Table 20). High correlation coefficients with NO (r=0.73) and CO (r=0.67) confirm that a large fraction of PAH are emitted by traffic during the night and the rest may be transported by the wind.

During winter week 3, PM2.5, temperature, and wind speed were able to resolve 94% of the total PAH variance. Only PM2.5, resolved 88% of the variance. Smaller contribution was observed by temperature and wind speed with 3% each. This analysis can be confirmed by high correlation coefficients between PAH concentrations and NO (r=0.91, Table 21), CO (r=0.94), and high negative correlation coefficient with wind speed (r= -0.55) which indicate that PAH are emitted in the particle phase by traffic and further dispersed by wind.

### n-alkane analysis during the day

Lifetime of n-alkanes against OH concentrations vary on the order of 0.5-1.4 day. Therefore, the dynamics of n-alkanes in the atmosphere is more complex than PAH. They are capable of dispersing, accumulating, and transporting from nearby locations. Overall, less variation of the n-alkanes could be resolved by linear regression analysis compared to PAH, particularly during the day, which is when radiation, boundary layer height, mixing coefficients, and concentration of oxidants are higher.

During winter week 1, 61% of the variation was resolved by pressure, dew point, traffic, ventilation coefficients, and particulate matter. Pressure alone was able to resolve 35% of the variance. Variations in dew point and traffic resolved 22 and 4% of the n-alkane concentrations, respectively. During winter week 1 at daytime, PAH concentrations showed high correlation with temperature (r=-56). N-alkanes on the other hand, showed high negative correlation with dew point (r=-0.58). During winter week 1, diurnal variations of temperature ranged from 2.5-6 °C, while dew point ranged -0.75-0.5°C. It is possible that since n-alkanes show a wider range of physicochemical properties, their condensation on fine particles is better represented by dew point temperature.

During winter week 2, humidity, traffic, precipitation, dew point, and PM2.5 resolved 42% of the n-alkane concentration. Humidity alone was able to resolve 21% of the variation, while traffic, precipitation, dew point, and PM resolved approximately 4-6% each. During week 2, high humidity and precipitation event were observed. A decrease in PM concentrations was also observed during the precipitation event. It is possible that low correlation coefficients during week 2 are due to the presence of high humidity, precipitation events, and lower boundary layer. These conditions may have contributed to a decrease in concentrations due to dry and wet deposition, and increased photochemistry, respectively. Significant correlations were observed with SO2 (r= 0.53) and temperature (r=0.54), however, the correlations can't be explained at the moment.

During spring, 56% of the variation in n-alkane concentrations during the day is explained by dew point (40%), wind direction (3%), pressure (8%), and precipitation (5%). During summer, 33% of the variance is resolved by pressure, mixing layer height, and solar radiation. Mixing layer height is the factor that contributes the most to the variance of n-alkanes with 31%. It is possible that the complex dynamics of the atmosphere caused by increased radiation, mixing layer height, and various precipitation events throughout spring sampling week is responsible for mixing, dispersion, transport and deposition of n-alkanes and therefore a greater fraction of the concentration is unexplained by the linear regression model.

During the fall, 40% of the variance of high-time resolved n-alkanes observed during daytime was explained by mixing layer height, precipitation, dew point, solar radiation, pressure, and PM2.5 concentrations. 20%, 11%, and 5% of the variance were due to mixing layer height, precipitation, and dew point, respectively. This coincides with negative correlation coefficients between n-alkane concentrations and boundary layer height (r=-0.51) and precipitation (r=-0.34), and positive correlation coefficient with dew point (r=0.42).

During the winter, 42% of the variance is explained by boundary layer height (20%), PM2.5 concentration (6%), solar radiation (5%), wind direction (5%), dew point (4%), and traffic (2%). Concentrations of n-alkanes during winter week 3 were the highest overall due to low dispersion conditions as can be observed by high correlations with boundary layer height (r=-0.5) and ventilation coefficients (r=-0.47). High correlations with PM2.5 (r=0.44), CO (0.4), and NO (r=0.57) indicate a fraction of n-alkanes are associated to traffic emissions.

### n-alkane analysis during the night

During the night, due to less variations in meteorological conditions, high correlations are obtained with less number of variables. Overall, two and three variables resolved over 74% of the variance. At night, PM2.5 concentration was usually the most important factor for all seasons.

During winter week 1, PM2.5 and traffic resolved 89% of the variance of n-alkane concentrations at night. Variations of PM2.5 concentrations and traffic alone resolved 65% and 24% of the n-alkane concentrations at night. These results coincide with high Pearson correlation coefficients between n-alkanes and PM2.5 and traffic with r=0.81 and r=-0.54, respectively. Correlation coefficients with traffic may be a good indicator about the effect of emissions to PM2.5, PAH, and n-alkanes. However, in Barvaros Bulevar traffic congestion which is quantified as low traffic flow, may contribute to higher emissions of SVOCs and PM2.5, therefore, small or even negative correlation coefficients may result. During week 1, a negative high correlation was observed, which is an indicator for higher emissions at low traffic counts. This is corroborated with high Pearson correlations with CO (r=0.55) and NO (0.78) which are emitted by traffic. As observed before, dew point is an important variable that influences condensation of n-alkanes to the particle phase. High correlation coefficient of r=-0.61 was obtained between n-alkanes and dew point.

During winter week 2, 74% of the variance was resolved by PM2.5, temperature, and boundary layer height. During this week, solar radiation, boundary layer height, and ventilation coefficients decreased (Fig. 22). In addition, wind direction was predominantly from southern directions (Fig. 62), and a precipitation event and high relative humidity were observed throughout the week (Fig. 16). This may have caused accumulation of n-alkanes at night due to lower mixing and dry and wet deposition due to high humidity and precipitation, respectively. Significant correlations were obtained with CO (r=0.84), traffic (r=0.41), precipitation (r=-0.42). It is possible that low correlation with NO (r=0.13) is due to its higher solubility in water (56 mg/L, 20C) compared to CO (27 mg/L, 25C). NO can combine with water to produce nitrous acid (HNO2). During winter week 2, high humidity and low dew point, a slight precipitation event with scattered rain, and fog were observed throughout the week (Fig. 16, Fig. 22, (https://www.timeanddate.com/weather/@745044/historic?month=2&year=2017)

During spring, 96% of the variance was resolved by PM2.5, boundary layer height, and wind direction. PM2.5, alone was able to resolve 83% of the n-alkane variance during the night. Whereas Boundary layer height and wind direction contributed to 5 and 7%, respectively. High correlations of n-alkanes

with PM2.5 (r=0.76), NO (0.51), and CO (0.82) indicate that an important fraction of n-alkane are related to vehicle emissions. While negative correlation with ozone (r=-0.67) and ventilation coefficient (r=-0.64) indicate oxidation and dispersion at night. A lower contribution to the variance of 7% from wind direction (r=0.43) may be due to ship emissions since high concentrations of SVOCs are associated to short northern trajectories from the Bosphorous.

During summer, 76% of the variance is resolved by wind direction (48%), temperature (20%), and humidity (8%). During summer high concentrations of n-alkanes were observed. As it can be observed in Fig. 64, the short air mass trajectories favored the northern direction. High correlations with NO (0.88) and CO (0.80) and wind speed of 3 m/s during the night, low boundary layer heights and inversion layer (Fig 24, Table 5) indicate that concentrations of n-alkanes are partly due to vehicle emissions close to the sampling site and ship emissions and transport from the Bosphorous. High negative correlations with temperature (r=-0.54) indicate that during the night, the decrease in temperature from 26 to 21°C favors condensation on the particle phase.

During the fall, 82% of the variance was resolved by PM2.5, dew point, and wind direction. The majority of the variance is due to PM2.5 concentrations (66%), followed by 15% due to dew point. Wind direction contributed to 2% of the variance of n-alkane concentrations at night. During the night, temperature inversions were observed all days in the fall season. For this reason, due to high stability in the atmosphere, very high positive and negative correlation coefficients were observed with PM2.5 (0.97), NO (0.86), CO (0.98), traffic (r= 0.77), wind speed (r=-0.7), boundary layer height (r=-0.92), ventilation coefficient (r=-0.87), and ozone (-0.72).

During winter week 3, 98% of the total variance of n-alkane concentrations was resolved by PM2.5 and relative humidity. Only PM2.5 concentrations resolved 95% of the variance. The remaining 4% was due to relative humidity. During winter week 3, temperature inversions were observed all days, except on 10 jan 2018. In addition, very low wind speed of 1.3 m/s was observed at night (Fig 26). Due to very high stability of the atmosphere during winter week 3 (Table 5), significant positive and negative correlation coefficients were observed with PM2.5 (0.97), NO (0.95), CO (0.97), traffic (r= 0.46), wind speed (r=-0.57), and boundary layer height (r=-0.49). Significant correlation coefficients with ozone were not observed during winter week 3 at night due to very low photochemical production of ozone and possibly OH, the background concentration at night was very low.

Table 14. Optimized cumulative $R^2$ obtained with multiple regression analysis

| | PAH | | n-alkanes | |
|---|---|---|---|---|
| | **R2** | **variables** | **R2** | **Variables** |
| **Winter week 1** | | | | |
| **Day** | 0.73 | PM, T, RH, WD | 0.60 | P, DewP, traff |
| **Night** | 0.95 | PM, RH, WD | 0.89 | PM, traffi |
| **Winter week 2** | | | | |
| **Day** | 0.57 | WD, DewP, traff | 0.42 | RH, traff, precip, DewP, PM |
| **Night** | 0.97 | DewP, P, Precip | 0.74 | PM, T, BLH |
| **Spring** | | | | |
| **Day** | 0.42 | T, WD, WS, Precip, DewP, P, Solar | 0.56 | DewP, WD, P, Precip |
| **Night** | 0.96 | Solar, NOAAB, PM | 0.96 | PM, BLH, WD |
| **Summer** | | | | |
| **Day** | 0.43 | PM, Solar, P, T, RH, DewP | 0.33 | P, BLH, Solar |
| **Night** | 0.37 | RH, WS, P | 0.76 | WD, T, RH |
| **Fall** | | | | |
| **Day** | 0.3 | traff, BLH, P, Solar, WS | 0.4 | BLH, Precip, DewP, Solar, P, PM2.5 |
| **Night** | 0.74 | Precip, WD | 0.83 | PM, DewP, WD |
| **Winter week 3** | | | | |
| **Day** | 0.69 | PM, traffi, solar, WS, RH, DewP, BLH | 0.42 | BLH, PM2.5, Solar, WD, DewP, traffi |
| **Night** | 0.94 | PM, T, WS | 0.98 | PM, RH |

Table 15. Correlation coefficients during winter week 1

| | Day | | | Night | | |
|---|---|---|---|---|---|---|
| | PAH | nalkanes | PM2.5 | PAH | nalkanes | PM2.5 |
| PAH | 1.00 | | | 1.00 | | |
| nalkanes | 0.30 | 1.00 | | 0.73 | 1.00 | |
| PM2.5 | 0.46 | 0.30 | 1.00 | 0.94 | 0.81 | 1.00 |
| O3 ppb | -0.62 | -0.17 | -0.55 | -0.70 | -0.62 | -0.87 |
| NO ppb | 0.14 | 0.39 | 0.81 | 0.92 | 0.78 | 0.98 |
| CO ppb | 0.43 | -0.26 | 0.41 | 0.89 | 0.55 | 0.94 |
| NOx | 0.13 | 0.38 | 0.83 | 0.91 | 0.78 | 0.98 |
| Ox | -0.56 | -0.05 | -0.09 | -0.67 | -0.53 | -0.79 |
| SO2 | -0.28 | 0.02 | 0.28 | 0.22 | 0.41 | 0.50 |
| NO2 | -0.03 | 0.16 | 0.62 | 0.38 | 0.52 | 0.59 |
| Temperature °C | -0.56 | -0.38 | -0.07 | -0.18 | -0.41 | -0.06 |
| Dew Point °C | -0.36 | -0.58 | -0.30 | -0.24 | -0.61 | -0.19 |
| Humidity % | 0.34 | -0.31 | -0.34 | -0.23 | -0.71 | -0.42 |
| Wind Direction | 0.22 | -0.24 | 0.44 | 0.21 | -0.05 | 0.39 |
| Pressure hPa | 0.43 | 0.60 | 0.39 | 0.35 | 0.60 | 0.32 |
| Precip. Rate. mm | #DIV/0! | #DIV/0! | #DIV/0! | #DIV/0! | #DIV/0! | #DIV/0! |
| Solar w/m² | -0.26 | 0.01 | 0.37 | #DIV/0! | #DIV/0! | #DIV/0! |
| wind speed (m/s) | -0.34 | 0.18 | -0.44 | -0.83 | -0.62 | -0.94 |
| NOAA Boundary Layer (m) | -0.06 | 0.10 | -0.29 | -0.47 | -0.11 | -0.50 |
| traffic (263) | -0.15 | 0.17 | 0.21 | -0.11 | -0.54 | -0.06 |
| ventilation | -0.22 | 0.29 | -0.32 | -0.52 | 0.15 | -0.65 |

Table 16. Correlation coefficients during winter week 2

| | Day | | | Night | | |
|---|---|---|---|---|---|---|
| | PAH | nalkanes | PM2.5 | PAH | nalkanes | PM2.5 |
| PAH | 1.00 | | | 1.00 | | |
| nalkanes | -0.13 | 1.00 | | 0.42 | 1.00 | |
| PM2.5 | 0.29 | 0.13 | 1.00 | 0.79 | 0.37 | 1.00 |
| O3 ppb | -0.47 | 0.18 | -0.36 | -0.82 | -0.15 | -0.83 |
| NO ppb | 0.33 | 0.12 | 0.75 | 0.83 | 0.13 | 0.94 |
| CO ppb | -0.03 | 0.09 | -0.38 | 0.76 | 0.84 | 0.80 |
| NOx | 0.30 | 0.13 | 0.77 | 0.81 | 0.10 | 0.94 |
| Ox | -0.50 | 0.18 | -0.29 | -0.67 | -0.23 | -0.63 |
| SO2 | -0.48 | 0.53 | 0.00 | -0.40 | -0.03 | 0.19 |
| NO2 | -0.19 | 0.05 | 0.07 | 0.29 | -0.23 | 0.41 |
| Temperature °C | -0.60 | 0.54 | -0.33 | -0.70 | 0.11 | -0.46 |
| Dew Point °C | -0.49 | 0.31 | -0.61 | -0.88 | -0.01 | -0.71 |
| Humidity % | 0.20 | -0.29 | -0.20 | 0.00 | -0.21 | -0.22 |
| Wind Direction | -0.65 | 0.27 | -0.06 | -0.68 | -0.12 | -0.23 |
| Pressure hPa | 0.60 | -0.12 | 0.53 | 0.80 | 0.31 | 0.65 |
| Precip. Rate. mm | 0.03 | 0.04 | -0.25 | -0.35 | -0.42 | -0.43 |
| Solar w/m² | -0.28 | 0.04 | 0.27 | #DIV/0! | #DIV/0! | #DIV/0! |
| wind speed (m/s) | -0.24 | -0.09 | -0.25 | -0.76 | 0.04 | -0.73 |
| NOAA Boundary Layer (m) | -0.29 | -0.10 | -0.21 | -0.18 | 0.37 | -0.41 |
| traffic (263) | -0.12 | -0.29 | 0.08 | 0.64 | 0.41 | 0.74 |
| ventilation | -0.33 | -0.05 | -0.22 | -0.45 | 0.30 | -0.61 |

Table 17. Correlation coefficients during winter week 3

| | Day | | | Night | | |
|---|---|---|---|---|---|---|
| | PAH | nalkanes | PM2.5 | PAH | nalkanes | PM2.5 |
| PAH | 1.00 | | | 1.00 | | |
| nalkanes | -0.14 | 1.00 | | 0.65 | 1.00 | |
| PM2.5 | 0.18 | -0.12 | 1.00 | 0.29 | 0.76 | 1.00 |
| O3 ppb | -0.11 | 0.08 | -0.67 | -0.57 | -0.67 | -0.20 |
| NO ppb | 0.21 | 0.09 | 0.78 | 0.60 | 0.51 | 0.09 |
| CO ppb | -0.15 | -0.38 | 0.04 | 0.56 | 0.82 | 0.45 |
| NOx | 0.22 | 0.03 | 0.78 | 0.57 | 0.60 | 0.13 |
| Ox | 0.12 | -0.17 | -0.29 | 0.02 | 0.35 | 0.09 |
| SO2 | -0.18 | 0.40 | -0.06 | -0.08 | -0.18 | -0.40 |
| NO2 | 0.19 | -0.19 | 0.50 | 0.43 | 0.67 | 0.19 |
| Temperature °C | -0.42 | 0.48 | -0.39 | -0.20 | -0.12 | -0.13 |
| Dew Point °C | -0.35 | 0.62 | -0.09 | -0.29 | -0.39 | -0.57 |
| Humidity % | 0.38 | -0.35 | 0.41 | -0.05 | -0.21 | -0.36 |
| Wind Direction | -0.18 | -0.13 | -0.07 | 0.39 | 0.43 | -0.05 |
| Pressure hPa | 0.18 | -0.49 | 0.13 | 0.26 | 0.37 | 0.63 |
| Precip. Rate. mm | -0.04 | -0.33 | 0.03 | -0.11 | 0.11 | -0.22 |
| Solar w/m² | -0.25 | 0.26 | -0.31 | 0.70 | 0.65 | 0.66 |
| wind speed (m/s) | -0.10 | 0.15 | -0.20 | -0.31 | -0.66 | -0.41 |
| NOAA Boundary Layer (m) | -0.28 | -0.08 | -0.23 | 0.31 | -0.19 | -0.73 |
| traffic (263) | #DIV/0! | #DIV/0! | #DIV/0! | #DIV/0! | #DIV/0! | #DIV/0! |
| ventilation | -0.21 | 0.25 | -0.35 | 0.00 | -0.64 | -0.57 |

Table 18. Correlation coefficients during winter week 4

| | Day | | | Night | | |
|---|---|---|---|---|---|---|
| | PAH | nalkanes | PM2.5 | PAH | nalkanes | PM2.5 |
| PAH | 1.00 | | | 1.00 | | |
| nalkanes | 0.03 | 1.00 | | 0.26 | 1.00 | |
| PM2.5 | 0.46 | -0.15 | 1.00 | -0.52 | -0.22 | 1.00 |
| O3 ppb | -0.57 | 0.20 | -0.64 | 0.19 | -0.56 | 0.17 |
| NO ppb | 0.61 | -0.24 | 0.78 | -0.03 | 0.88 | -0.20 |
| CO ppb | 0.15 | 0.27 | 0.37 | -0.03 | 0.80 | 0.07 |
| NOx | 0.52 | -0.20 | 0.75 | -0.27 | 0.80 | 0.05 |
| Ox | -0.63 | 0.22 | -0.51 | -0.36 | -0.08 | 0.61 |
| SO2 | -0.08 | 0.01 | 0.16 | -0.46 | -0.02 | 0.41 |
| NO2 | 0.20 | -0.08 | 0.51 | -0.57 | 0.57 | 0.39 |
| Temperature °C | -0.32 | 0.12 | -0.21 | -0.17 | -0.54 | 0.55 |
| Dew Point °C | 0.07 | 0.02 | 0.01 | 0.38 | -0.68 | -0.20 |
| Humidity % | 0.30 | -0.12 | 0.18 | 0.52 | -0.37 | -0.54 |
| Wind Direction | -0.07 | 0.11 | 0.29 | -0.10 | -0.38 | 0.11 |
| Pressure hPa | -0.13 | -0.10 | -0.04 | 0.06 | -0.10 | -0.55 |
| Precip. Rate. mm | #DIV/0! | #DIV/0! | #DIV/0! | #DIV/0! | #DIV/0! | #DIV/0! |
| Solar w/m² | -0.42 | -0.13 | -0.29 | 0.34 | 0.03 | 0.02 |
| wind speed (m/s) | -0.30 | 0.15 | -0.47 | 0.52 | -0.09 | -0.77 |
| NOAA Boundary Layer (m) | -0.33 | 0.08 | -0.30 | 0.51 | -0.26 | -0.86 |
| traffic (263) | #DIV/0! | #DIV/0! | #DIV/0! | #DIV/0! | #DIV/0! | #DIV/0! |
| ventilation | -0.28 | 0.11 | -0.27 | 0.56 | -0.19 | -0.81 |

Table 19. Correlation coefficients during winter week 5

| | Day | | | Night | | |
|---|---|---|---|---|---|---|
| | PAH | nalkanes | PM2.5 | PAH | nalkanes | PM2.5 |
| PAH | 1.00 | | | 1.00 | | |
| nalkanes | 0.24 | 1.00 | | 0.61 | 1.00 | |
| PM2.5 | 0.55 | -0.06 | 1.00 | 0.61 | 0.97 | 1.00 |
| O3 ppb | -0.21 | 0.10 | -0.31 | -0.77 | -0.72 | -0.73 |
| NO ppb | 0.10 | 0.29 | 0.36 | 0.73 | 0.86 | 0.77 |
| CO ppb | 0.26 | 0.28 | 0.47 | 0.67 | 0.98 | 0.97 |
| NOx | 0.14 | 0.33 | 0.41 | 0.74 | 0.91 | 0.83 |
| Ox | 0.08 | 0.28 | 0.21 | 0.36 | 0.81 | 0.85 |
| SO2 | -0.01 | 0.10 | -0.06 | 0.38 | 0.51 | 0.54 |
| NO2 | 0.21 | 0.27 | 0.45 | 0.65 | 0.96 | 0.95 |
| Temperature °C | -0.02 | 0.26 | 0.06 | -0.18 | 0.18 | 0.12 |
| Dew Point °C | 0.39 | 0.42 | 0.37 | -0.22 | 0.49 | 0.68 |
| Humidity % | 0.29 | -0.01 | 0.15 | 0.01 | 0.19 | 0.30 |
| Wind Direction | 0.46 | 0.22 | 0.80 | -0.29 | 0.24 | 0.33 |
| Pressure hPa | 0.16 | -0.12 | 0.29 | 0.19 | 0.22 | 0.41 |
| Precip. Rate. mm | -0.14 | -0.34 | 0.06 | -0.63 | -0.64 | -0.55 |
| Solar w/m² | -0.06 | 0.16 | 0.27 | #DIV/0! | #DIV/0! | #DIV/0! |
| wind speed (m/s) | -0.35 | -0.34 | -0.46 | -0.02 | -0.70 | -0.68 |
| NOAA Boundary Layer (m) | -0.44 | -0.51 | -0.63 | -0.59 | -0.92 | -0.91 |
| traffic (263) | -0.56 | 0.09 | -0.49 | 0.05 | 0.77 | 0.82 |
| ventilation | -0.36 | -0.43 | -0.47 | -0.44 | -0.87 | -0.83 |

Table 20. Correlation coefficients during winter week 6

| | Day | | | Night | | |
|---|---|---|---|---|---|---|
| | PAH | nalkanes | PM2.5 | PAH | nalkanes | PM2.5 |
| PAH | 1.00 | | | 1.00 | | |
| nalkanes | 0.44 | 1.00 | | 0.93 | 1.00 | |
| PM2.5 | 0.54 | 0.44 | 1.00 | 0.94 | 0.97 | 1.00 |
| O3 ppb | -0.31 | -0.34 | -0.45 | -0.06 | 0.21 | 0.26 |
| NO ppb | 0.81 | 0.57 | 0.75 | 0.91 | 0.95 | 0.99 |
| CO ppb | 0.59 | 0.40 | 0.39 | 0.94 | 0.97 | 0.93 |
| NOx | 0.79 | 0.58 | 0.75 | 0.91 | 0.96 | 0.99 |
| Ox | 0.34 | 0.38 | 0.36 | 0.73 | 0.92 | 0.88 |
| SO2 | -0.05 | 0.20 | 0.17 | 0.26 | 0.53 | 0.38 |
| NO2 | 0.54 | 0.60 | 0.64 | 0.80 | 0.96 | 0.91 |
| Temperature °C | -0.33 | 0.02 | 0.05 | -0.44 | -0.21 | -0.29 |
| Dew Point °C | -0.19 | 0.04 | 0.34 | -0.49 | -0.47 | -0.40 |
| Humidity % | 0.18 | 0.00 | 0.16 | -0.05 | -0.30 | -0.13 |
| Wind Direction | 0.04 | 0.30 | 0.21 | 0.45 | 0.63 | 0.53 |
| Pressure hPa | -0.13 | -0.06 | 0.23 | -0.09 | 0.09 | 0.00 |
| Precip. Rate. mm | #DIV/0! | #DIV/0! | #DIV/0! | #DIV/0! | #DIV/0! | #DIV/0! |
| Solar w/m² | -0.37 | -0.19 | 0.00 | #DIV/0! | #DIV/0! | #DIV/0! |
| wind speed (m/s) | -0.15 | -0.20 | 0.13 | -0.55 | -0.57 | -0.48 |
| NOAA Boundary Layer (m) | -0.54 | -0.50 | -0.71 | -0.42 | -0.49 | -0.40 |
| NOAA mixing coefficient (m2/s) | -0.47 | -0.38 | -0.67 | -0.55 | -0.55 | -0.58 |
| traffic (263) | -0.45 | -0.02 | -0.17 | 0.64 | 0.46 | 0.54 |
| ventilation | -0.53 | -0.47 | -0.51 | -0.32 | -0.37 | -0.24 |

## 6. CONCLUSİONS AND RECOMMENDATİONS

In this work, 295 high-volume samples were collected at high-time resolution for 2h during the day and 12h during the night for six weeks during one year in order to understand diurnal and seasonal variations of selected SVOCs (i.e., n-alkanes and PAH), respectively. Low-volume samples were also collected during 24h for determination of PM2.5 concentrations and for study of organic carbon and elemental carbon concentrations. Thermal desorption coupled to gas chromatography and mass spectrometry was used under optimized method conditions. A total of 15 PAH and 28 n-alkanes were identified and quantified in the samples for the first time in Istanbul and Turkey. The developed method is able to quantitatively recover two additional n-alkanes and 1 PAH, however, due to their high volatilities, they were not identified in the particle phase.

According to the daily average standard, 3.6% and 31-46% and of the days in summer and winter-spring-fall exceeded the regulation, respectively. However, according to the hourly recommendation, approximately 50% of the days in the winter-spring-fall, and 33% of the days in the summer had fair, poor, and very poor air quality. In addition, a better idea about the magnitude of the exceedances is obtained with the hourly system, in which is it understood that between 20-30% in the winter, spring, and fall, and 5% of the days in the summer had air quality with potential effects on human health. This suggested metric can be a better alternative for comparison of air quality among urban areas and implementation of control strategies. Similarly, OC concentrations were approximately twice as high during the fall and winter than during the summer and they were found 46% and 3.5x higher than concentrations observed in USA and Europe and comparable to China. EC concentrations were 6.5x and 1.6x higher than USA and Europe, respectively, mostly due to the increase use of diesel vehicles for private use.

During all seasons, except fall, Pearson correlations between high-time resolved PM2.5 concentrations and NO varied as R=0.70-0.80. Only during the fall, the correlation coefficient was R=0.45. Similarly, high correlations were found with CO during winter weeks 1, 3, and fall with R=0.55-0.63. Although high correlations between PM2.5, and NO and CO were found, low correlations with traffic were observed (R<0.49). This is likely due to the fact that during high congestion, low traffic counts are recorded, however, when cars are stationary high emissions occur and are collected at our station. This proves that since an important fraction of PM2.5 is emitted by traffic, correlations with high time resolved CO and NO are a better metric than traffic counts.

Ventilation coefficients can be used as an indicator of air quality and the impact of mixing or accumulation of pollutants vs. emissions can be determined accordingly. In this work it was found that Although ventilation coefficients at night during the winter weeks are still in the category that indicates poor air pollution, the impact of having ventilation coefficients 5 times greater has great impacts on PM2.5 concentrations at night. During spring and summer, maximum concentrations observed early in the morning and at night are less than half the concentrations observed during the winter weeks. Although poor air quality conditions are found in spring (97.6%) and summer (50%) due to low ventilation coefficients, 70 and 76% of PM2.5 concentrations are in the categories of good and fair during spring and summer, respectively. During the summer, at night, minimum n-alkane concentrations of 40 ng/m3 were observed. On the contrary, during the winter, concentrations observed at night ranged 100-135 ng/m3. Concentrations of 40 ng/m3 are partly due to low traffic counts during the night. This shows that although poor ventilation coefficients can be found at all seasons, the use of high quality of fuel for residential heating is the most important management strategy for the decrease of PM2.5 concentrations during the winter.

Similarly to PM2.5 and OC/EC concentrations, the highest concentrations of PAH and n-alkanes were observed during the winter, followed by fall, and spring and summer. And significant diurnal variations were observed during all weeks. Comparison of concentrations of PAH and n-alkanes with other megacities, urban areas, and rural areas in the world show that the highest concentrations are found in the Megacity of Guangzhou and although PAH concentrations in Istanbul are lower than China, they can be comparable. Concentrations of n-alkanes with $n_C$>24 are lower than China, however, n-alkanes with $n_C$=17-24 are higher than China but comparable to Germany. In general, this type of study is necessary in other regions in the world to improve comparisons according to local anthropogenic activities, to perform epidemiological studies in order to understand the effects of these observed concentrations on human health, and to potentially improve air quality regulations at high-time resolution.

The study of diurnal variations of PAH and n-alkanes provided significant insight into their lifetime and interactions in the atmosphere according to changes in meteorology and traffic. PAH are able to react with OH, NO3, and O3 and their lifetimes vary on the order of 2.1-12 hours when they react with OH. n-alkanes have a wide range of volatility and react with OH and NO3 radicals at different rates. They are more stable than PAH and since they have longer lifetimes, they can be transported. In this work, diurnal variations of PAH are due to variations in traffic, photochemical reactions, and ventilation conditions. n-alkanes followed two diurnal variations: (1) during the fall and winter sampling weeks with marked behavior with respect to traffic and photochemistry and possibly enhanced due to lower

boundary layer height, and (2) during spring and summer slight variations with photochemistry and traffic, possibly due to dilution and lack of residential heating.

Multiple regression analysis is a useful statistical tool that can be used to quantify the effect of meteorological variables and emission sources such as traffic on high-time resolved PAH and n-alkane concentrations. The discussion is improved by combining results from Spearman correlations with individual gas-phase pollutants, particle-phase pollutants, meteorological parameters, and traffic. Since optimizing the multiple regression model for each variable for each season is time consuming, prior knowledge of individual correlation coefficients is useful. In addition, the sign of the correlation coefficient is useful to understand the physical and chemical effect of the variables on the concentrations.

Overall, multiple regression analysis identified PM2.5 concentrations and traffic as the most important variables that contributed to the variance of PAH concentrations during all seasons. Both PAH and n-alkanes showed high Pearson correlation coefficients with NO and CO which are emitted by traffic. However, due to longer lifetimes and greater variations in volatilities, dew point was identified as an important variable that determines condensation of n-alkanes on fine particles. Precipitation events during the spring and fall, and higher variations in boundary layer heights and radiation during the summer, may be the reason for lower variance explained by multiple regression analysis. During the night, due to less variations in meteorological conditions, high correlations are obtained with a less number of variables. Overall, two or three variables resolved over 94% and 74% of the variance of PAH and n-alkane concentrations, respectively. Except during the summer in which only 37% of the variance of PAH concentrations was resolved.

Understanding the effect of mixed meteorological variables and traffic is useful for improvement of models on local and regional levels to understand sources, transport, and sink of organic aerosol components. In addition, it is helpful for prediction of concentrations and implementation of air quality control strategies at the local level.

Although thermal desorption is more time efficient than solvent extraction, the developed TD-GC-MS method allowed processing of only 4 samples per day and the instruments are expensive and regular maintenance is required. In the future, acquisition of an automatic TD-GC-MS such as the one developed by Williams et al., 2006 will be more helpful for comprehensive study of a larger set of SVOCs at higher time-resolution and in various sampling locations.

In Istanbul, stringent control measures such as limiting the number of diesel vehicles for private use, control of fuel used in transatlantic ships and local ferries, controlling the quality or banning of fuels

used for residential heating, or controlling the number of vehicles that circulate during the week are necessary in order to reduce the concentrations of PM2,5, OC/EC, PAH, and n-alkanes, particularly during the fall and winter.

## References


[1] Aydin Coskun, A., Türker, O., Velioglu, N., 2011. "Air pollution regulations in Turkey and harmonization with the EU legislation", iForest - Biogeosciences and Forestry, 4, 181-185.
[2] Brook, J.R., Demerjian, K.L., Hidy, G., Molina, L.T., Pennell, W.T., Scheffe, R., 2009. "New Directions: Results-oriented multi-pollutant air quality management", Atmospheric Environment, 43, 2091-2093.
[3] Cabada, J.C., Pandis, S.N., Subramanian, R., Robinson, A.L., Polidori, A., Turpin, B., 2004. "Estimating the Secondary Organic Aerosol Contribution to PM2.5 Using the EC Tracer Method Special Issue of Aerosol Science and Technology on Findings from the Fine Particulate Matter Supersites Program", Aerosol Science and Technology, 38, 140-155.
[4] Chang, Y., Deng, C., Cao, F., Cao, C., Zou, Z., Liu, S., Lee, X., Li, J., Zhang, G., Zhang, Y., 2017. "Assessment of carbonaceous aerosols in Shanghai, China – Part 1: long-term evolution, seasonal variations, and meteorological effects", Atmospheric Chemistry and Physics, 17, 9945-9964.
[5] Chow, J.C., Doraiswamy, P., Watson, J.G., Chen, L.-W.A., Ho, S.S.H., Sodeman, D.A., 2008. "Advances in integrated and continuous measurements for particle mass and chemical composition", Journal of the Air & Waste Management Association, 58, 141-163.
[6] Chow, J.C., Watson, J., 2012. "Chemical analyses of particle filter deposits", Aerosols Handbook: Measurement, Dosimetry, and Health Effects, 2, 177-202.
[7] Chuersuwan, N., Turpin, B.J., Pietarinen, C., 2000. "Evaluation of Time-Resolved PM2.5 Data in Urban/Suburban Areas of New Jersey", Journal of the Air & Waste Management Association, 50, 1780-1789.
[8] Crippa, M., Canonaco, F., Lanz, V.A., Äijälä, M., Allan, J.D., Carbone, S., Capes, G., Ceburnis, D., Dall'Osto, M., Day, D.A., DeCarlo, P.F., Ehn, M., Eriksson, A., Freney, E., Hildebrandt Ruiz, L., Hillamo, R., Jimenez, J.L., Junninen, H., Kiendler-Scharr, A., Kortelainen, A.M., Kulmala, M., Laaksonen, A., Mensah, A.A., Mohr, C., Nemitz, E., O'Dowd, C., Ovadnevaite, J., Pandis, S.N., Petäjä, T., Poulain, L., Saarikoski, S., Sellegri, K., Swietlicki, E., Tiitta, P., Worsnop, D.R., Baltensperger, U., Prévôt, A.S.H., 2014. "Organic aerosol components derived from 25 AMS data sets across Europe using a consistent ME-2 based source apportionment approach", Atmospheric Chemistry and Physics, 14, 6159-6176.
[9] Derwent, R.G., Jenkin, M.E., Utembe, S.R., Shallcross, D.E., Murrells, T.P., Passant, N.R., 2010. "Secondary organic aerosol formation from a large number of reactive man-made organic compounds", Science of the Total Environment, 408, 3374-3381.
[10] Elsasser, M., Crippa, M., Orasche, J., DeCarlo, P.F., Oster, M., Pitz, M., Cyrys, J., Gustafson, T.L., Pettersson, J.B.C., Schnelle-Kreis, J., Prévôt, A.S.H., Zimmermann, R., 2012. "Organic molecular markers and signature from wood combustion particles in winter ambient aerosols: aerosol mass spectrometer (AMS) and high time-resolved GC-MS measurements in Augsburg, Germany", Atmospheric Chemistry and Physics, 12, 6113-6128.
[11] EPA, U., 1999. EPA Method IO-2.1. Sampling of Ambient Air for Total Suspended Particulate Matter (SPM) and PM10 Using High Volume (HV) Sampler, http://www.epa.gov/ttnamti1/files/ambient/inorganic/mthd-2-1.pdf.
[12] EPA, U., 2007. Method 8270D. Semivolatile organic compounds by gas chromatography/mass spectrometry (GC/MS), http://www.epa.gov/osw/hazard/testmethods/sw846/pdfs/8270d.pdf.
[13] EPA, U., 2013. Environmental Protection Agency 40 CFR Part 50 National Ambient Air Quality Standards for Particulate Matter; Final Rule. Tuesday January 15, 2013.
[14] EPA, U., 2015. Particulate Matter (PM) Standards, http://www.epa.gov/ttn/naaqs/standards/pm/s_pm_index.html.
[15] EPA, V., 2018. "PM2.5 particles in air. Available at https://www.epa.vic.gov.au/your-environment/air/air-pollution/pm25-particles-in-air", Accessed on 27 February 2019.
[16] Erdun, H., Öztürk, A., Çapraz, Ö., Toros, H., Dursun, S., Deniz, A., 2015. Spatial Variation of PM10 in Turkey, in: Deniz, A., Efe, B., Durna, B., Cavuz, P.C. (Eds.), VII Atmospheric Sciences Symposium, ITU and IAU, pp. 311-323.
[17] EU, 2004. Comparison of the EU and US Air Quality Standards and Planning Requirements, http://ec.europa.eu/environment/archives/cafe/activities/pdf/case_study2.pdf.
[18] EU, 2008. Directive 2008/50/EC of the European Parliament and of the Council of 21 May 2008 on Ambient Air Quality and Cleaner Air for Europe. Available at https://eur-lex.europa.eu/legal-content/EN/ALL/?uri=CELEX:32008L0050.
[19] Goldstein, A.H., Galbally, I.E., 2007. "Known and unexplored organic constituents in the earth's atmosphere", Environmental Science & Technology, 41, 1514-1521.
[20] Graham, L.A., Tong, A., Poole, G., Ding, L., Ke, F., Wang, D., Caravaggio, G., Charland, J.-P., MacDonald, P., Hall, A., Cheng, Y., Brook, J.R., 2010. "A comparison of direct thermal desorption with solvent extraction for gas chromatography-mass spectrometry analysis of semivolatile organic compounds in diesel particulate matter", International Journal of Environmental Analytical Chemistry, 90, 511-534.
[21] Hanedar, A., Alp, K., Kaynak, B., Avşar, E., 2014. "Toxicity evaluation and source apportionment of Polycyclic Aromatic Hydrocarbons (PAHs) at three stations in Istanbul, Turkey", Science of the Total Environment, 488–489, 437-446.
[22] Hays, M.D., Lavrich, R.J., 2007. "Developments in direct thermal extraction gas chromatography-mass spectrometry of fine aerosols", TRAC Trends in Analytical Chemistry, 26, 88-102.
[23] He, K., Yang, F., Ma, Y., Zhang, Q., Yao, X., Chan, C.K., Cadle, S., Chan, T., Mulawa, P., 2001. "The characteristics of PM2. 5 in Beijing, China", Atmospheric Environment, 35, 4959-4970.
[24] Huang, L., Bohac, S., Chernyak, S., Batterman, S., 2013. "Composition and Integrity of PAHs, Nitro-PAHs, Hopanes, and Steranes in Diesel Exhaust Particulate Matter", Water, Air, & Soil Pollution, 224, 1-14.

[25] Huang, X.F., He, L.Y., Hu, M., Canagaratna, M.R., Sun, Y., Zhang, Q., Zhu, T., Xue, L., Zeng, L.W., Liu, X.G., Zhang, Y.H., Jayne, J.T., Ng, N.L., Worsnop, D.R., 2010. "Highly time-resolved chemical characterization of atmospheric submicron particles during 2008 Beijing Olympic Games using an Aerodyne High-Resolution Aerosol Mass Spectrometer", Atmospheric Chemistry and Physics, 10, 8933-8945.
[26] Huang, X.F., He, L.Y., Xue, L., Sun, T.L., Zeng, L.W., Gong, Z.H., Hu, M., Zhu, T., 2012. "Highly time-resolved chemical characterization of atmospheric fine particles during 2010 Shanghai World Expo", Atmospheric Chemistry and Physics, 12, 4897-4907.
[27] Im, U., Kanakidou, M., 2012. "Impacts of East Mediterranean megacity emissions on air quality", Atmospheric Chemistry and Physics, 12, 6335-6355.
[28] Im, U., Ketzel, M., Brandt, J., 2015. Integrated modeling of air pollution and associated health impacts, in: Deniz, A., Efe, B., Durna, B., Cavuz, P.C. (Eds.), VII Atmospheric Sciences Symposium, ITU and IAU, p. 113.
[29] Incecik, S., Im, U., 2012. "Air Pollution in Mega Cities: A Case Study of Istanbul", Air Pollution–Monitoring, Modeling and Health, Rijeka and Shanghai: InTech, 77-116.
[30] Isaacman, G., Kreisberg, N.M., Yee, L.D., Worton, D.R., Chan, A.W.H., Moss, J.A., Hering, S.V., Goldstein, A.H., 2014. "Online derivatization for hourly measurements of gas- and particle-phase semi-volatile oxygenated organic compounds by thermal desorption aerosol gas chromatography (SV-TAG)", Atmos. Meas. Tech., 7, 4417-4429.
[31] Jimenez, J.L., Canagaratna, M.R., Donahue, N.M., Prevot, A.S.H., Zhang, Q., Kroll, J.H., DeCarlo, P.F., Allan, J.D., Coe, H., Ng, N.L., Aiken, A.C., Docherty, K.S., Ulbrich, I.M., Grieshop, A.P., Robinson, A.L., Duplissy, J., Smith, J.D., Wilson, K.R., Lanz, V.A., Hueglin, C., Sun, Y.L., Tian, J., Laaksonen, A., Raatikainen, T., Rautiainen, J., Vaattovaara, P., Ehn, M., Kulmala, M., Tomlinson, J.M., Collins, D.R., Cubison, M.J., E., Dunlea, J., Huffman, J.A., Onasch, T.B., Alfarra, M.R., Williams, P.I., Bower, K., Kondo, Y., Schneider, J., Drewnick, F., Borrmann, S., Weimer, S., Demerjian, K., Salcedo, D., Cottrell, L., Griffin, R., Takami, A., Miyoshi, T., Hatakeyama, S., Shimono, A., Sun, J.Y., Zhang, Y.M., Dzepina, K., Kimmel, J.R., Sueper, D., Jayne, J.T., Herndon, S.C., Trimborn, A.M., Williams, L.R., Wood, E.C., Middlebrook, A.M., Kolb, C.E., Baltensperger, U., Worsnop, D.R., 2009. "Evolution of Organic Aerosols in the Atmosphere", Science, 326, 1525-1529.
[32] Kanakidou, M., Mihalopoulos, N., Kindap, T., Im, U., Vrekoussis, M., Gerasopoulos, E., Dermitzaki, E., Unal, A., Koçak, M., Markakis, K., Melas, D., Kouvarakis, G., Youssef, A.F., Richter, A., Hatzianastassiou, N., Hilboll, A., Ebojie, F., Wittrock, F., von Savigny, C., Burrows, J.P., Ladstaetter-Weissenmayer, A., Moubasher, H., 2011. "Megacities as hot spots of air pollution in the East Mediterranean", Atmospheric Environment, 45, 1223-1235.
[33] Karaca, F., 2013. "Mapping the corrosion impact of air pollution on the historical peninsula of Istanbul", Journal of Cultural Heritage, 14, 129-137.
[34] Karaca, F., Alagha, O., Ertürk, F., 2005. "Statistical characterization of atmospheric PM10 and PM2.5 concentrations at a non-impacted suburban site of Istanbul, Turkey", Chemosphere, 59, 1183-1190.
[35] Karaca, F., Alagha, O., Ertürk, F., Yılmaz, Y.Z., Özkara, T., 2008. "Seasonal Variation of Source Contributions to Atmospheric Fine and Coarse Particles at Suburban Area in Istanbul, Turkey", Environmental Engineering Science, 25, 767-782.
[36] Karaca, F., Anil, I., Alagha, O., 2009. "Long-range potential source contributions of episodic aerosol events to PM10 profile of a megacity", Atmospheric Environment, 43, 5713-5722.
[37] Karaca, F., Camci, F., 2010. "Distant source contributions to PM10 profile evaluated by SOM based cluster analysis of air mass trajectory sets", Atmospheric Environment, 44, 892-899.
[38] Kim, B.M., Teffera, S., Zeldin, M.D., 2000. "Characterization of PM25 and PM10 in the South Coast air basin of Southern California: part 1—spatial variations", Journal of the Air & Waste Management Association, 50, 2034-2044.
[39] Kim, S.-Y., Dutton, S.J., Sheppard, L., Hannigan, M.P., Miller, S.L., Milford, J.B., Peel, J.L., Vedal, S., 2015. "The short-term association of selected components of fine particulate matter and mortality in the Denver Aerosol Sources and Health (DASH) study", Environmental Health, 14, 49.
[40] Kim, S.-Y., Peel, J.L., Hannigan, M.P., Dutton, S.J., Sheppard, L., Clark, M.L., Vedal, S., 2012. "The temporal lag structure of short-term associations of fine particulate matter chemical constituents and cardiovascular and respiratory hospitalizations", Environmental Health Perspectives, 120, 1094-1099.
[41] Kindap, T., Unal, A., Chen, S.H., Hu, Y., Odman, M.T., Karaca, M., 2006. "Long-range aerosol transport from Europe to Istanbul, Turkey", Atmospheric Environment, 40, 3536-3547.
[42] Kuzu, S.L., Saral, A., Summak, G., Çoltu, H., Demir, S., 2014. "Ambient polychlorinated biphenyl levels and their evaluation in a metropolitan city", Science of the Total Environment, 472, 13-19.
[43] Lambe, A., Chacon-Madrid, H., Nguyen, N., Weitkamp, E., Kreisberg, N., Hering, S., Goldstein, A., Donahue, N., Robinson, A., 2010. "Organic Aerosol Speciation: Intercomparison of Thermal Desorption Aerosol GC/MS (TAG) and Filter-Based Techniques", Aerosol Science and Technology, 44, 141-151.
[44] Li, J., Wang, G., Aggarwal, S.G., Huang, Y., Ren, Y., Zhou, B., Singh, K., Gupta, P.K., Cao, J., Zhang, R., 2014. "Comparison of abundances, compositions and sources of elements, inorganic ions and organic compounds in atmospheric aerosols from Xi'an and New Delhi, two megacities in China and India", Science of the Total Environment, 476–477, 485-495.
[45] Lin, J.J., Tai, H.-S., 2001. "Concentrations and distributions of carbonaceous species in ambient particles in Kaohsiung City, Taiwan", Atmospheric Environment, 35, 2627-2636.
[46] Long, C.M., Suh, H.H., Catalano, P.J., Koutrakis, P., 2001. "Using Time- and Size-Resolved Particulate Data To Quantify Indoor Penetration and Deposition Behavior", Environmental Science & Technology, 35, 2089-2099.

[47] Lu, Z., Streets, D.G., Winijkul, E., Yan, F., Chen, Y., Bond, T.C., Feng, Y., Dubey, M.K., Liu, S., Pinto, J.P., Carmichael, G.R., 2015. "Light Absorption Properties and Radiative Effects of Primary Organic Aerosol Emissions", Environmental Science & Technology, 49, 4868-4877.
[48] Ma, Y., Xu, X., Song, W., Geng, F., Wang, L., 2014. "Seasonal and diurnal variations of particulate organosulfates in urban Shanghai, China", Atmospheric Environment, 85, 152-160.
[49] Mahowald, N., Ward, D.S., Kloster, S., Flanner, M.G., Heald, C.L., Heavens, N.G., Hess, P.G., Lamarque, J.-F., Chuang, P.Y., 2011. "Aerosol Impacts on Climate and Biogeochemistry", Annual Review of Environment and Resources, 36, 45-74.
[50] Mauderly, J.L., Chow, J.C., 2008. "Health Effects of Organic Aerosols", Inhalation Toxicology, 20, 257-288.
[51] McDonald, J.D., Eide, I., Seagrave, J., Zielinska, B., Whitney, K., Lawson, D.R., Mauderly, J.L., 2004. "Relationship between Composition and Toxicity of Motor Vehicle Emission Samples", Environmental Health Perspectives, 112, 1527-1538.
[52] Miyazaki, Y., Kondo, Y., Takegawa, N., Komazaki, Y., Fukuda, M., Kawamura, K., Mochida, M., Okuzawa, K., Weber, R.J., 2006a. "Time-resolved measurements of water-soluble organic carbon in Tokyo", Journal of Geophysical Research: Atmospheres, 111, D23206.
[53] Miyazaki, Y., Kondo, Y., Takegawa, N., Komazaki, Y., Fukuda, M., Kawamura, K., Mochida, M., Okuzawa, K., Weber, R.J., 2006b. "Time-resolved measurements of water-soluble organic carbon in Tokyo", Journal of Geophysical Research: Atmospheres, 111, n/a-n/a.
[54] Mycock, J.C., McKenna, J.D., Theodore, L., 1995. Handbook of air pollution control engineering and technology. CRC Press Boca Raton, FL.
[55] Na, K., Sawant, A.A., Song, C., Cocker, D.R., 2004. "Primary and secondary carbonaceous species in the atmosphere of Western Riverside County, California", Atmospheric Environment, 38, 1345-1355.
[56] NEPC, 2015. "National Environment Protection (Ambient Air Quality) Measure. available at https://www.legislation.gov.au/Series/F2007B01142".
[57] Onat, B., Şahin, Ü.A., 2012. "Trafik Kaynaklı Partikül Madde Boyutlarının ve Siyah Duman İle İlişkisinin Araştırılması.", Ekoloji Dergisi 21, 77-83.
[58] Onat, B., Stakeeva, B., 2014. "Assessment of fine particulate matters in the subway system of Istanbul", Indoor and Built Environment, 23, 574-583.
[59] Orasche, J., Schnelle-Kreis, J., Abbaszade, G., Zimmermann, R., 2011. "Technical Note: In-situ derivatization thermal desorption GC-TOFMS for direct analysis of particle-bound non-polar and polar organic species", Atmospheric Chemistry and Physics, 11, 8977-8993.
[60] Ozdemir, H., Pozzoli, L., Kindap, T., Demir, G., Mertoglu, B., Mihalopoulos, N., Theodosi, C., Kanakidou, M., Im, U., Unal, A., 2014. "Spatial and temporal analysis of black carbon aerosols in Istanbul megacity", Science of the Total Environment, 473–474, 451-458.
[61] Öztürk, F., Keleş, M., 2016. "Wintertime chemical compositions of coarse and fine fractions of particulate matter in Bolu, Turkey", Environmental Science and Pollution Research, 23, 14157-14172.
[62] Park, S.S., Kim, Y.J., Fung, K., 2002. "PM2. 5 carbon measurements in two urban areas: Seoul and Kwangju, Korea", Atmospheric Environment, 36, 1287-1297.
[63] Peré-Trepat, E., Kim, E., Paatero, P., Hopke, P.K., 2007. "Source apportionment of time and size resolved ambient particulate matter measured with a rotating DRUM impactor", Atmospheric Environment, 41, 5921-5933.
[64] Perrino, C., Canepari, S., Pappalardo, S., Marconi, E., 2010. "Time-resolved measurements of water-soluble ions and elements in atmospheric particulate matter for the characterization of local and long-range transport events", Chemosphere, 80, 1291-1300.
[65] Rutter, A.P., Snyder, D.C., Stone, E.A., Shelton, B., DeMinter, J., Schauer, J.J., 2014. "Preliminary assessment of the anthropogenic and biogenic contributions to secondary organic aerosols at two industrial cities in the upper Midwest", Atmospheric Environment, 84, 307-313.
[66] Scheffe, R., Brook, J., Demerjian, K., 2011. "Air Quality Measurements", in: Hidy, G.M., Brook, J.R., Demerjian, K.L., Molina, L.T., Pennell, W.T., Scheffe, R.D. (Eds.), Technical Challenges of Multipollutant Air Quality Management. Springer Netherlands, pp. 339-393.
[67] Schnelle-Kreis, J., Welthagen, W., Sklorz, M., Zimmermann, R., 2005. "Application of direct thermal desorption gas chromatography and comprehensive two-dimensional gas chromatography coupled to time of flight mass spectrometry for analysis of organic compounds in ambient aerosol particles", Journal of Separation Science, 28, 1648-1657.
[68] Sevimoglu, O., 2015. Greenhouse gas mitigation works and measures taken against climate change: Case of Istanbul, in: Deniz, A., Efe, B., Durna, B., Cavuz, P.C. (Eds.), VII Atmospheric Sciences Symposium, ITU and IAU, pp. 686-697.
[69] Sun, Y.L., Zhang, Q., Schwab, J.J., Demerjian, K.L., Chen, W.N., Bae, M.S., Hung, H.M., Hogrefe, O., Frank, B., Rattigan, O.V., Lin, Y.C., 2011. "Characterization of the sources and processes of organic and inorganic aerosols in New York city with a high-resolution time-of-flight aerosol mass apectrometer", Atmospheric Chemistry and Physics, 11, 1581-1602.
[70] Tanriover, Ş., Kahraman, A., Incecik, S., Deniz, A., Toros, H., Celebi, H., Ozturk, A., Sezen, Î., 2014. "Meteorological Modeling of the PM10 Episode in the Creek Valley of Golden Horn Harbour, Istanbul Under Very Stable Conditions for November 6–9, 2010 Episode", in: Steyn, D.G., Builtjes, P.J.H., Timmermans, R.M.A. (Eds.), Air Pollution Modeling and its Application XXII. Springer Netherlands, pp. 685-692.
[71] Tayanç, M., 2000. "An assessment of spatial and temporal variation of sulfur dioxide levels over Istanbul, Turkey", Environmental Pollution, 107, 61-69.

[72] Tolocka, M.P., Solomon, P.A., Mitchell, W., Norris, G.A., Gemmill, D.B., Wiener, R.W., Vanderpool, R.W., Homolya, J.B., Rice, J., 2001. "East versus west in the US: chemical characteristics of PM2. 5 during the winter of 1999", Aerosol Science & Technology, 34, 88-96.
[73] Toros, H., Geertsema, G., Cats, G., 2014. "Evaluation of the HIRLAM and HARMONIE Numerical Weather Prediction Models during an Air Pollution Episode over Greater İstanbul Area", CLEAN – Soil, Air, Water, 42, 863-870.
[74] Unal, Y.S., Toros, H., Deniz, A., Incecik, S., 2011. "Influence of meteorological factors and emission sources on spatial and temporal variations of PM10 concentrations in Istanbul metropolitan area", Atmospheric Environment, 45, 5504-5513.
[75] Vedal, S., Hannigan, M., Dutton, S., Miller, S., Milford, J., Rabinovitch, N., Kim, S.-Y., Sheppard, L., 2009. "The Denver Aerosol Sources and Health (DASH) study: overview and early findings", Atmospheric Environment, 43, 1666-1673.
[76] Viana, M., Fann, N., Tobías, A., Querol, X., Rojas-Rueda, D., Plaza, A., Aynos, G., Conde, J.A., Fernández, L., Fernández, C., 2015. "Environmental and Health Benefits from Designating the Marmara Sea and the Turkish Straits as an Emission Control Area (ECA)", Environmental Science & Technology, 49, 3304-3313.
[77] Wang, J., Ho, S.S.H., Ma, S., Cao, J., Dai, W., Liu, S., Shen, Z., Huang, R., Wang, G., Han, Y., 2016. "Characterization of PM2.5 in Guangzhou, China: uses of organic markers for supporting source apportionment", Science of the Total Environment, 550, 961-971.
[78] Wexler, A.S., Johnston, M.V., 2008. "What Have We Learned from Highly Time-Resolved Measurements during EPA's Supersites Program and Related Studies?", Journal of the Air & Waste Management Association, 58, 303-319.
[79] Williams, B.J., Goldstein, A.H., Kreisberg, N.M., Hering, S.V., 2006. "An In-Situ Instrument for Speciated Organic Composition of Atmospheric Aerosols: Thermal Desorption Aerosol GC/MS-FID (TAG)", Aerosol Science and Technology, 40, 627-638.
[80] Williams, B.J., Goldstein, A.H., Kreisberg, N.M., Hering, S.V., Worsnop, D.R., Ulbrich, I.M., Docherty, K.S., Jimenez, J.L., 2010. "Major components of atmospheric organic aerosol in southern California as determined by hourly measurements of source marker compounds", Atmospheric Chemistry and Physics, 10, 11577-11603.
[81] Williams, B.J., Jayne, J.T., Lambe, A.T., Hohaus, T., Kimmel, J.R., Sueper, D., Brooks, W., Williams, L.R., Trimborn, A.M., Martinez, R.E., Hayes, P.L., Jimenez, J.L., Kreisberg, N.M., Hering, S.V., Worton, D.R., Goldstein, A.H., Worsnop, D.R., 2014. "The First Combined Thermal Desorption Aerosol Gas Chromatograph—Aerosol Mass Spectrometer (TAG-AMS)", Aerosol Science and Technology, 48, 358-370.
[82] Worton, D.R., Kreisberg, N.M., Isaacman, G., Teng, A.P., McNeish, C., Górecki, T., Hering, S.V., Goldstein, A.H., 2011. "Thermal Desorption Comprehensive Two-Dimensional Gas Chromatography: An Improved Instrument for In-Situ Speciated Measurements of Organic Aerosols", Aerosol Science and Technology, 46, 380-393.
[83] Xie, M., Barsanti, K.C., Hannigan, M.P., Dutton, S.J., Vedal, S., 2013. "Positive matrix factorization of PM2.5 – eliminating the effects of gas/particle partitioning of semivolatile organic compounds", Atmospheric Chemistry and Physics, 13, 7381-7393.
[84] Xu, L., Suresh, S., Guo, H., Weber, R.J., Ng, N.L., 2015. "Aerosol characterization over the southeastern United States using high resolution aerosol mass spectrometry: spatial and seasonal variation of aerosol composition, sources, and organic nitrates", Atmos. Chem. Phys. Discuss., 15, 10479-10552.
[85] Yalçın, E., Tecer, L.H., Yurdakul, S., Tuncel, G., 2015. Measured VOC concentrations in Balikesir ambient atmosphere, in: Deniz, A., Efe, B., Durna, B., Cavuz, P.C. (Eds.), VII Atmospheric Sciences Symposium, ITU and IAU, pp. 198-203.
[86] Zakey, A.S., Solmon, F., Giorgi, F., 2006. "Implementation and testing of a desert dust module in a regional climate model", Atmospheric Chemistry and Physics, 6, 4687-4704.
[87] Zhao, W., Hopke, P.K., Karl, T., 2004. "Source Identification of Volatile Organic Compounds in Houston, Texas", Environmental Science & Technology, 38, 1338-1347.
[88] Zhao, Y., Kreisberg, N.M., Worton, D.R., Teng, A.P., Hering, S.V., Goldstein, A.H., 2012. "Development of an In Situ Thermal Desorption Gas Chromatography Instrument for Quantifying Atmospheric Semi-Volatile Organic Compounds", Aerosol Science and Technology, 47, 258-266.
[89] Zhao, Y., Kreisberg, N.M., Worton, D.R., Teng, A.P., Hering, S.V., Goldstein, A.H., 2013. "Development of an In Situ Thermal Desorption Gas Chromatography Instrument for Quantifying Atmospheric Semi-Volatile Organic Compounds", Aerosol Science and Technology, 47, 258-266.

# *Appendix A*

**Weather forecasts for week 1**

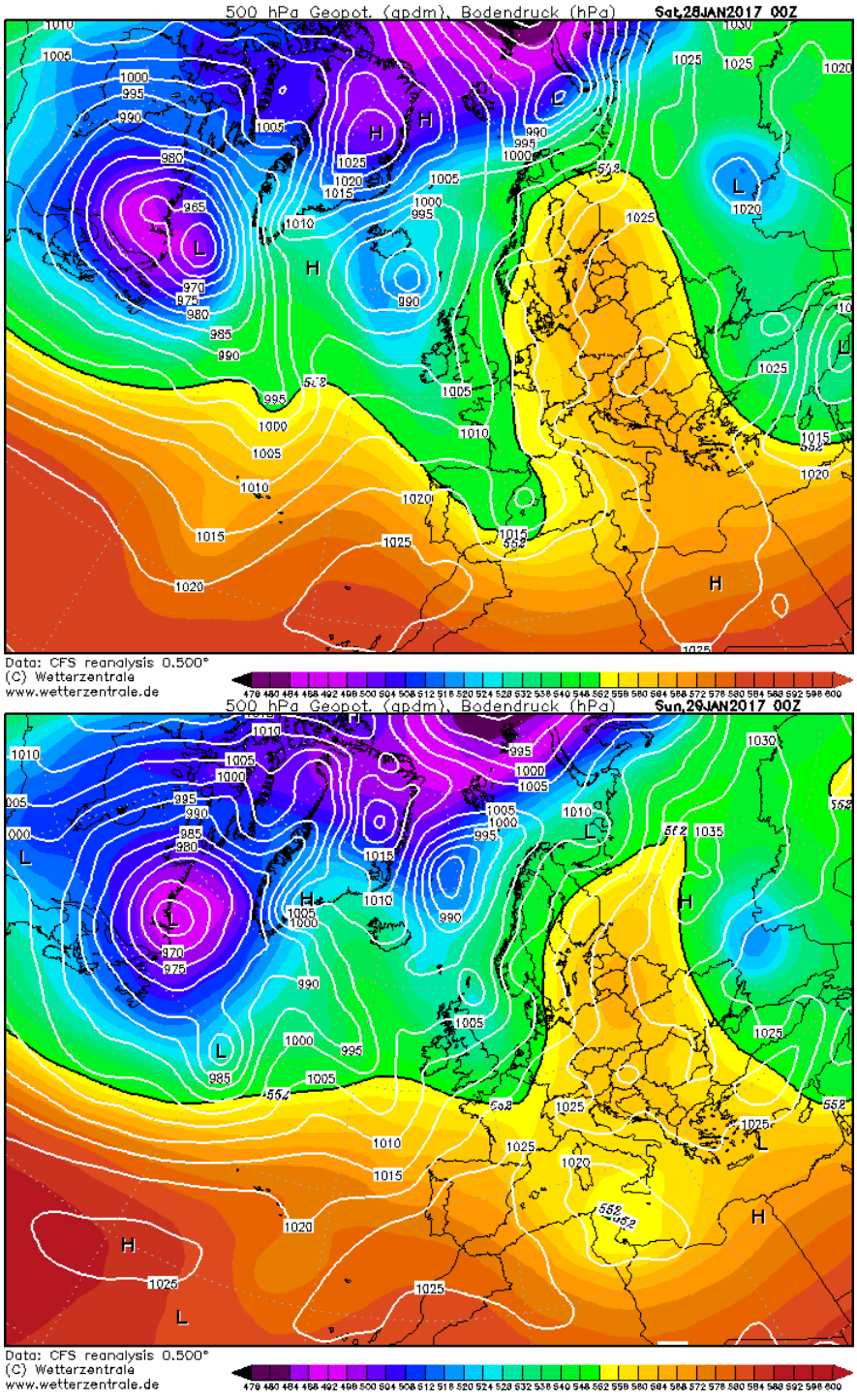

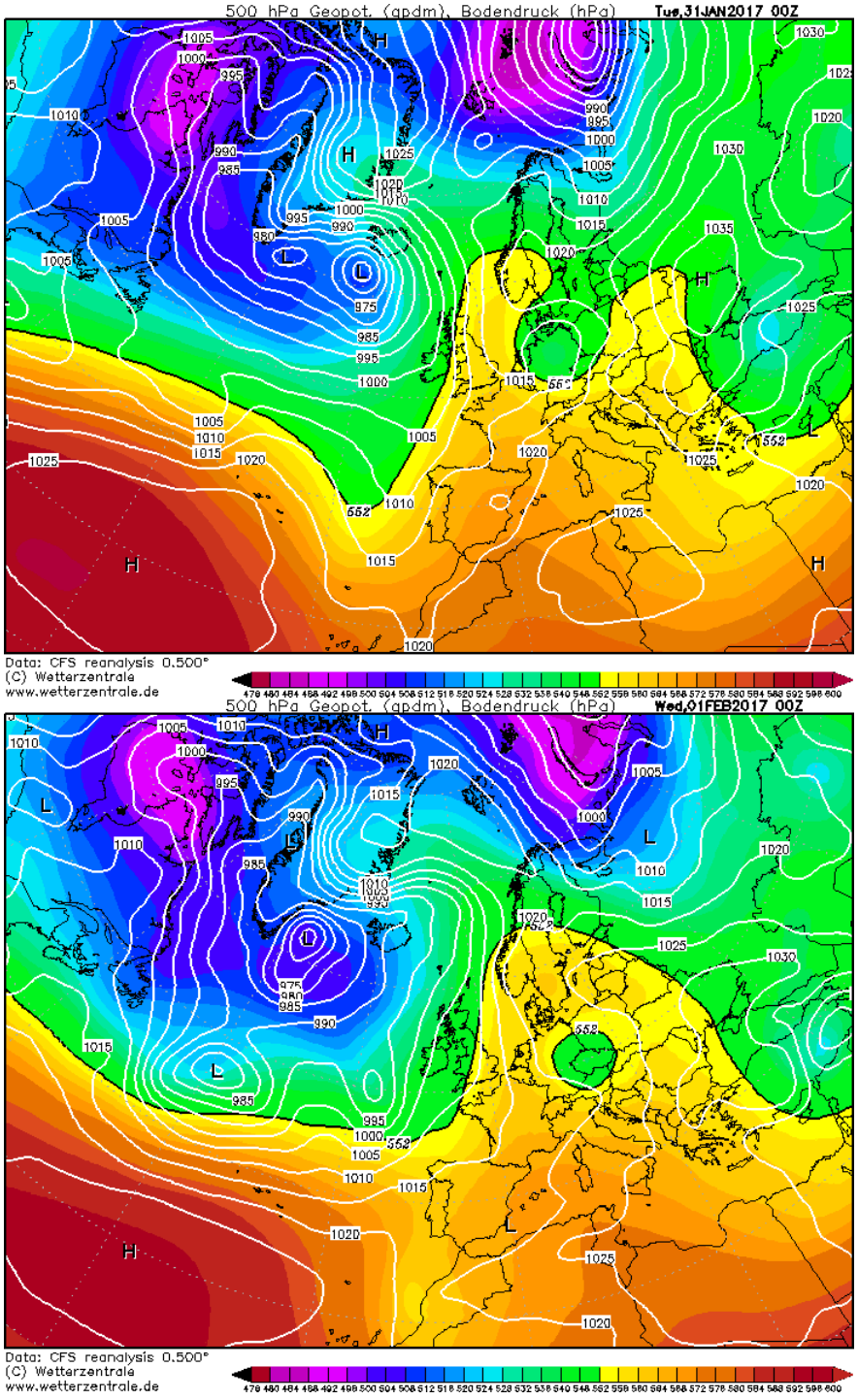
500 hPa Geopot. (gpdm), Bodendruck (hPa)
Tue,31JAN2017 00Z
Data: CFS reanalysis 0.500°
(C) Wetterzentrale
www.wetterzentrale.de
500 hPa Geopot. (gpdm), Bodendruck (hPa)
Wed,01FEB2017 00Z
Data: CFS reanalysis 0.500°
(C) Wetterzentrale
www.wetterzentrale.de

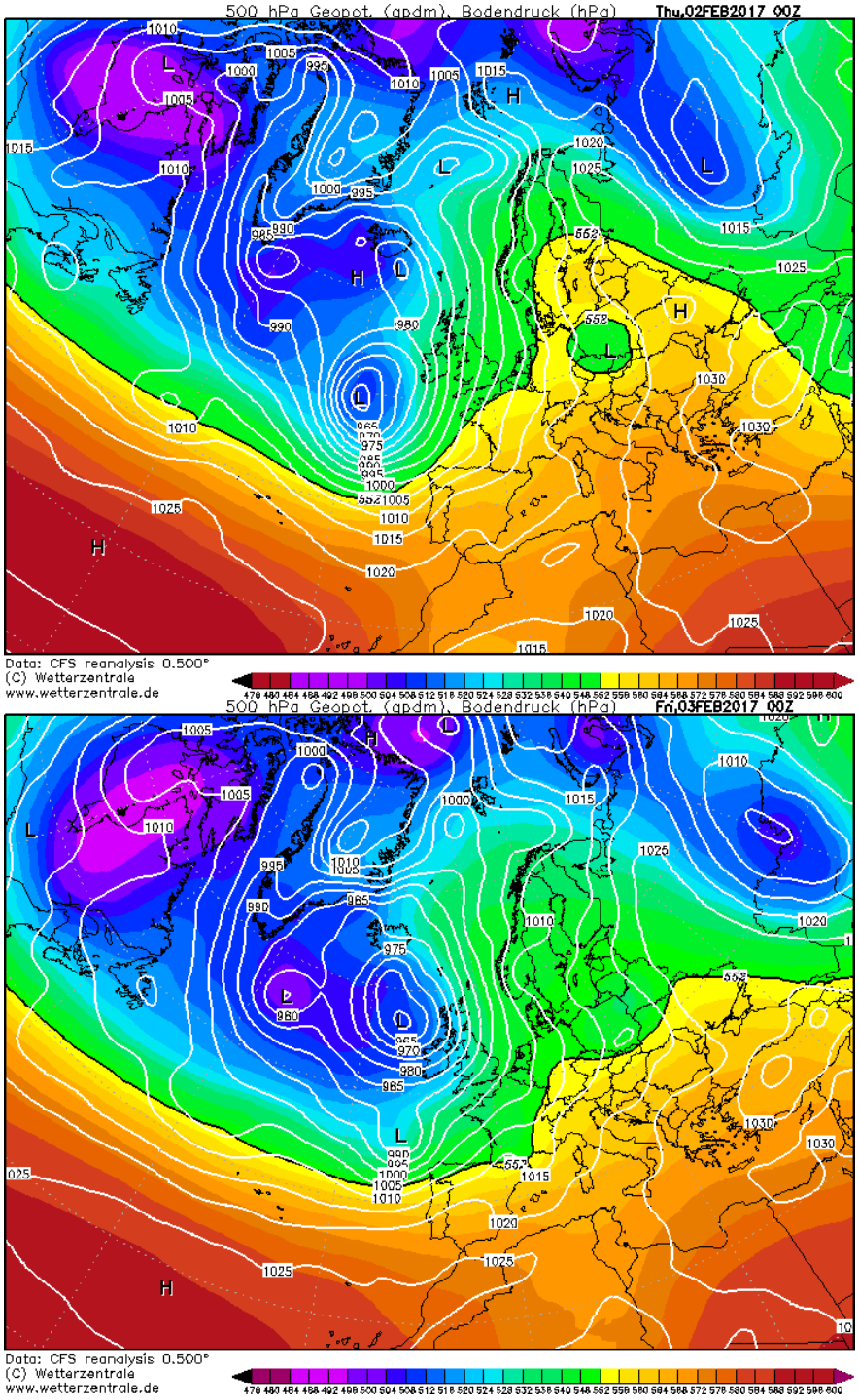
500 hPa Geopot. (gpdm), Bodendruck (hPa)
Thu,02FEB2017 00Z
Data: CFS reanalysis 0.500°
(C) Wetterzentrale
www.wetterzentrale.de
500 hPa Geopot. (gpdm), Bodendruck (hPa)
Fri,03FEB2017 00Z
Data: CFS reanalysis 0.500°
(C) Wetterzentrale
www.wetterzentrale.de

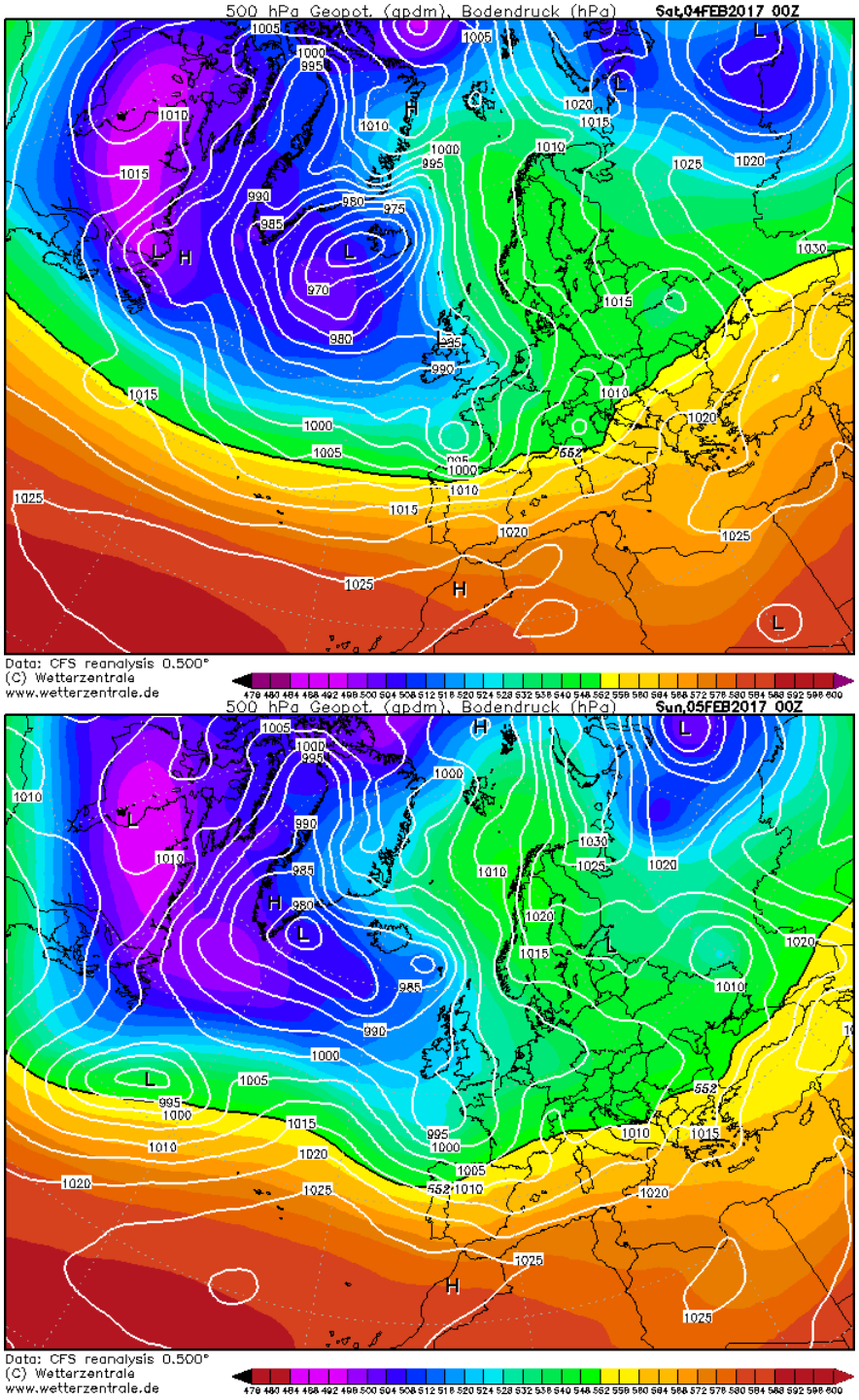
500 hPa Geopot. (gpdm), Bodendruck (hPa)
Sat,04FEB2017 00Z
Data: CFS reanalysis 0.500°
(C) Wetterzentrale
www.wetterzentrale.de
500 hPa Geopot. (gpdm), Bodendruck (hPa)
Sun,05FEB2017 00Z
Data: CFS reanalysis 0.500°
(C) Wetterzentrale
www.wetterzentrale.de

## Weather forecasts for week 2

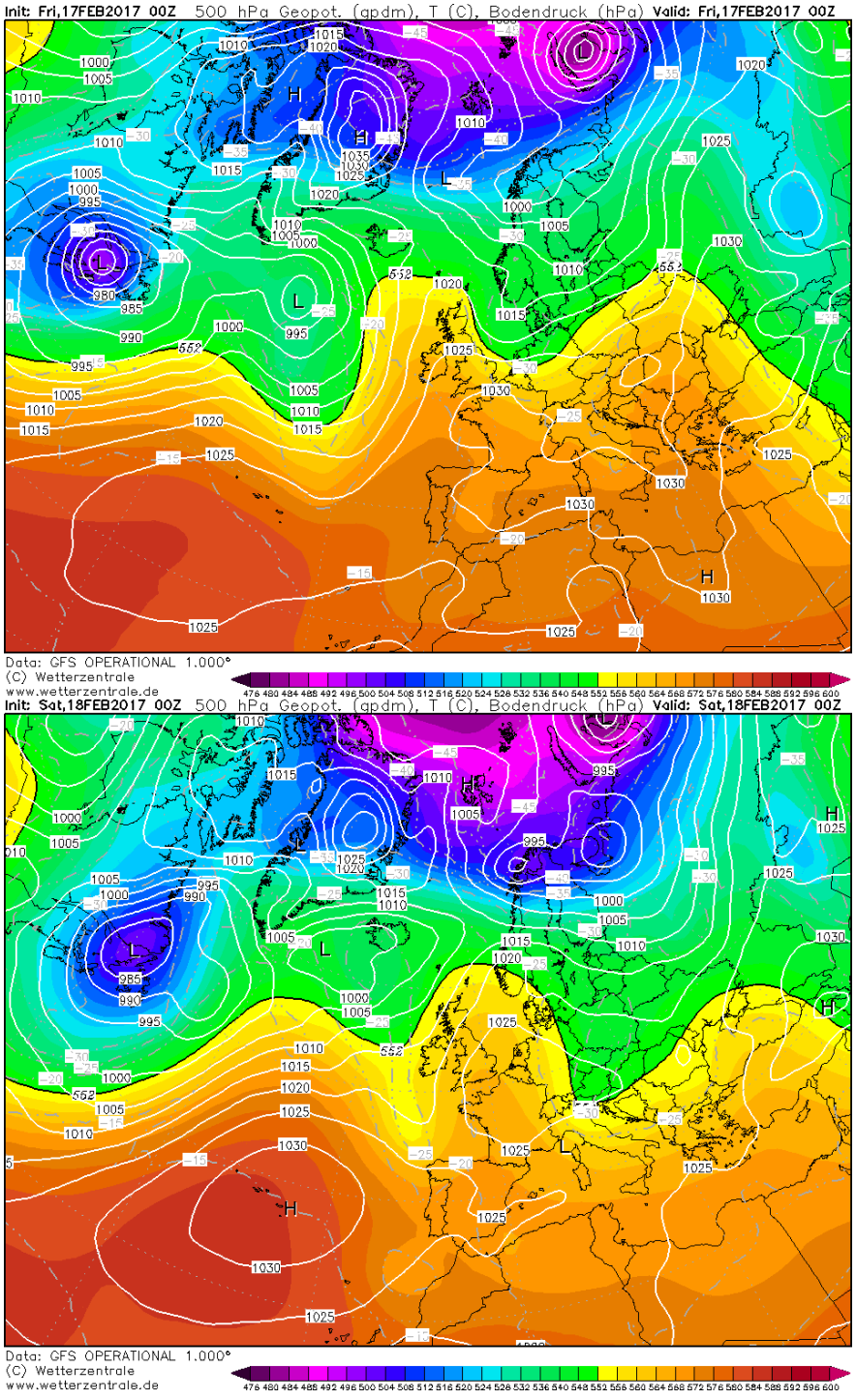

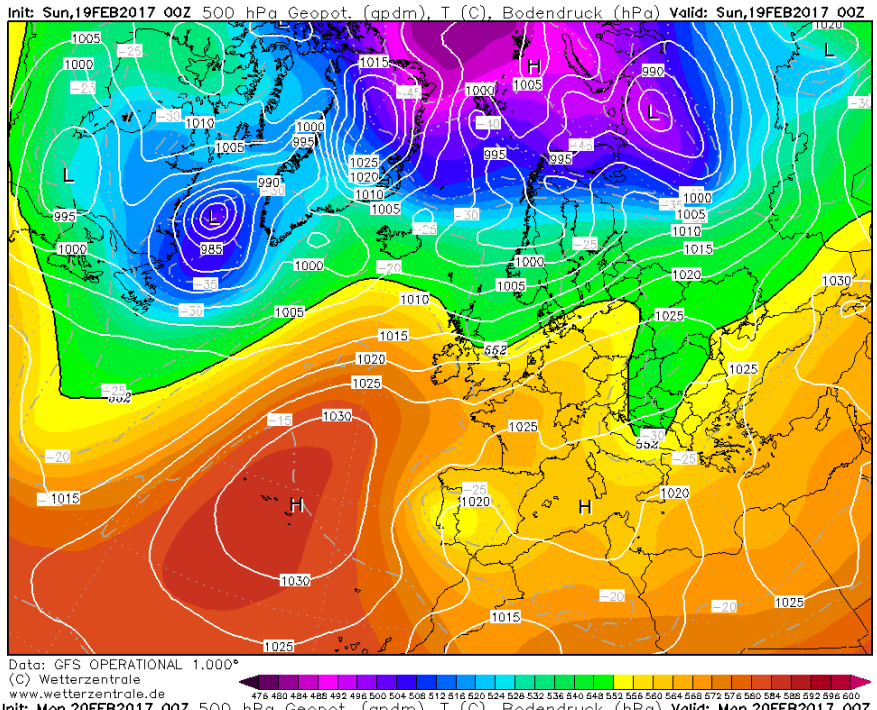
Init: Sun,19FEB2017 00Z 500 hPa Geopot. (gpdm), T (C), Bodendruck (hPa) Valid: Sun,19FEB2017 00Z
Data: GFS OPERATIONAL 1.000°
(C) Wetterzentrale
www.wetterzentrale.de
476 480 484 488 492 496 500 504 508 512 516 520 524 528 532 536 540 544 548 552 556 560 564 568 572 576 580 584 588 592 596 600

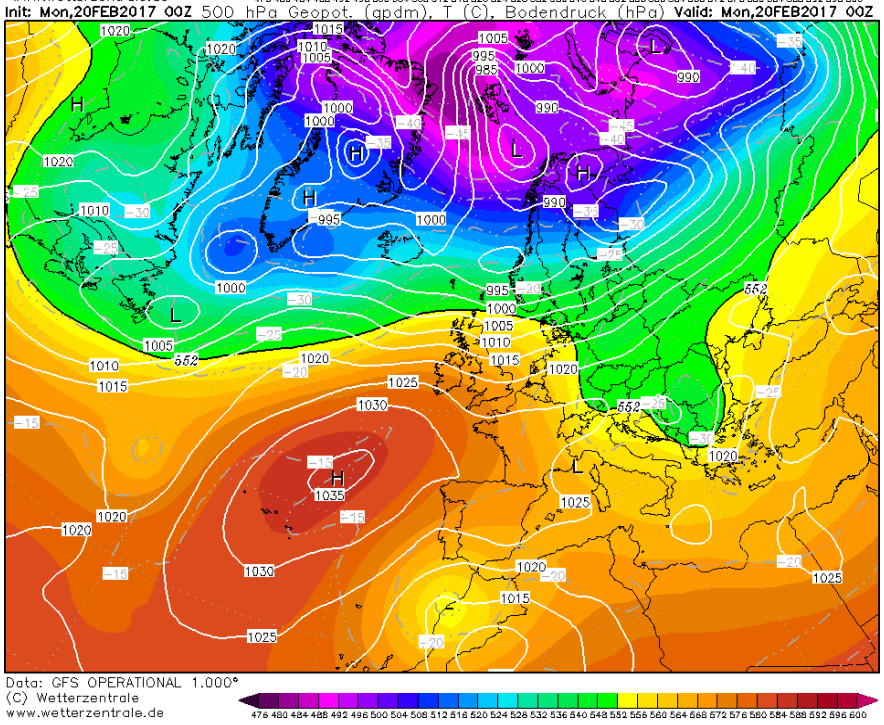
Init: Mon,20FEB2017 00Z 500 hPa Geopot. (gpdm), T (C), Bodendruck (hPa) Valid: Mon,20FEB2017 00Z
Data: GFS OPERATIONAL 1.000°
(C) Wetterzentrale
www.wetterzentrale.de
476 480 484 488 492 496 500 504 508 512 516 520 524 528 532 536 540 544 548 552 556 560 564 568 572 576 580 584 588 592 596 600

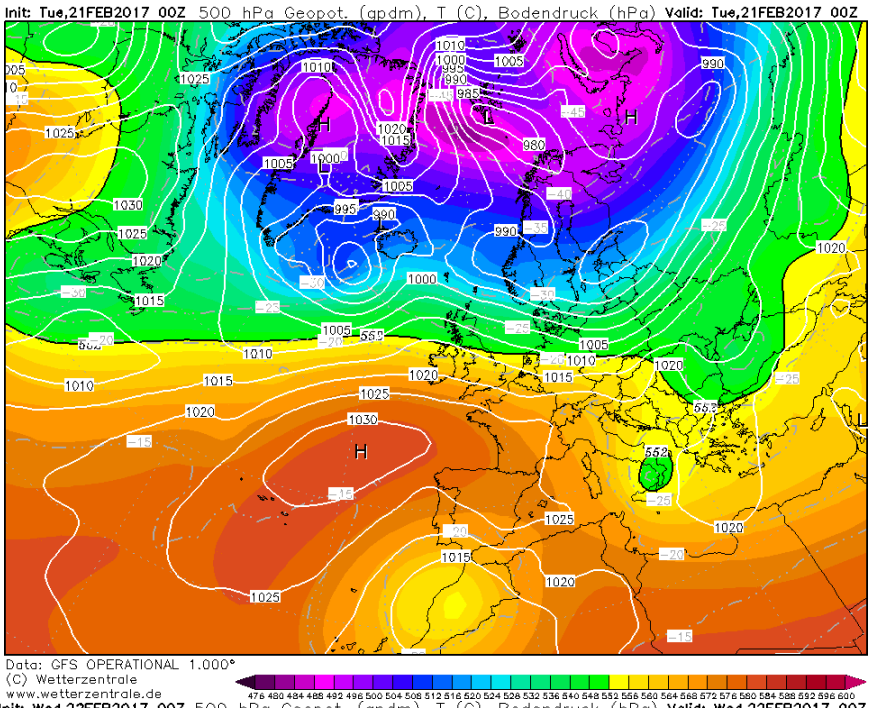
Init: Tue,21FEB2017 00Z 500 hPa Geopot. (gpdm), T (C), Bodendruck (hPa) Valid: Tue,21FEB2017 00Z
Data: GFS OPERATIONAL 1.000°
(C) Wetterzentrale
www.wetterzentrale.de
476 480 484 488 492 496 500 504 508 512 516 520 524 528 532 536 540 544 548 552 556 560 564 568 572 576 580 584 588 592 596 600

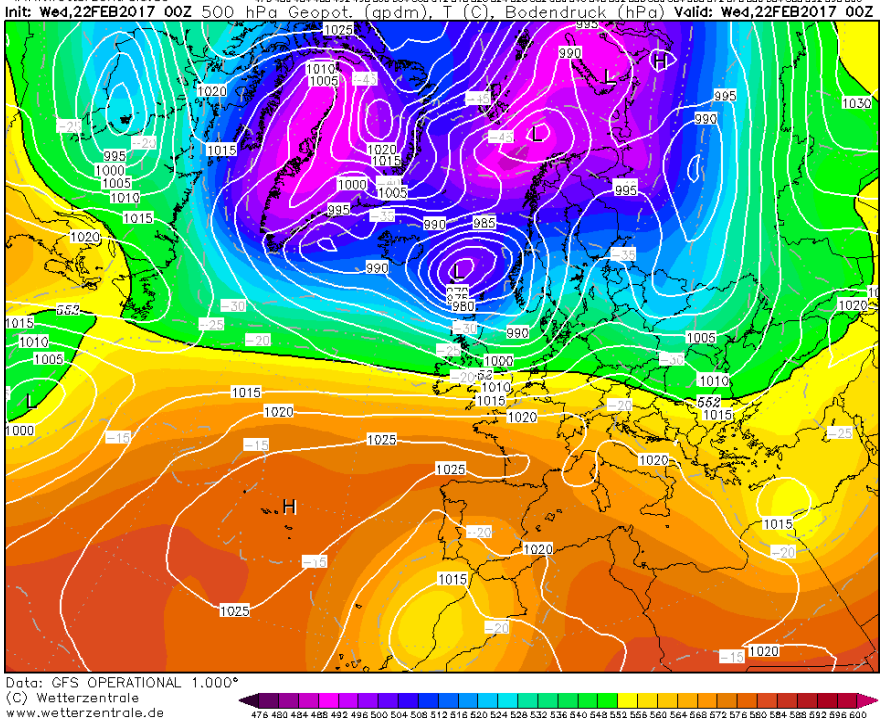
Init: Wed,22FEB2017 00Z 500 hPa Geopot. (gpdm), T (C), Bodendruck (hPa) Valid: Wed,22FEB2017 00Z
Data: GFS OPERATIONAL 1.000°
(C) Wetterzentrale
www.wetterzentrale.de
476 480 484 488 492 496 500 504 508 512 516 520 524 528 532 536 540 544 548 552 556 560 564 568 572 576 580 584 588 592 596 600

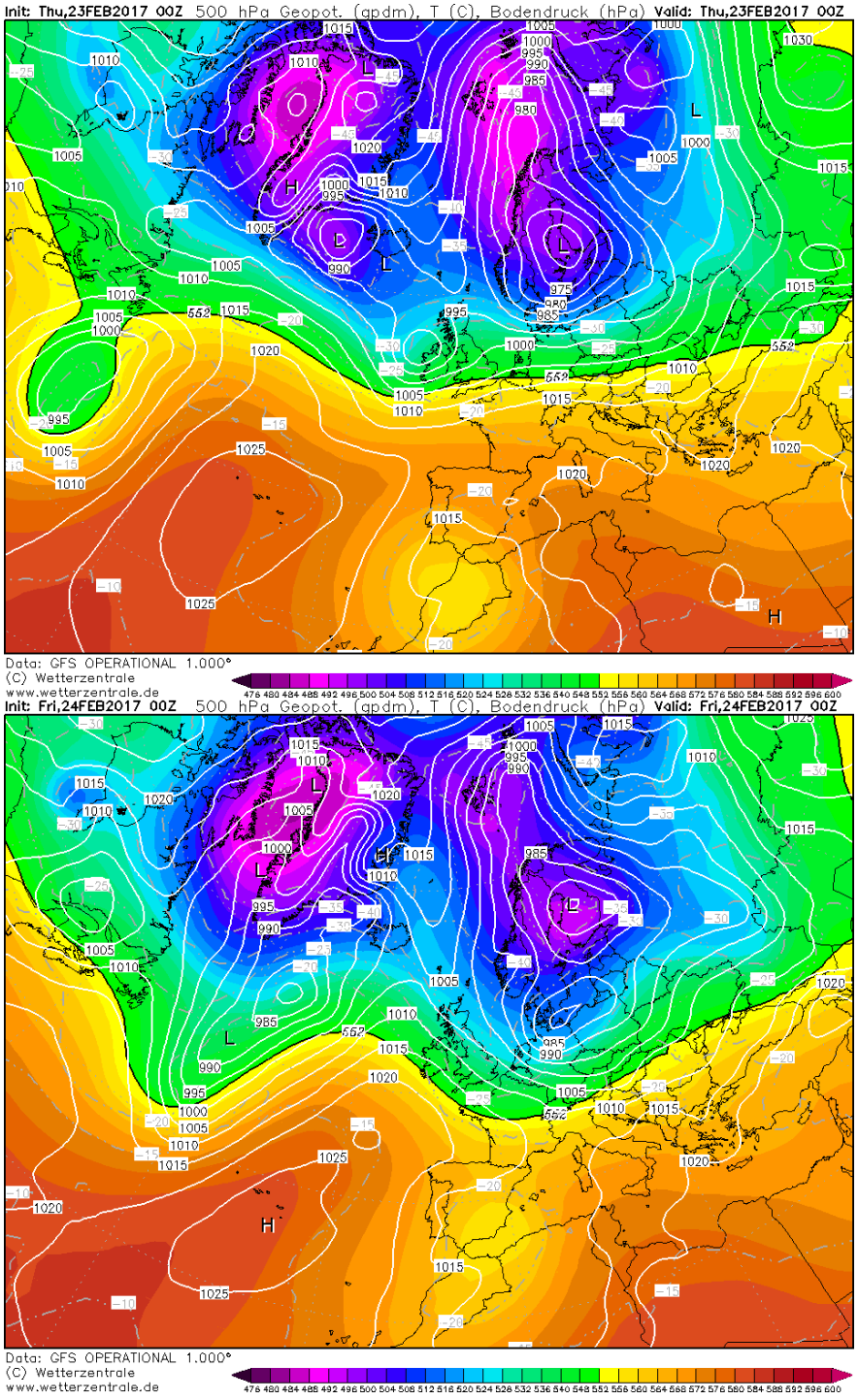


**Weather forecasts for week 3**

Meteorological forecasts for week 3

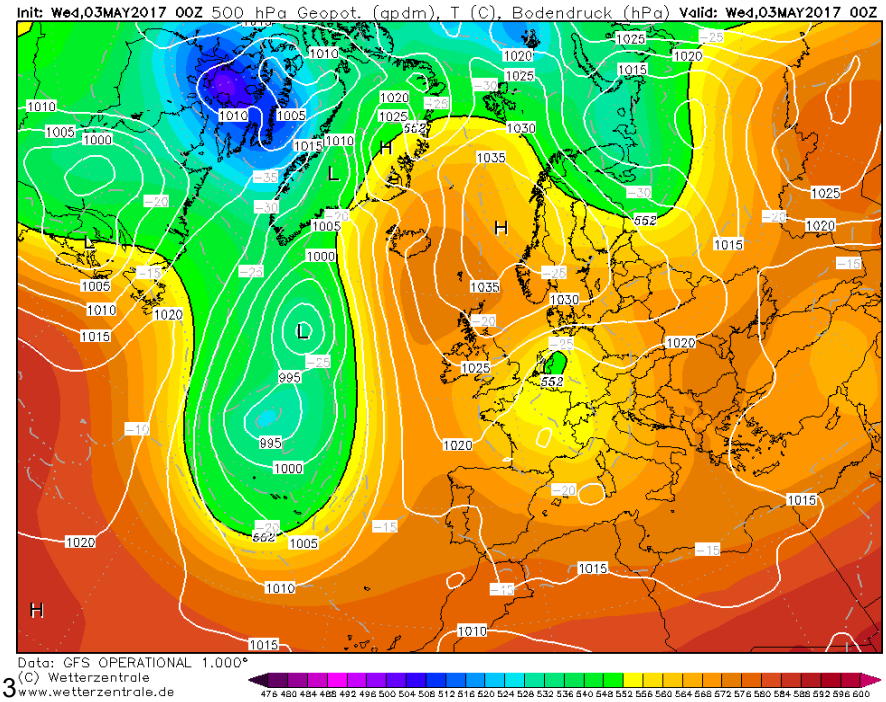


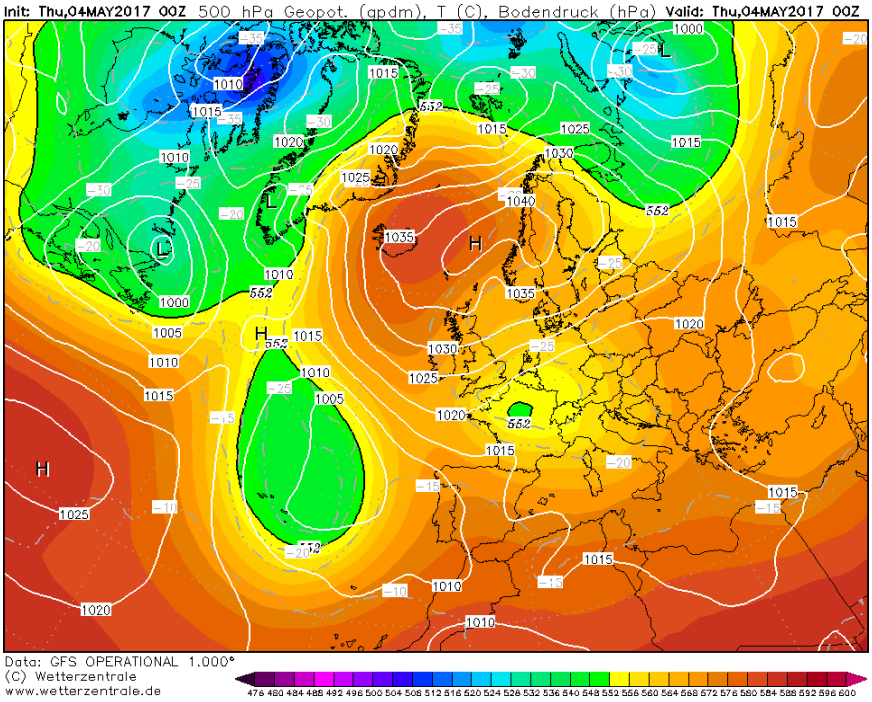

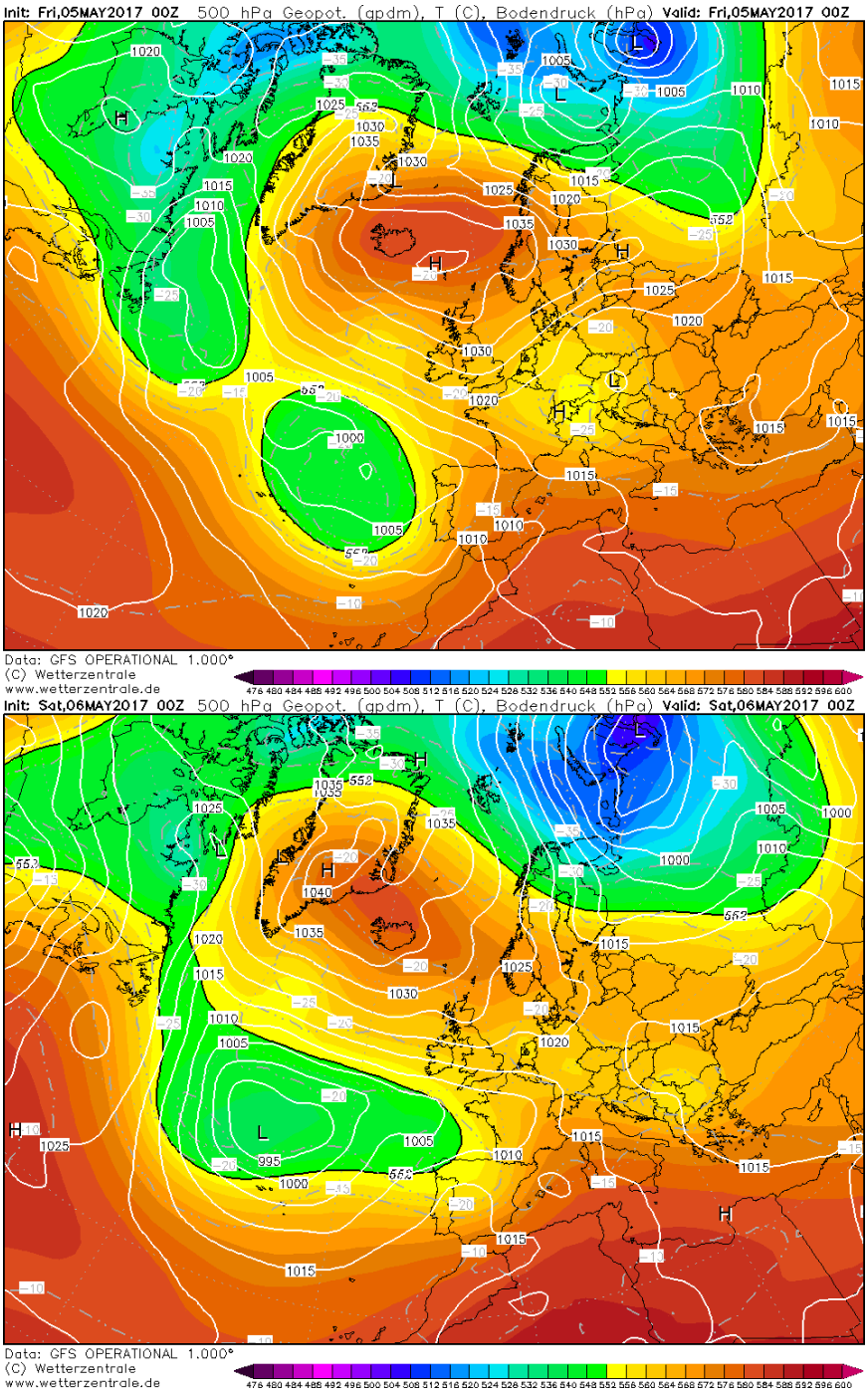
Init: Fri,05MAY2017 00Z 500 hPa Geopot. (gpdm), T (C), Bodendruck (hPa) Valid: Fri,05MAY2017 00Z
Data: GFS OPERATIONAL 1.000°
(C) Wetterzentrale
www.wetterzentrale.de
476 480 484 488 492 496 500 504 508 512 516 520 524 528 532 536 540 544 548 552 556 560 564 568 572 576 580 584 588 592 596 600
Init: Sat,06MAY2017 00Z 500 hPa Geopot. (gpdm), T (C), Bodendruck (hPa) Valid: Sat,06MAY2017 00Z
Data: GFS OPERATIONAL 1.000°
(C) Wetterzentrale
www.wetterzentrale.de
476 480 484 488 492 496 500 504 508 512 516 520 524 528 532 536 540 544 548 552 556 560 564 568 572 576 580 584 588 592 596 600

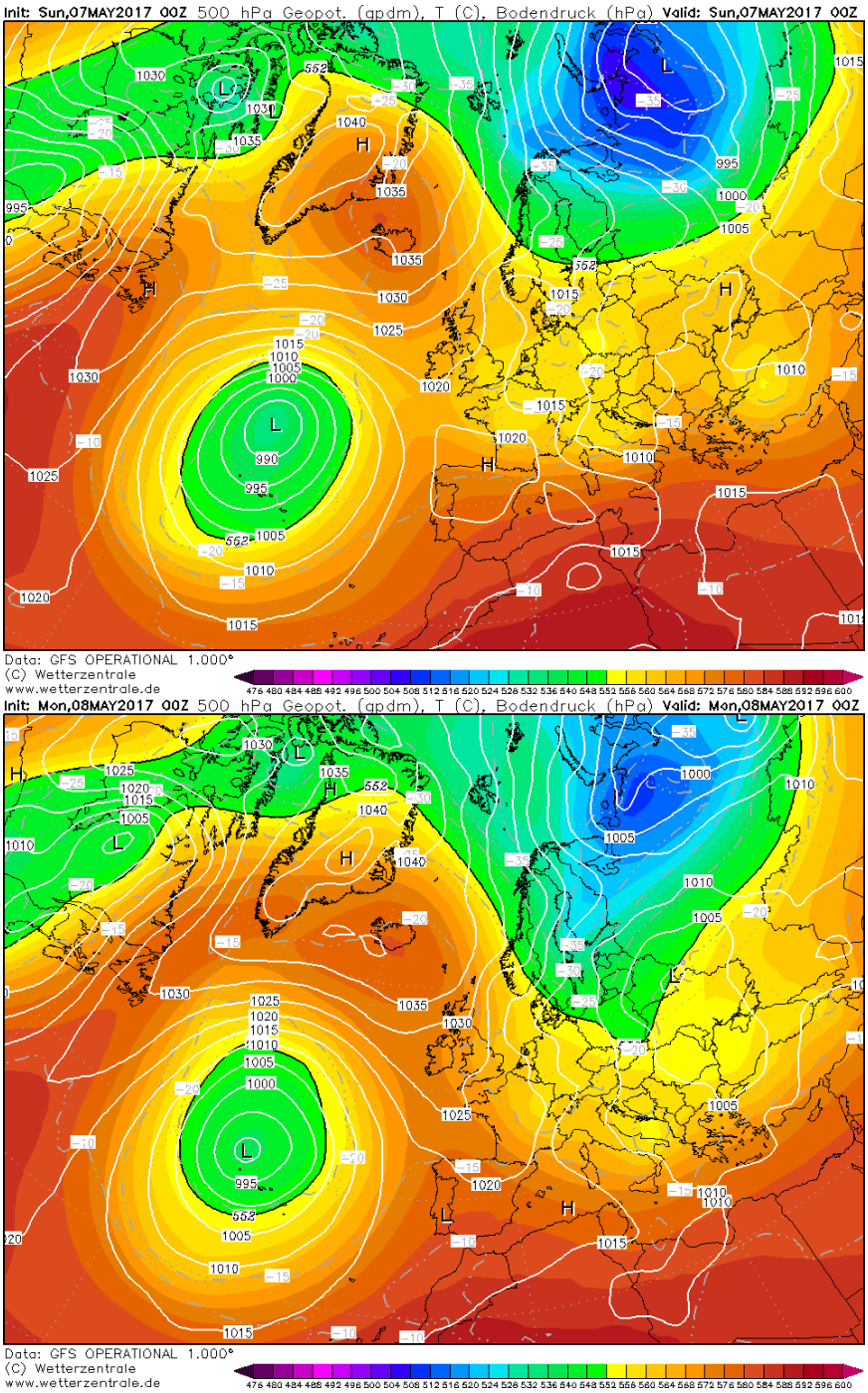
Init: Sun,07MAY2017 00Z 500 hPa Geopot. (gpdm), T (C), Bodendruck (hPa) Valid: Sun,07MAY2017 00Z
Data: GFS OPERATIONAL 1.000°
(C) Wetterzentrale
www.wetterzentrale.de
476 480 484 488 492 496 500 504 508 512 516 520 524 528 532 536 540 544 548 552 556 560 564 568 572 576 580 584 588 592 596 600
Init: Mon,08MAY2017 00Z 500 hPa Geopot. (gpdm), T (C), Bodendruck (hPa) Valid: Mon,08MAY2017 00Z
Data: GFS OPERATIONAL 1.000°
(C) Wetterzentrale
www.wetterzentrale.de
476 480 484 488 492 496 500 504 508 512 516 520 524 528 532 536 540 544 548 552 556 560 564 568 572 576 580 584 588 592 596 600

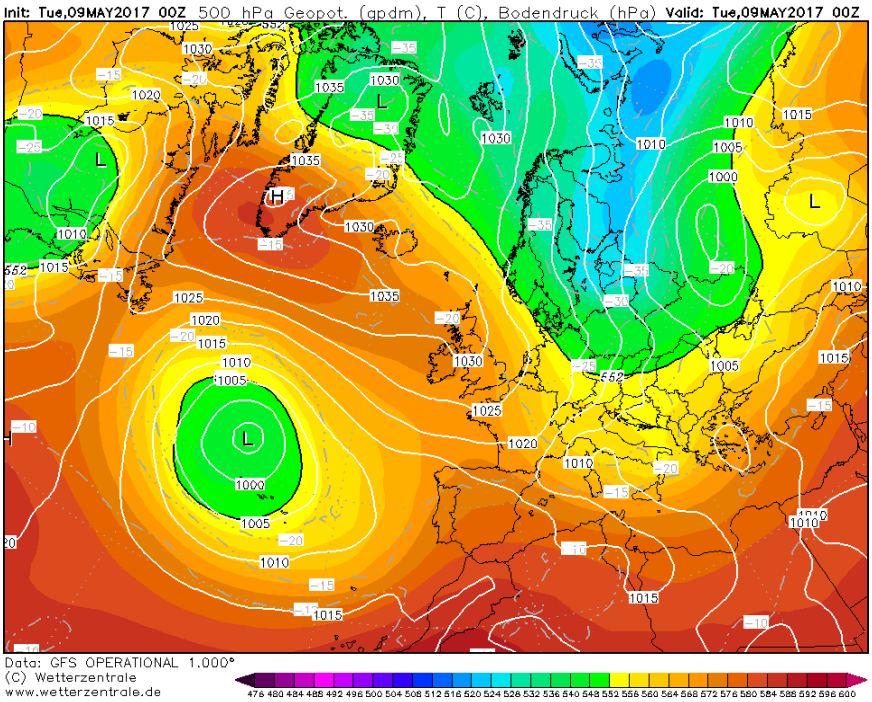


## Weather forecasts for week 4

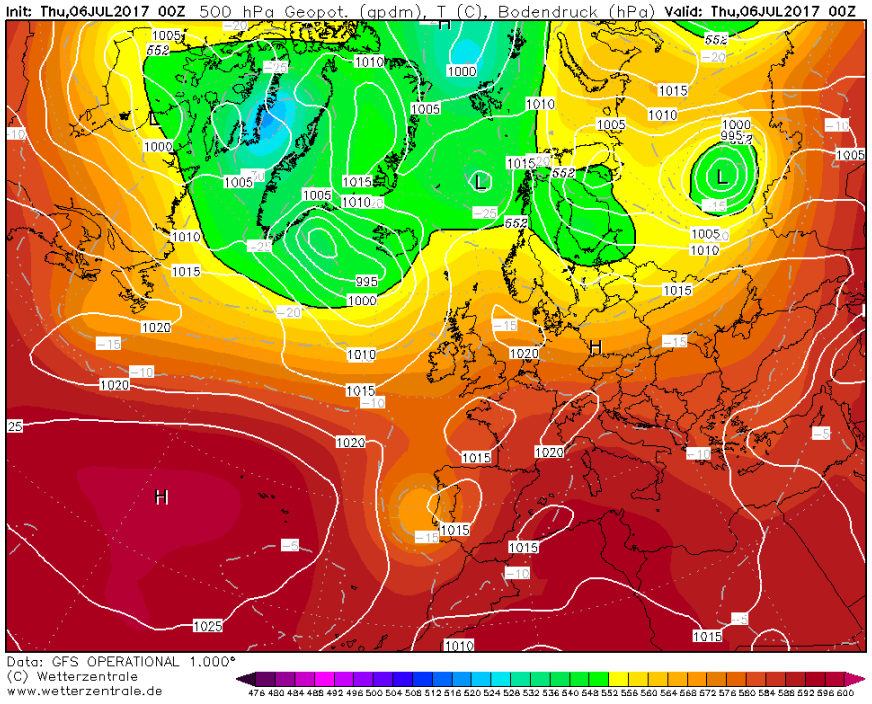

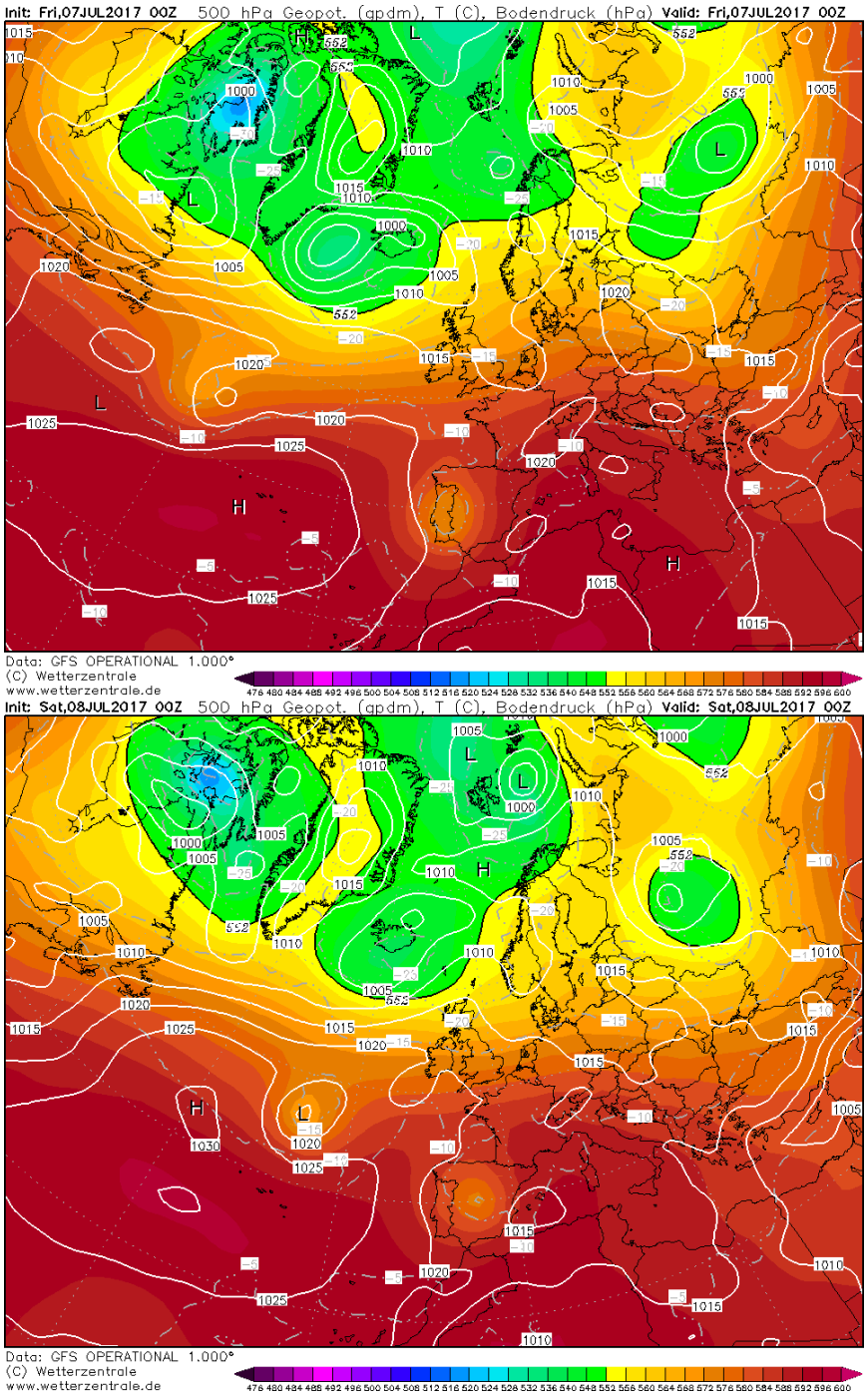
Init: Fri,07JUL2017 00Z 500 hPa Geopot. (gpdm), T (C), Bodendruck (hPa) Valid: Fri,07JUL2017 00Z
Data: GFS OPERATIONAL 1.000°
(C) Wetterzentrale
www.wetterzentrale.de
476 480 484 488 492 496 500 504 508 512 516 520 524 528 532 536 540 544 548 552 556 560 564 568 572 576 580 584 588 592 596 600
Init: Sat,08JUL2017 00Z 500 hPa Geopot. (gpdm), T (C), Bodendruck (hPa) Valid: Sat,08JUL2017 00Z
Data: GFS OPERATIONAL 1.000°
(C) Wetterzentrale
www.wetterzentrale.de
476 480 484 488 492 496 500 504 508 512 516 520 524 528 532 536 540 544 548 552 556 560 564 568 572 576 580 584 588 592 596 600

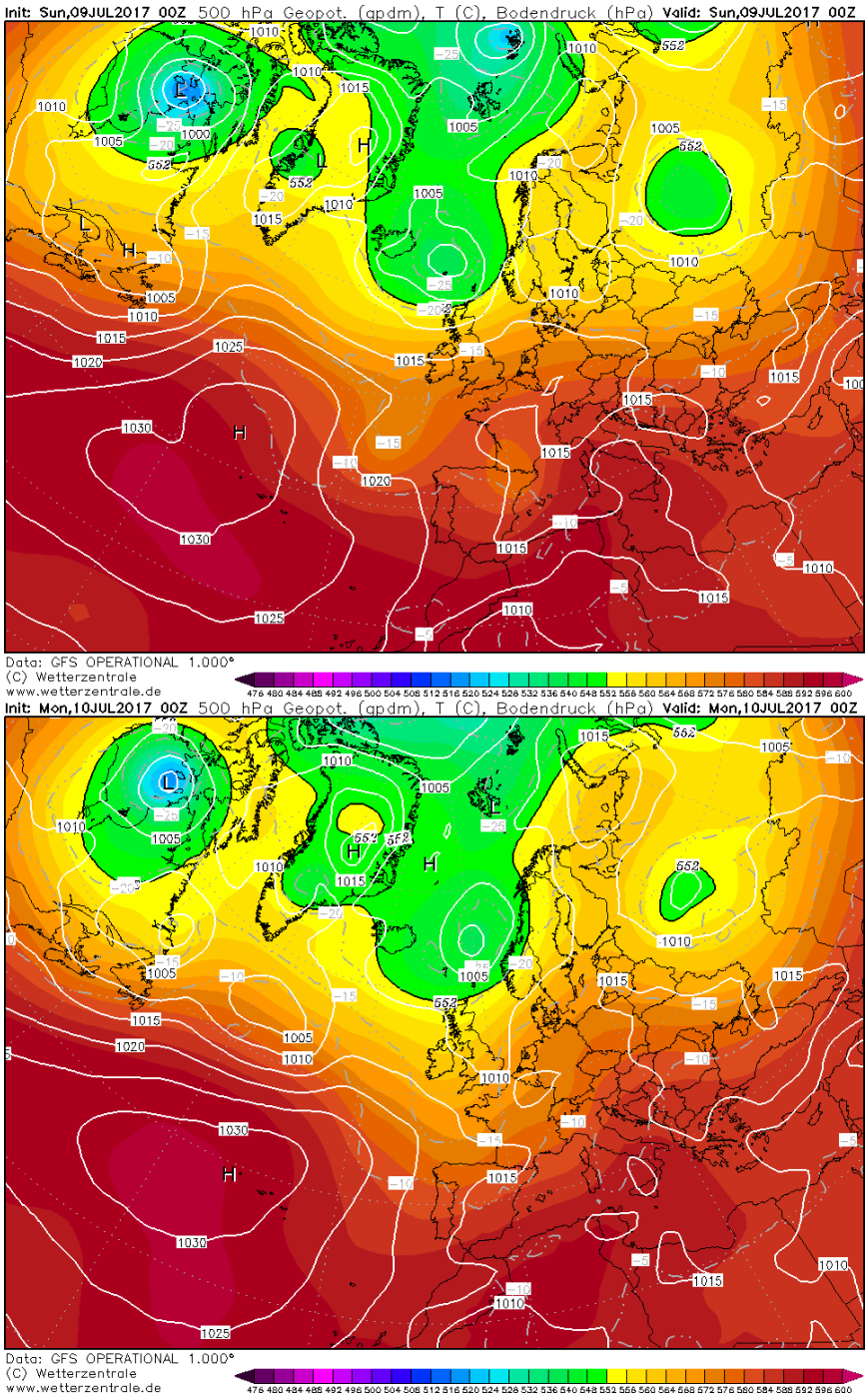
Init: Sun,09JUL2017 00Z 500 hPa Geopot. (gpdm), T (C), Bodendruck (hPa) Valid: Sun,09JUL2017 00Z
Data: GFS OPERATIONAL 1.000°
(C) Wetterzentrale
www.wetterzentrale.de
476 480 484 488 492 496 500 504 508 512 516 520 524 528 532 536 540 544 548 552 556 560 564 568 572 576 580 584 588 592 596 600
Init: Mon,10JUL2017 00Z 500 hPa Geopot. (gpdm), T (C), Bodendruck (hPa) Valid: Mon,10JUL2017 00Z
Data: GFS OPERATIONAL 1.000°
(C) Wetterzentrale
www.wetterzentrale.de
476 480 484 488 492 496 500 504 508 512 516 520 524 528 532 536 540 544 548 552 556 560 564 568 572 576 580 584 588 592 596 600

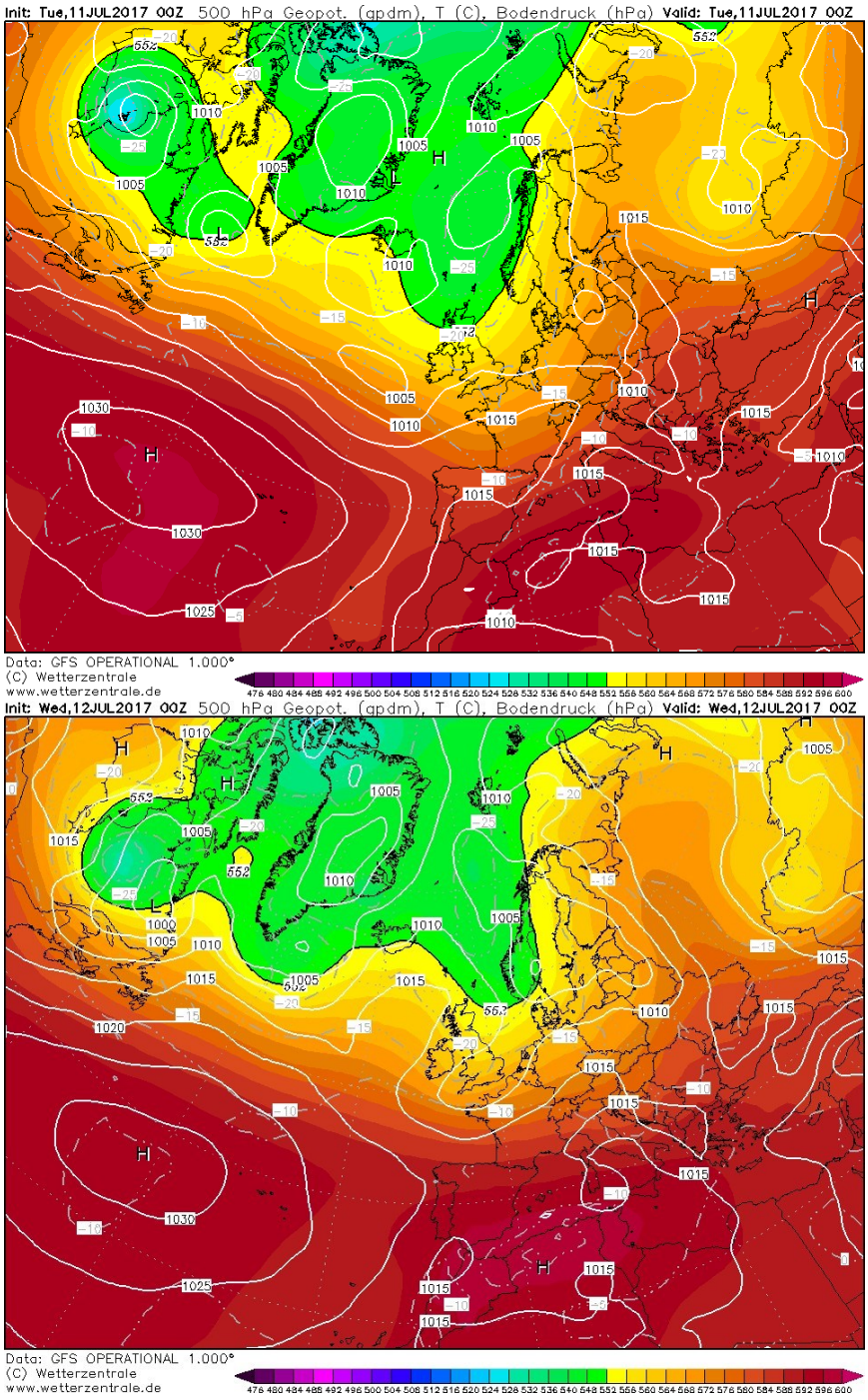


**Weather forecasts for week 5**

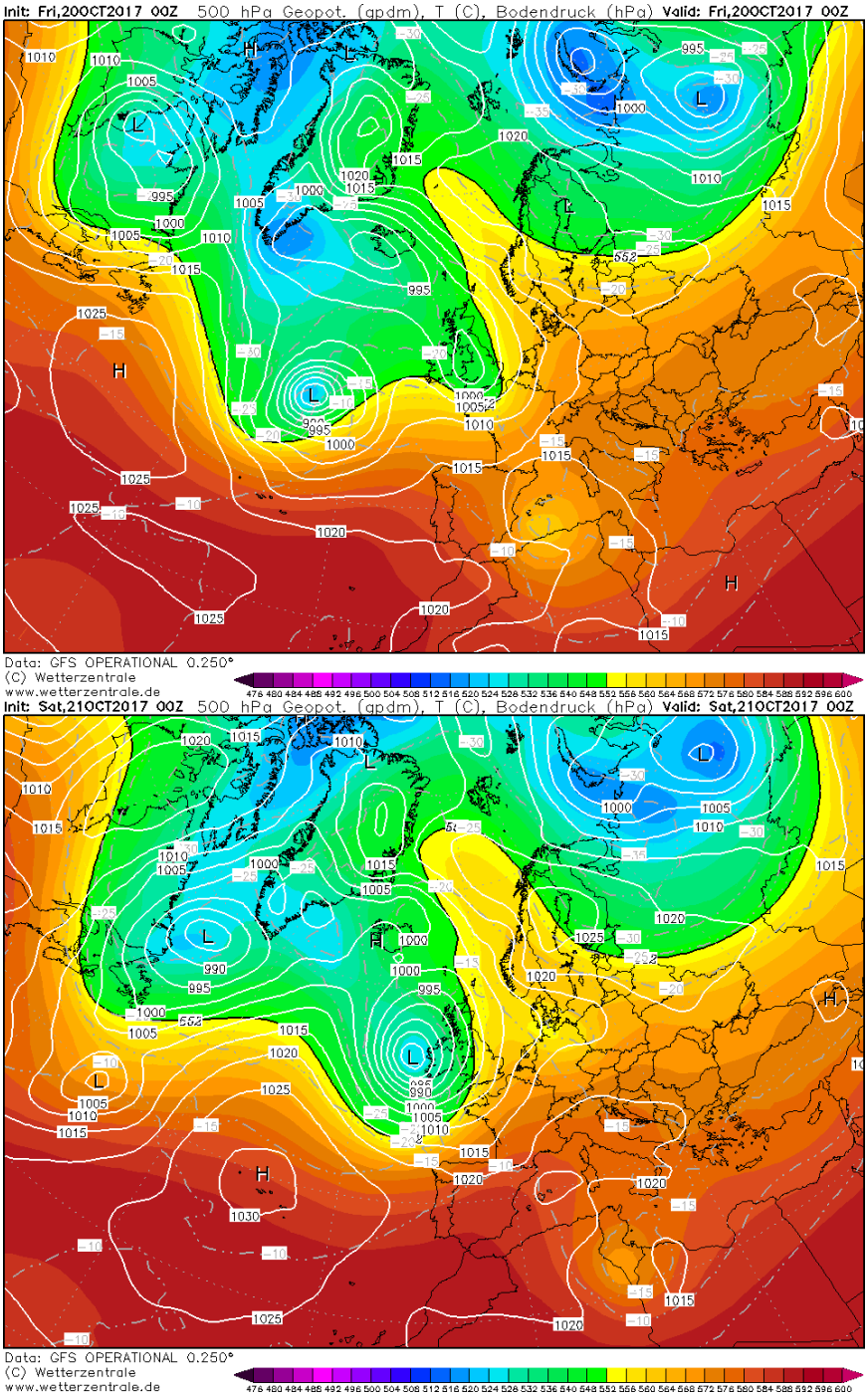
Init: Fri,20OCT2017 00Z 500 hPa Geopot. (gpdm), T (C), Bodendruck (hPa) Valid: Fri,20OCT2017 00Z
Data: GFS OPERATIONAL 0.250°
(C) Wetterzentrale
www.wetterzentrale.de
476 480 484 488 492 496 500 504 508 512 516 520 524 528 532 536 540 544 548 552 556 560 564 568 572 576 580 584 588 592 596 600
Init: Sat,21OCT2017 00Z 500 hPa Geopot. (gpdm), T (C), Bodendruck (hPa) Valid: Sat,21OCT2017 00Z
Data: GFS OPERATIONAL 0.250°
(C) Wetterzentrale
www.wetterzentrale.de
476 480 484 488 492 496 500 504 508 512 516 520 524 528 532 536 540 544 548 552 556 560 564 568 572 576 580 584 588 592 596 600

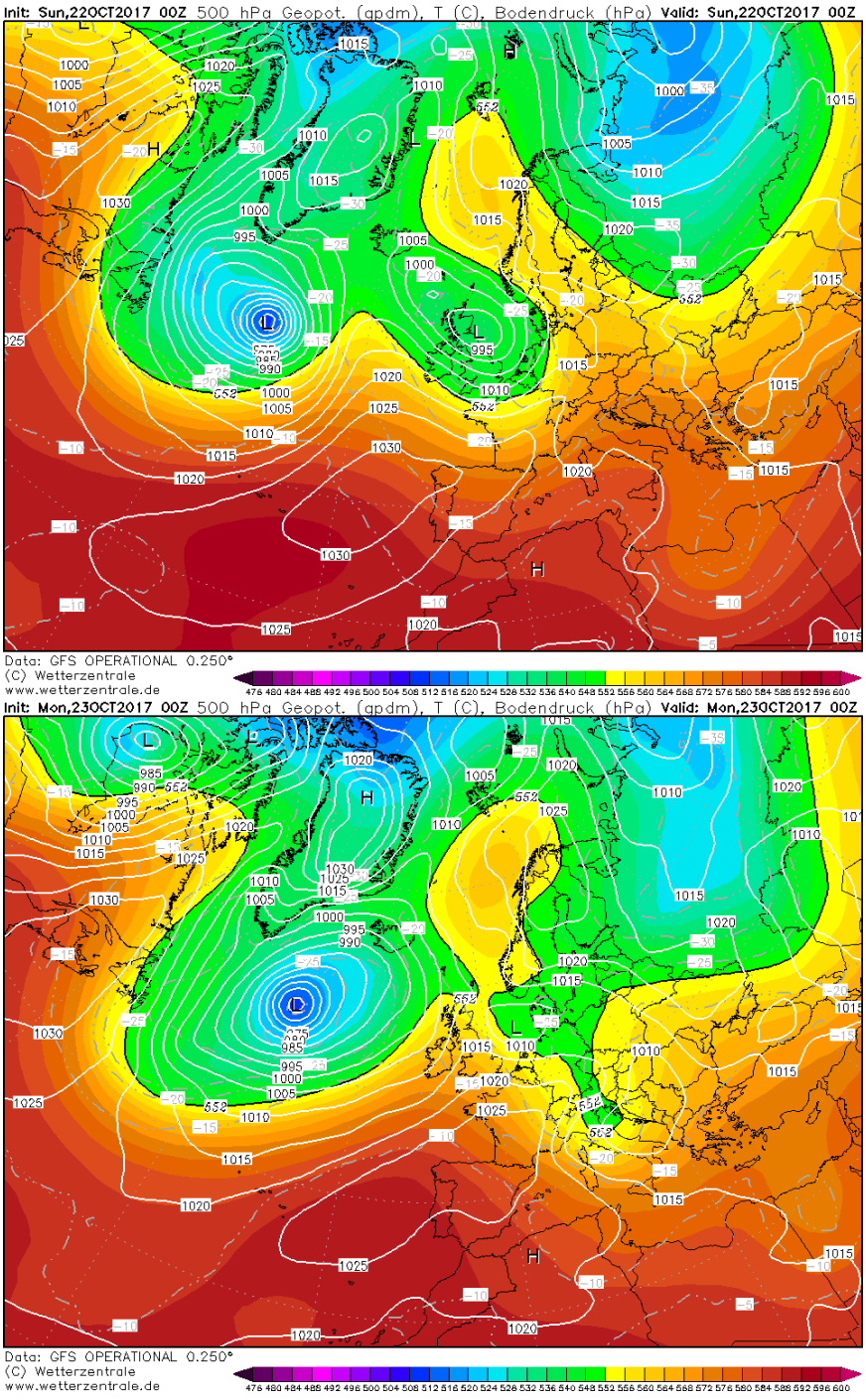
Init: Sun,22OCT2017 00Z 500 hPa Geopot. (gpdm), T (C), Bodendruck (hPa) Valid: Sun,22OCT2017 00Z
Data: GFS OPERATIONAL 0.250°
(C) Wetterzentrale
www.wetterzentrale.de
476 480 484 488 492 496 500 504 508 512 516 520 524 528 532 536 540 544 548 552 556 560 564 568 572 576 580 584 588 592 596 600
Init: Mon,23OCT2017 00Z 500 hPa Geopot. (gpdm), T (C), Bodendruck (hPa) Valid: Mon,23OCT2017 00Z
Data: GFS OPERATIONAL 0.250°
(C) Wetterzentrale
www.wetterzentrale.de
476 480 484 488 492 496 500 504 508 512 516 520 524 528 532 536 540 544 548 552 556 560 564 568 572 576 580 584 588 592 596 600

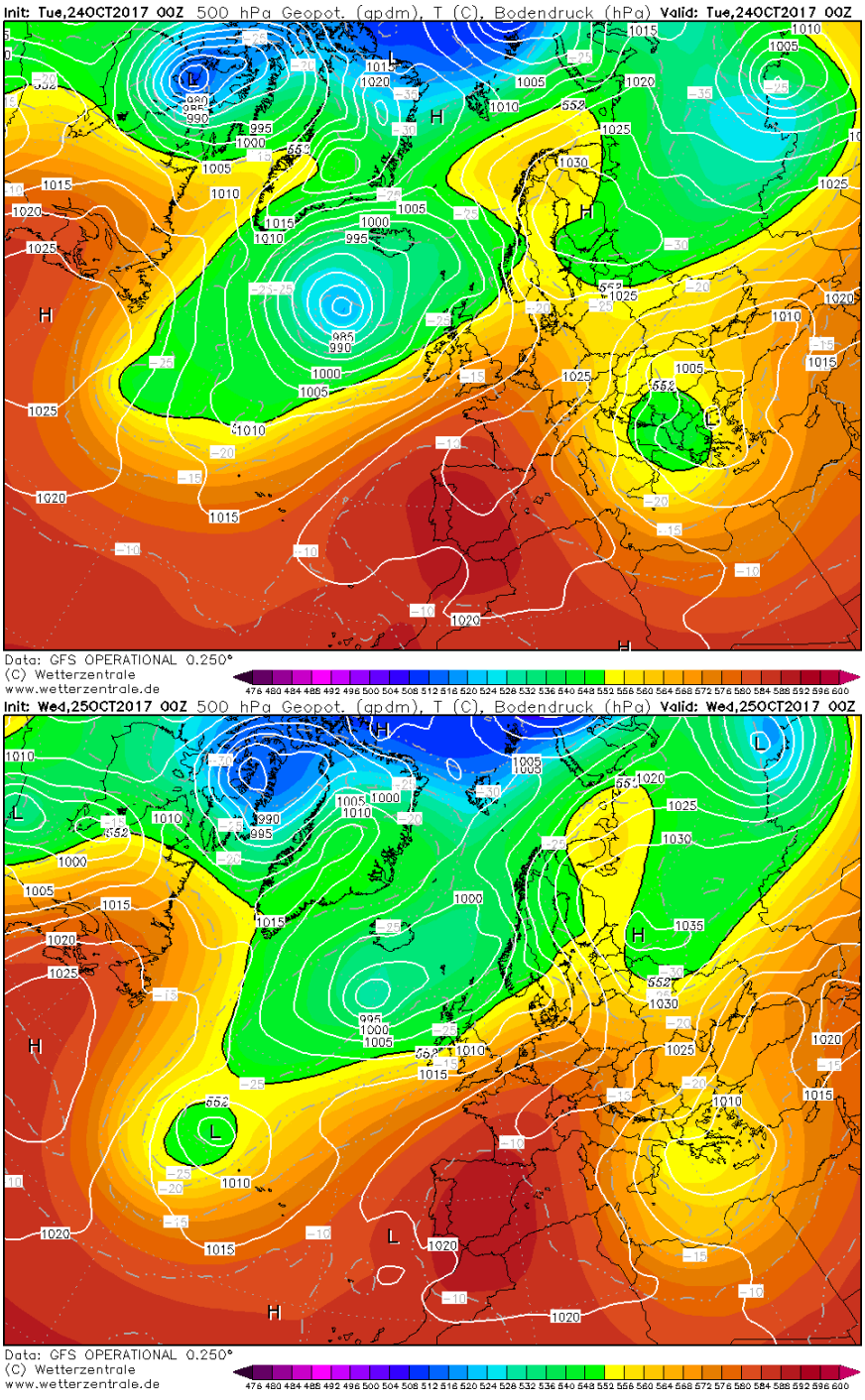
Init: Tue,24OCT2017 00Z 500 hPa Geopot. (gpdm), T (C), Bodendruck (hPa) Valid: Tue,24OCT2017 00Z
Data: GFS OPERATIONAL 0.250°
(C) Wetterzentrale
www.wetterzentrale.de
476 480 484 488 492 496 500 504 508 512 516 520 524 528 532 536 540 544 548 552 556 560 564 568 572 576 580 584 588 592 596 600
Init: Wed,25OCT2017 00Z 500 hPa Geopot. (gpdm), T (C), Bodendruck (hPa) Valid: Wed,25OCT2017 00Z
Data: GFS OPERATIONAL 0.250°
(C) Wetterzentrale
www.wetterzentrale.de
476 480 484 488 492 496 500 504 508 512 516 520 524 528 532 536 540 544 548 552 556 560 564 568 572 576 580 584 588 592 596 600

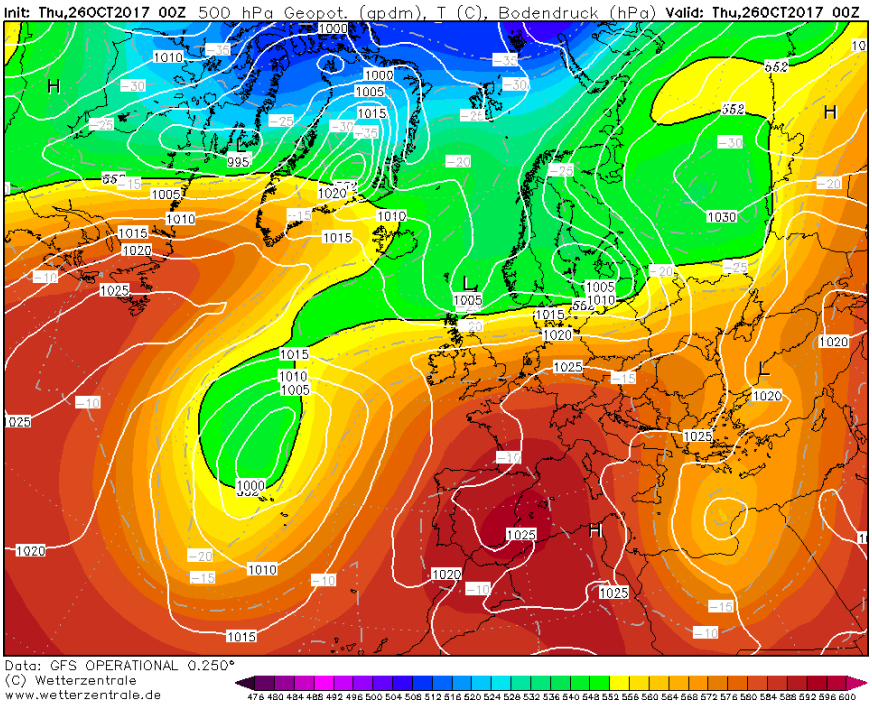


## Weather forecasts for week 6

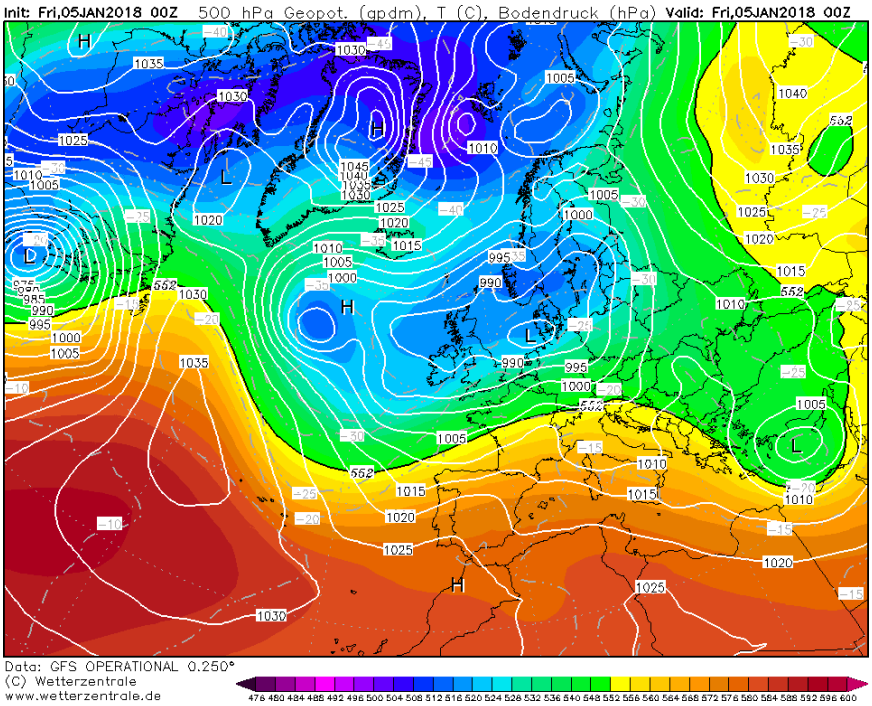

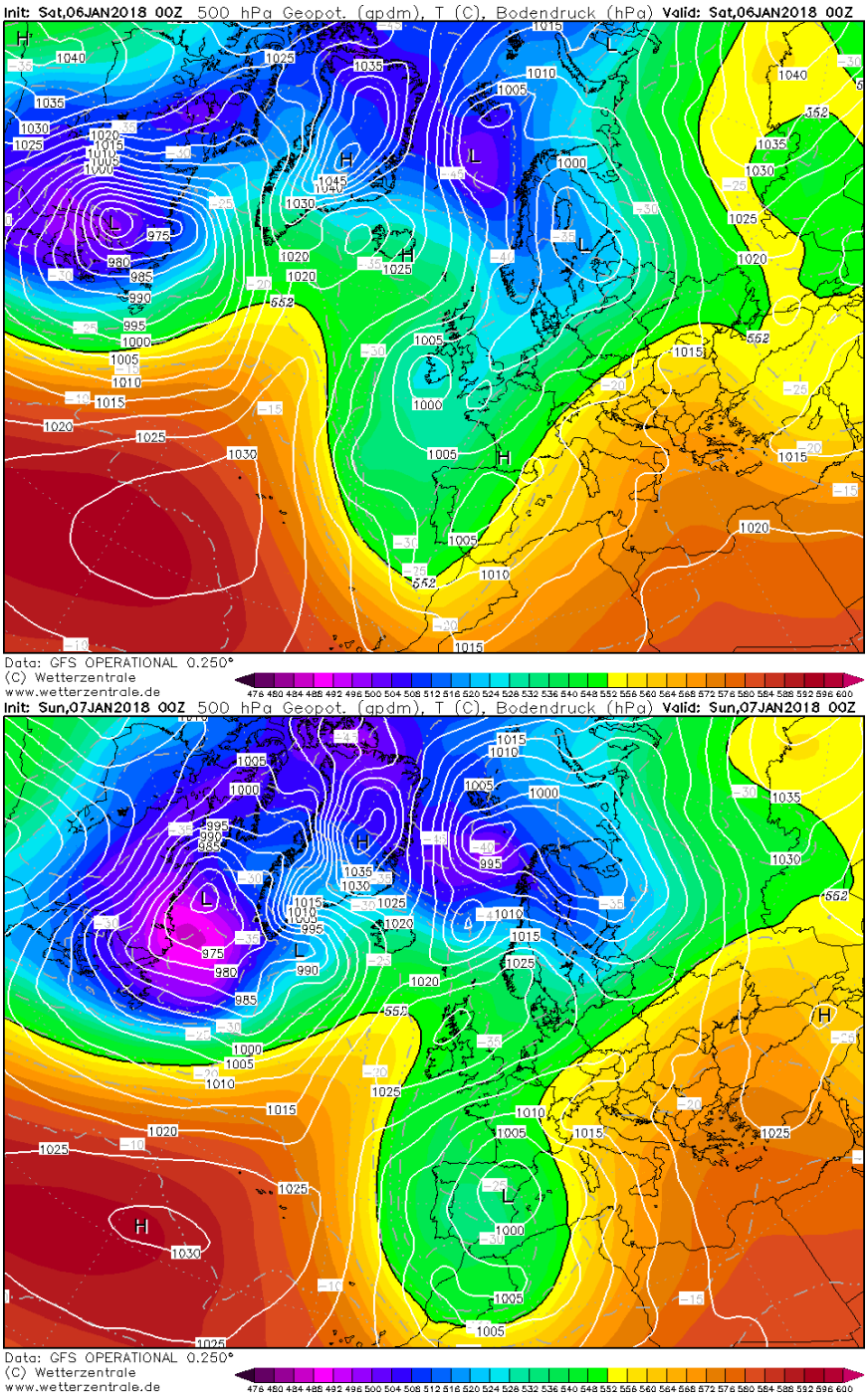
Init: Sat,06JAN2018 00Z 500 hPa Geopot. (gpdm), T (C), Bodendruck (hPa) Valid: Sat,06JAN2018 00Z
Data: GFS OPERATIONAL 0.250°
(C) Wetterzentrale
www.wetterzentrale.de
476 480 484 488 492 496 500 504 508 512 516 520 524 528 532 536 540 544 548 552 556 560 564 568 572 576 580 584 588 592 596 600
Init: Sun,07JAN2018 00Z 500 hPa Geopot. (gpdm), T (C), Bodendruck (hPa) Valid: Sun,07JAN2018 00Z
Data: GFS OPERATIONAL 0.250°
(C) Wetterzentrale
www.wetterzentrale.de
476 480 484 488 492 496 500 504 508 512 516 520 524 528 532 536 540 544 548 552 556 560 564 568 572 576 580 584 588 592 596 600

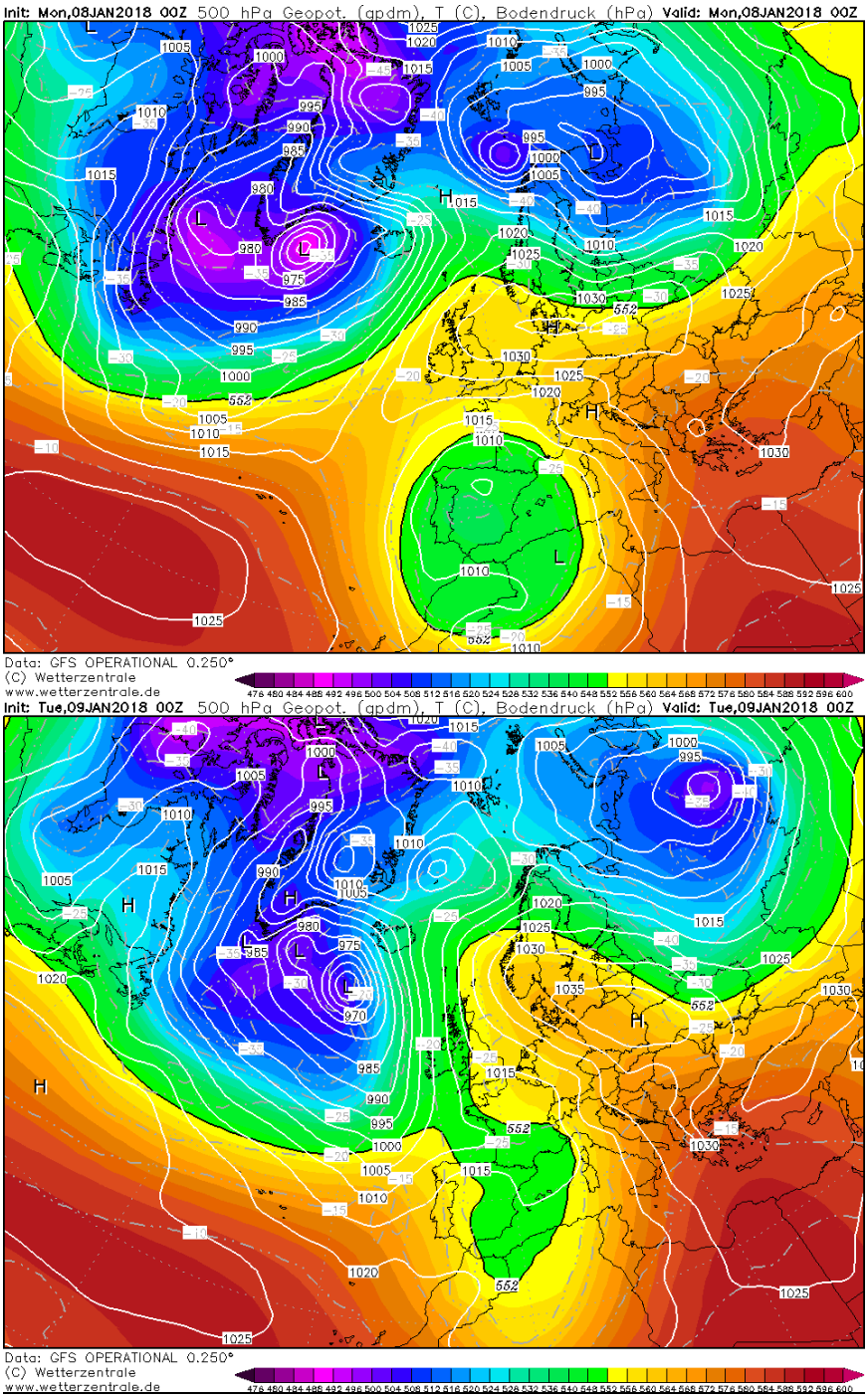
Init: Mon,08JAN2018 00Z 500 hPa Geopot. (gpdm), T (C), Bodendruck (hPa) Valid: Mon,08JAN2018 00Z
Data: GFS OPERATIONAL 0.250°
(C) Wetterzentrale
www.wetterzentrale.de
476 480 484 488 492 496 500 504 508 512 516 520 524 528 532 536 540 544 548 552 556 560 564 568 572 576 580 584 588 592 596 600
Init: Tue,09JAN2018 00Z 500 hPa Geopot. (gpdm), T (C), Bodendruck (hPa) Valid: Tue,09JAN2018 00Z
Data: GFS OPERATIONAL 0.250°
(C) Wetterzentrale
www.wetterzentrale.de
476 480 484 488 492 496 500 504 508 512 516 520 524 528 532 536 540 544 548 552 556 560 564 568 572 576 580 584 588 592 596 600

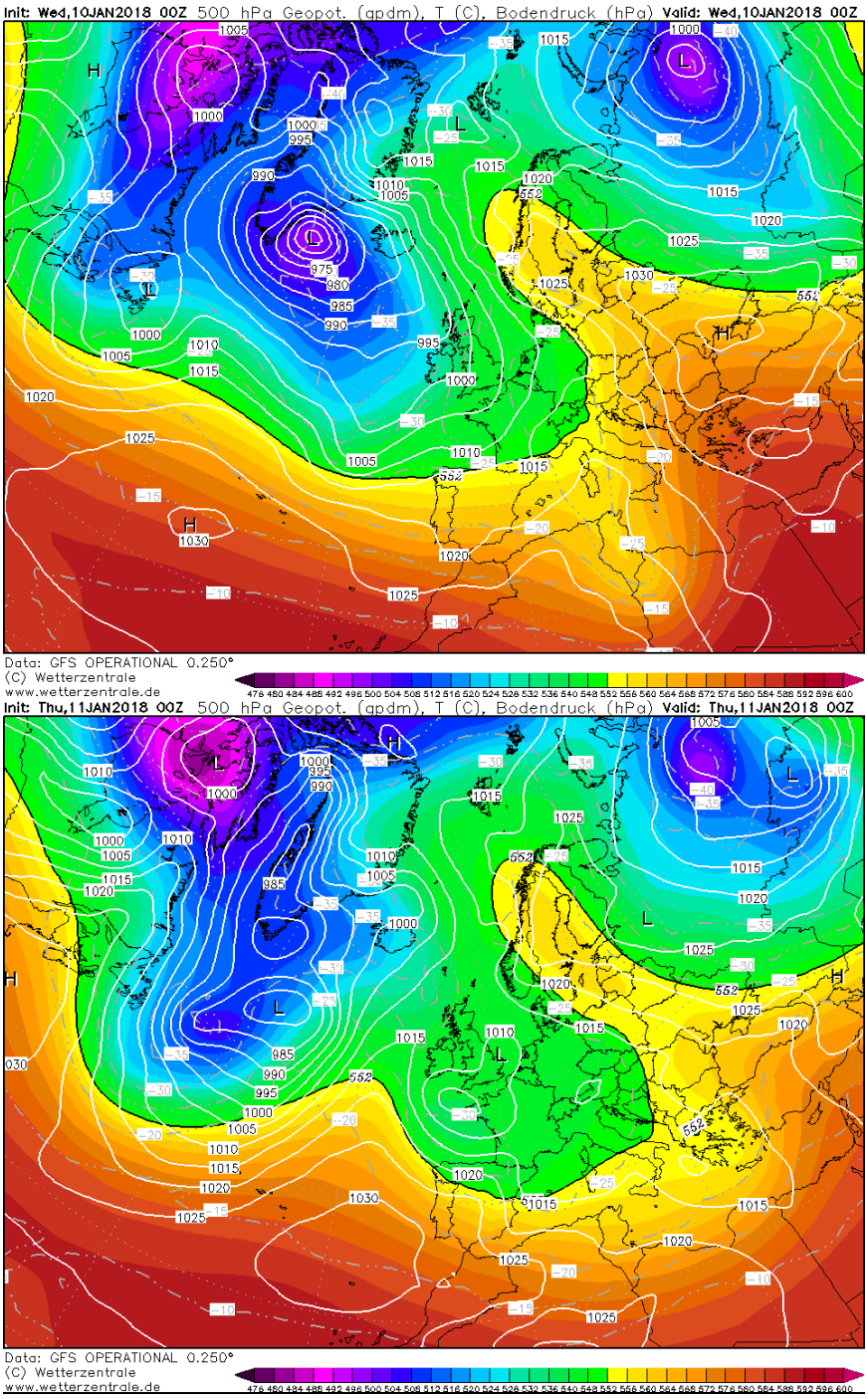
Init: Wed,10JAN2018 00Z 500 hPa Geopot. (gpdm), T (C), Bodendruck (hPa) Valid: Wed,10JAN2018 00Z
Data: GFS OPERATIONAL 0.250°
(C) Wetterzentrale
www.wetterzentrale.de
476 480 484 488 492 496 500 504 508 512 516 520 524 528 532 536 540 544 548 552 556 560 564 568 572 576 580 584 588 592 596 600
Init: Thu,11JAN2018 00Z 500 hPa Geopot. (gpdm), T (C), Bodendruck (hPa) Valid: Thu,11JAN2018 00Z
Data: GFS OPERATIONAL 0.250°
(C) Wetterzentrale
www.wetterzentrale.de
476 480 484 488 492 496 500 504 508 512 516 520 524 528 532 536 540 544 548 552 556 560 564 568 572 576 580 584 588 592 596 600

# *Appendix B*

**Radiosonde data for weeks 1 and 2**

17064 Istanbul Observations at 00Z 28 Jan 2017

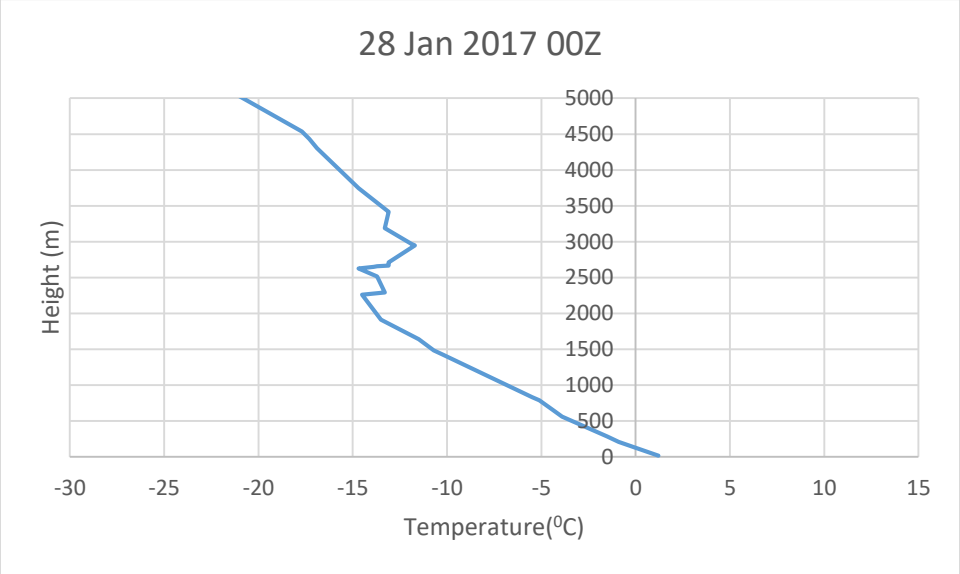


17064 Istanbul Observations at 12Z 28 Jan 2017

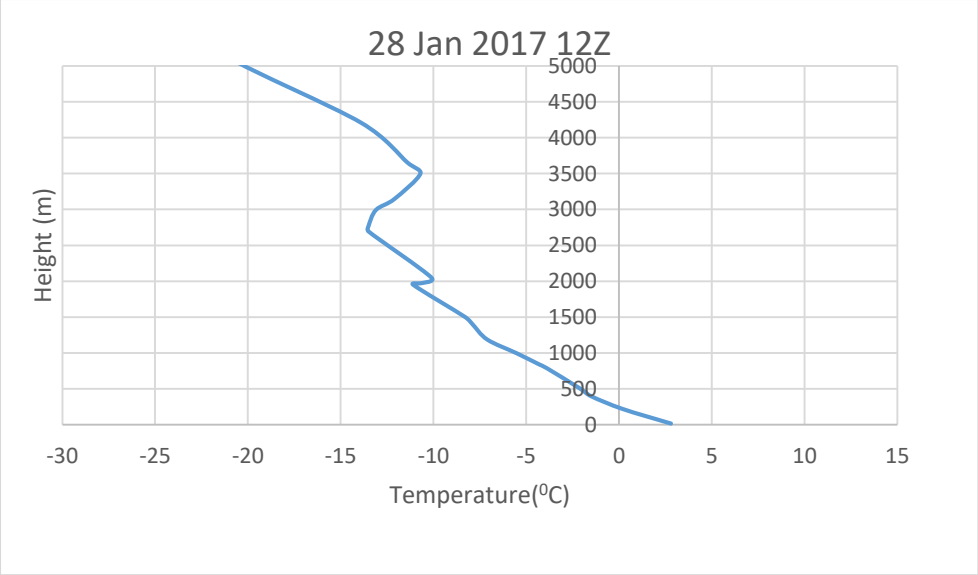


Radiosonde data and mixing height at 3am local time (top) and 3pm local time (bottom)

17064 Istanbul Observations at 00Z 29 Jan 2017

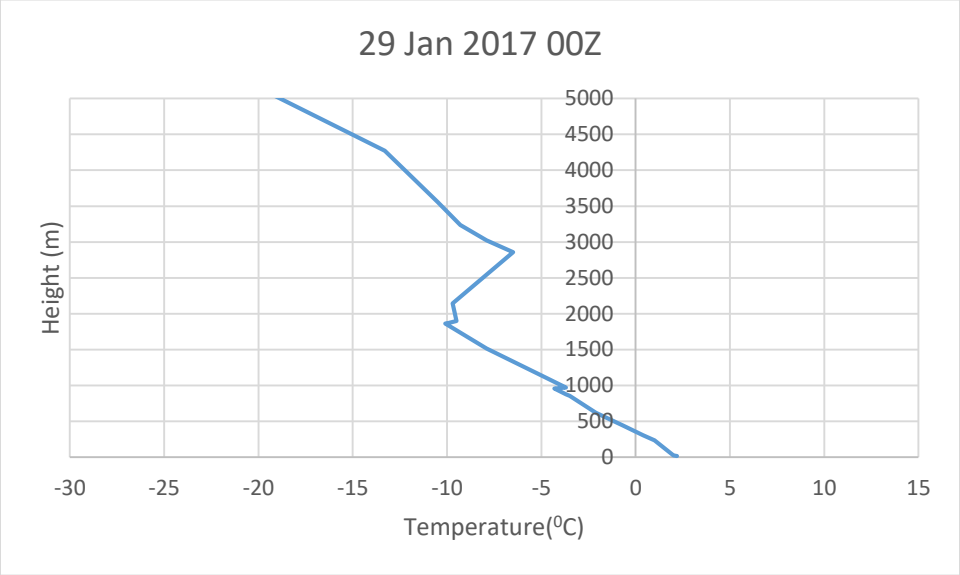


17064 Istanbul Observations at 12Z 29 Jan 2017

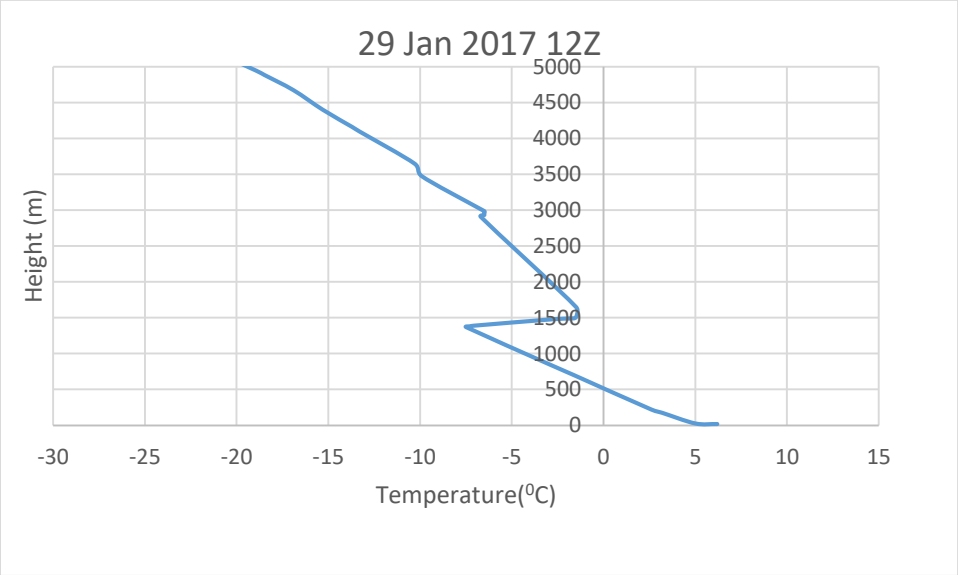


Radiosonde data and mixing height at 3am local time (top) and 3pm local time (bottom)

17064 Istanbul Observations at 00Z 30 Jan 2017

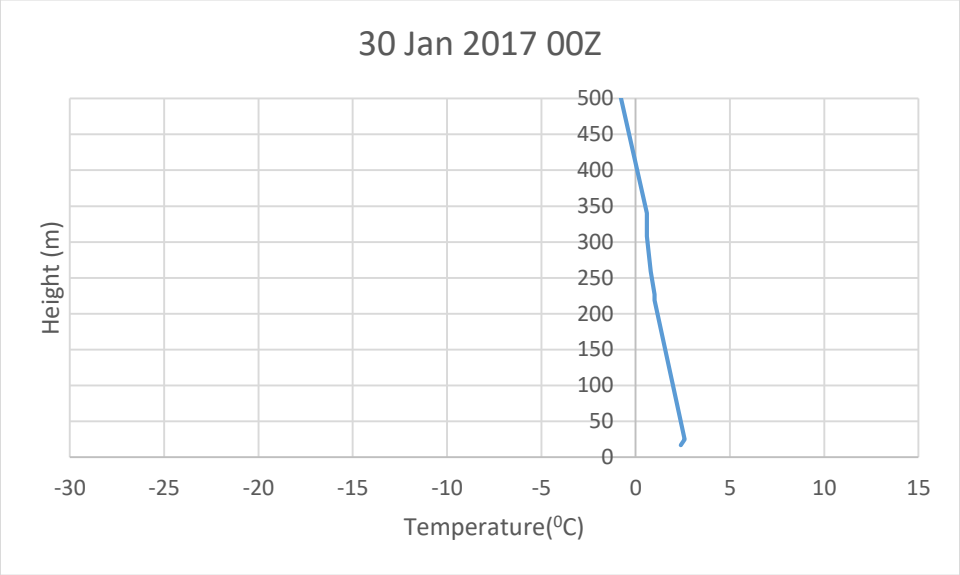


17064 Istanbul Observations at 12Z 30 Jan 2017

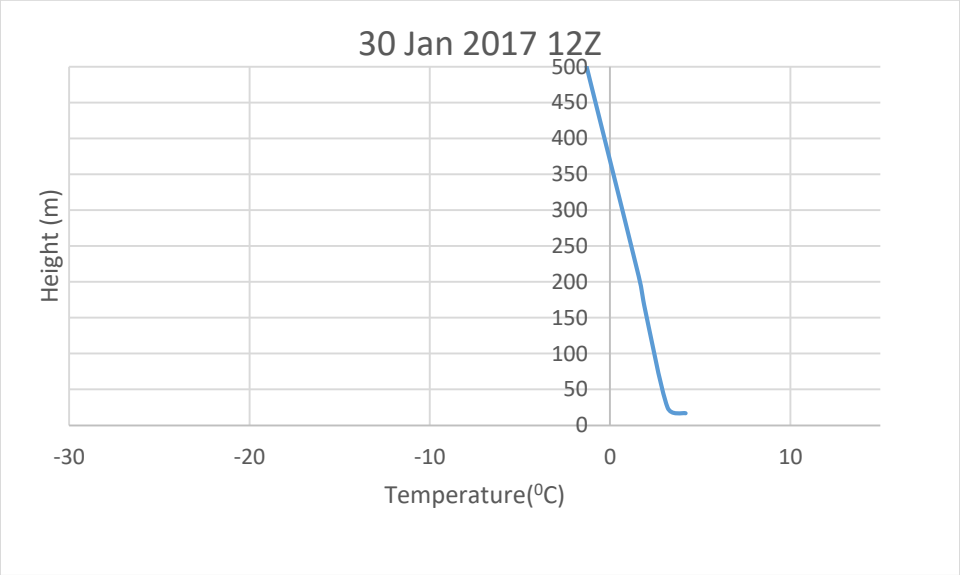


Radiosonde data and mixing height at 3am local time (top) and 3pm local time (bottom)

17064 Istanbul Observations at 00Z 31 Jan 2017

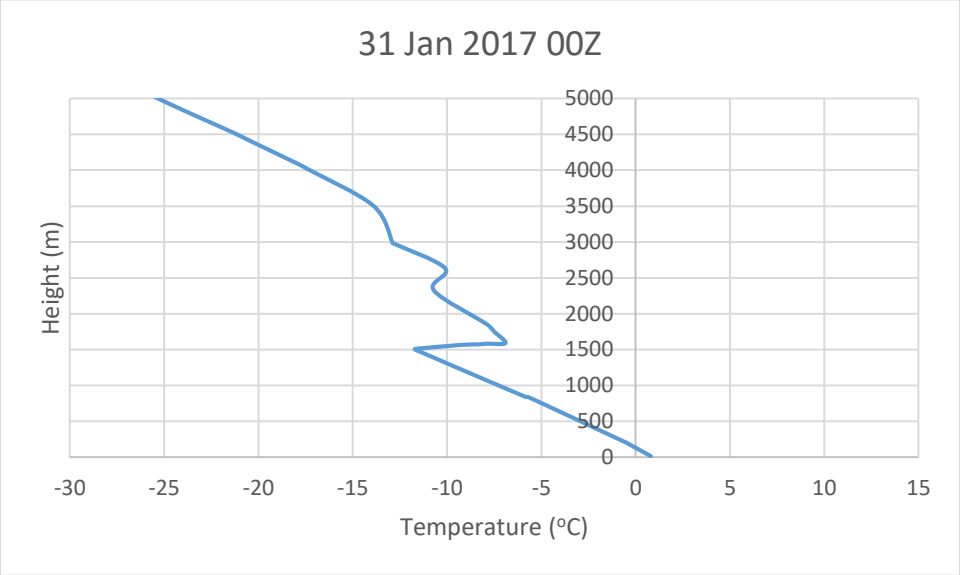


17064 Istanbul Observations at 12Z 31 Jan 2017

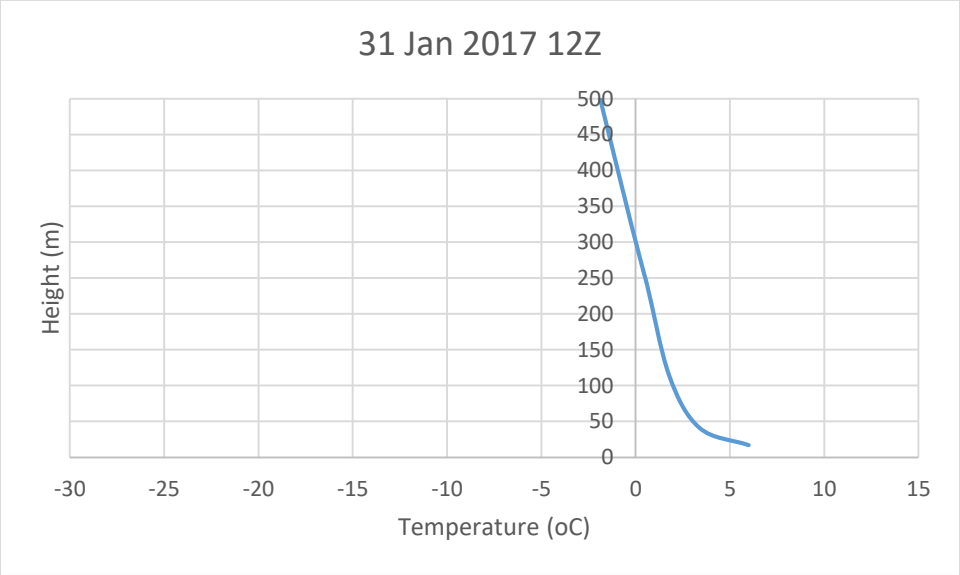


Radiosonde data and mixing height at 3am local time (top) and 3pm local time (bottom)

17064 Istanbul Observations at 00Z 01 February 2017

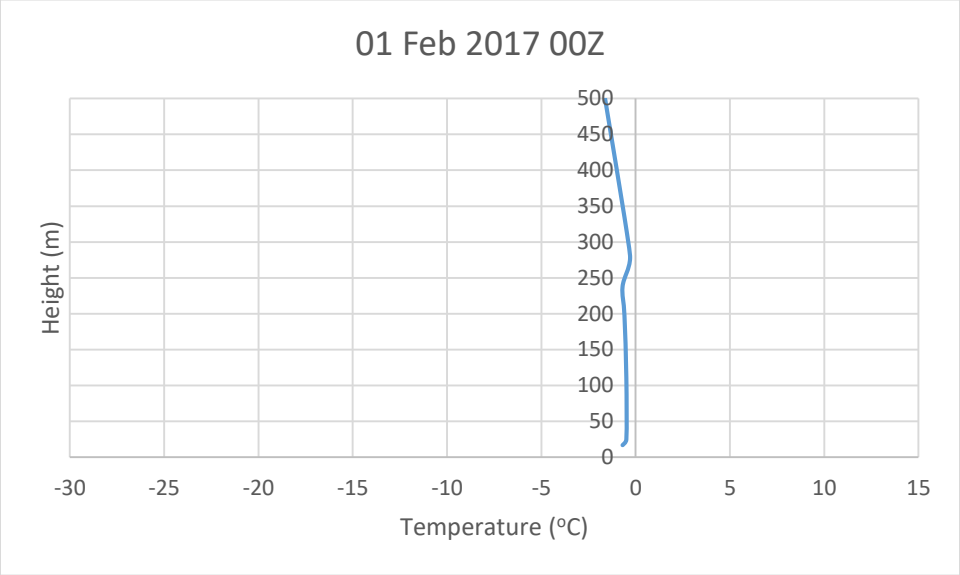


17064 Istanbul Observations at 12Z 01 February 2017

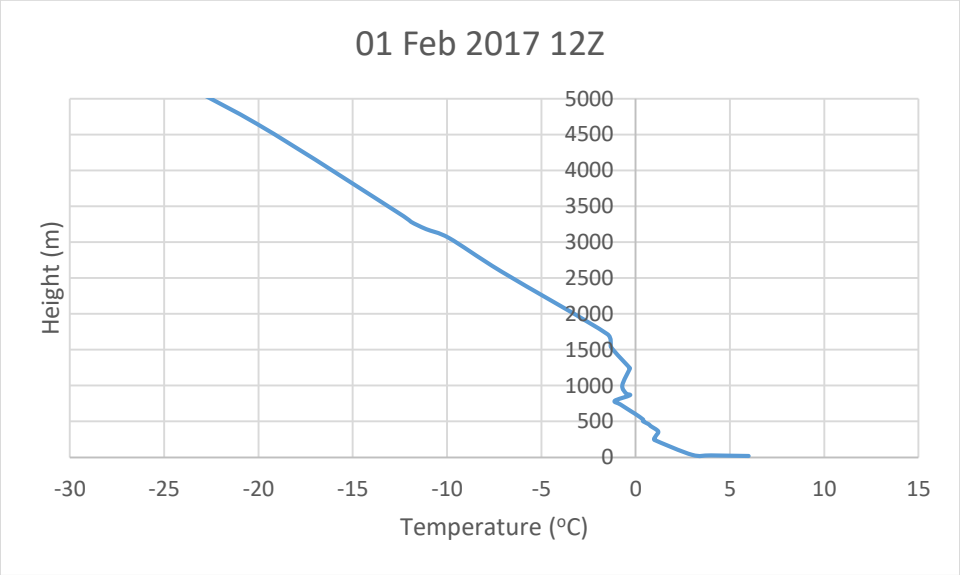


Radiosonde data and mixing height at 3am local time (top) and 3pm local time (bottom)

17064 Istanbul Observations at 00Z 02 February 2017

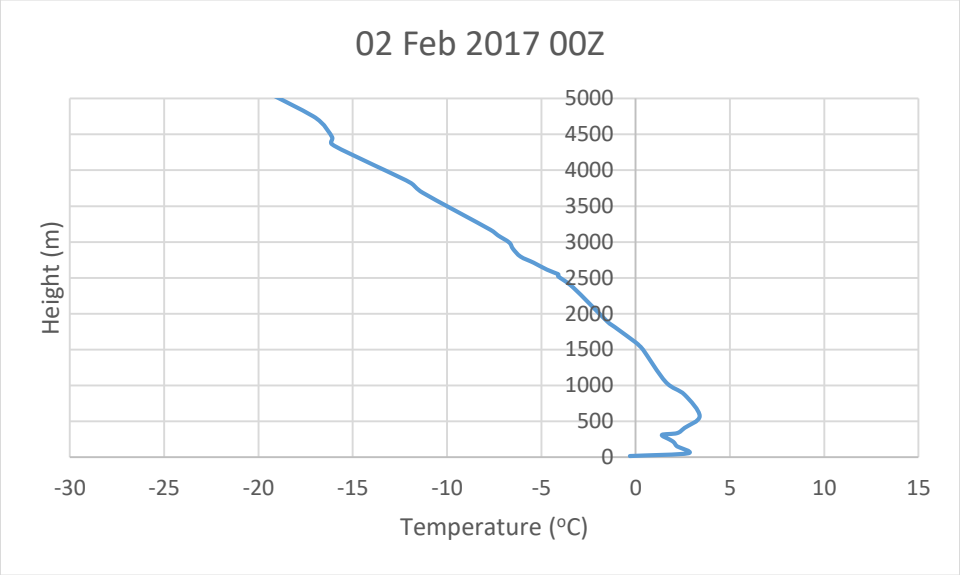


17064 Istanbul Observations at 12Z 02 February 2017

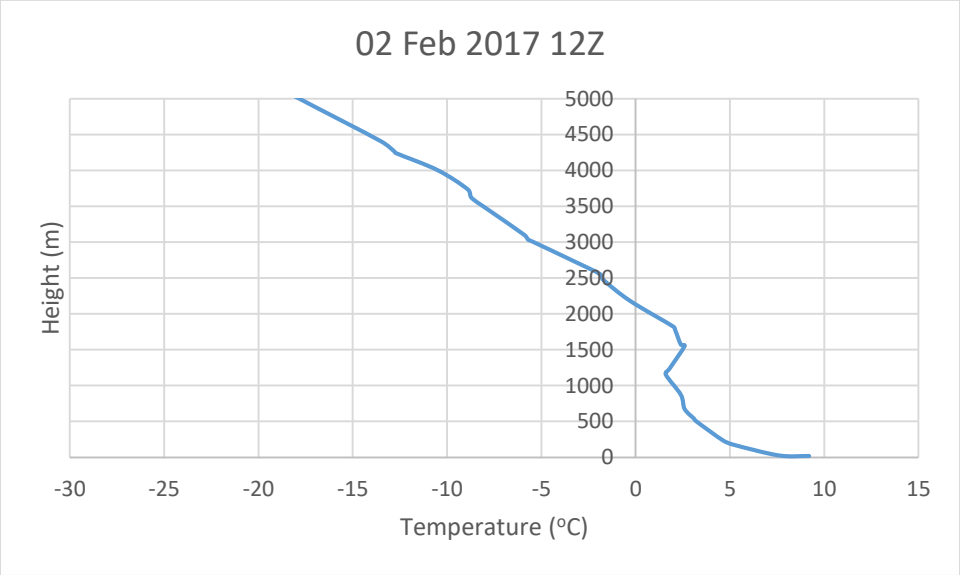


Radiosonde data and mixing height at 3am local time (top) and 3pm local time (bottom)

17064 Istanbul Observations at 00Z 03 February 2017

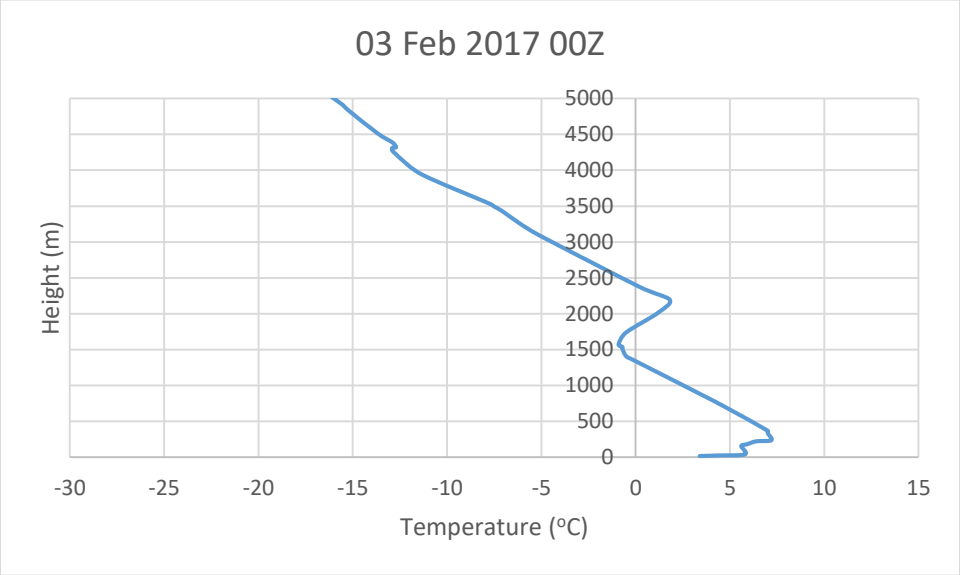


17064 Istanbul Observations at 12Z 03 February 2017

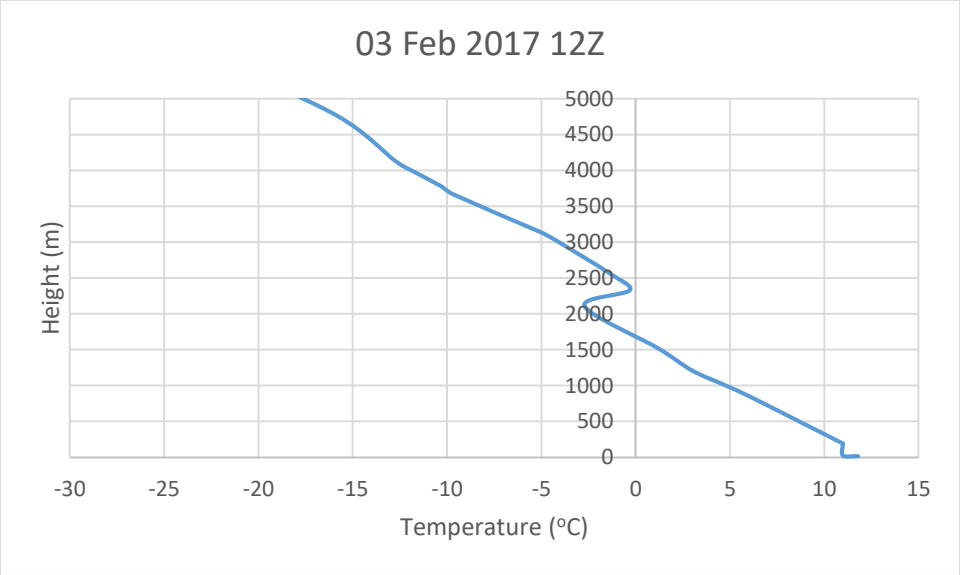


Radiosonde data and mixing height at 3am local time (top) and 3pm local time (bottom)

17064 Istanbul Observations at 00Z 04 February 2017

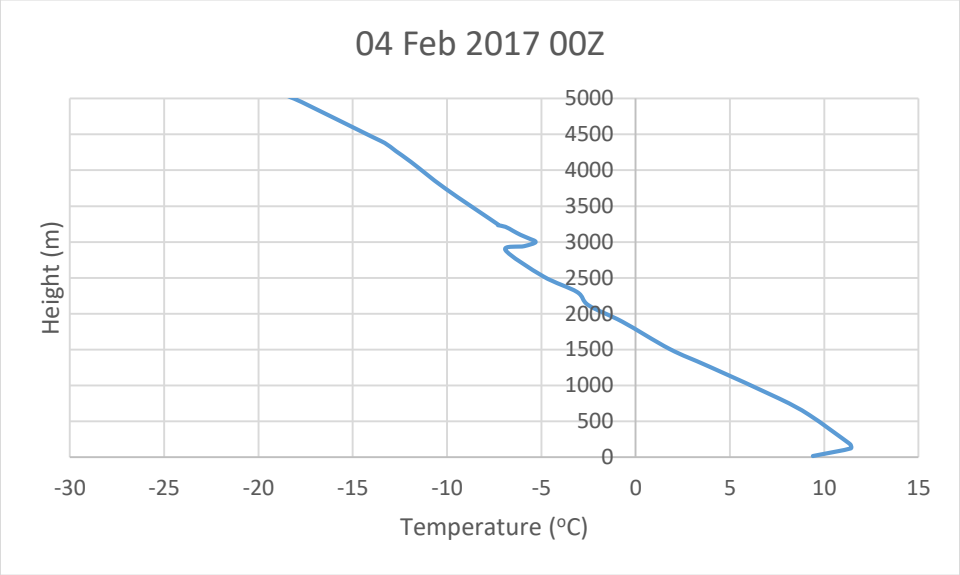


17064 Istanbul Observations at 12Z 04 February 2017

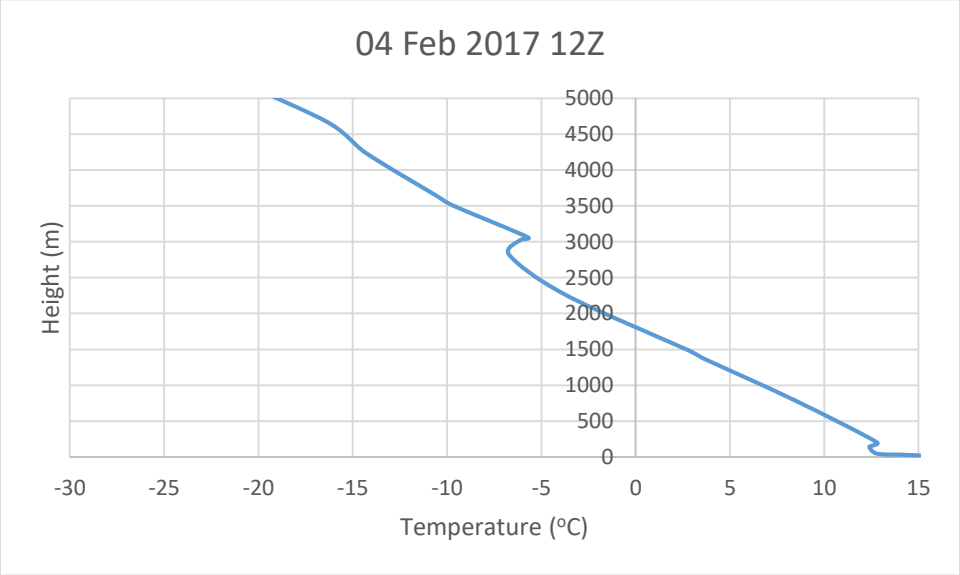


Radiosonde data and mixing height at 3am local time (top) and 3pm local time (bottom)

Mixing height: 00Z – 3am Istanbul Local time; 12Z – 3pm Istanbul local time

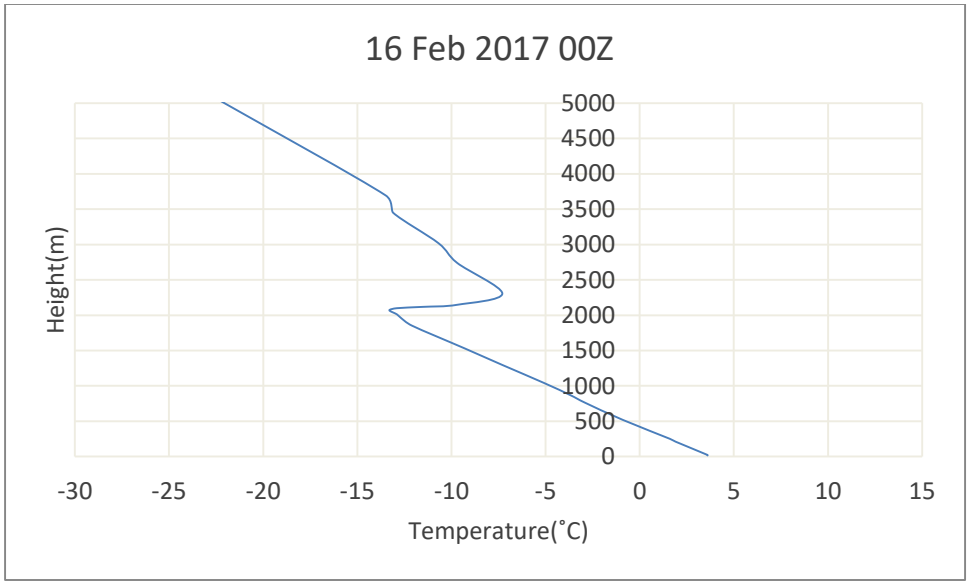


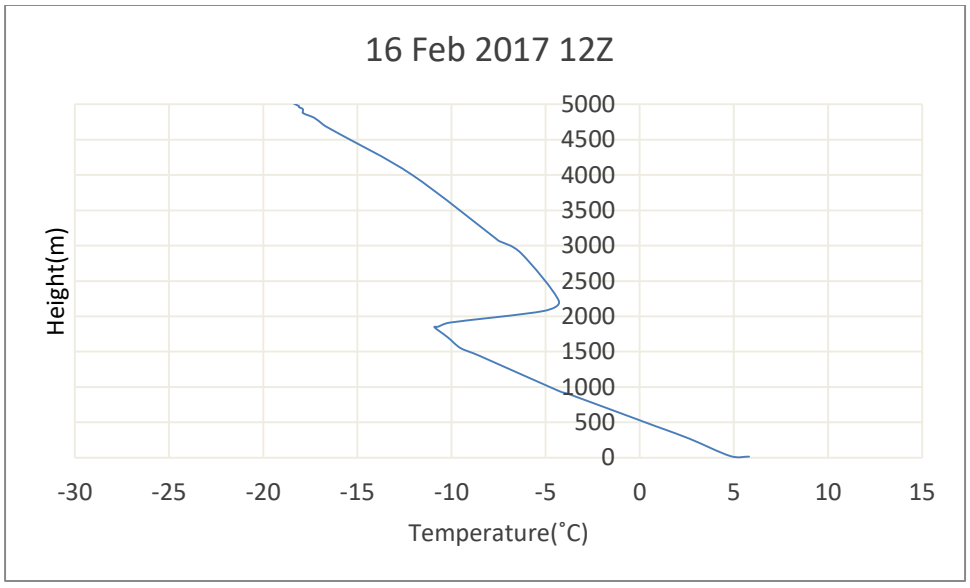


Radiosonde data and mixing height at 3am local time (top) and 3pm local time (bottom)

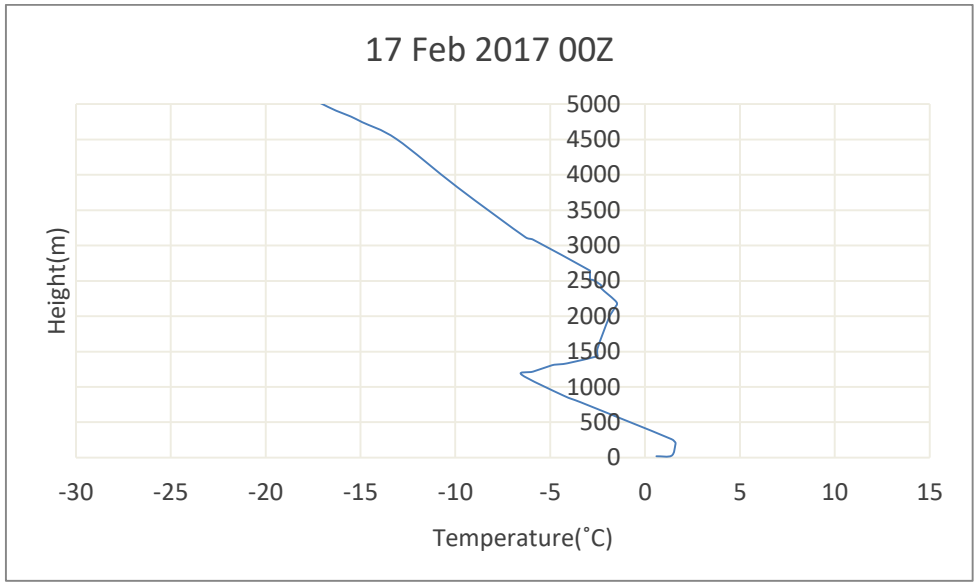


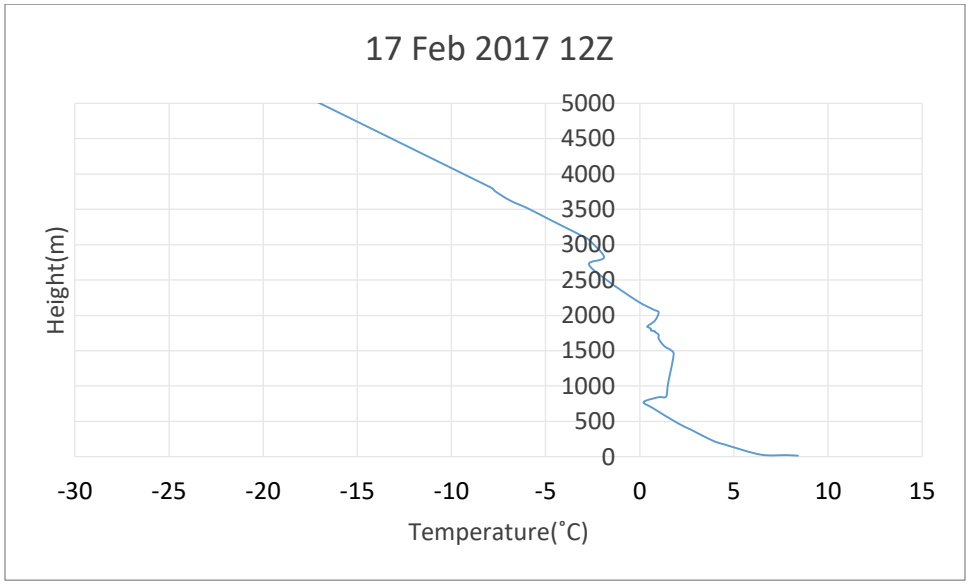


Radiosonde data and mixing height at 3am local time (top) and 3pm local time (bottom)

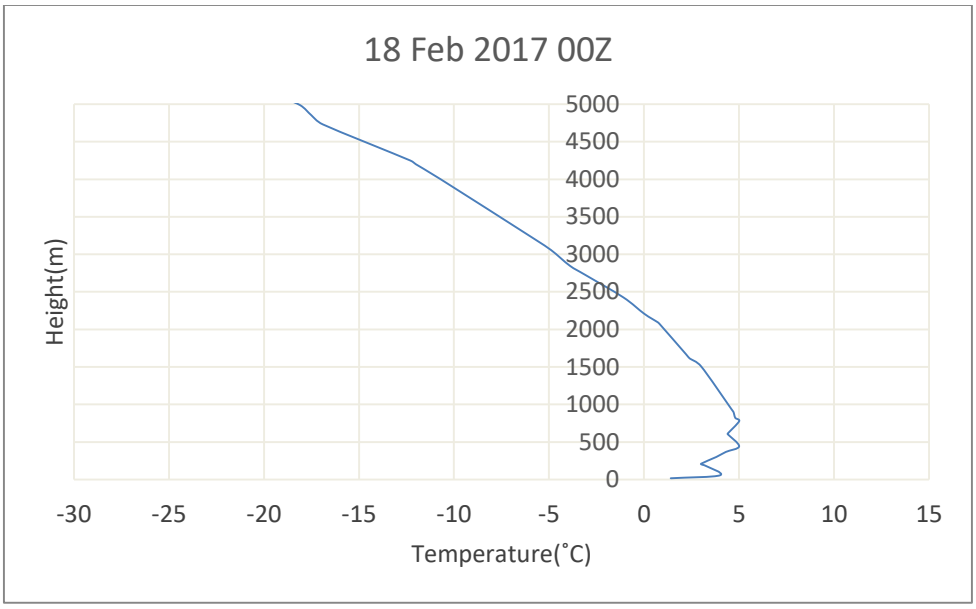


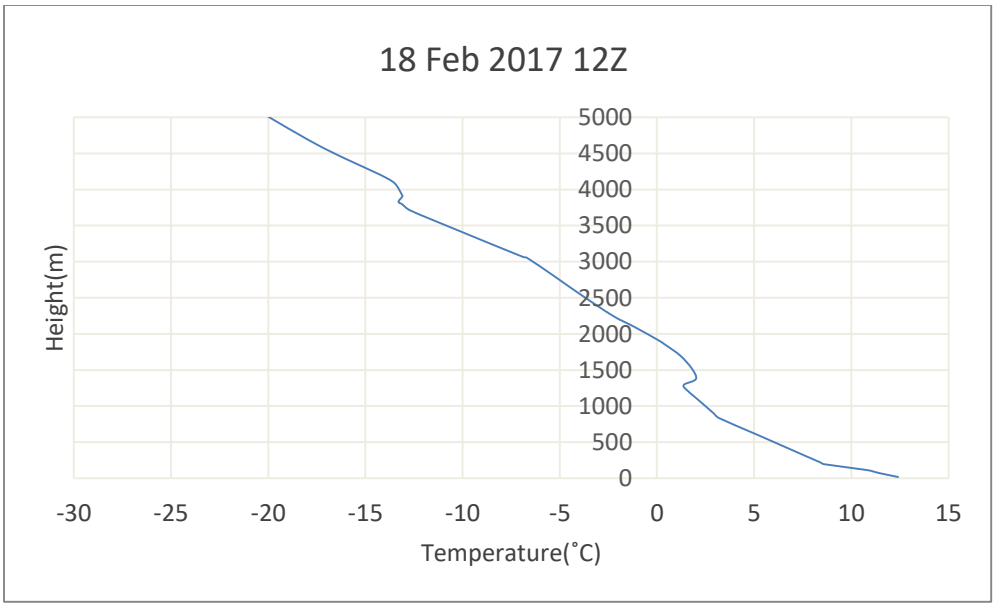


Radiosonde data and mixing height at 3am local time (top) and 3pm local time (bottom)

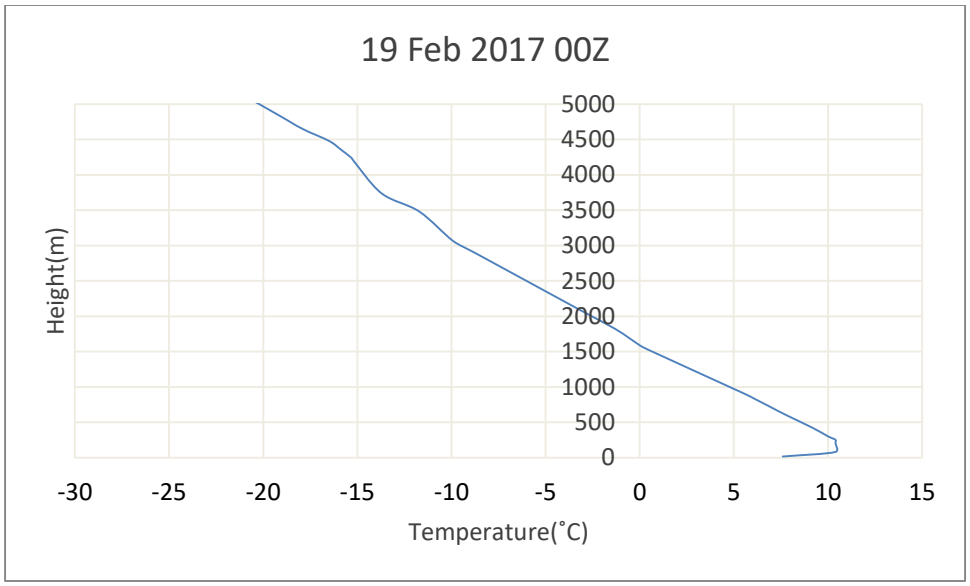


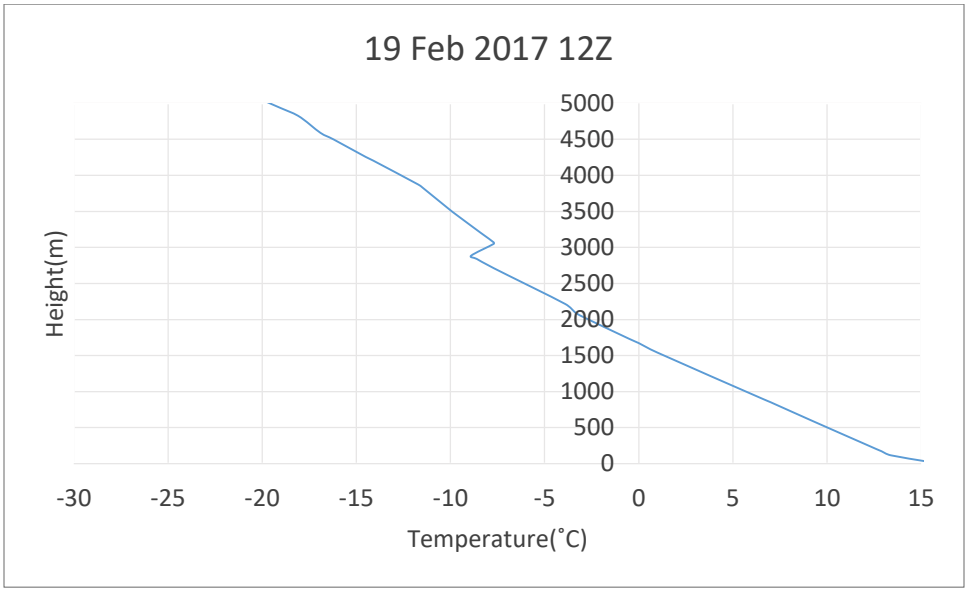


Radiosonde data and mixing height at 3am local time (top) and 3pm local time (bottom)

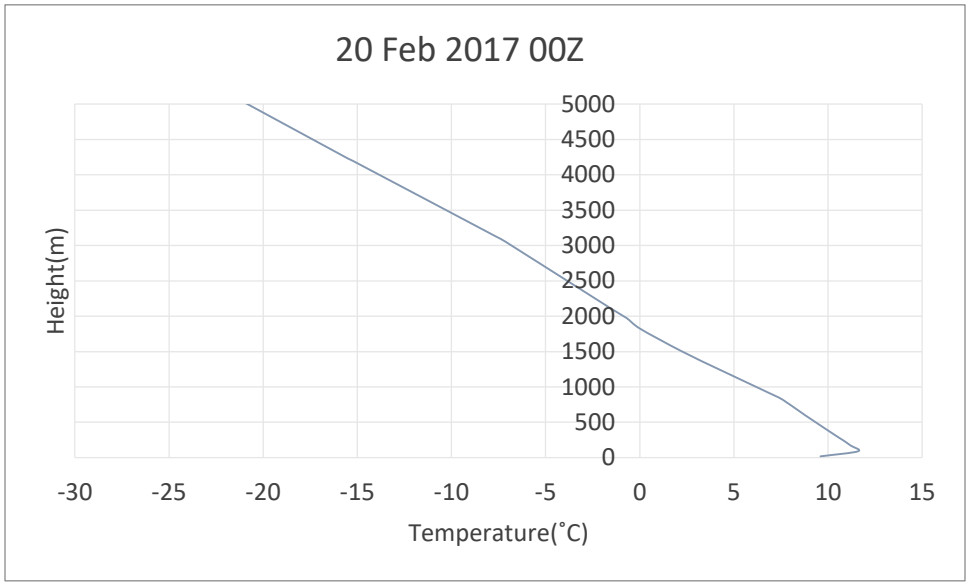


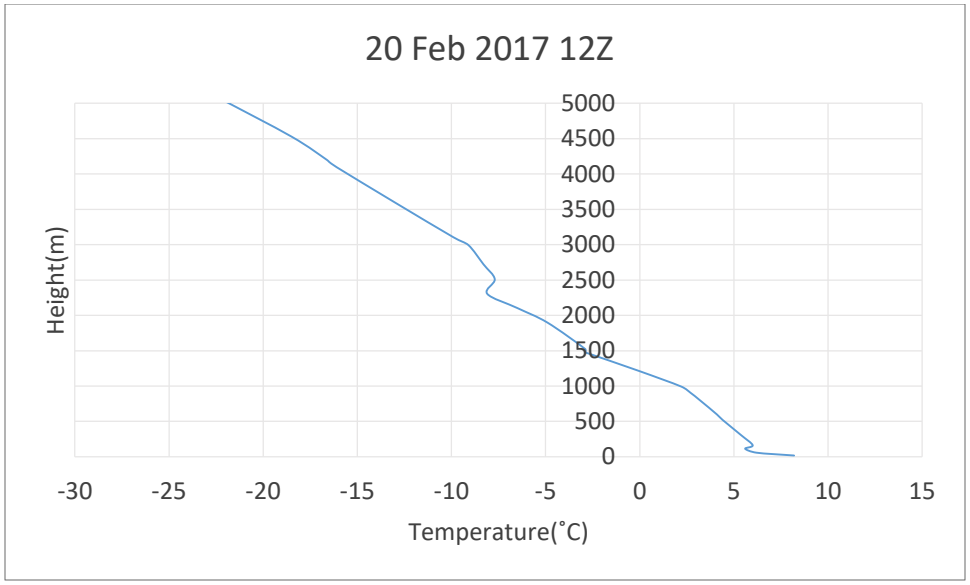


Radiosonde data and mixing height at 3am local time (top) and 3pm local time (bottom)

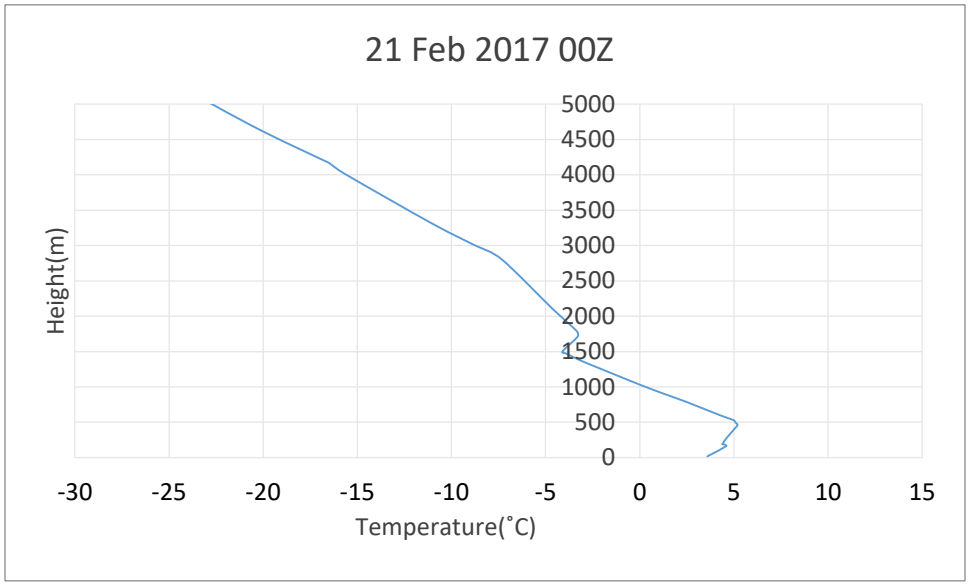


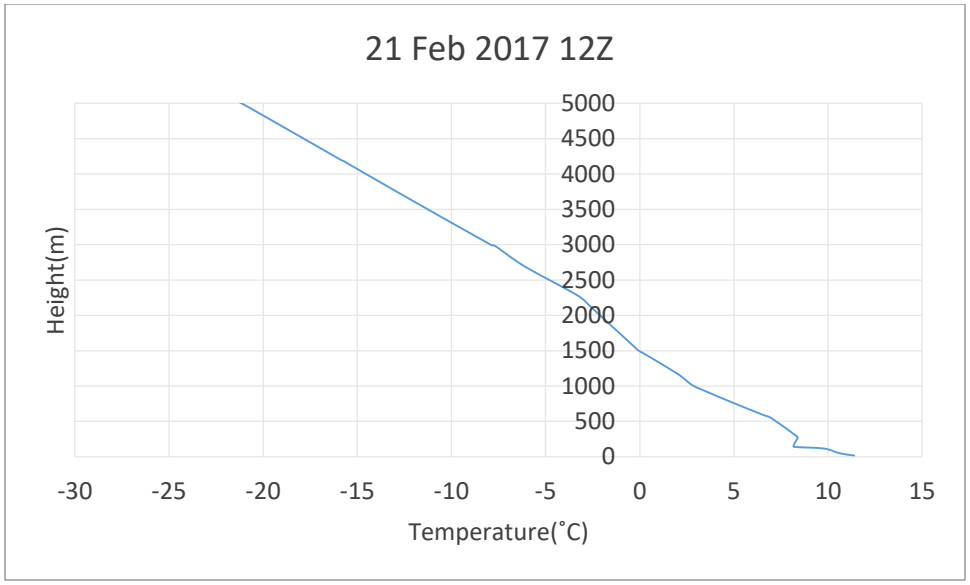


Radiosonde data and mixing height at 3am local time (top) and 3pm local time (bottom)

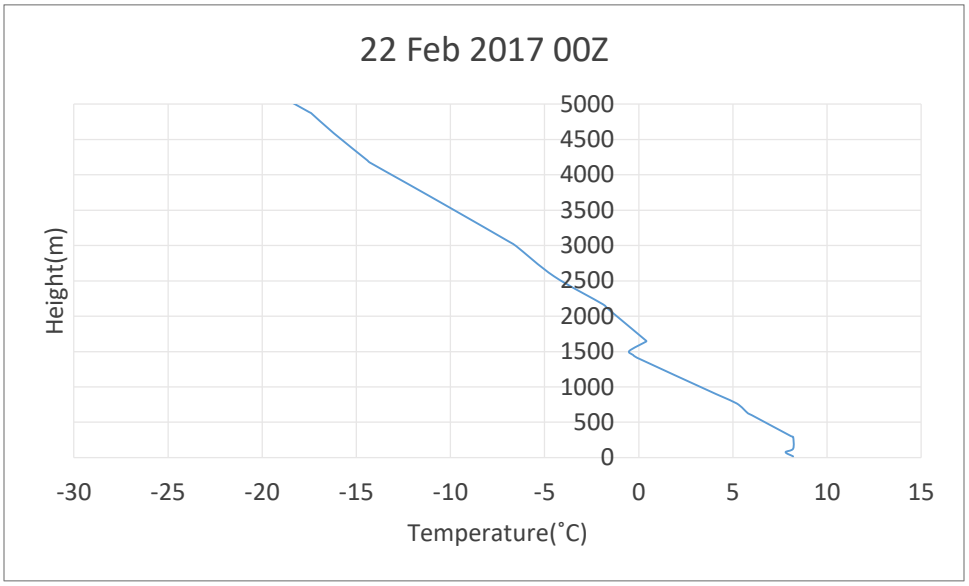


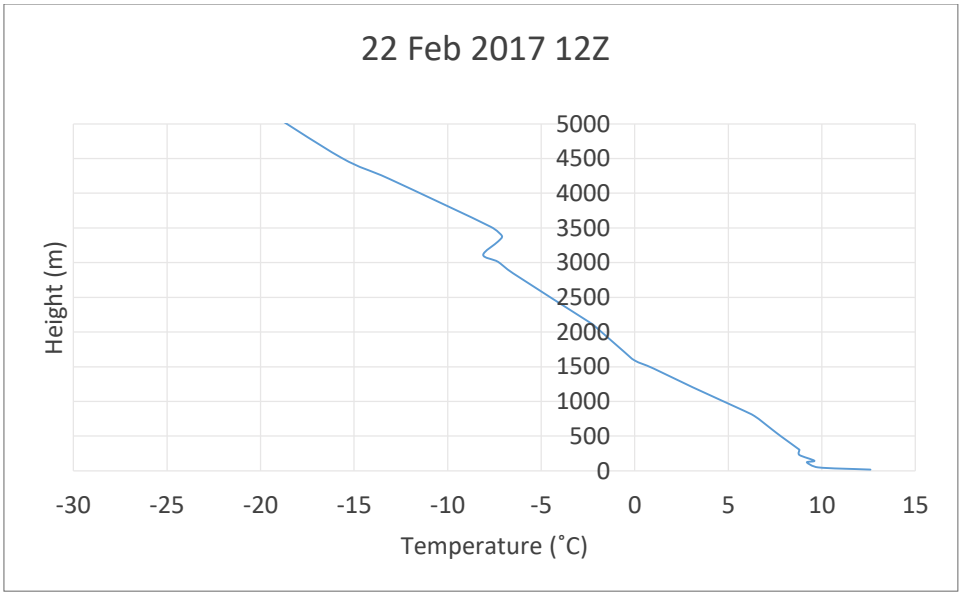


Radiosonde data and mixing height at 3am local time (top) and 3pm local time (bottom)

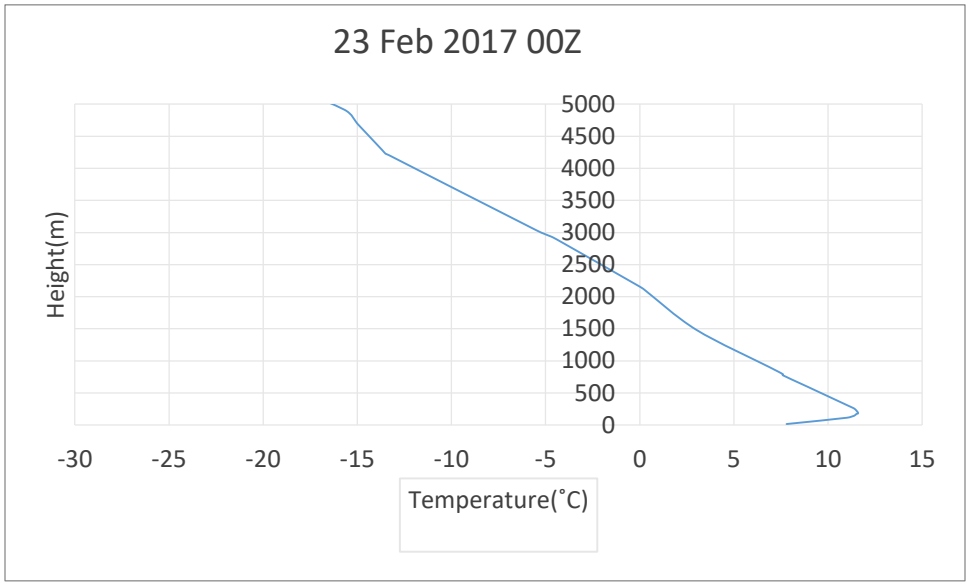


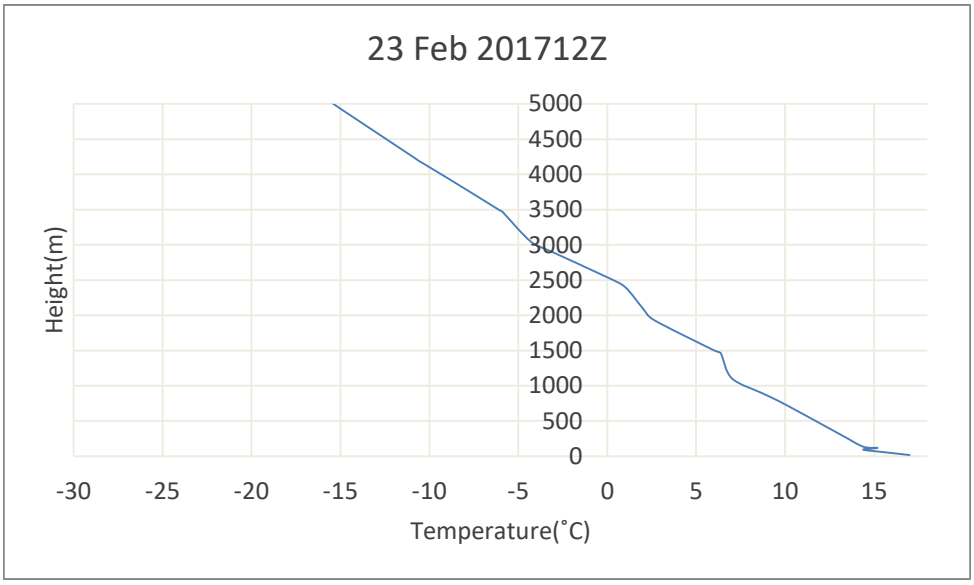


Radiosonde data and mixing height at 3am local time (top) and 3pm local time (bottom)

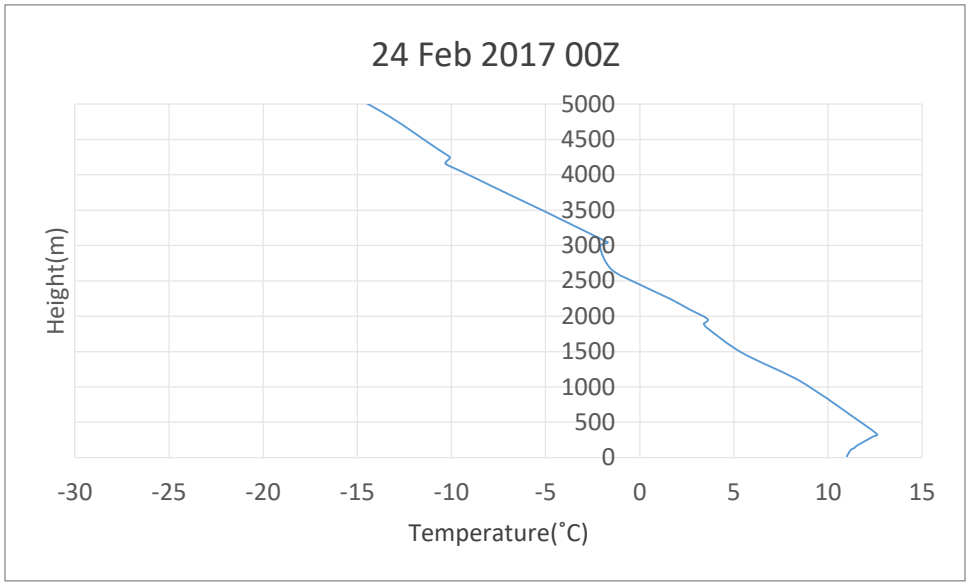


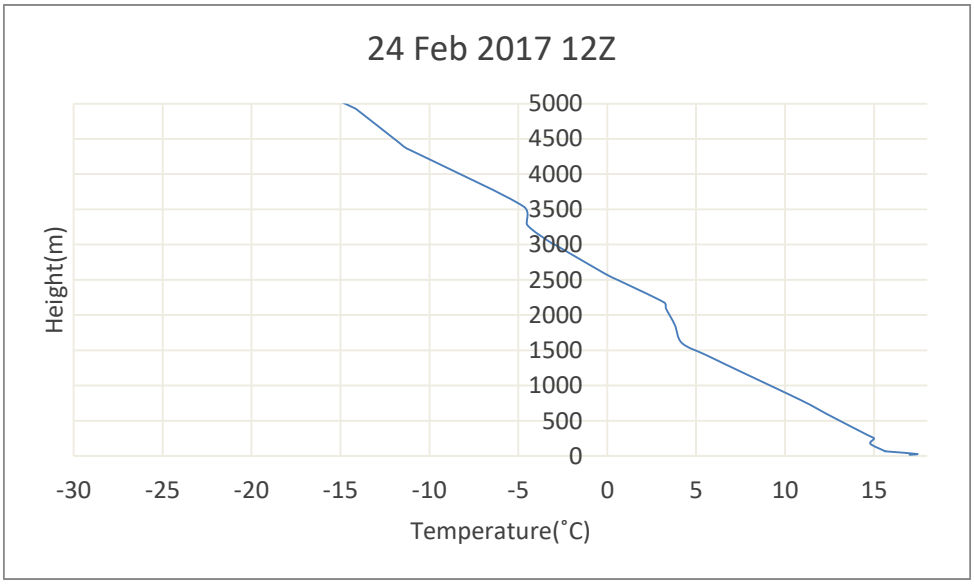


Radiosonde data and mixing height at 3am local time (top) and 3pm local time (bottom)

**Radiosonde data for weeks 3 and 4**

17064 Istanbul Observations at 3am local time on 03 May 2017

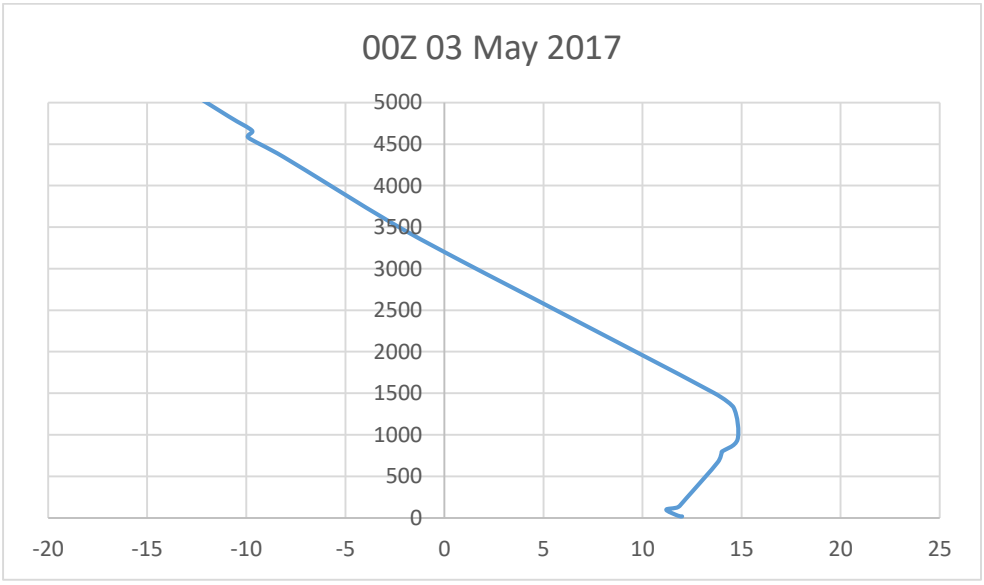


17064 Istanbul Observations at 3pm local time on 03 May 2017

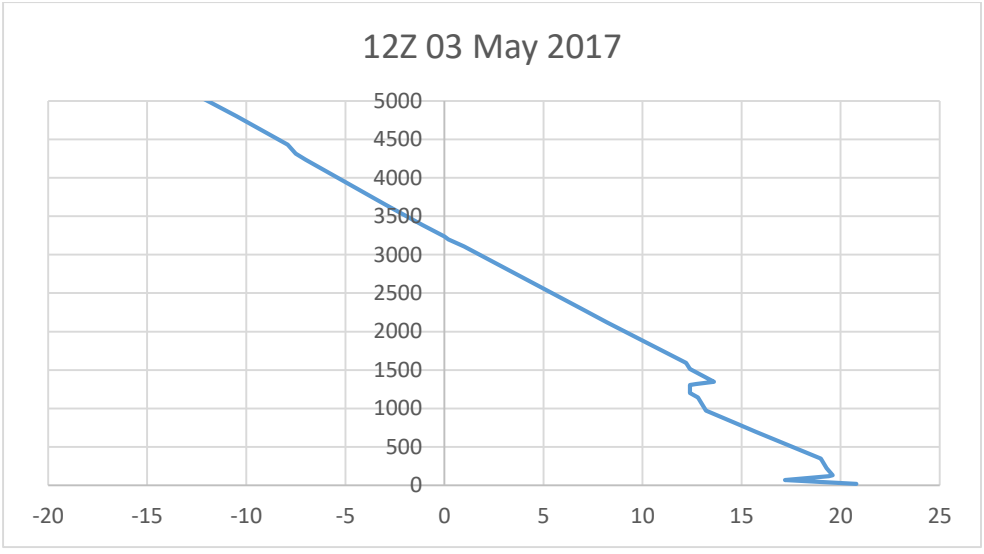


Radiosonde data and mixing height at 3am local time (top) and 3pm local time (bottom)

17064 Istanbul Observations at 3 am local time on 04 May 2017

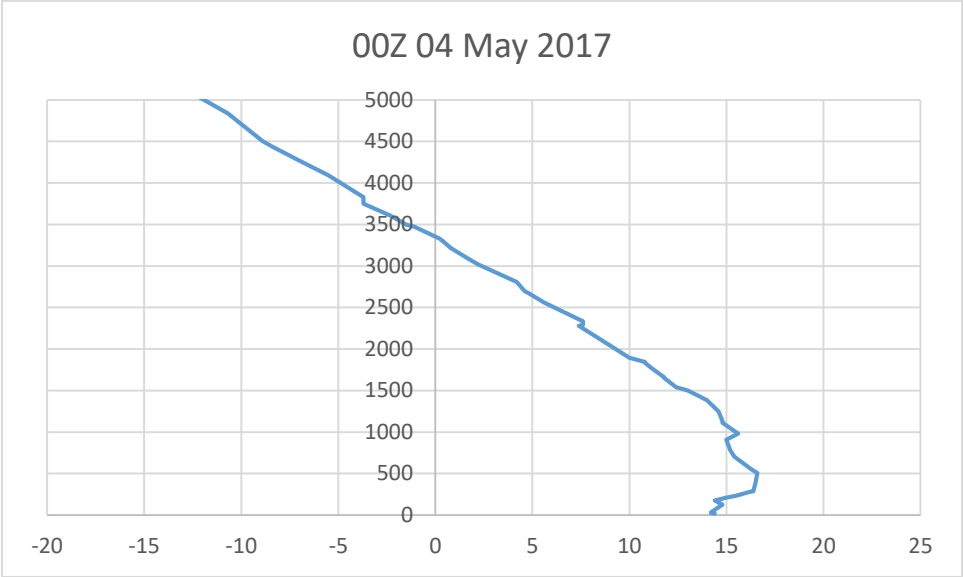


17064 Istanbul Observations at 3pm local time on 04 May 2017

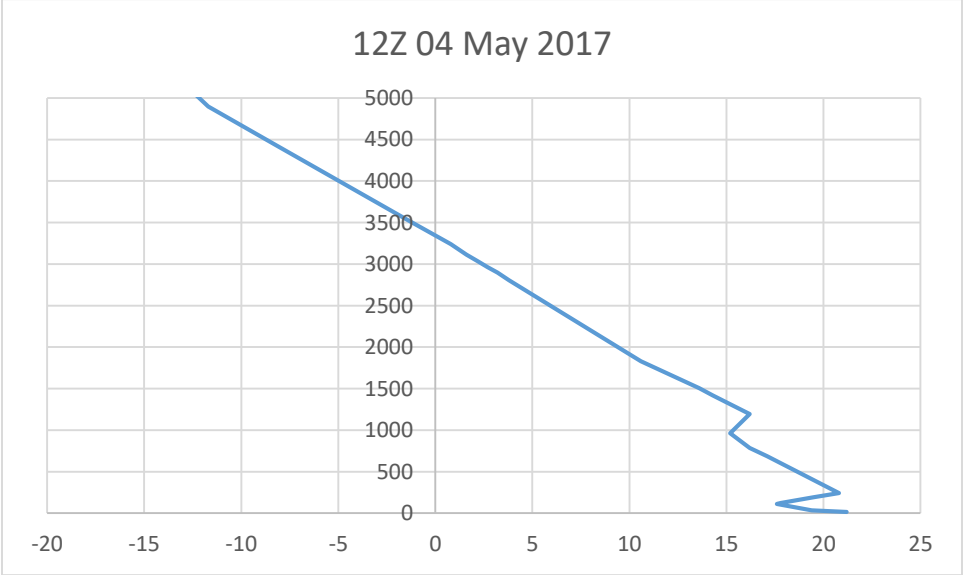


Radiosonde data and mixing height at 3am local time (top) and 3pm local time (bottom)

17064 Istanbul Observations at 3am local time on 5 May 2017

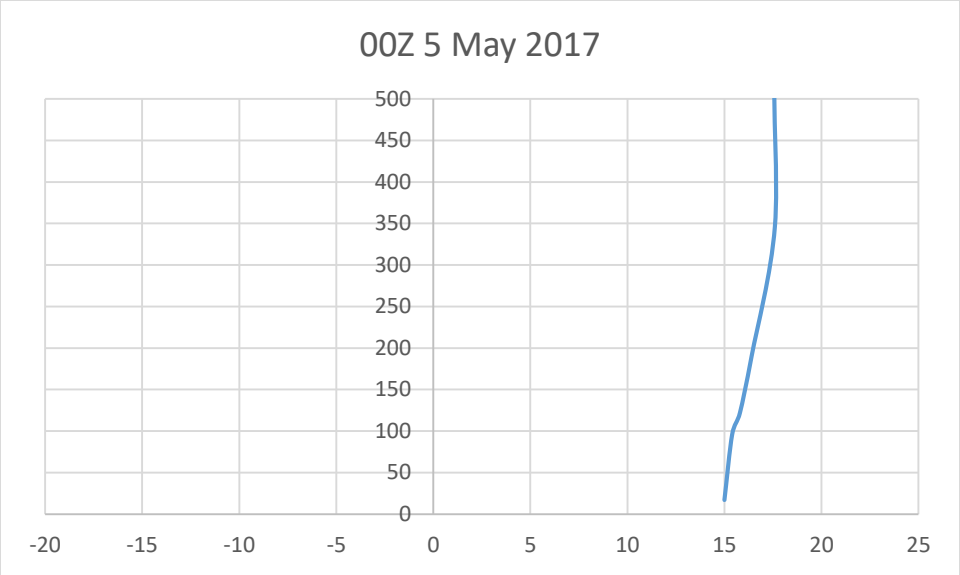


17064 Istanbul Observations at 3pm local time on 05 May 2017

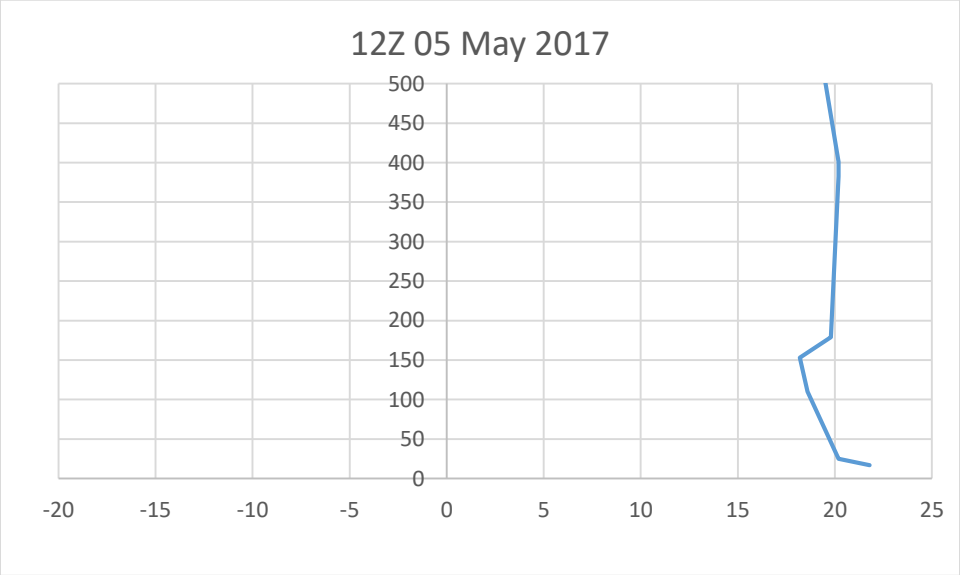


Radiosonde data and mixing height at 3am local time (top) and 3pm local time (bottom)

17064 Istanbul Observations at 3am local time on 06 May 2017

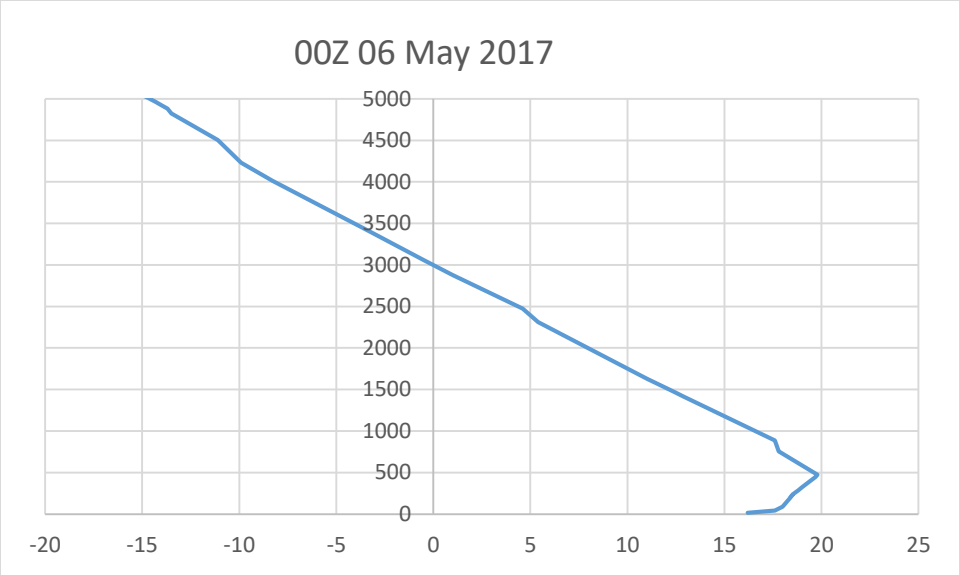


17064 Istanbul Observations at 3pm local time on 06 May 2017

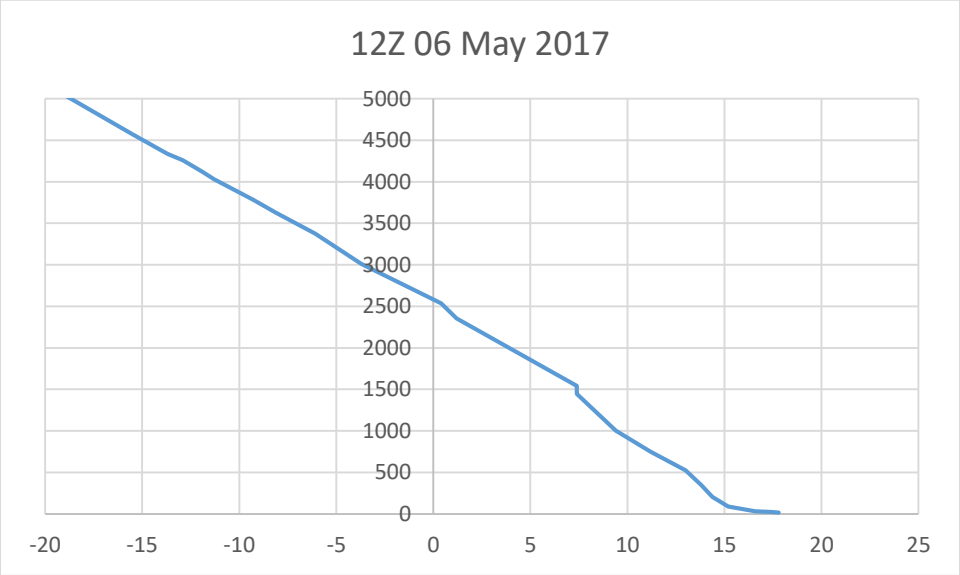


Radiosonde data and mixing height at 3am local time (top) and 3pm local time (bottom)

17064 Istanbul Observations at 3am local time on 07 May 2017

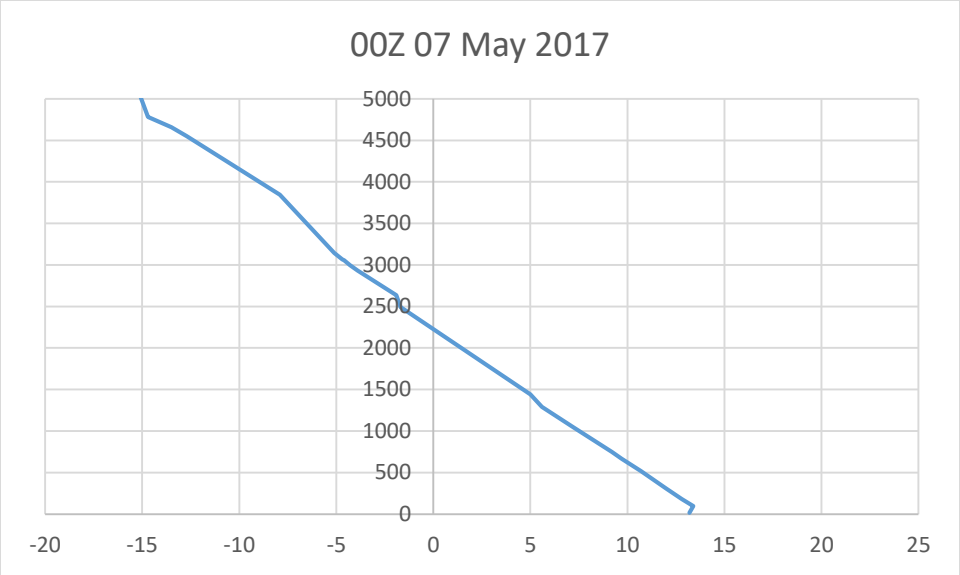


17064 Istanbul Observations at 3pm local time on 07 May 2017

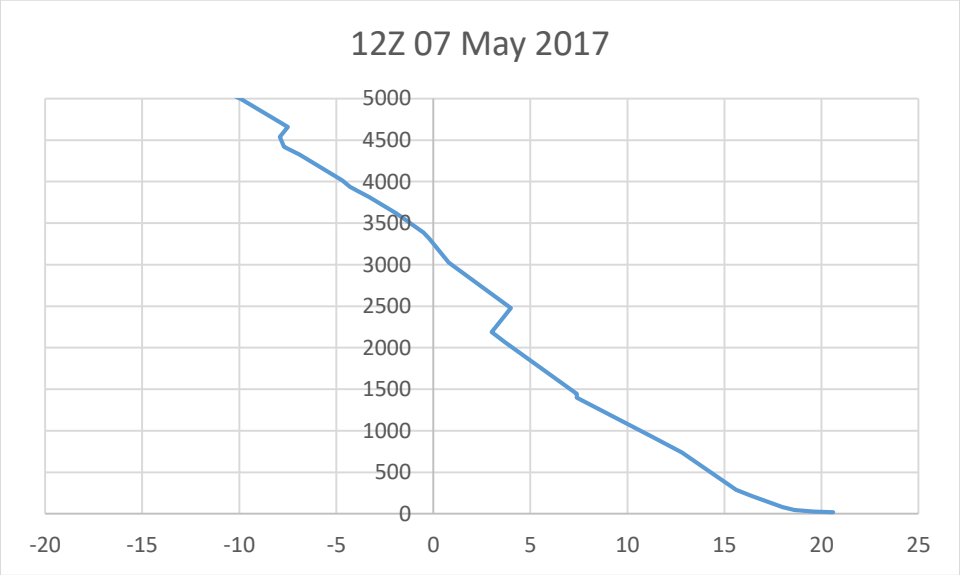


Radiosonde data and mixing height at 3am local time (top) and 3pm local time (bottom)

17064 Istanbul Observations at 3pm local time on 08 May 2017

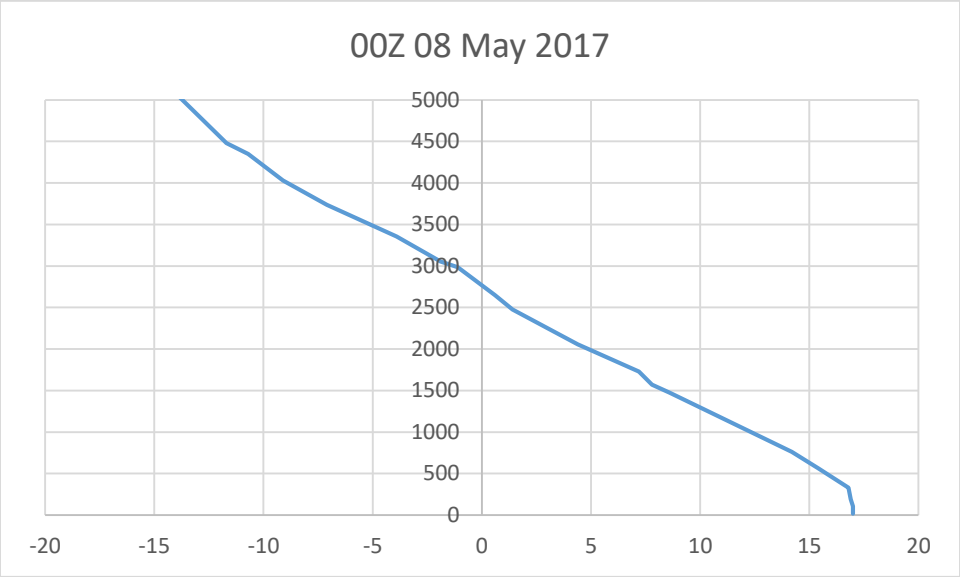


17064 Istanbul Observations at 3pm local time on 08 May 2017

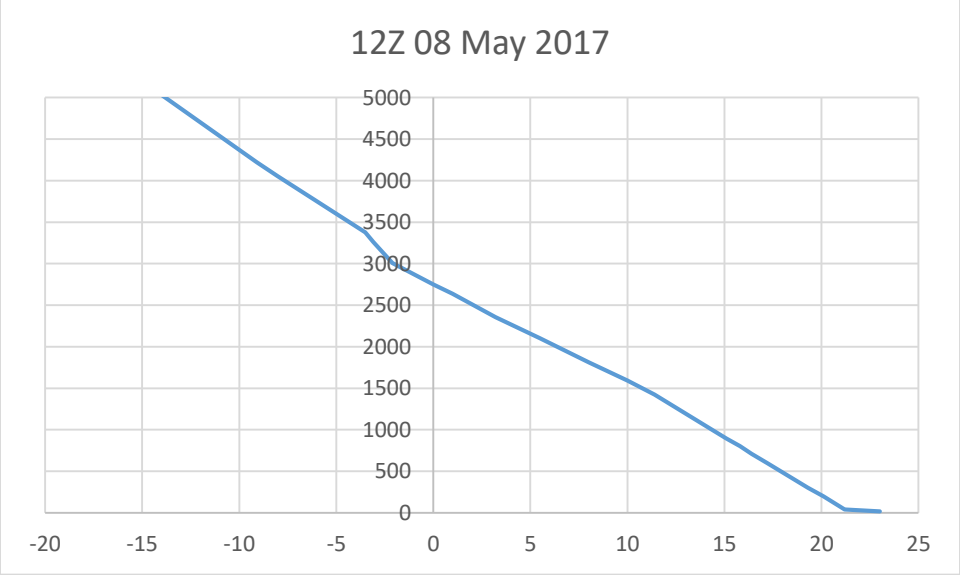


Radiosonde data and mixing height at 3am local time (top) and 3pm local time (bottom)

7064 Istanbul Observations at 3am local time on 09 May 2017

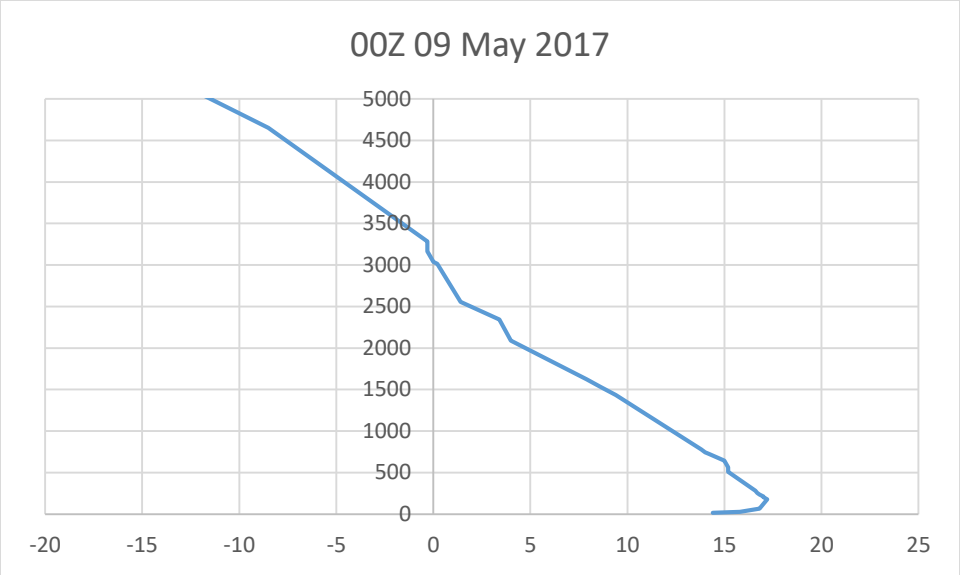


17064 Istanbul Observations at 3pm local time on 09 May 2017

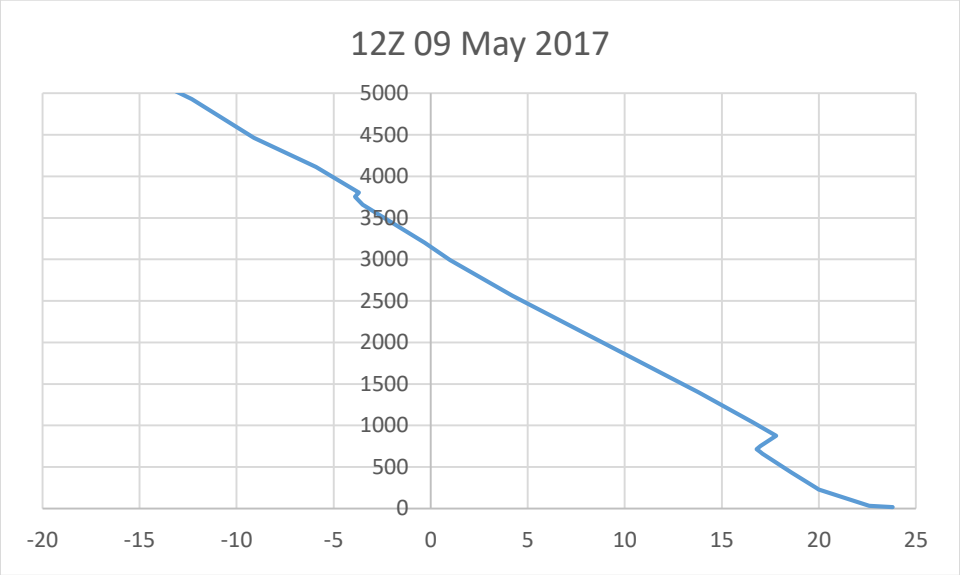


Radiosonde data and mixing height at 3am local time (top) and 3pm local time (bottom)

17064 Istanbul Observations at 3am local time on 06 JULY 2017

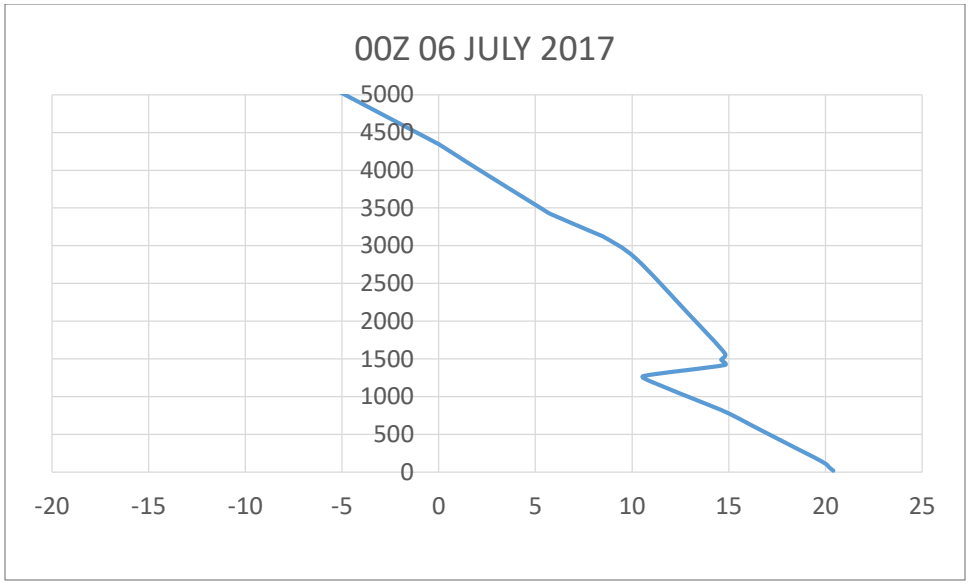


17064 Istanbul Observations at 3pm local time on 06 JULY 2017

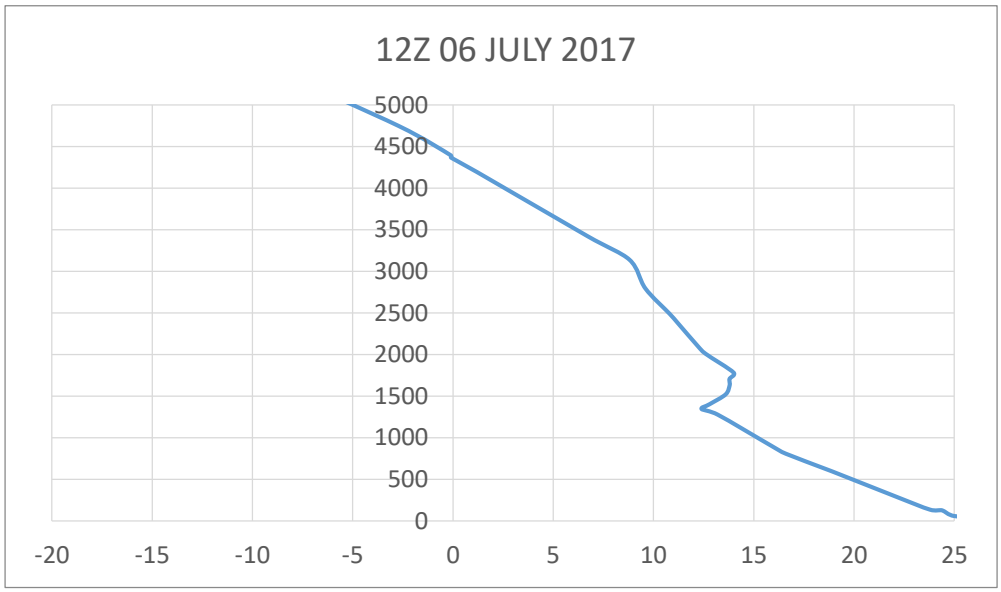


Radiosonde data and mixing height at 3am local time (top) and 3pm local time (bottom)

17064 Istanbul Observations at 3am local time on 07 JULY 2017

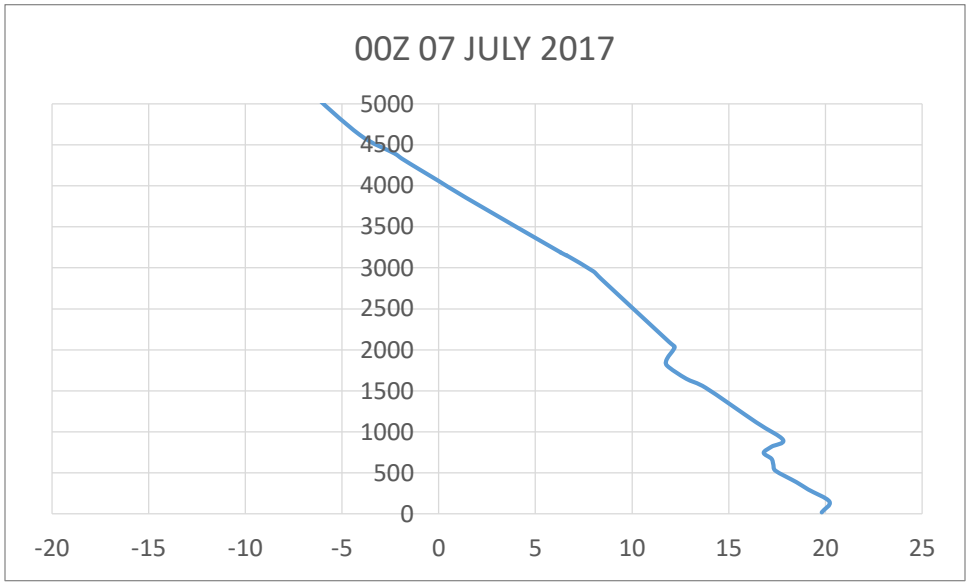


17064 Istanbul Observations at 3pm local time on 07 JULY 2017

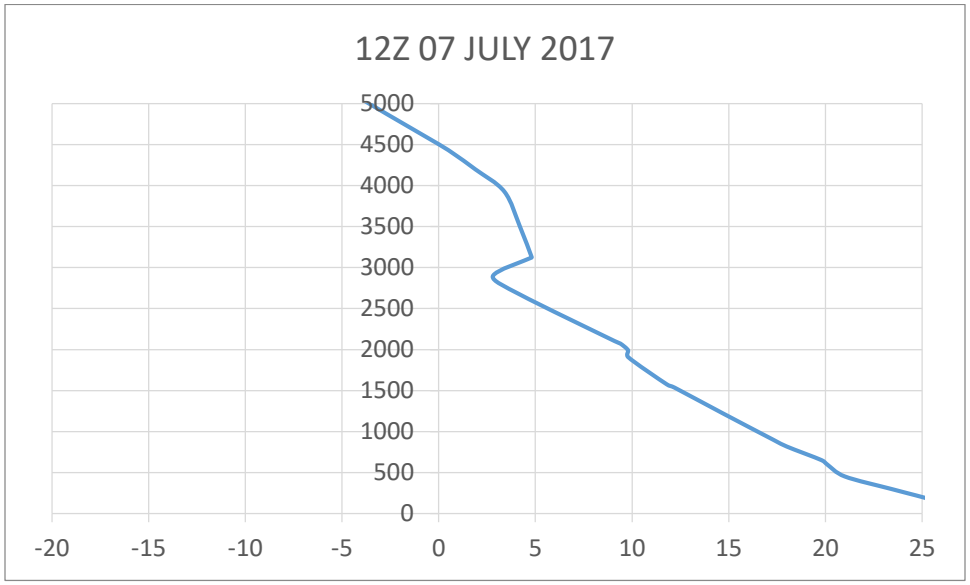


Radiosonde data and mixing height at 3am local time (top) and 3pm local time (bottom)

17064 Istanbul Observations at 3am local time on 08 JULY 2017

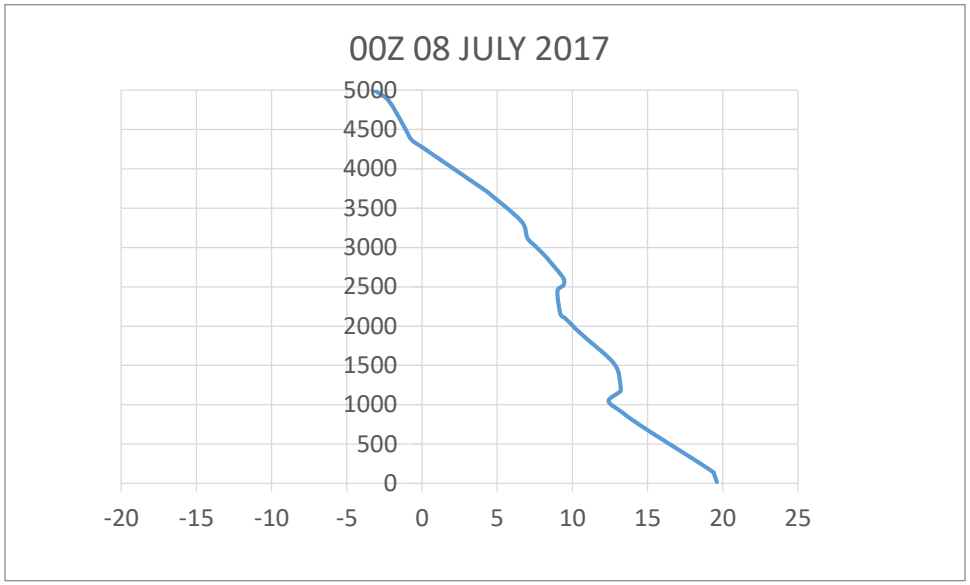


17064 Istanbul Observations at 3pm local time on 08 JULY 2017

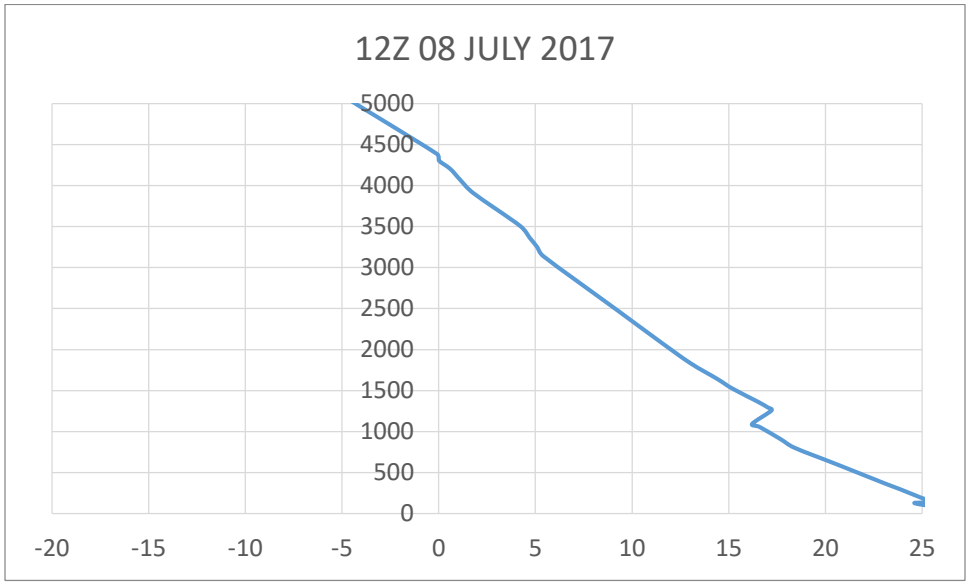


Radiosonde data and mixing height at 3am local time (top) and 3pm local time (bottom)

17064 Istanbul Observations at 3am local time on 09 JULY 2017

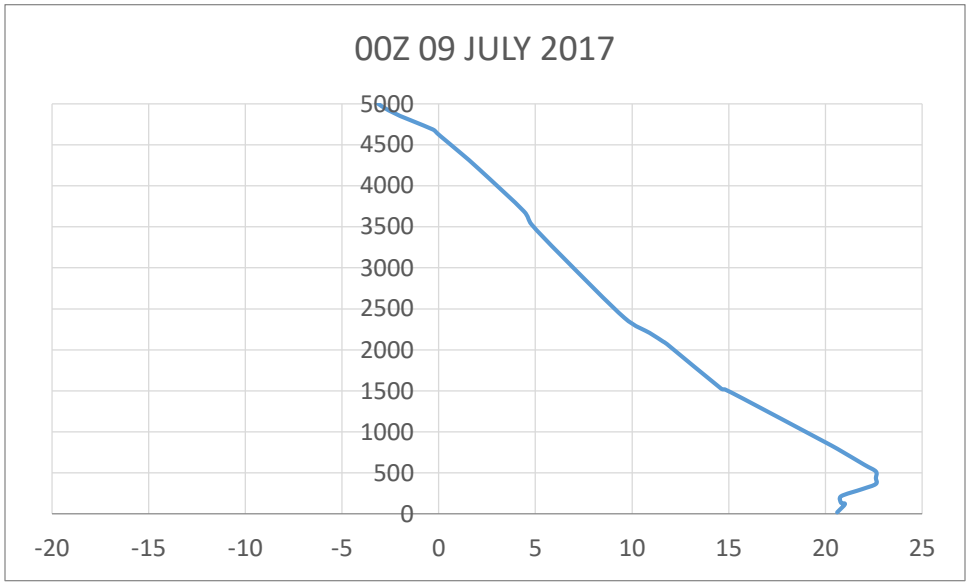


17064 Istanbul Observations at 3pm local time on 09 JULY 2017

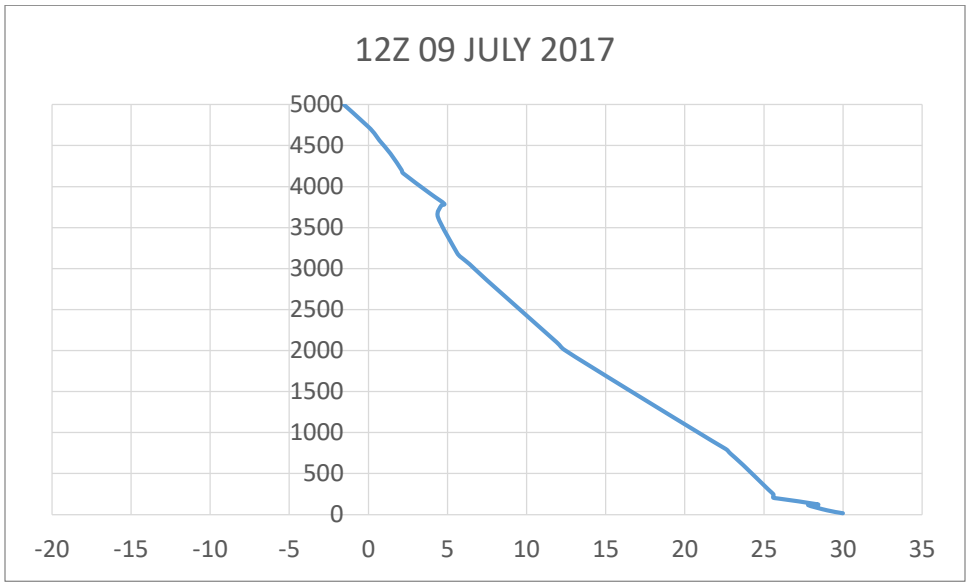


Radiosonde data and mixing height at 3am local time (top) and 3pm local time (bottom)

17064 Istanbul Observations at 3am local time on 10 JULY 2017

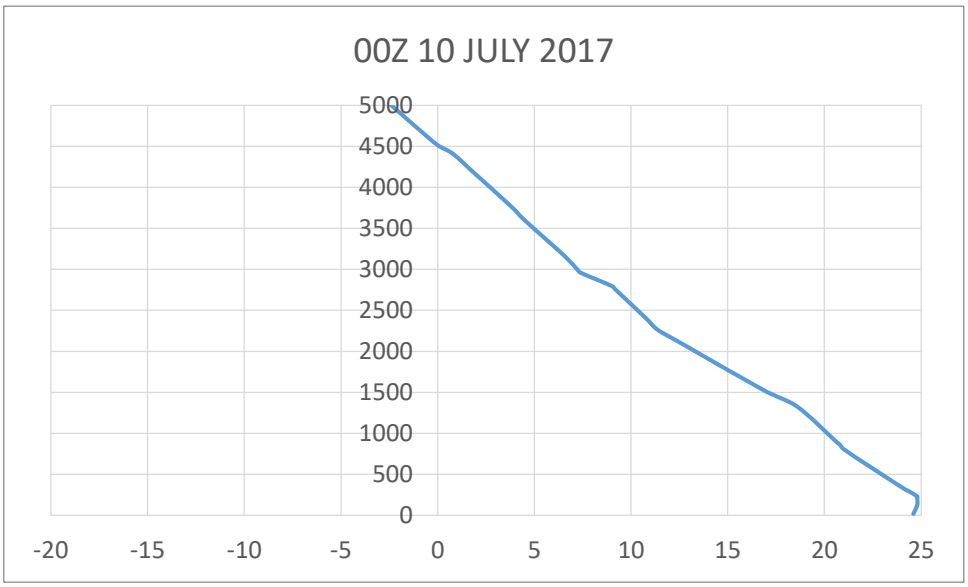


17064 Istanbul Observations at 3pm local time on 10 JULY 2017

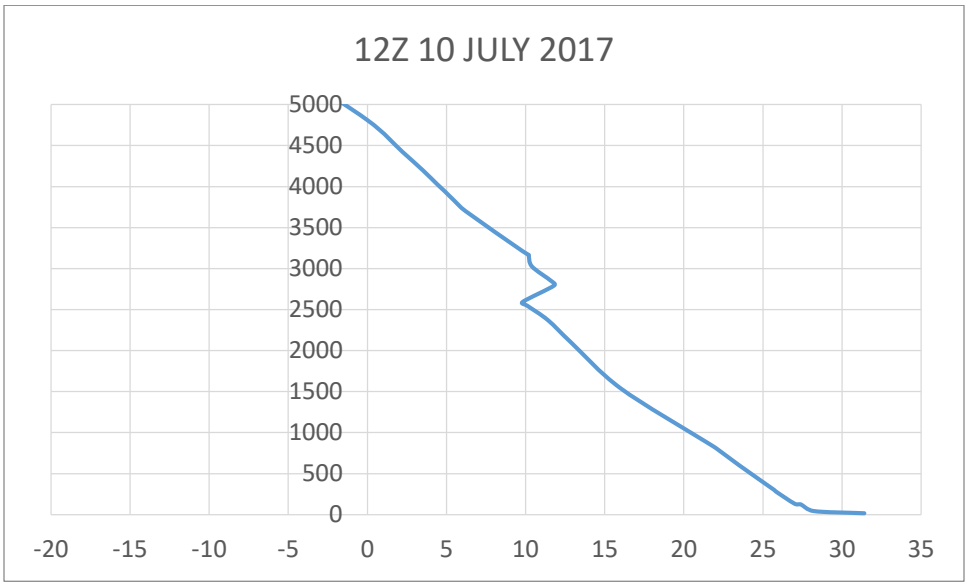


Radiosonde data and mixing height at 3am local time (top) and 3pm local time (bottom)

17064 Istanbul Observations at 3am local time on 11 JULY 2017

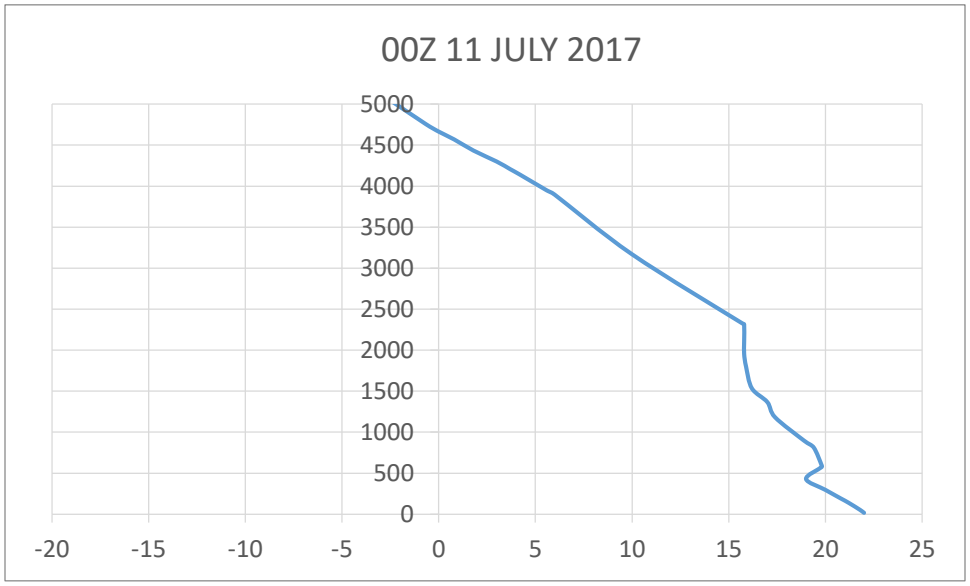


17064 Istanbul Observations at 3pm local time on 11 JULY 2017

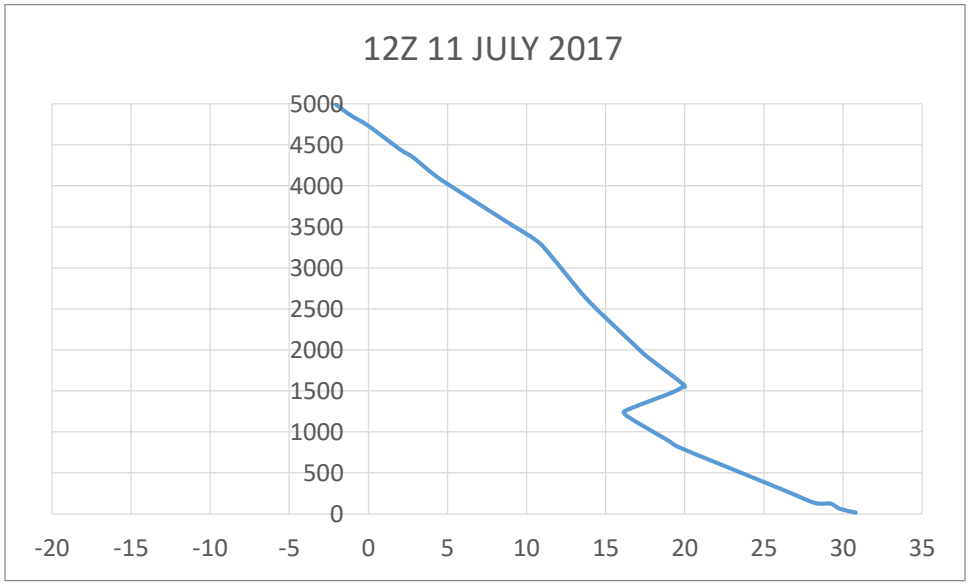


Radiosonde data and mixing height at 3am local time (top) and 3pm local time (bottom)

17064 Istanbul Observations at 3am local time on 12 JULY 2017

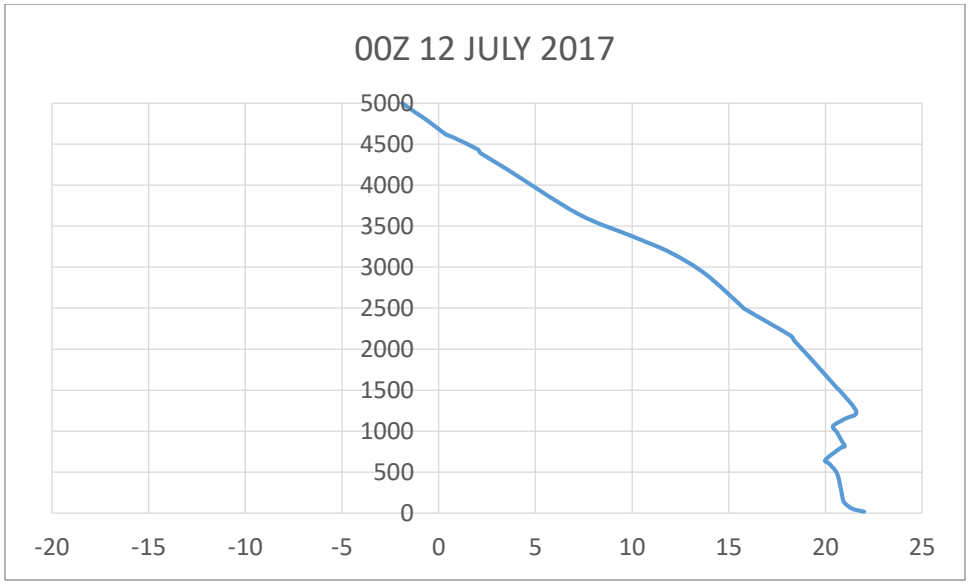


17064 Istanbul Observations at 3pm local time on 12 JULY 2017

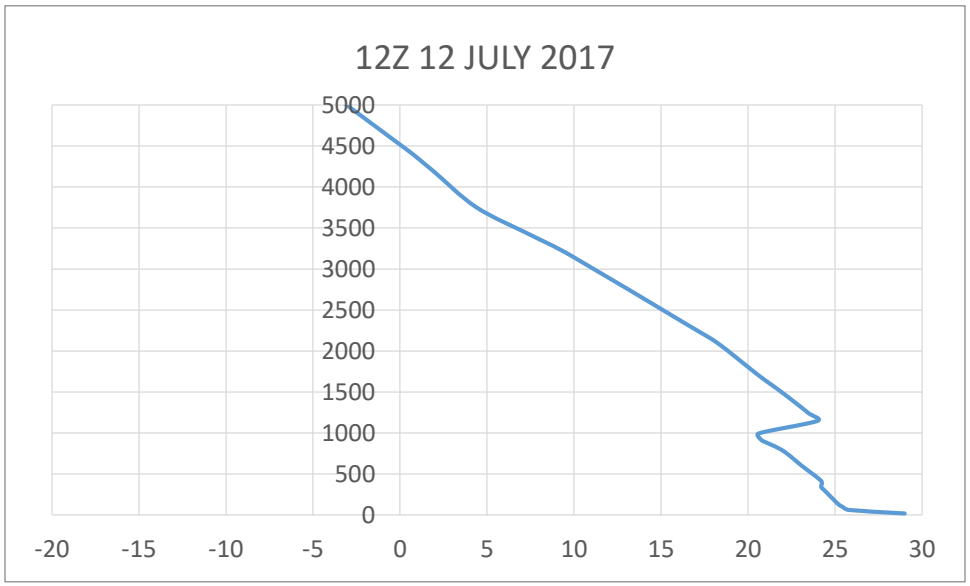


Radiosonde data and mixing height at 3am local time (top) and 3pm local time (bottom)

**Radiosonde data for weeks 5 and 6**

17064 Istanbul Observations at 00Z 20 OCT 2017

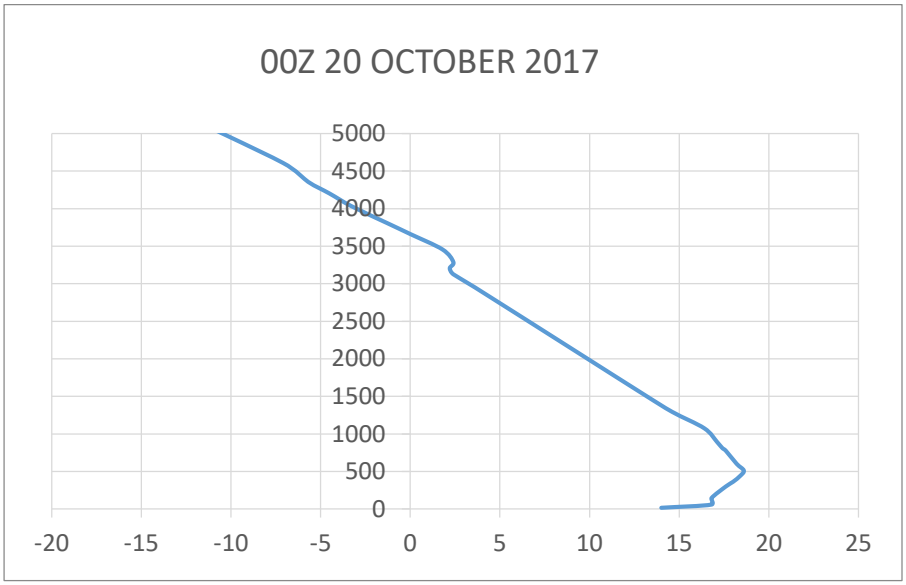


17064 Istanbul Observations at 12Z 20 OCT 2017

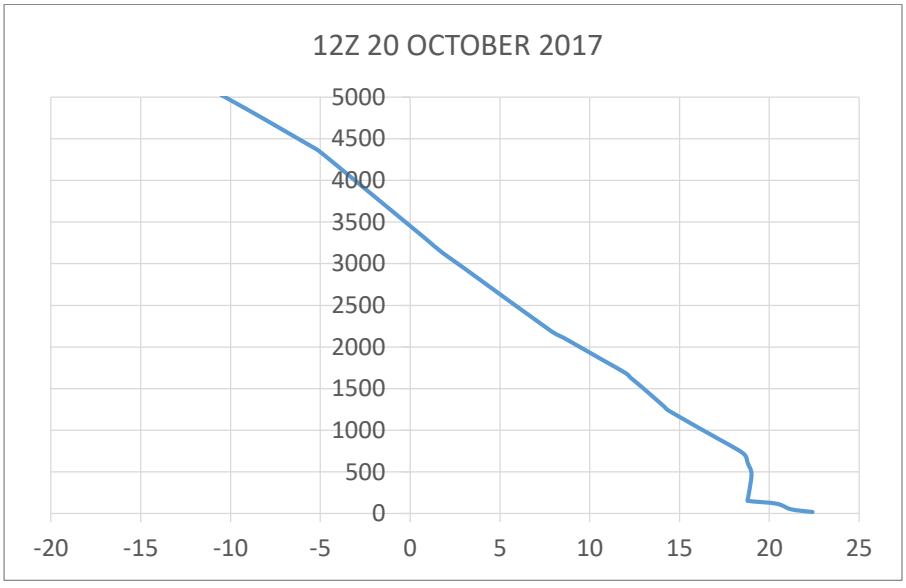


Radiosonde data and mixing height at 3am local time (top) and 3pm local time (bottom)

17064 Istanbul Observations at 00Z 21 OCT 2017

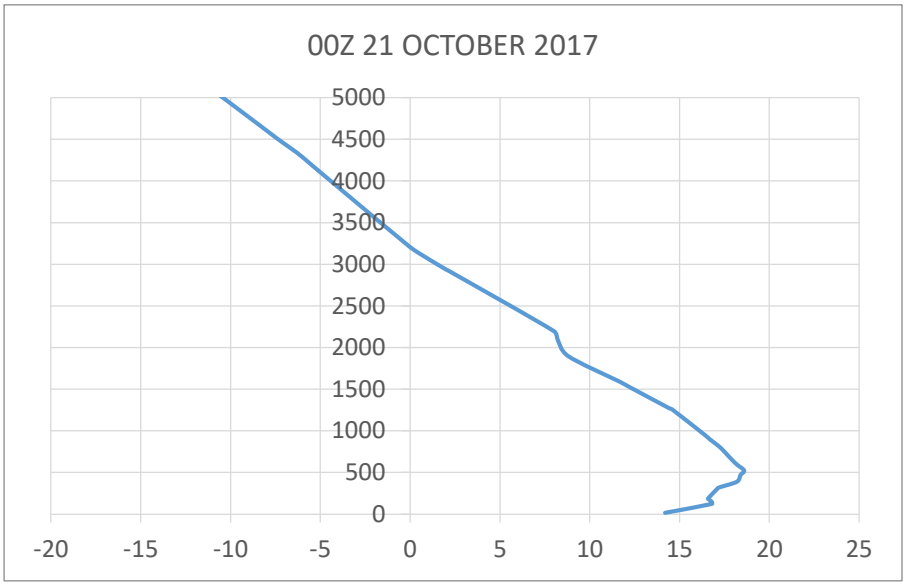


17064 Istanbul Observations at 12Z 21 OCT 2017

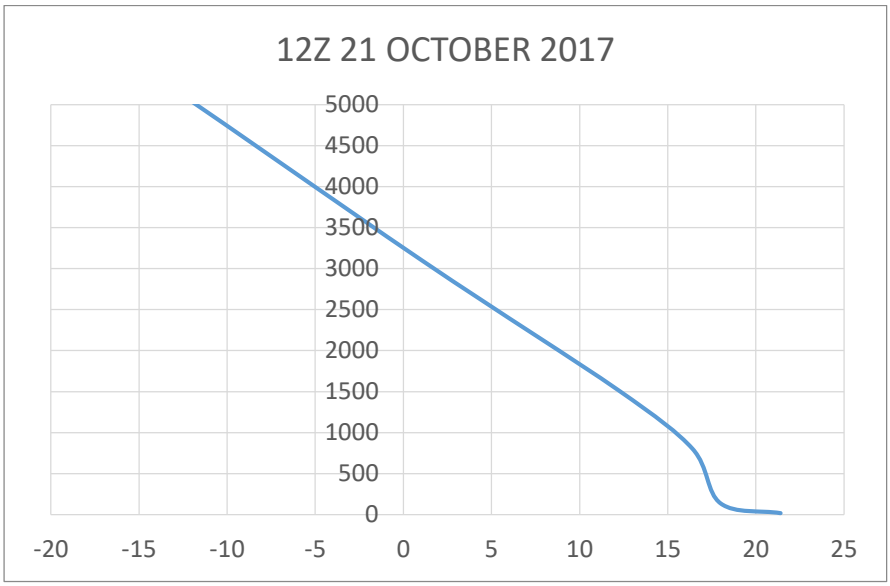


Radiosonde data and mixing height at 3am local time (top) and 3pm local time (bottom)

17064 Istanbul Observations at 00Z 22 OCT 2017

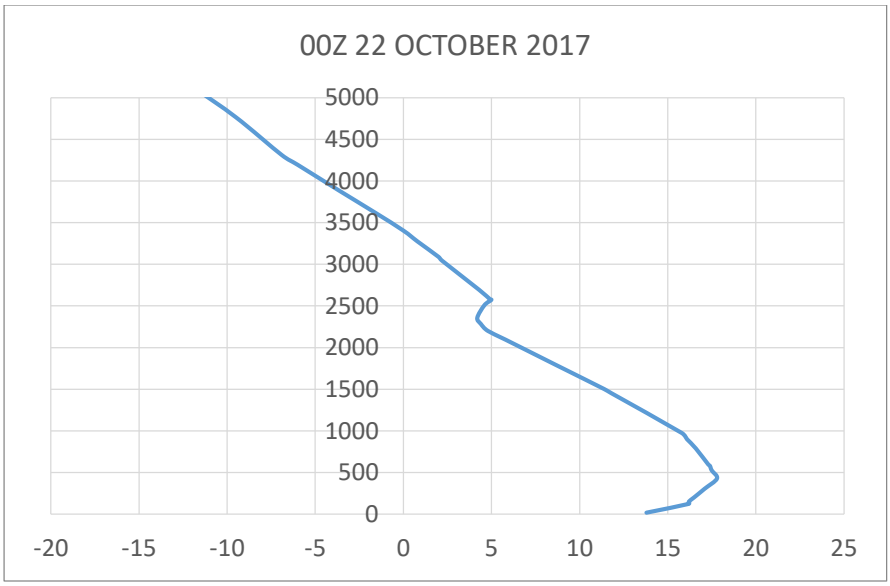


17064 Istanbul Observations at 12Z 22 OCT 2017

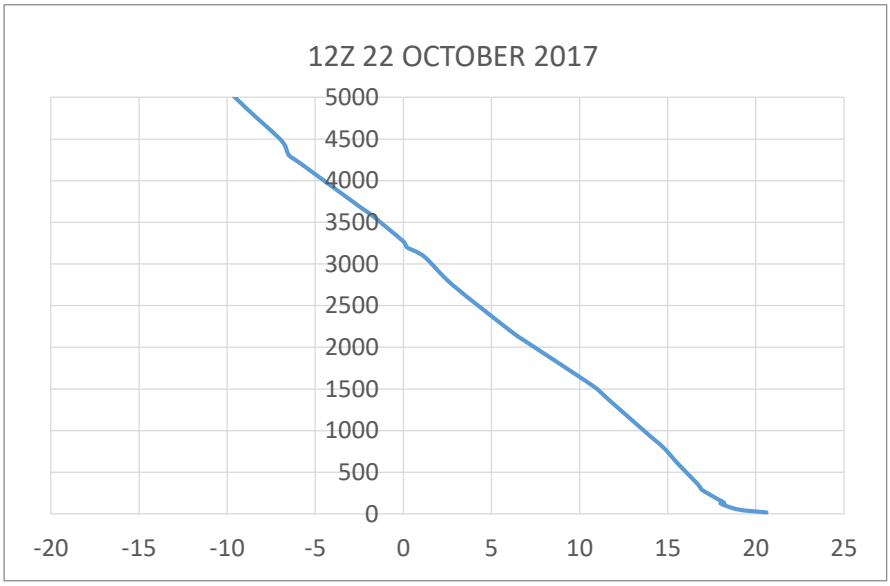


Radiosonde data and mixing height at 3am local time (top) and 3pm local time (bottom)

17064 Istanbul Observations at 00Z 23 OCT 2017

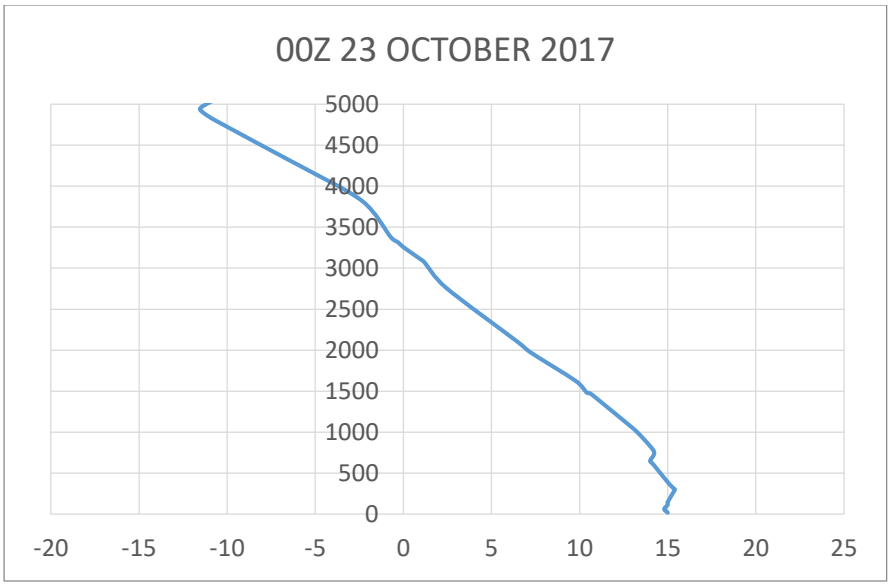


17064 Istanbul Observations at 12Z 23 OCT 2017

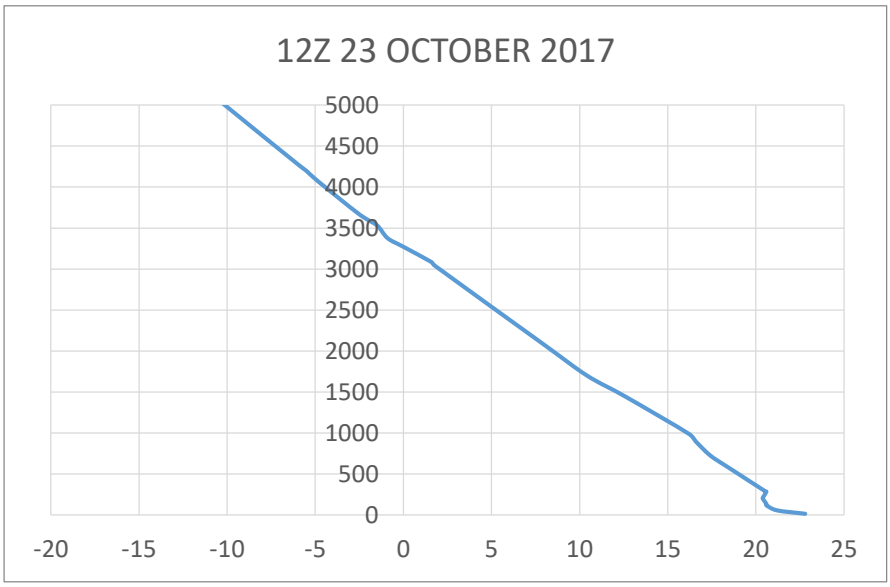


Radiosonde data and mixing height at 3am local time (top) and 3pm local time (bottom)

17064 Istanbul Observations at 00Z 24 OCT 2017

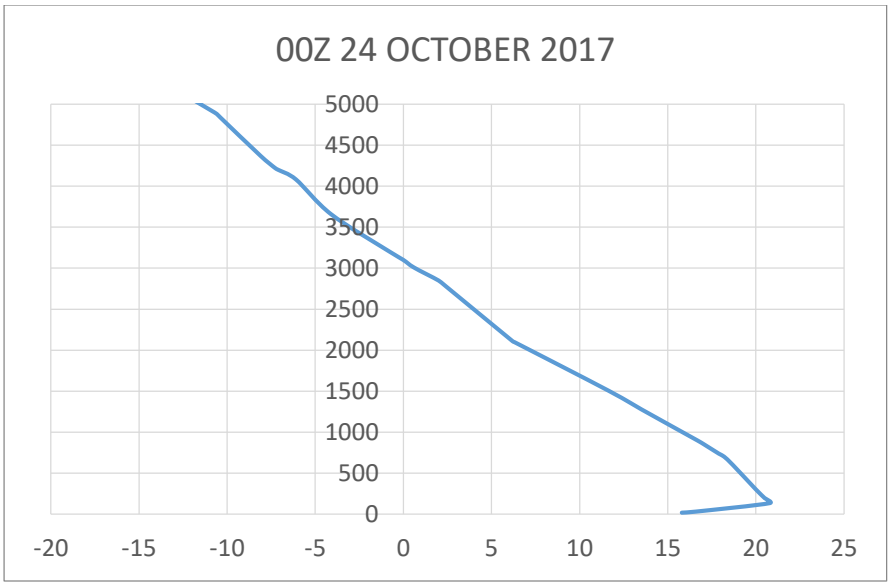


17064 Istanbul Observations at 12Z 24 OCT 2017

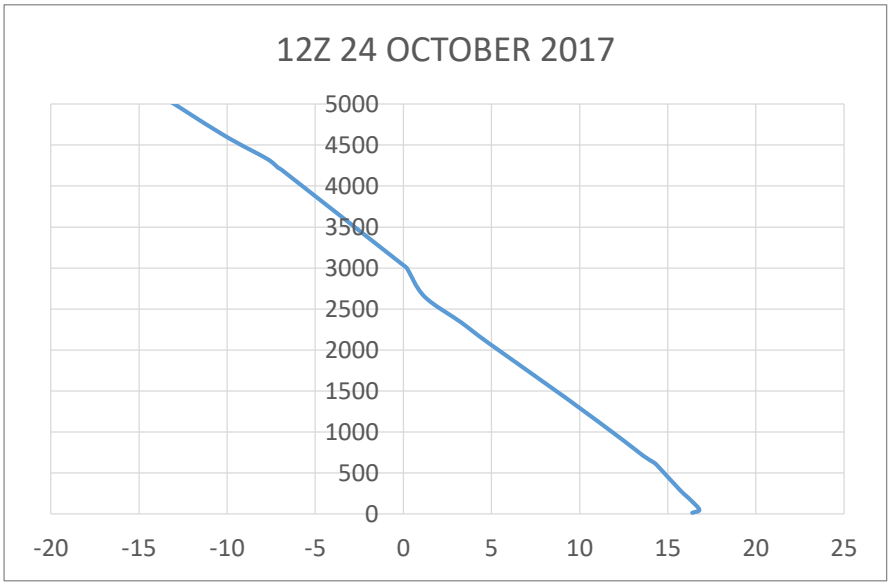


Radiosonde data and mixing height at 3am local time (top) and 3pm local time (bottom)

17064 Istanbul Observations at 00Z 25 OCT 2017

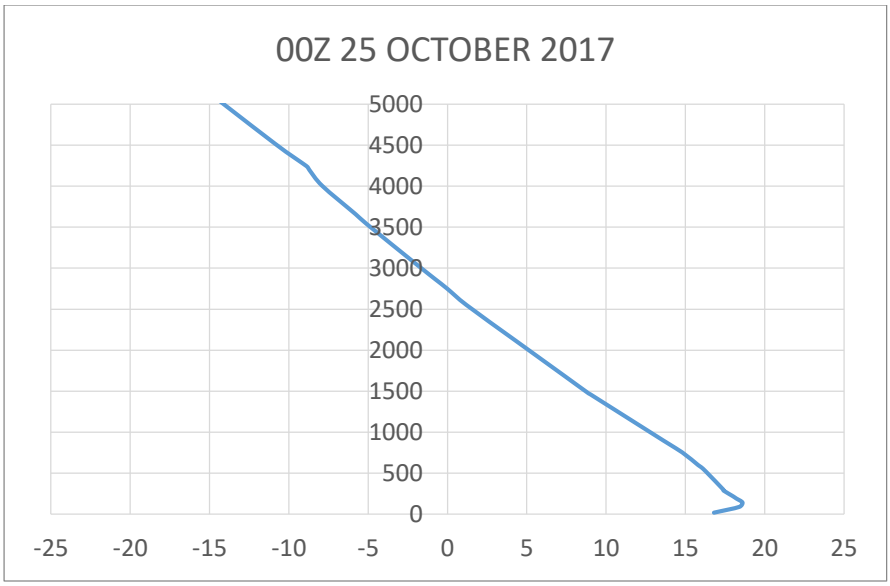


17064 Istanbul Observations at 12Z 25 OCT 2017

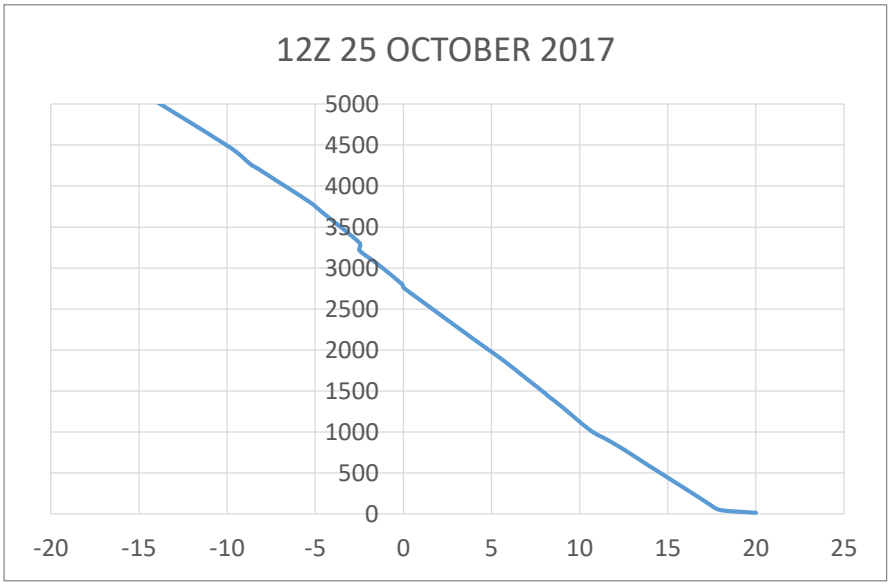


Radiosonde data and mixing height at 3am local time (top) and 3pm local time (bottom)

17064 Istanbul Observations at 00Z 26 OCT 2017

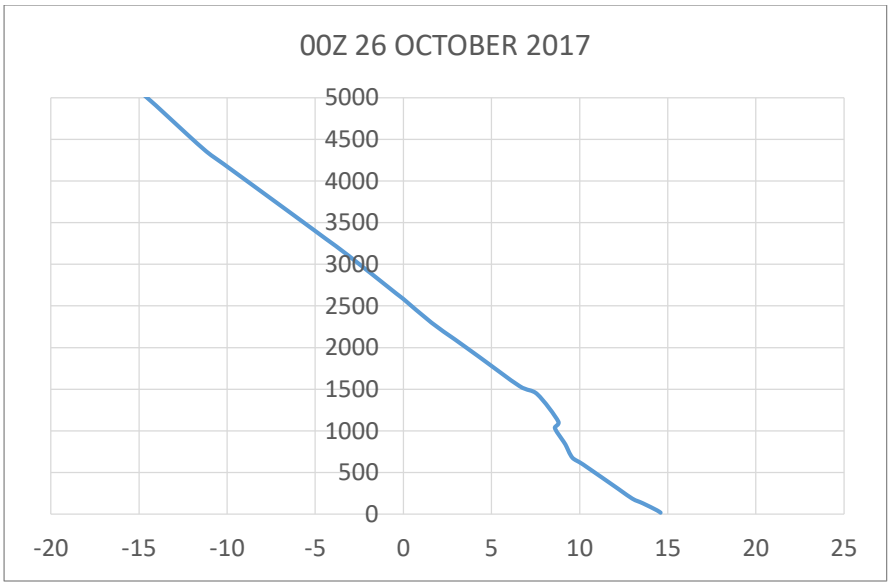


17064 Istanbul Observations at 12Z 26 OCT 2017

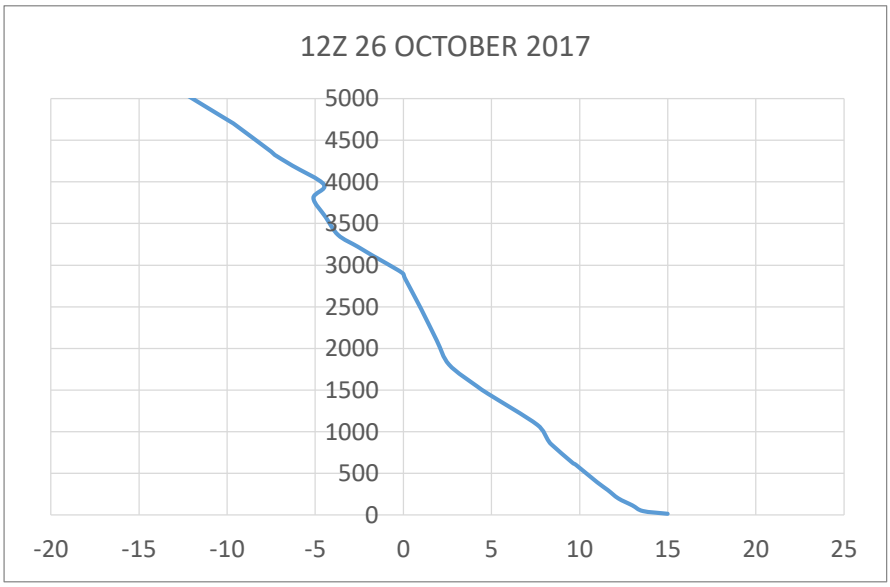


Radiosonde data and mixing height at 3am local time (top) and 3pm local time (bottom)

17064 Istanbul Observations at 00Z 05 JAN 2018

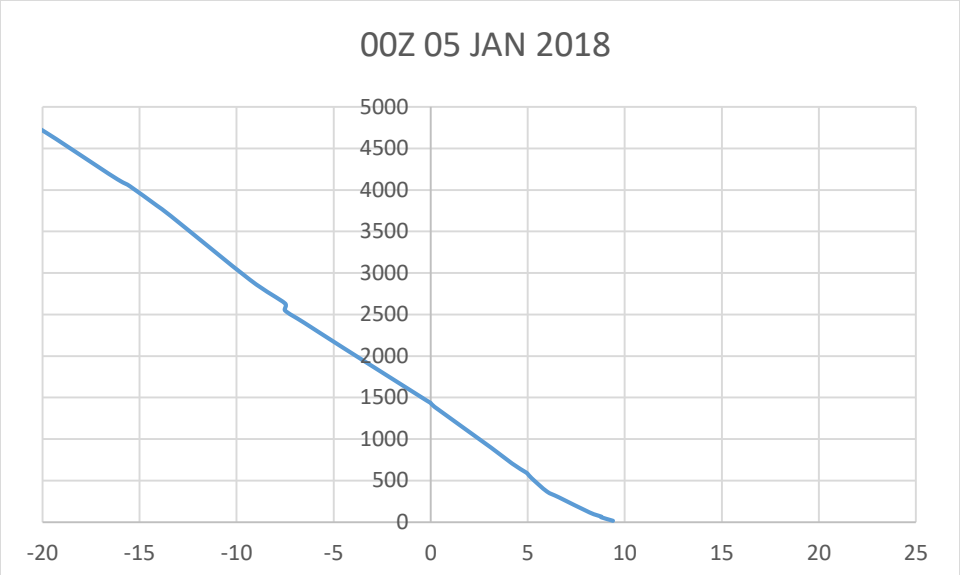


17064 Istanbul Observations at 12Z 05 JAN 2018

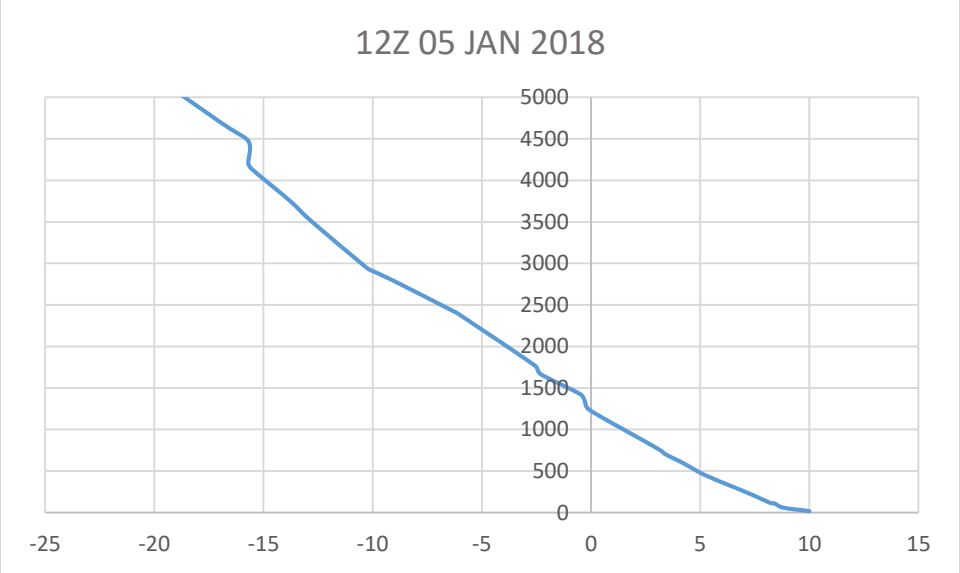


Radiosonde data and mixing height at 3am local time (top) and 3pm local time (bottom)

17064 Istanbul Observations at 00Z 06 JAN 2018

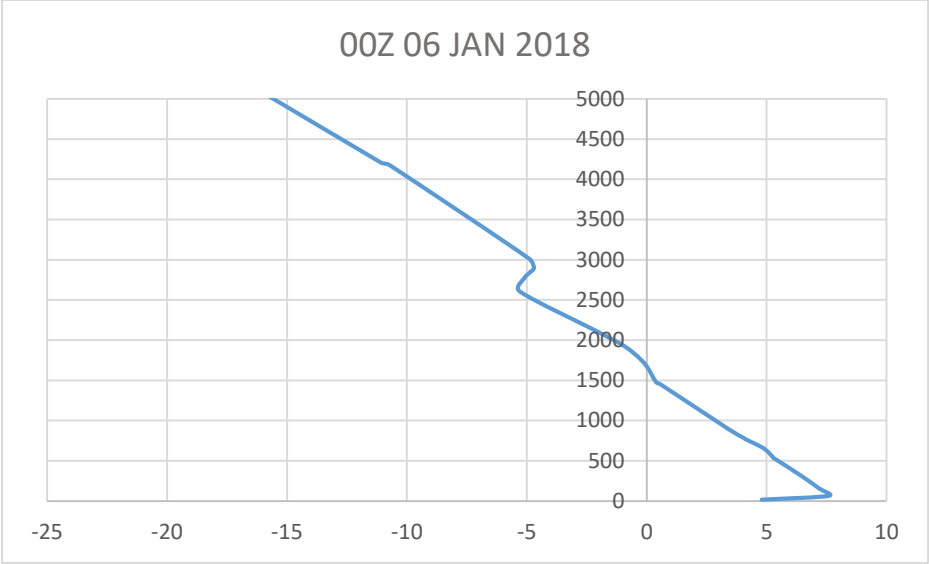


17064 Istanbul Observations at 12Z 06 JAN 2018

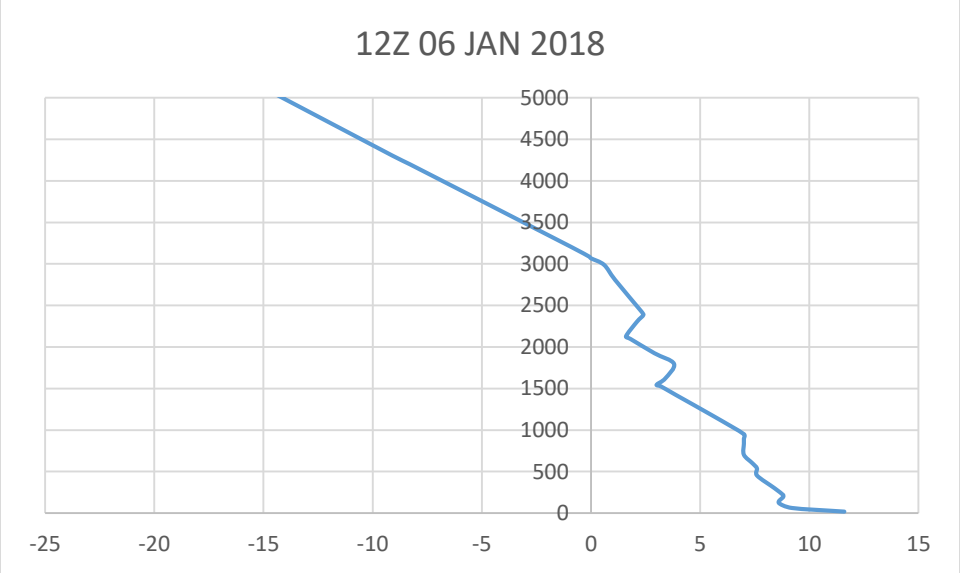


Radiosonde data and mixing height at 3am local time (top) and 3pm local time (bottom)

17064 Istanbul Observations at 00Z 07 JAN 2018

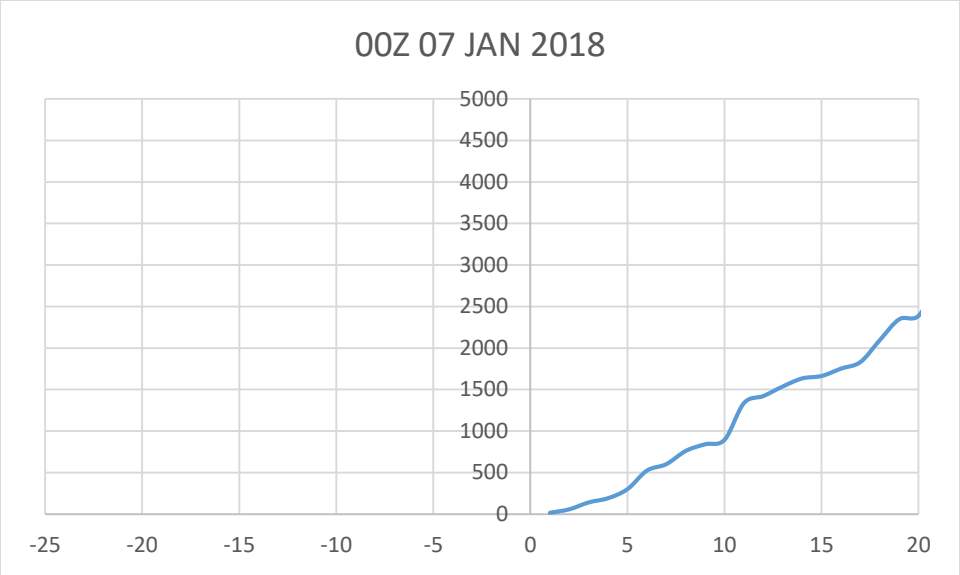


17064 Istanbul Observations at 12Z 07 JAN 2018

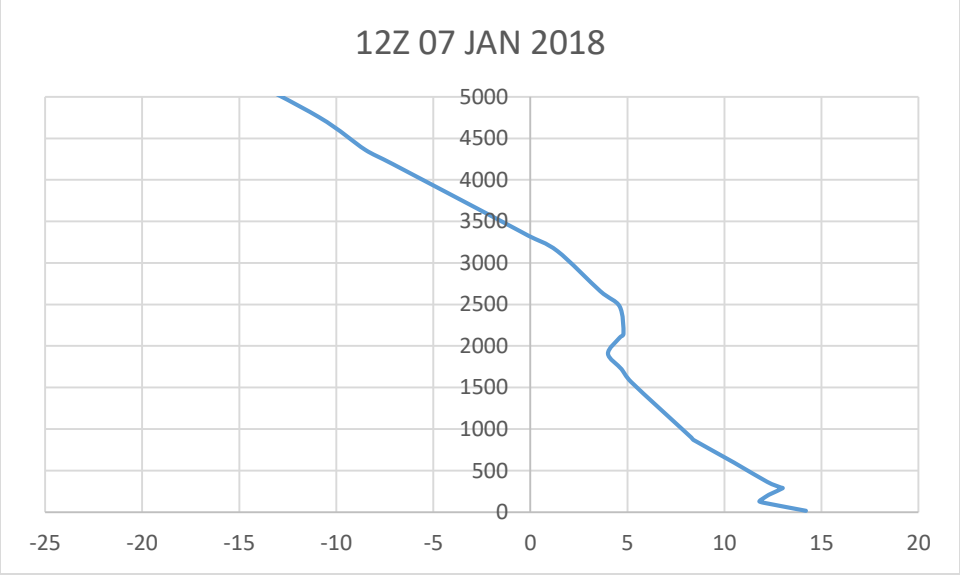


Radiosonde data and mixing height at 3am local time (top) and 3pm local time (bottom)

17064 Istanbul Observations at 00Z 08 JAN 2018

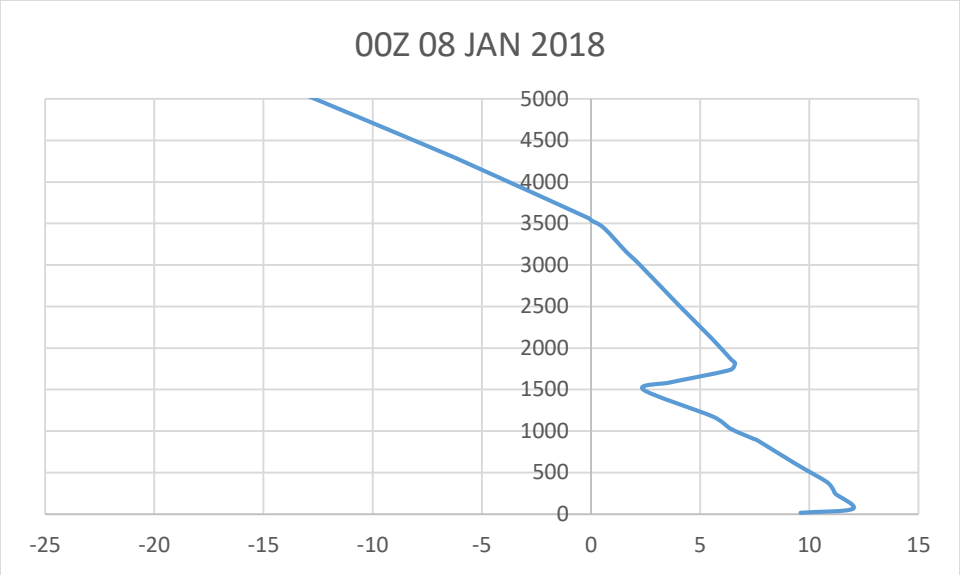


17064 Istanbul Observations at 12Z 08 JAN 2018

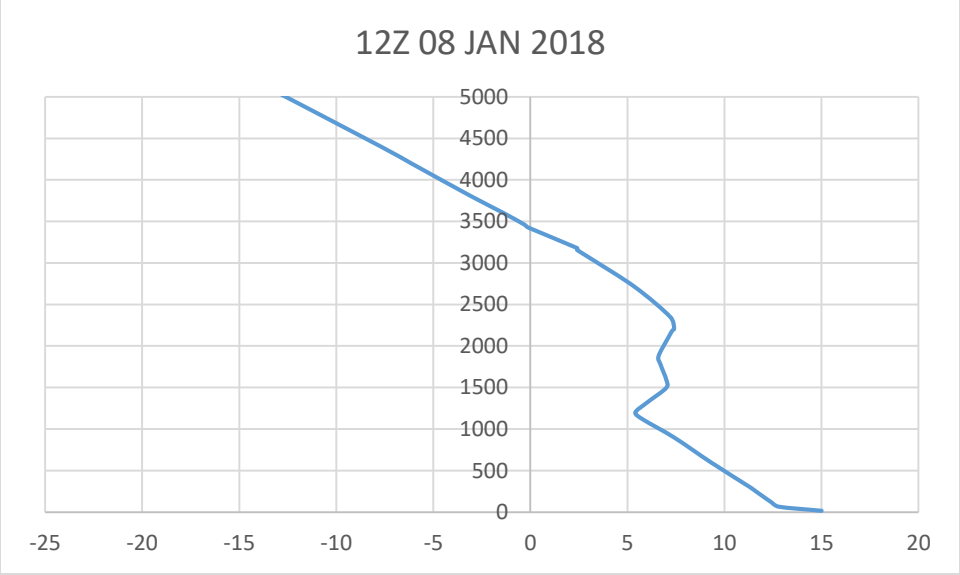


Radiosonde data and mixing height at 3am local time (top) and 3pm local time (bottom)

17064 Istanbul Observations at 00Z 09 JAN 2018

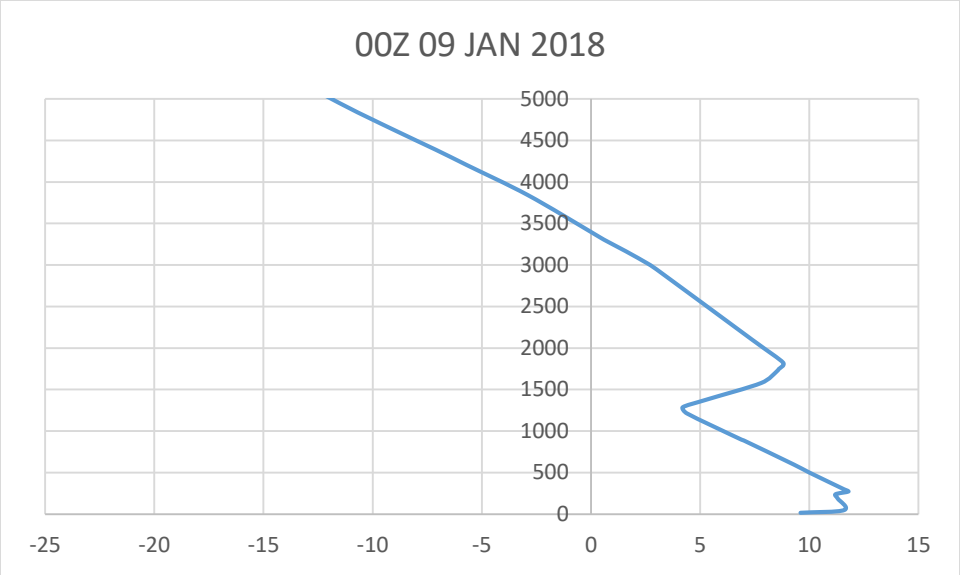


17064 Istanbul Observations at 12Z 09 JAN 2018

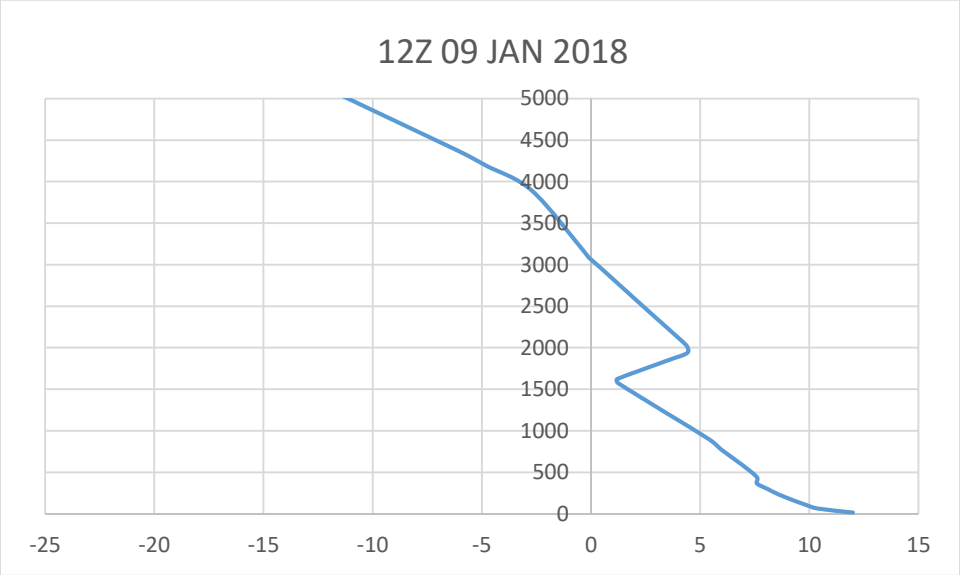


Radiosonde data and mixing height at 3am local time (top) and 3pm local time (bottom)

17064 Istanbul Observations at 00Z 10 JAN 2018

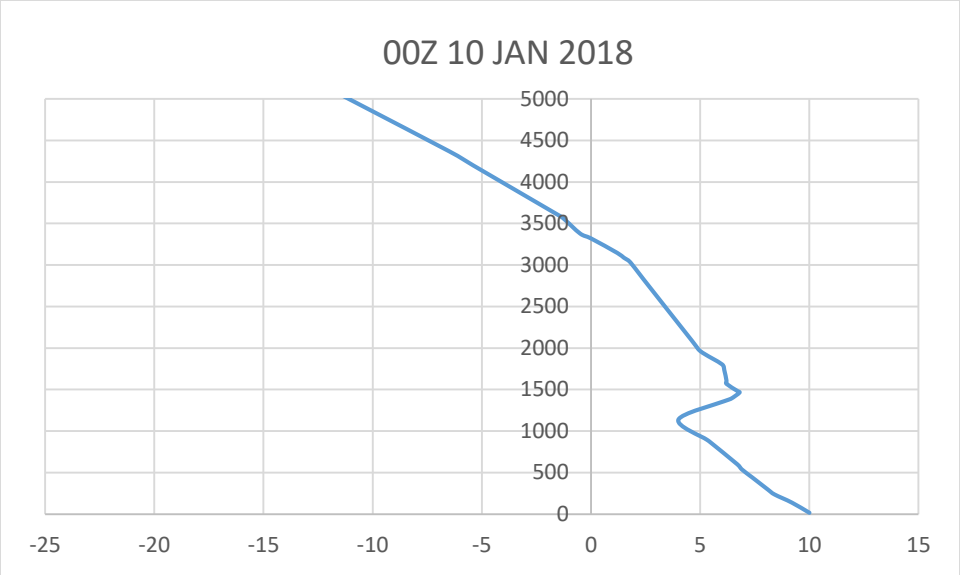


17064 Istanbul Observations at 12Z 10 JAN 2018

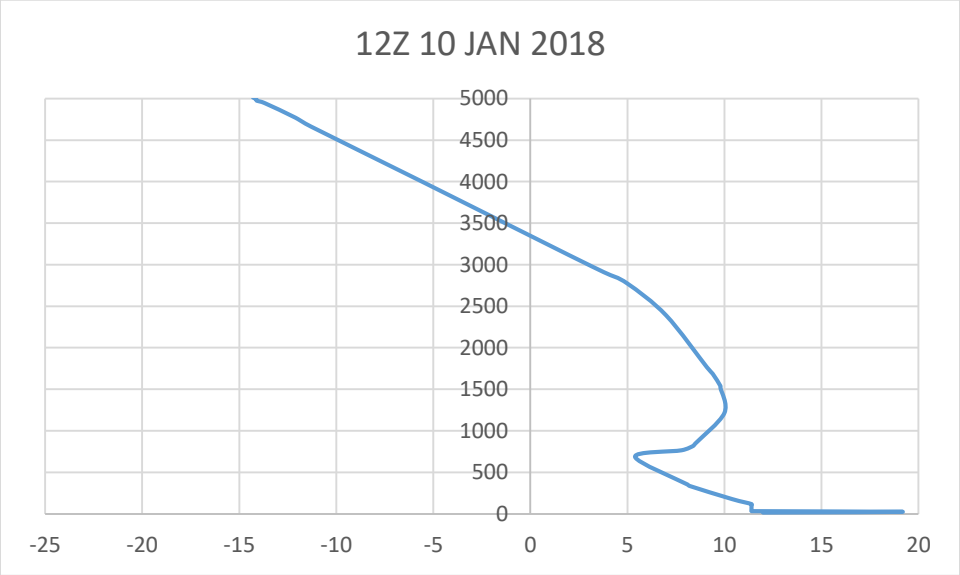


Radiosonde data and mixing height at 3am local time (top) and 3pm local time (bottom)

17064 Istanbul Observations at 00Z 11 JAN 2018

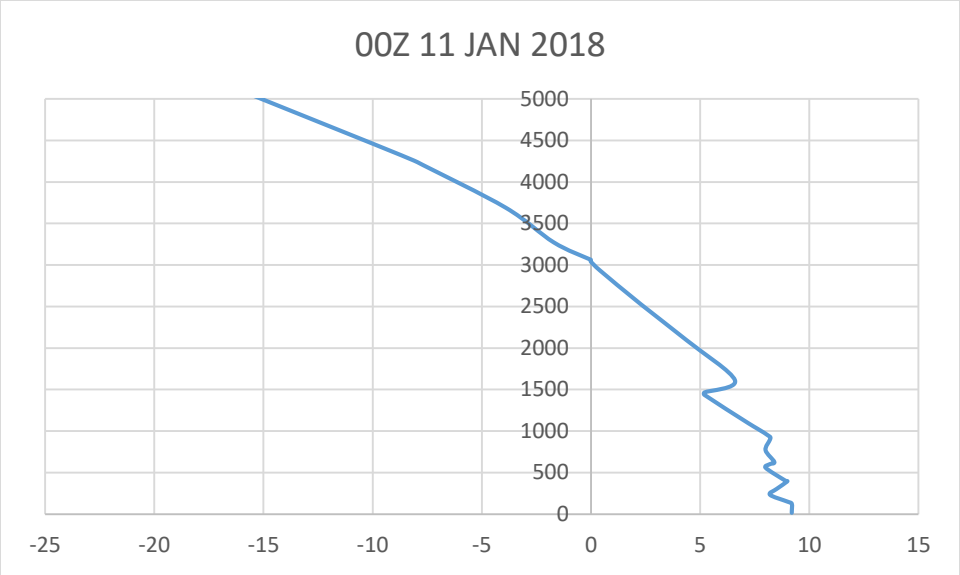


17064 Istanbul Observations at 12Z 11 JAN 2018

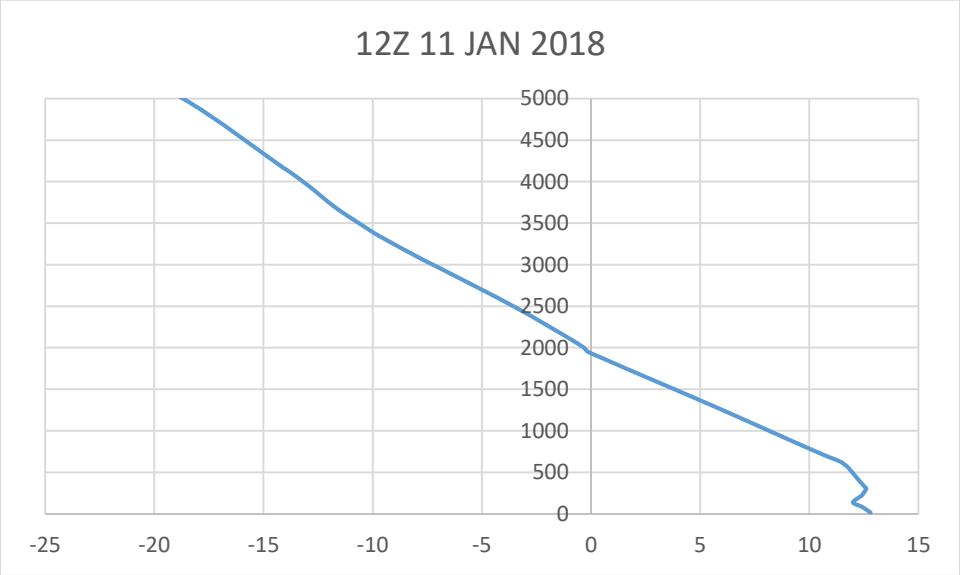


Radiosonde data and mixing height at 3am local time (top) and 3pm local time (bottom)

## *Appendix C*

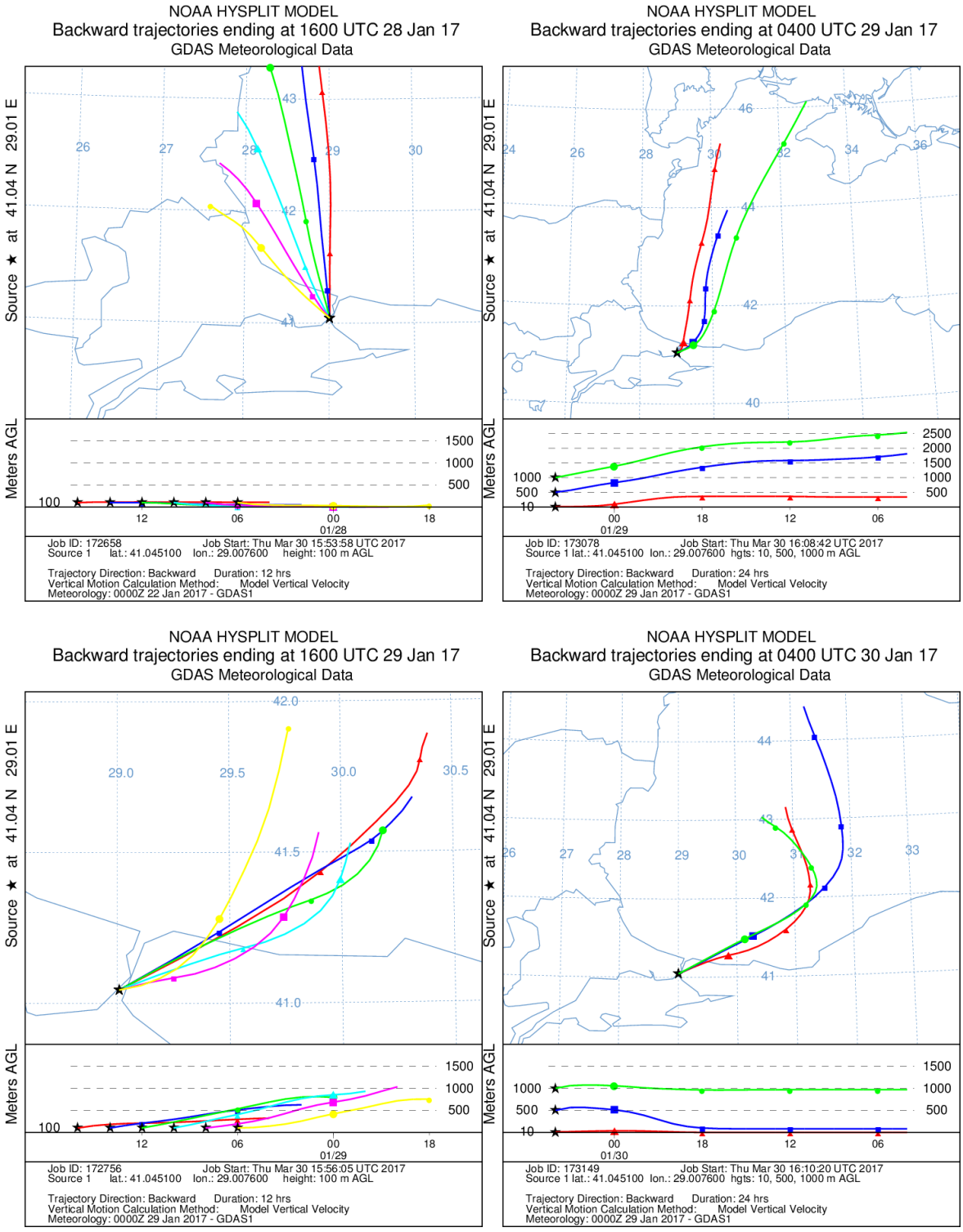


Two-hour air mass backward trajectories that correspond to daytime air samples (left) and 12-h air mass backward trajectories that correspond to nighttime air samples (right).

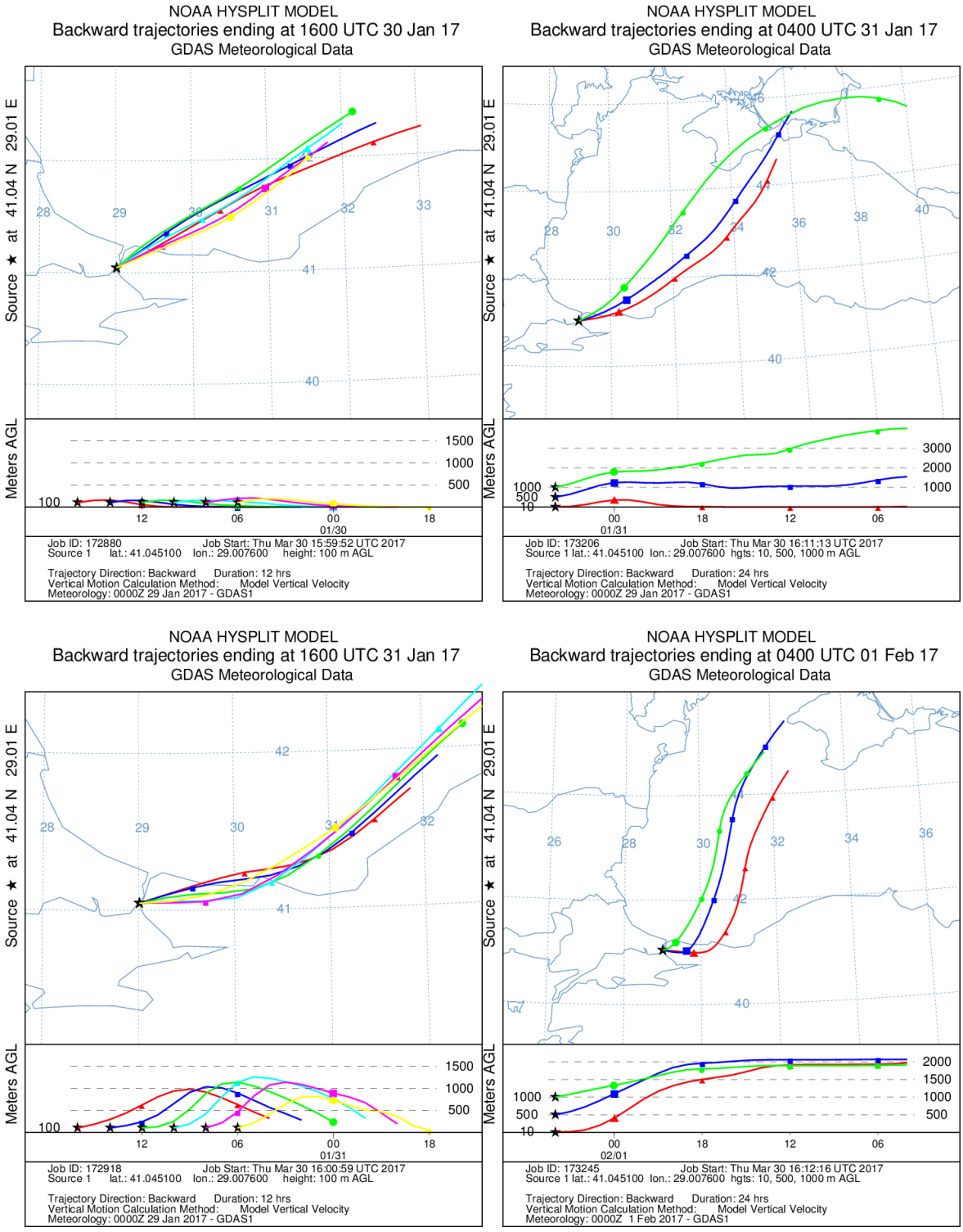


Two-hour air mass backward trajectories that correspond to daytime air samples (left) and 12-h air mass backward trajectories that correspond to nighttime air samples (right).

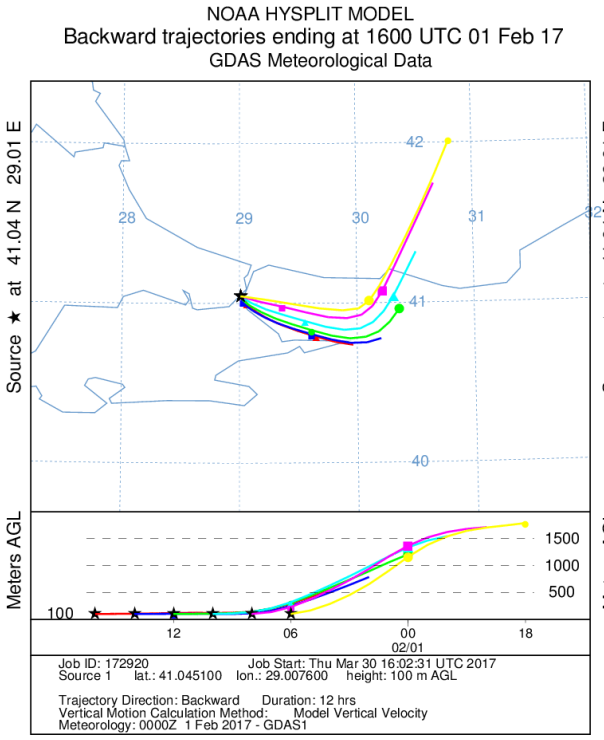


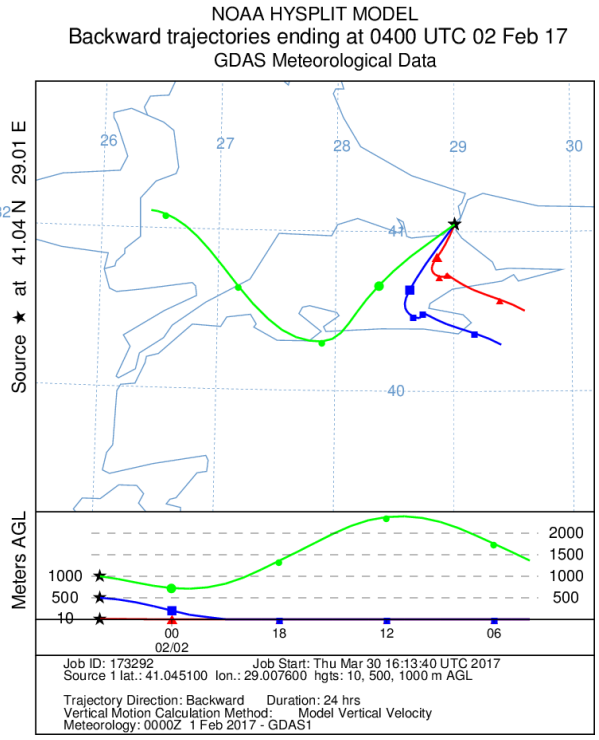


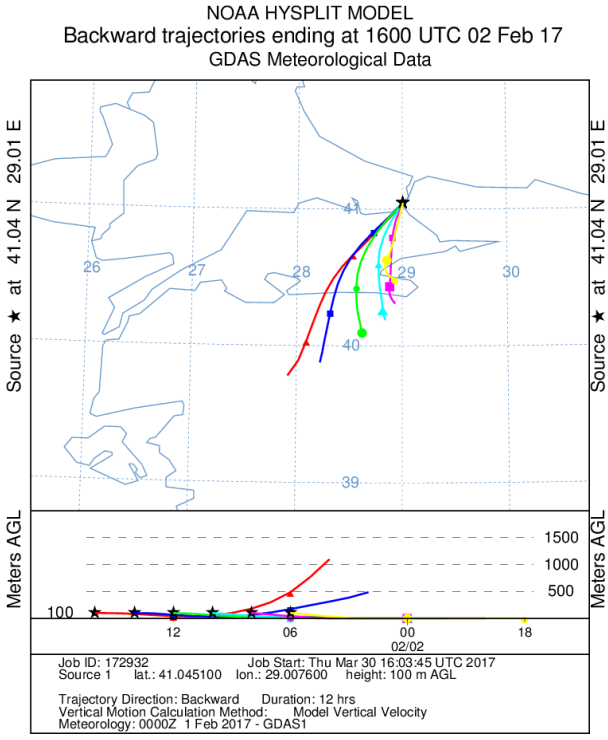


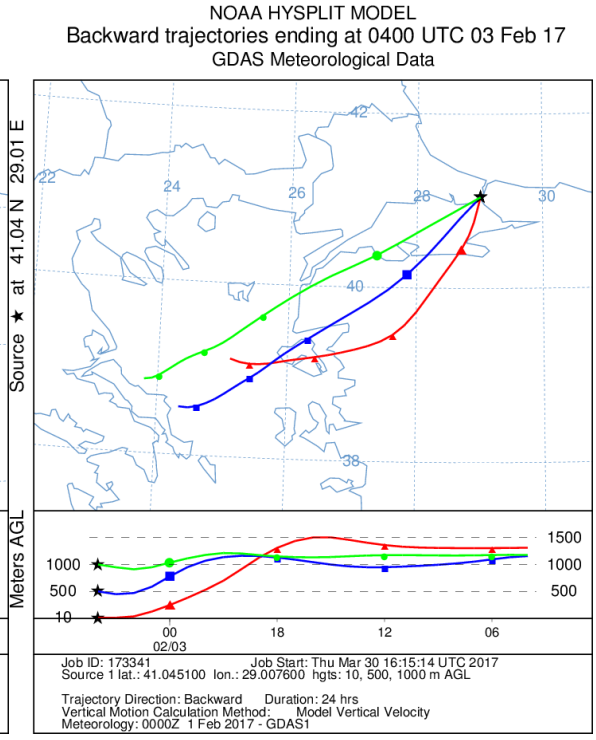


Two-hour air mass backward trajectories that correspond to daytime air samples (left) and 12-h air mass backward trajectories that correspond to nighttime air samples (right).

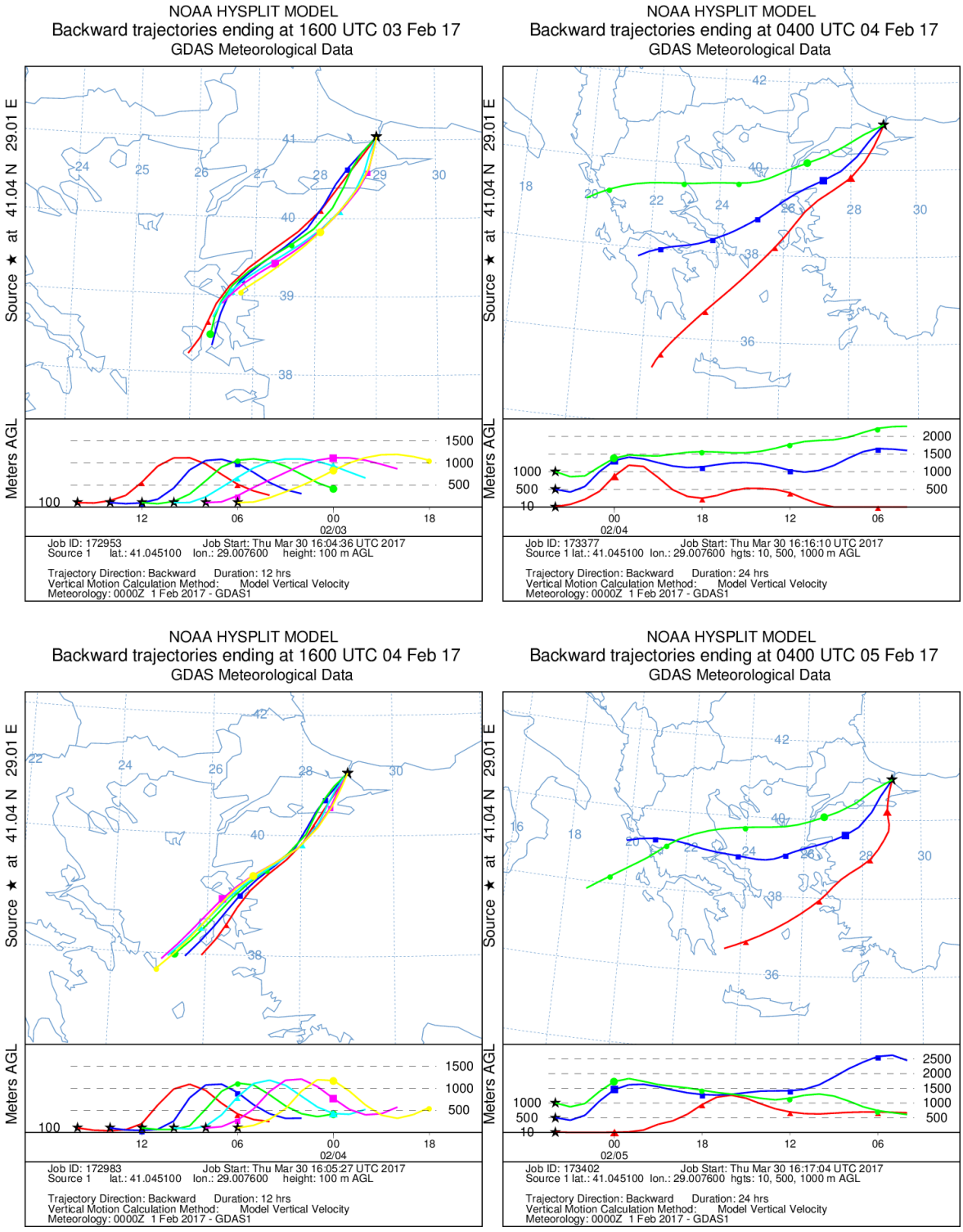


Two-hour air mass backward trajectories that correspond to daytime air samples (left) and 12-h air mass backward trajectories that correspond to nighttime air samples (right).

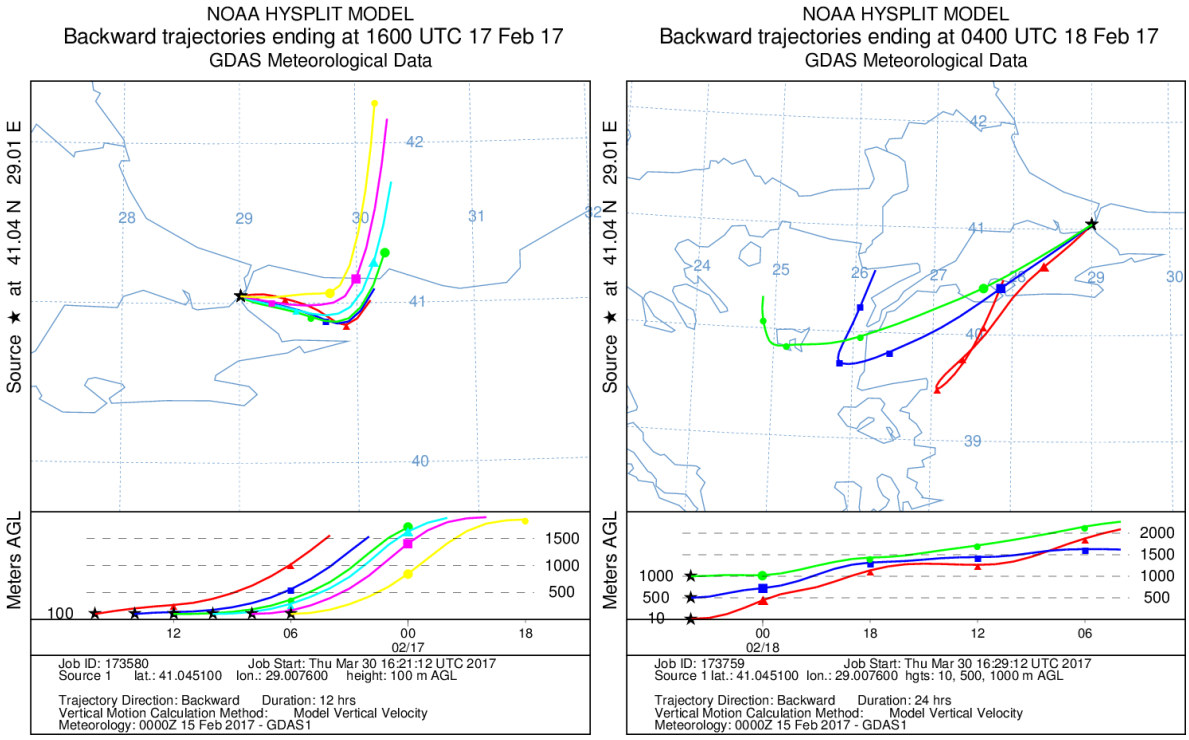


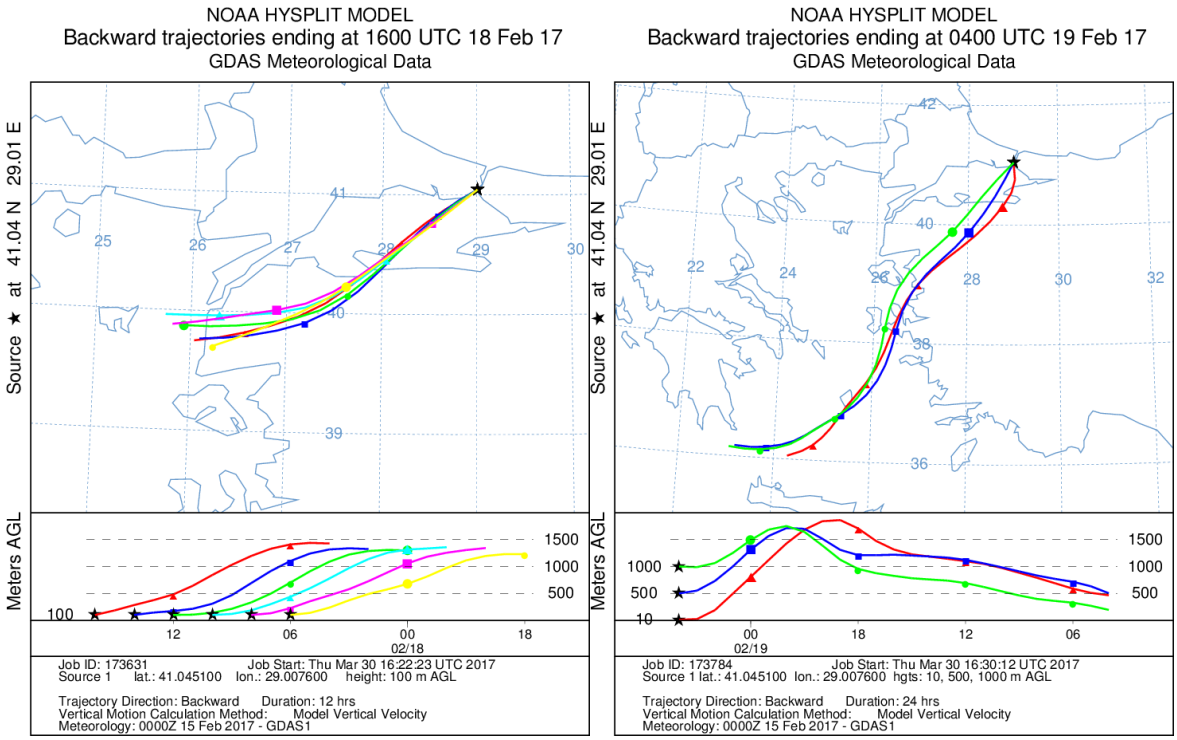


Two-hour air mass backward trajectories that correspond to daytime air samples (left) and 12-h air mass backward trajectories that correspond to nighttime air samples (right).

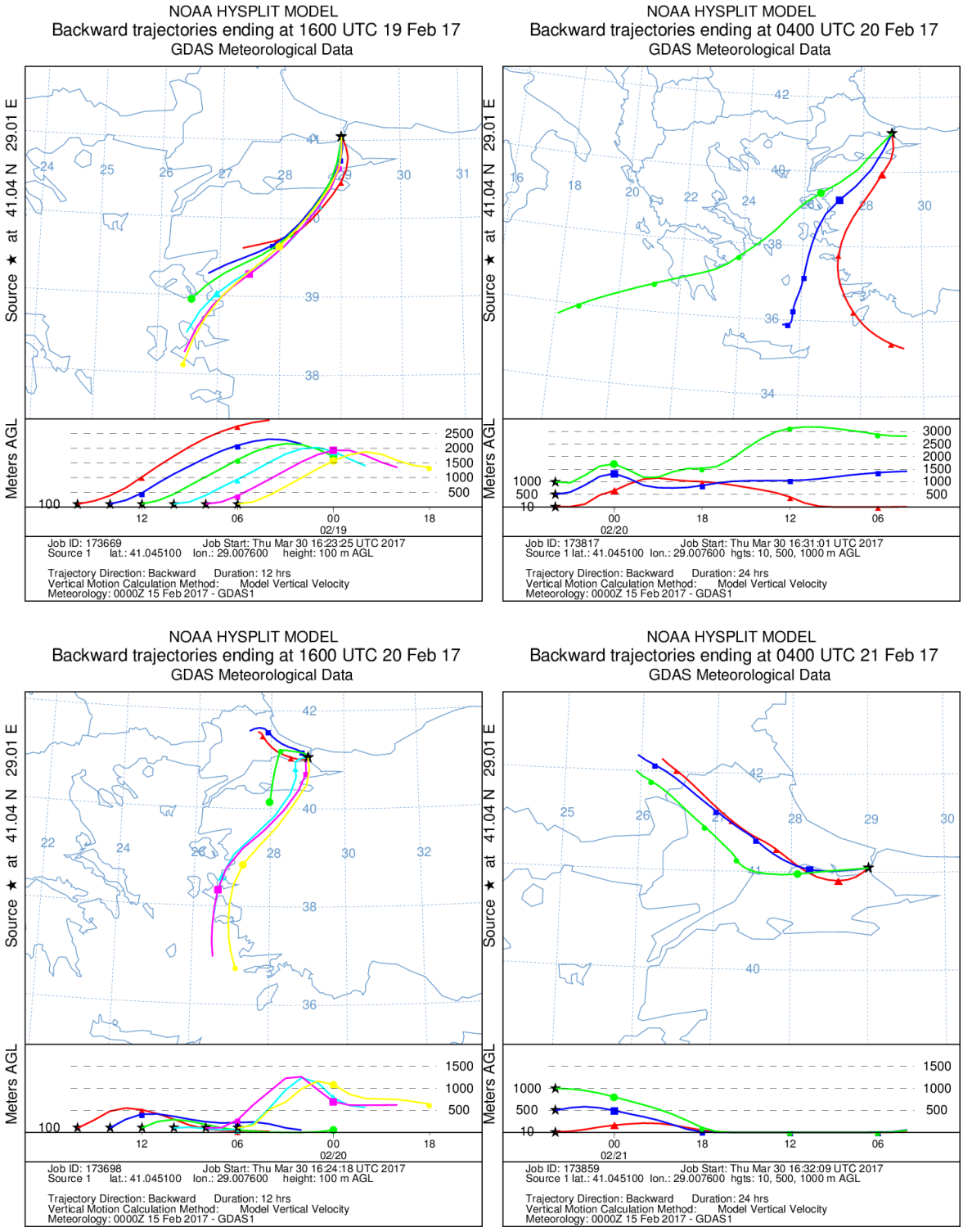


Two-hour air mass backward trajectories that correspond to daytime air samples (left) and 12-h air mass backward trajectories that correspond to nighttime air samples (right).

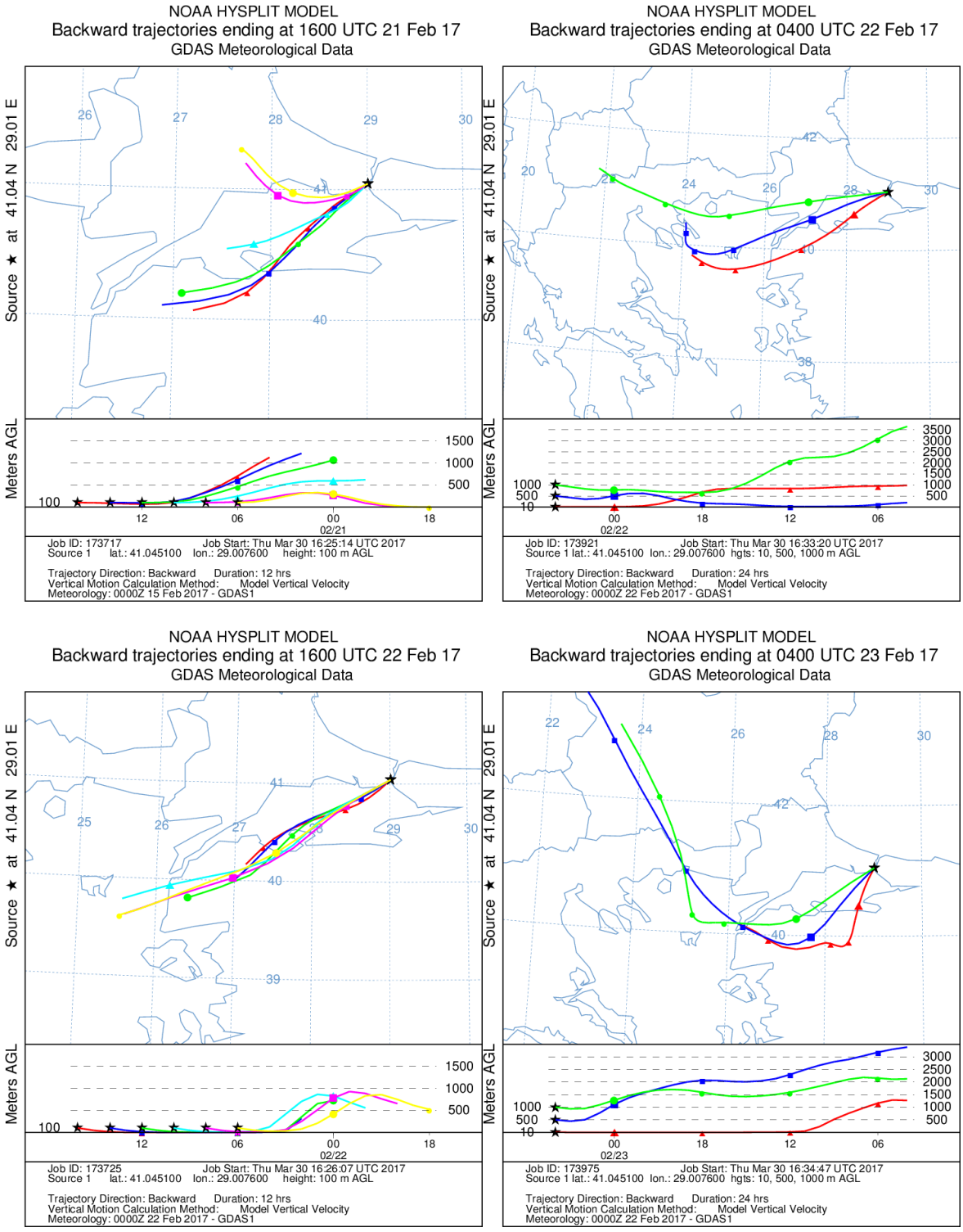


Two-hour air mass backward trajectories that correspond to daytime air samples (left) and 12-h air mass backward trajectories that correspond to nighttime air samples (right).

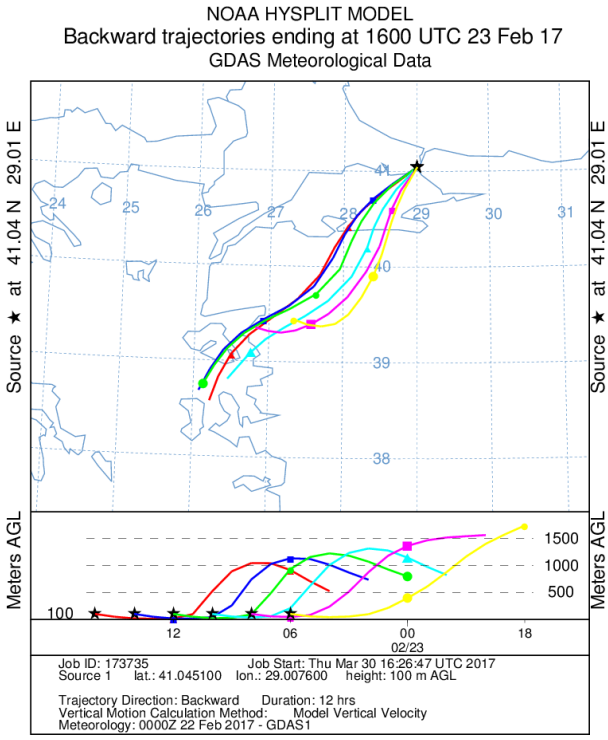


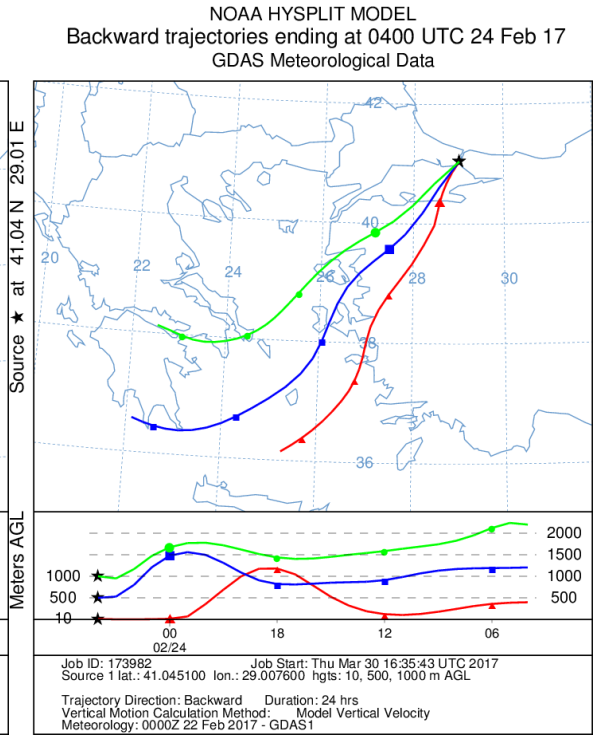


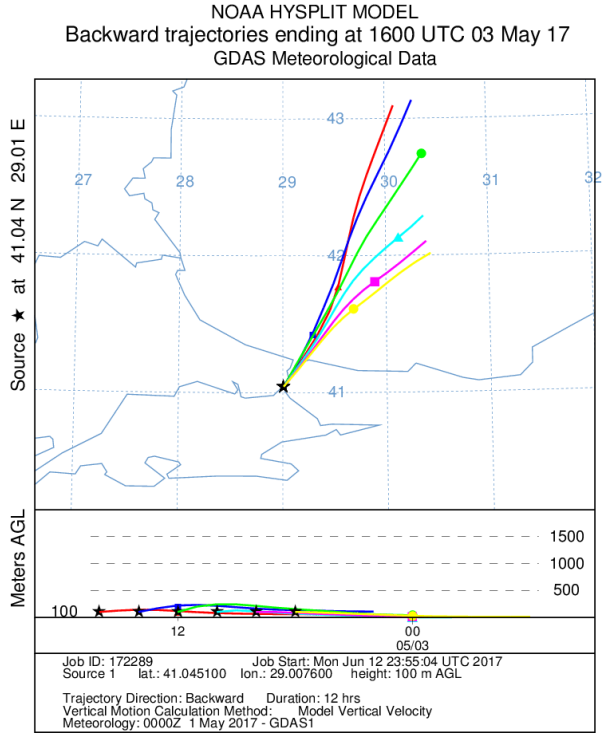


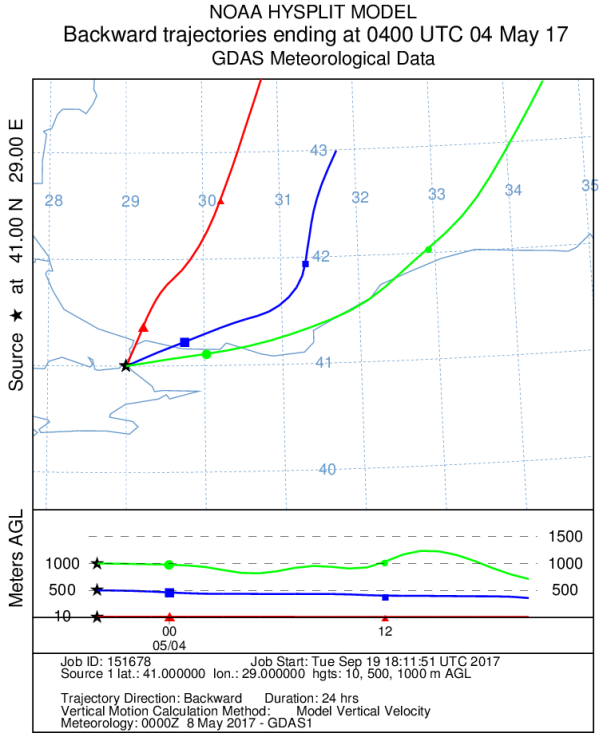


Two-hour air mass backward trajectories that correspond to daytime air samples (left) and 12-h air mass backward trajectories that correspond to nighttime air samples (right).

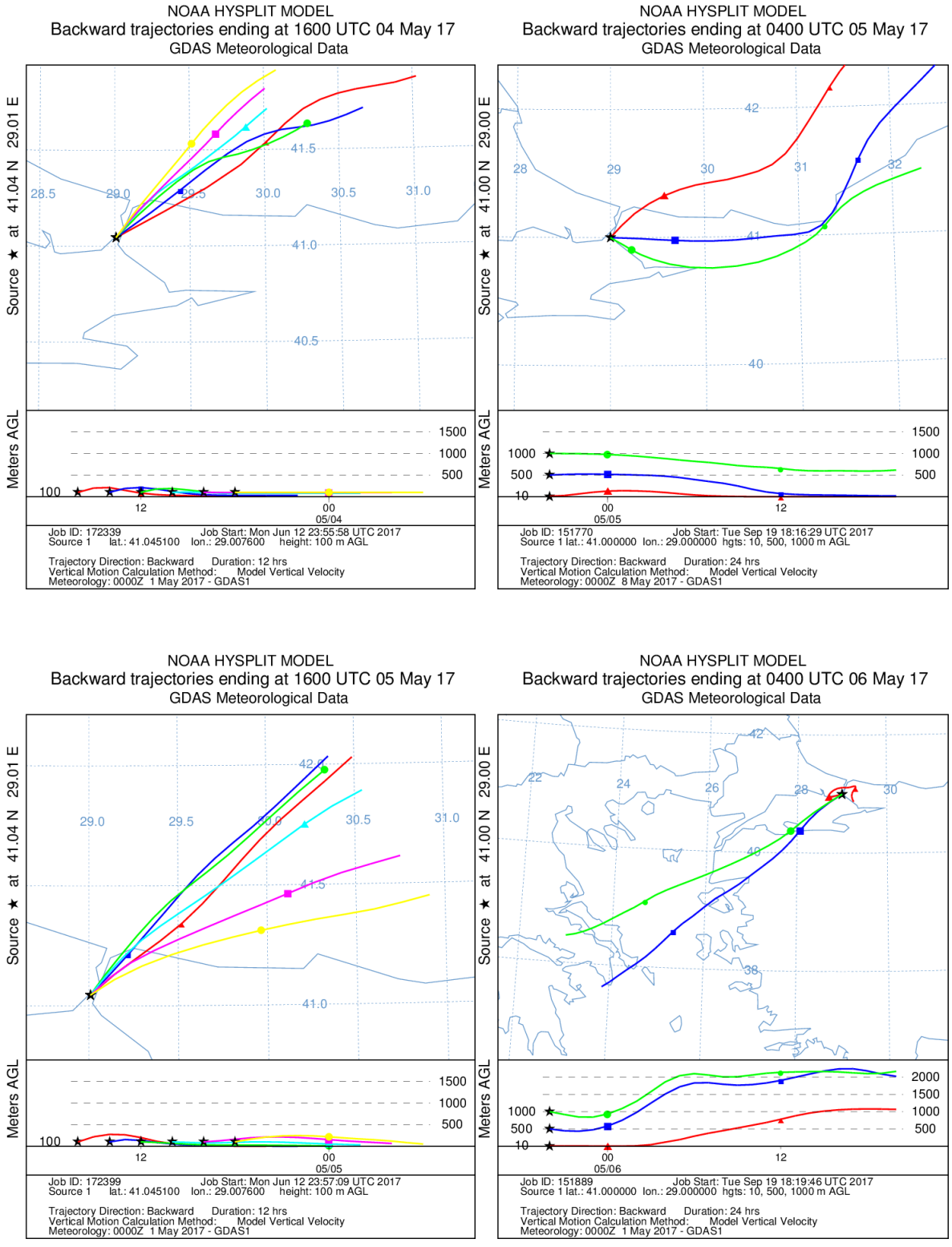


Two-hour air mass backward trajectories that correspond to daytime air samples (left) and 12-h air mass backward trajectories that correspond to nighttime air samples (right).

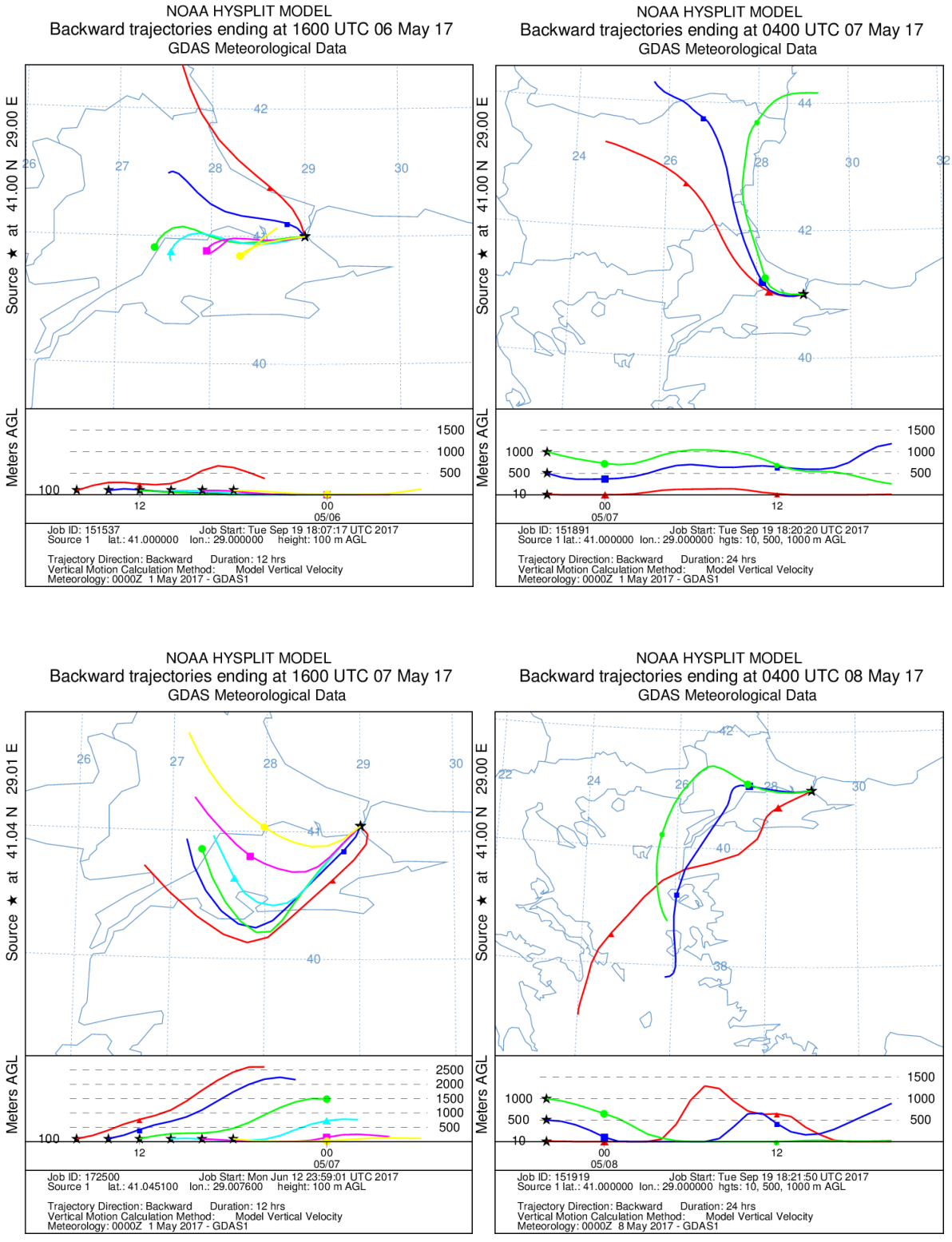


6.3

Two-hour air mass backward trajectories that correspond to daytime air samples (left) and 12-h air mass backward trajectories that correspond to nighttime air samples (right).

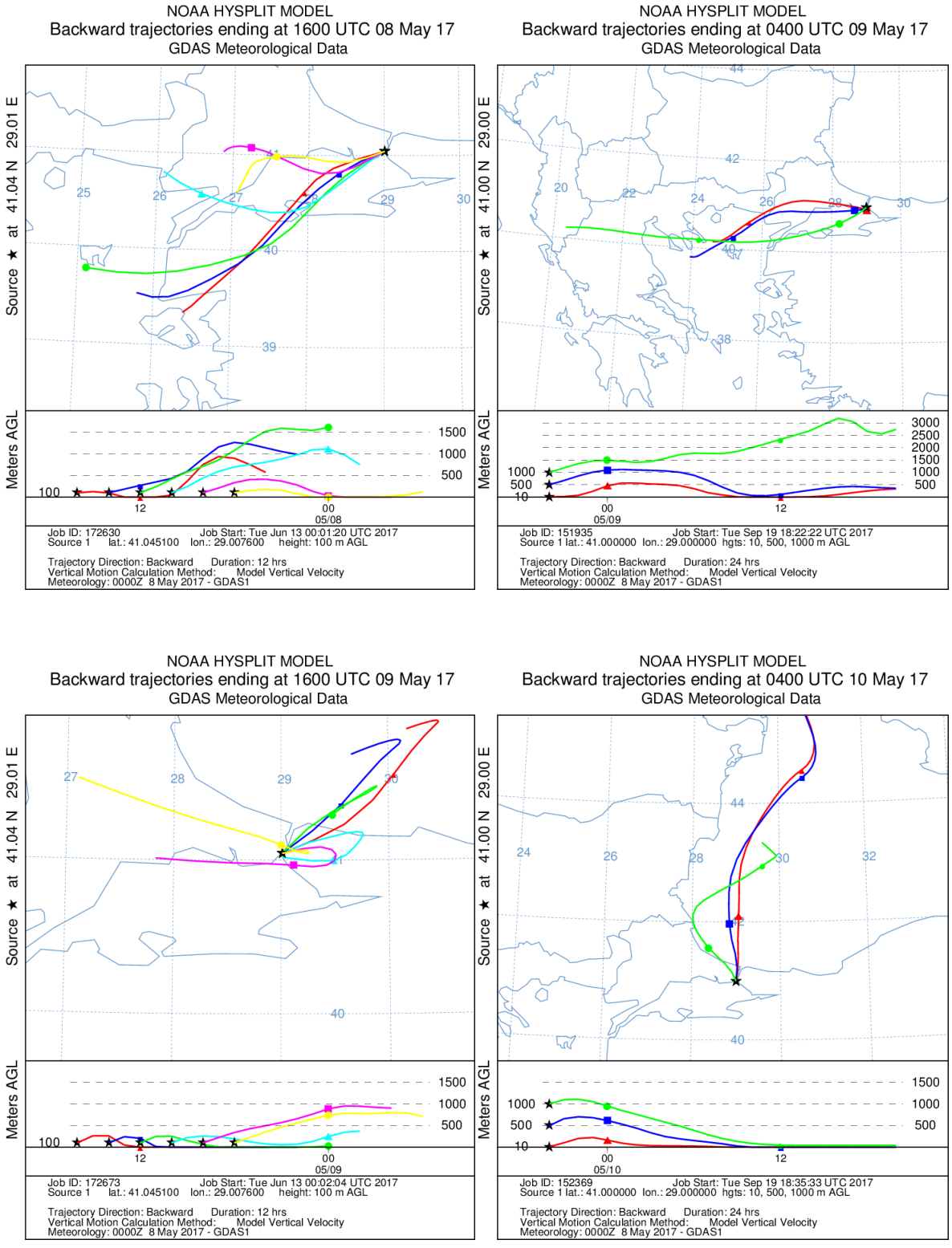


Two-hour air mass backward trajectories that correspond to daytime air samples (left) and 12-h air mass backward trajectories that correspond to nighttime air samples (right).

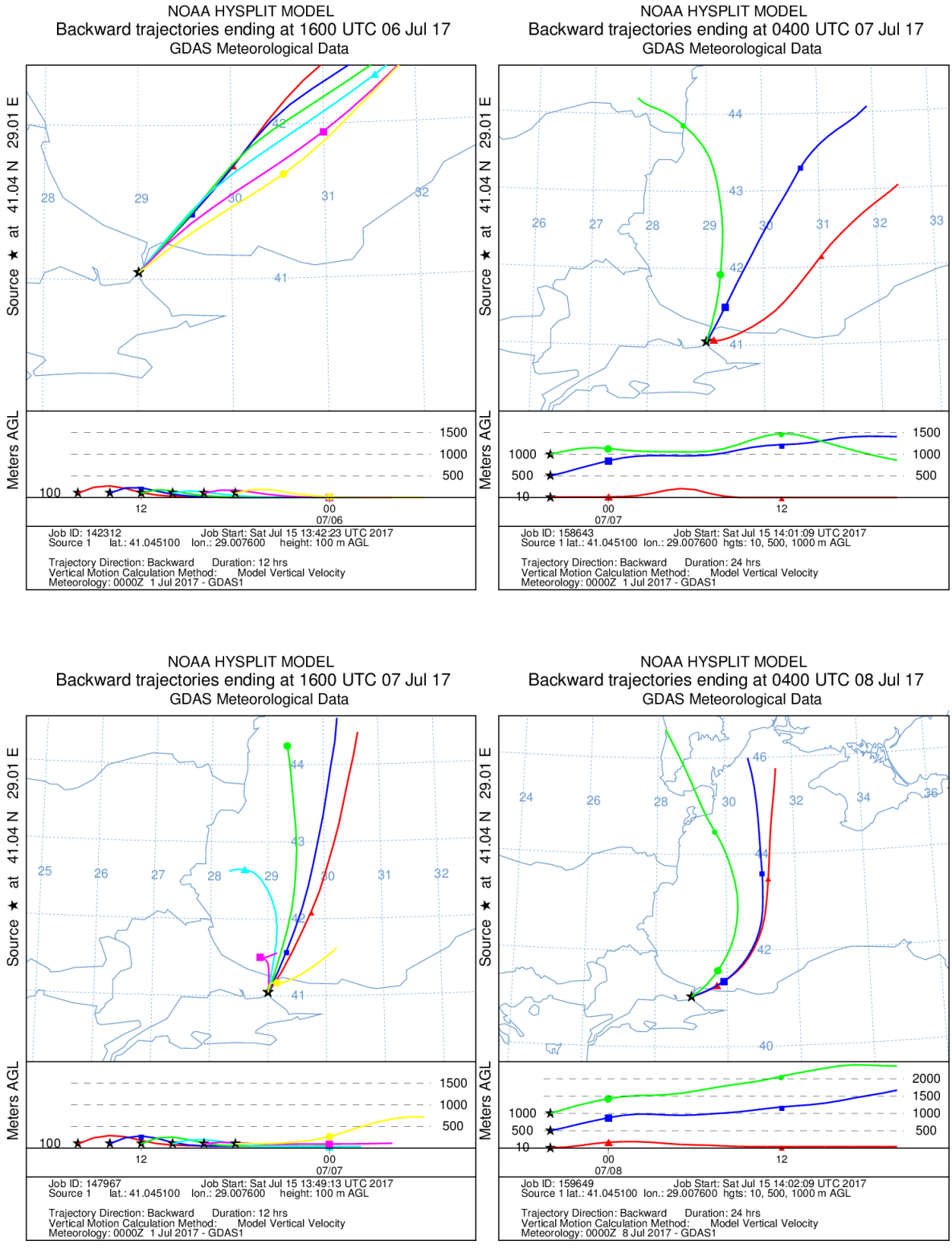


Two-hour air mass backward trajectories that correspond to daytime air samples (left) and 12-h air mass backward trajectories that correspond to nighttime air samples (right).

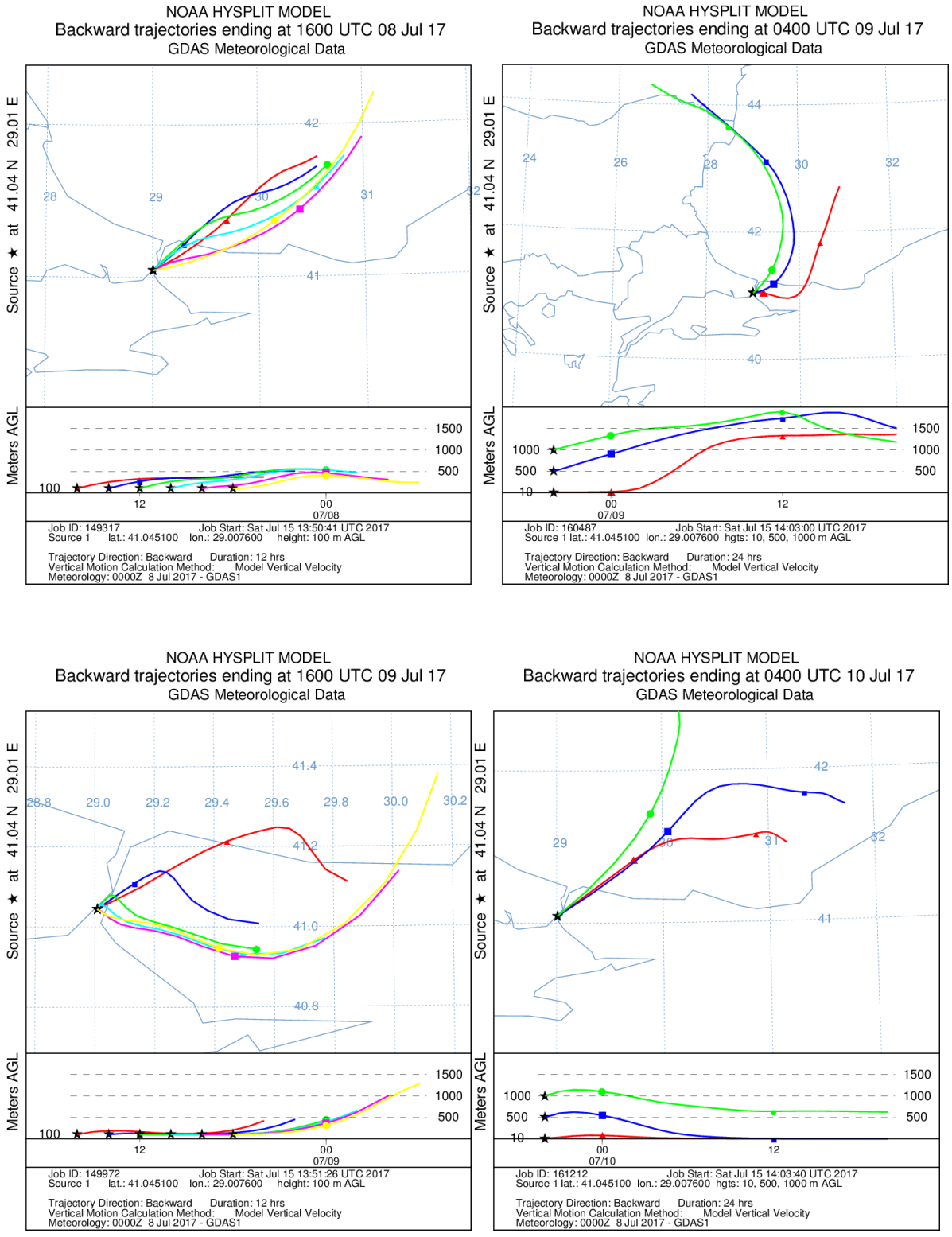


Two-hour air mass backward trajectories that correspond to daytime air samples (left) and 12-h air mass backward trajectories that correspond to nighttime air samples (right).

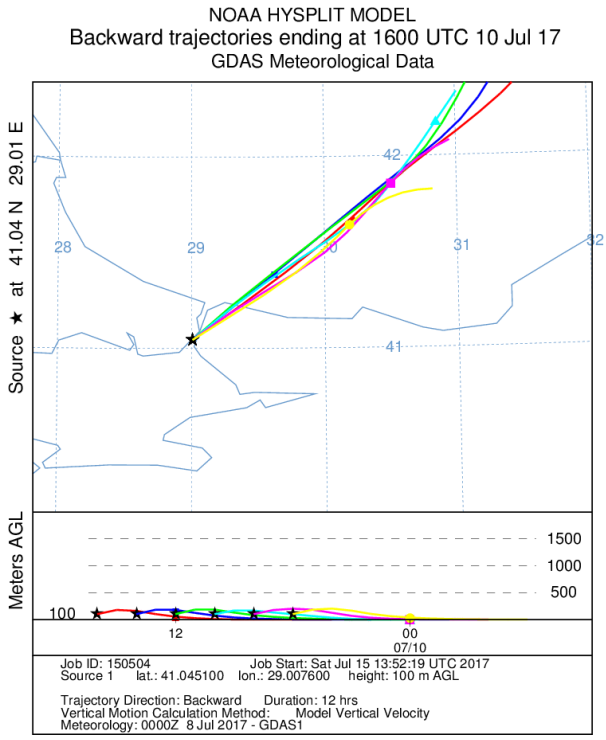


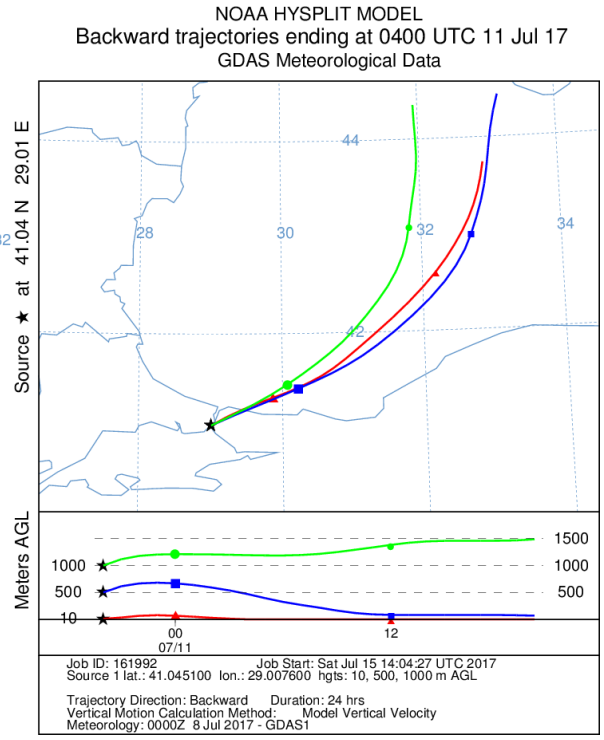


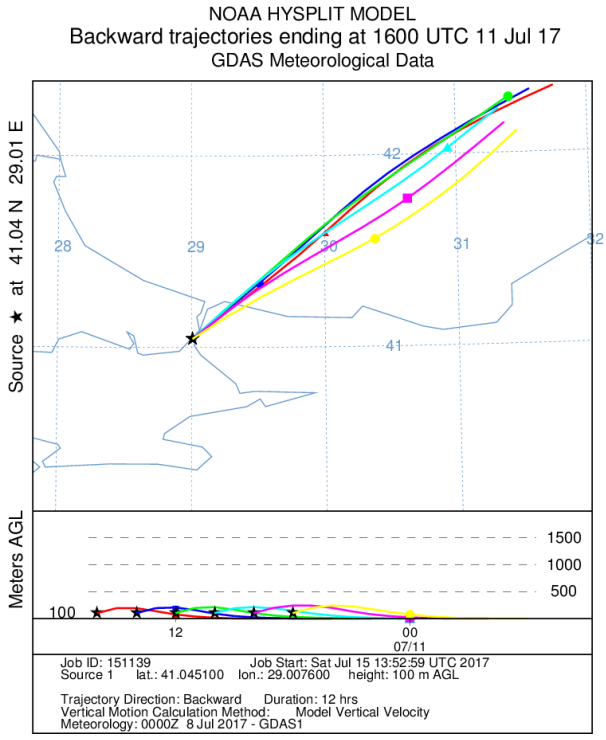


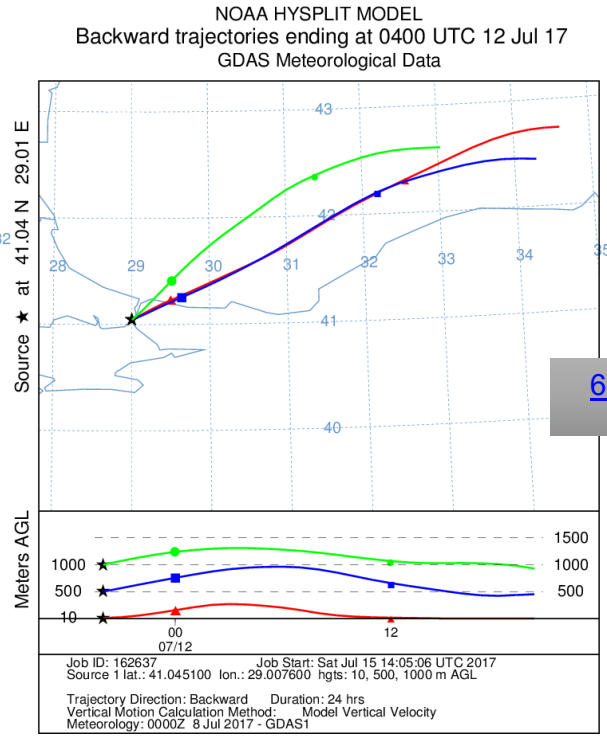


6.3

Two-hour air mass backward trajectories that correspond to daytime air samples (left) and 12-h air mass backward trajectories that correspond to nighttime air samples (right).

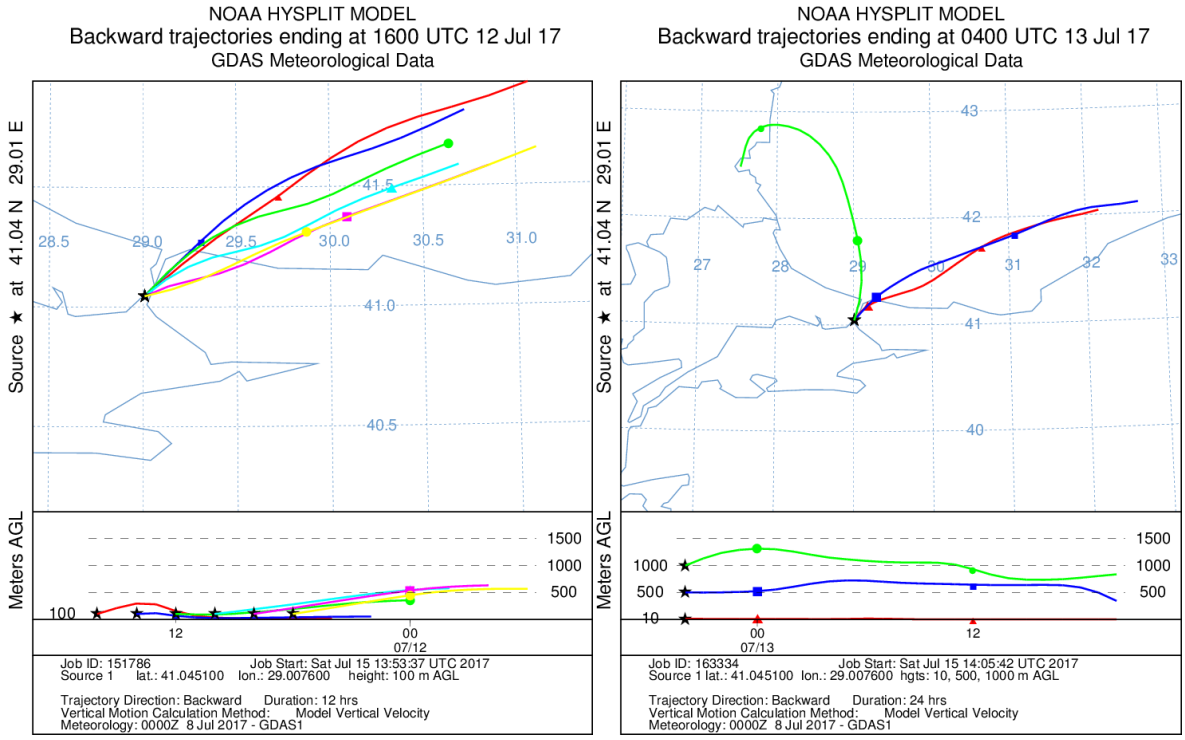


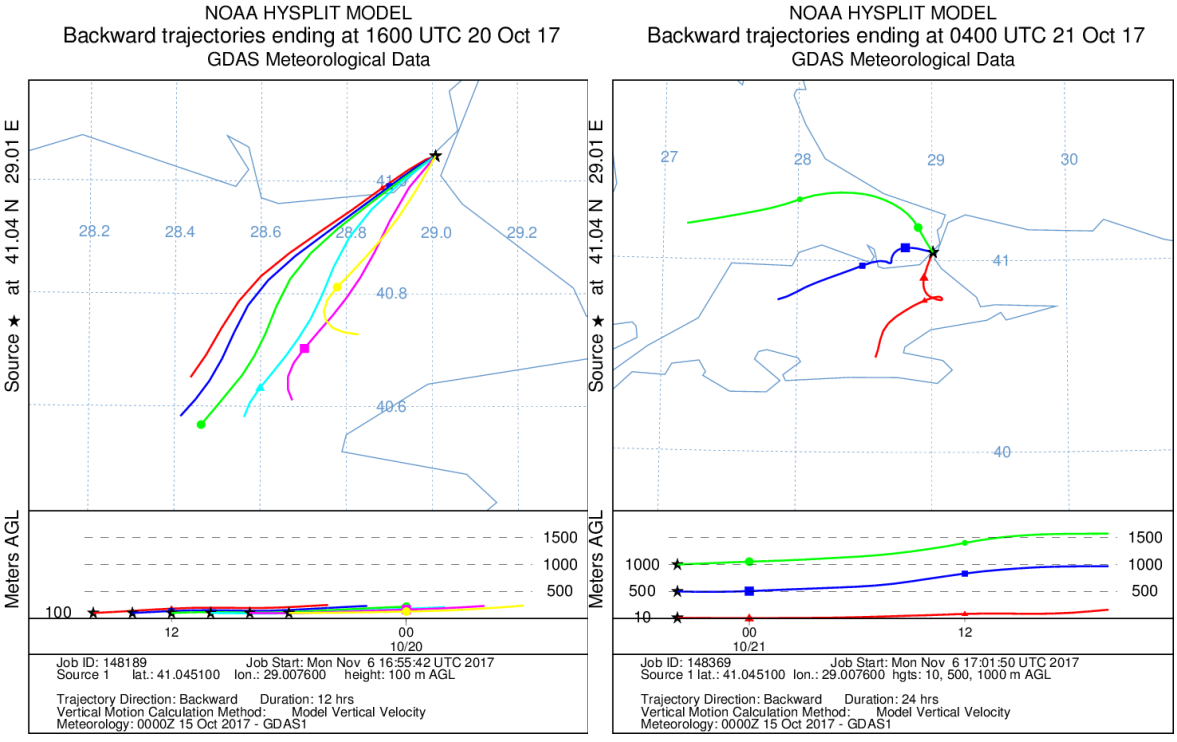


Two-hour air mass backward trajectories that correspond to daytime air samples (left) and 12-h air mass backward trajectories that correspond to nighttime air samples (right).

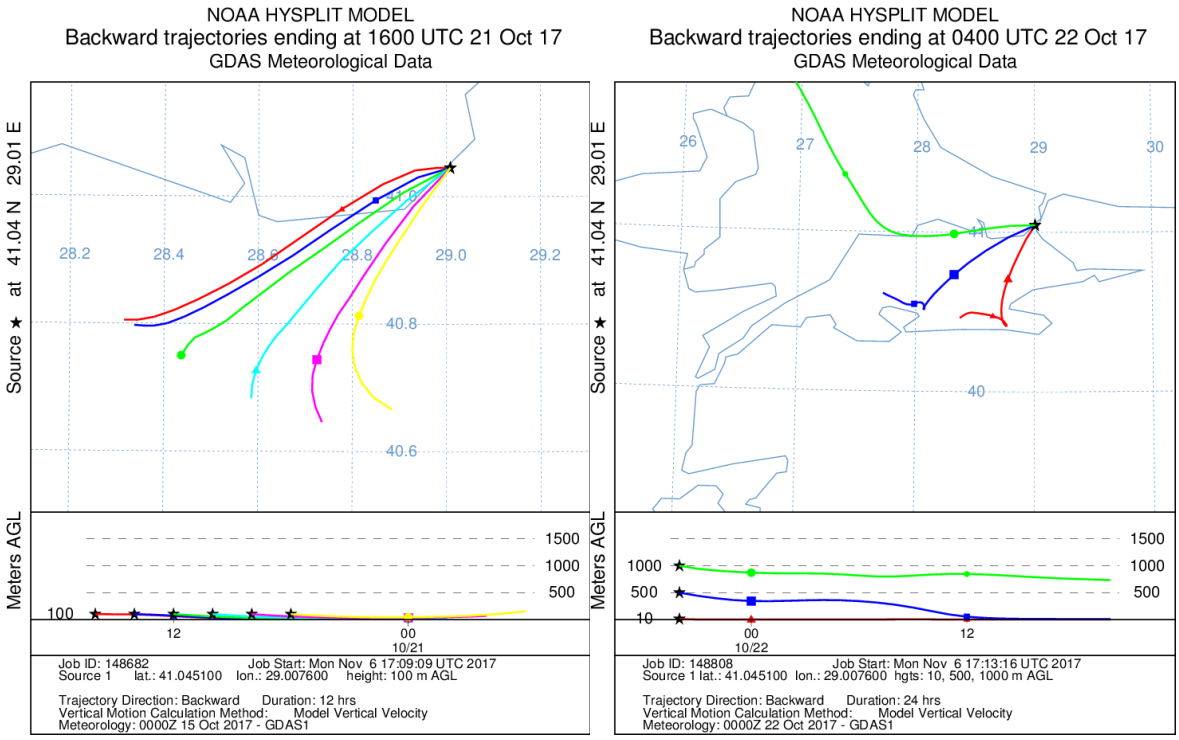


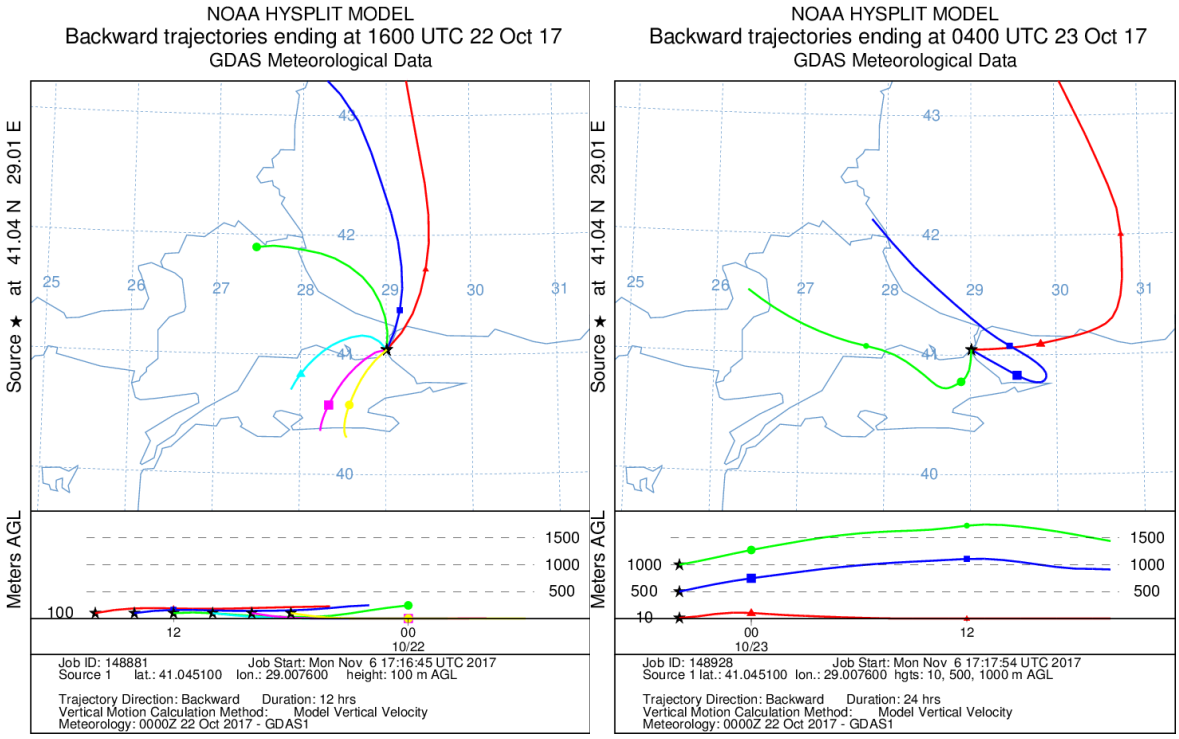


Two-hour air mass backward trajectories that correspond to daytime air samples (left) and 12-h air mass backward trajectories that correspond to nighttime air samples (right).

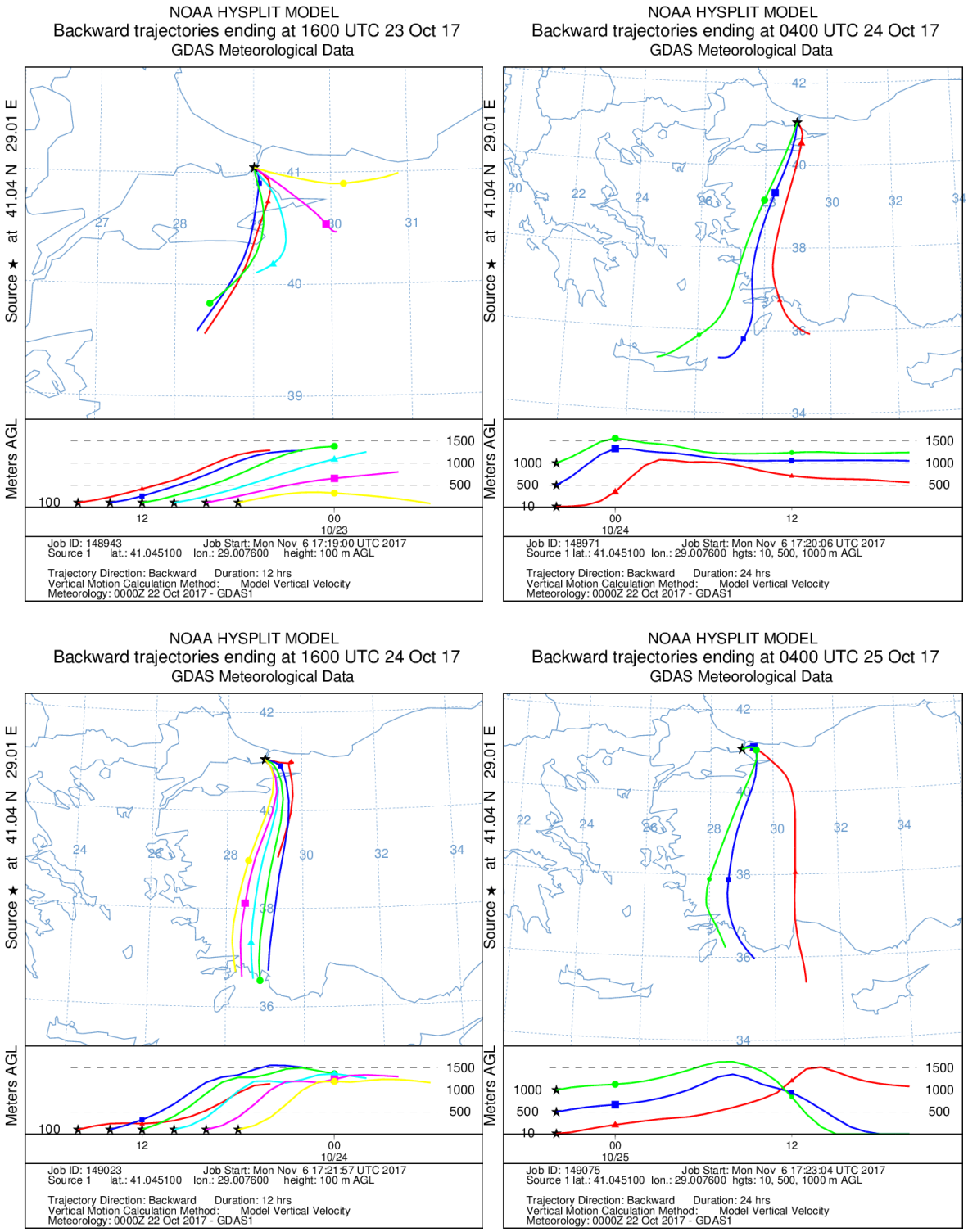


Two-hour air mass backward trajectories that correspond to daytime air samples (left) and 12-h air mass backward trajectories that correspond to nighttime air samples (right).

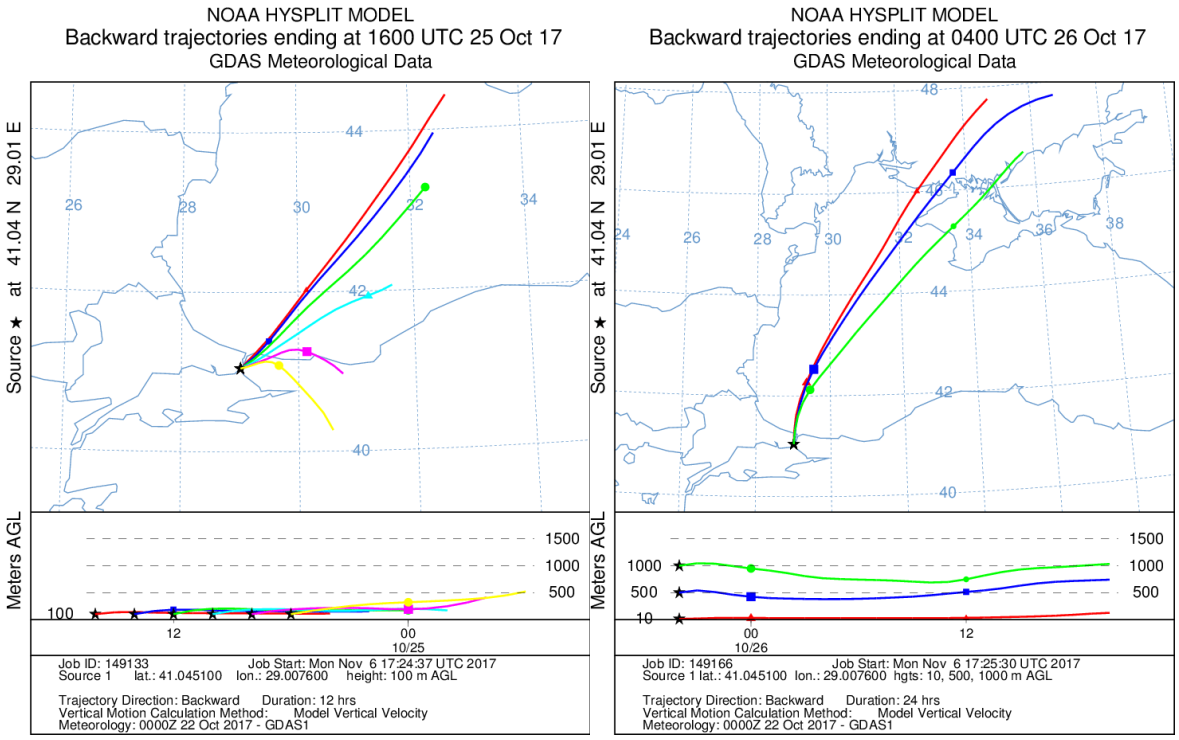


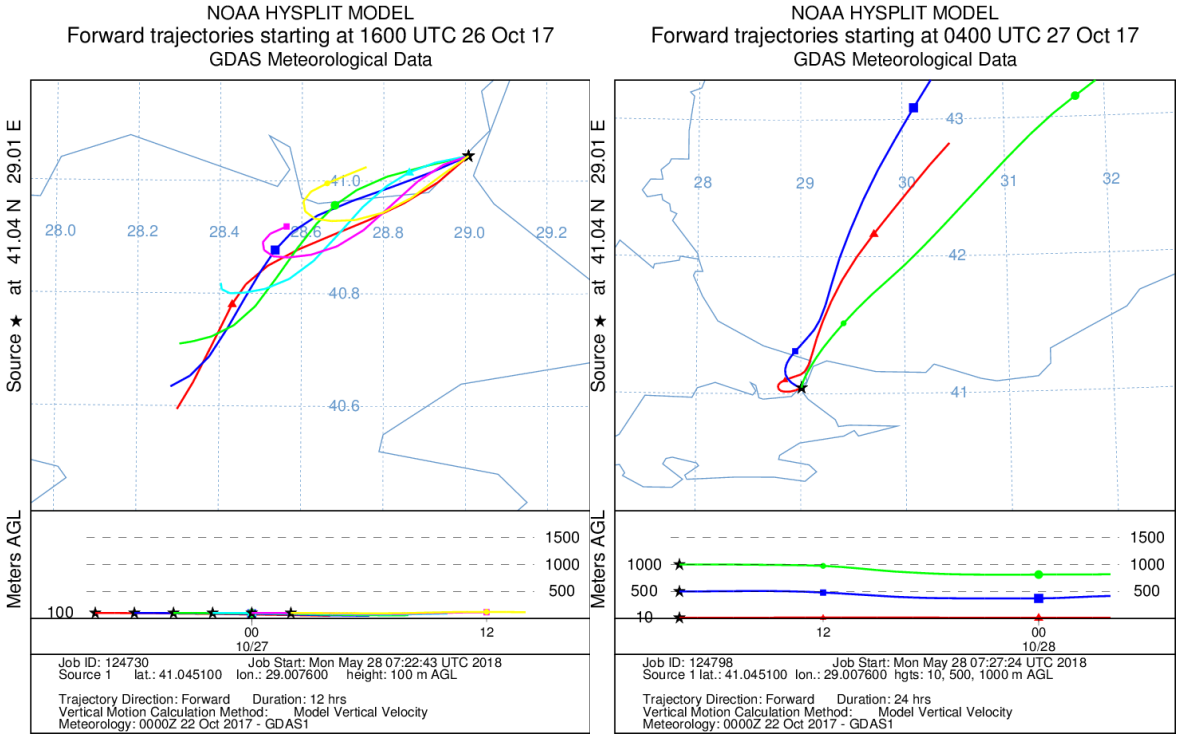


Two-hour air mass backward trajectories that correspond to daytime air samples (left) and 12-h air mass backward trajectories that correspond to nighttime air samples (right).

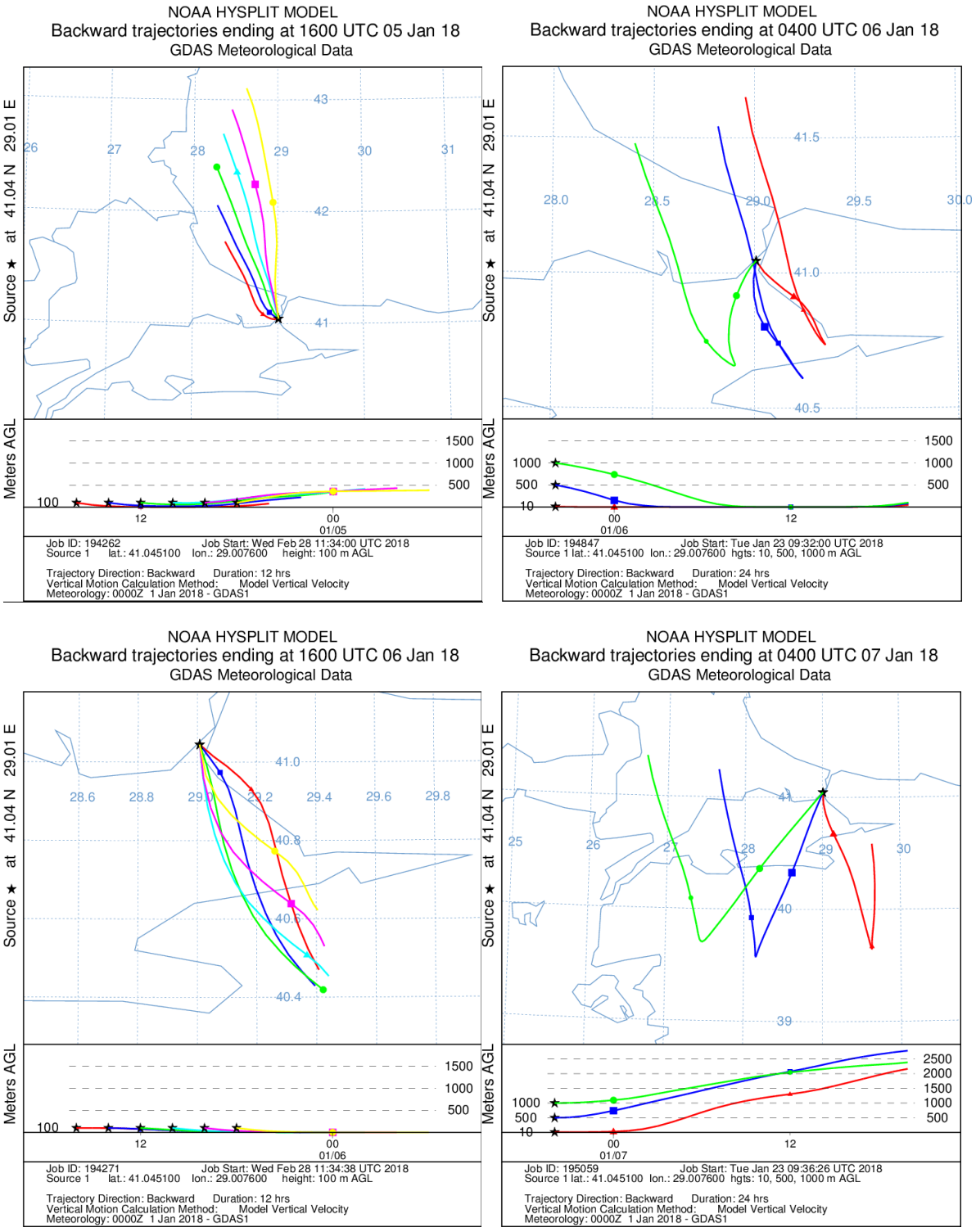


Two-hour air mass backward trajectories that correspond to daytime air samples (left) and 12-h air mass backward trajectories that correspond to nighttime air samples (right).

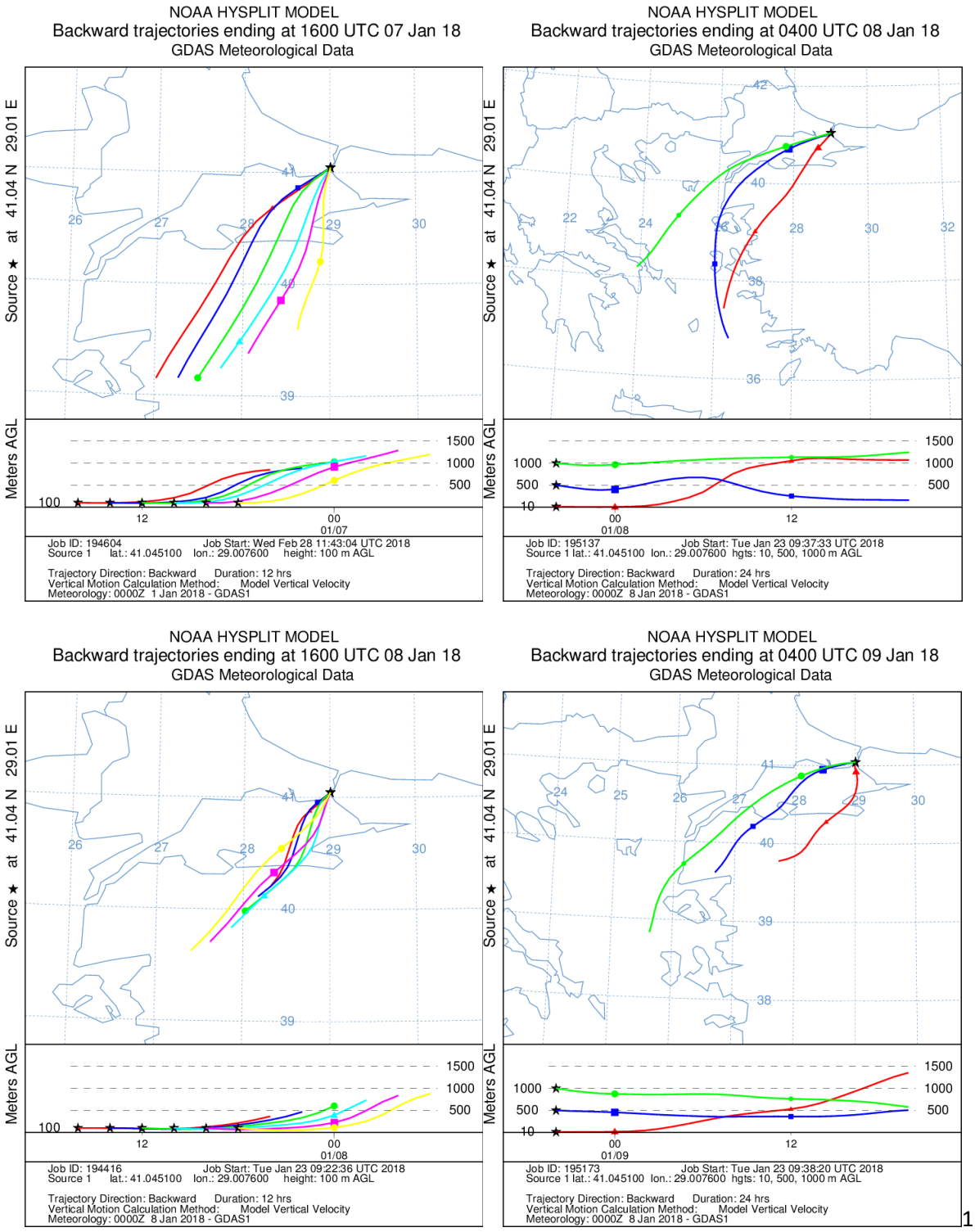


12

Two-hour air mass backward trajectories that correspond to daytime air samples (left) and 12-h air mass backward trajectories that correspond to nighttime air samples (right).

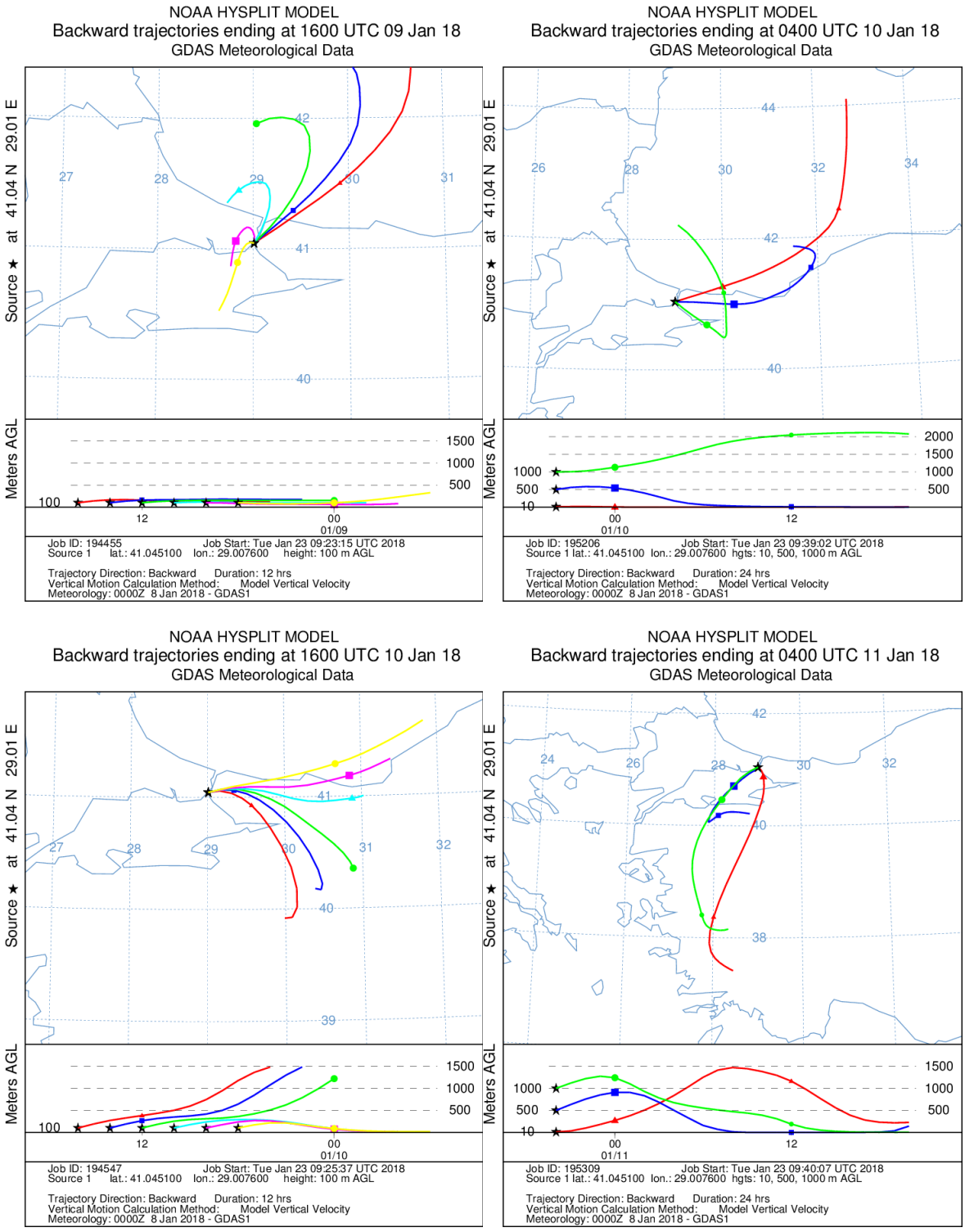


Two-hour air mass backward trajectories that correspond to daytime air samples (left) and 12-h air mass backward trajectories that correspond to nighttime air samples (right).

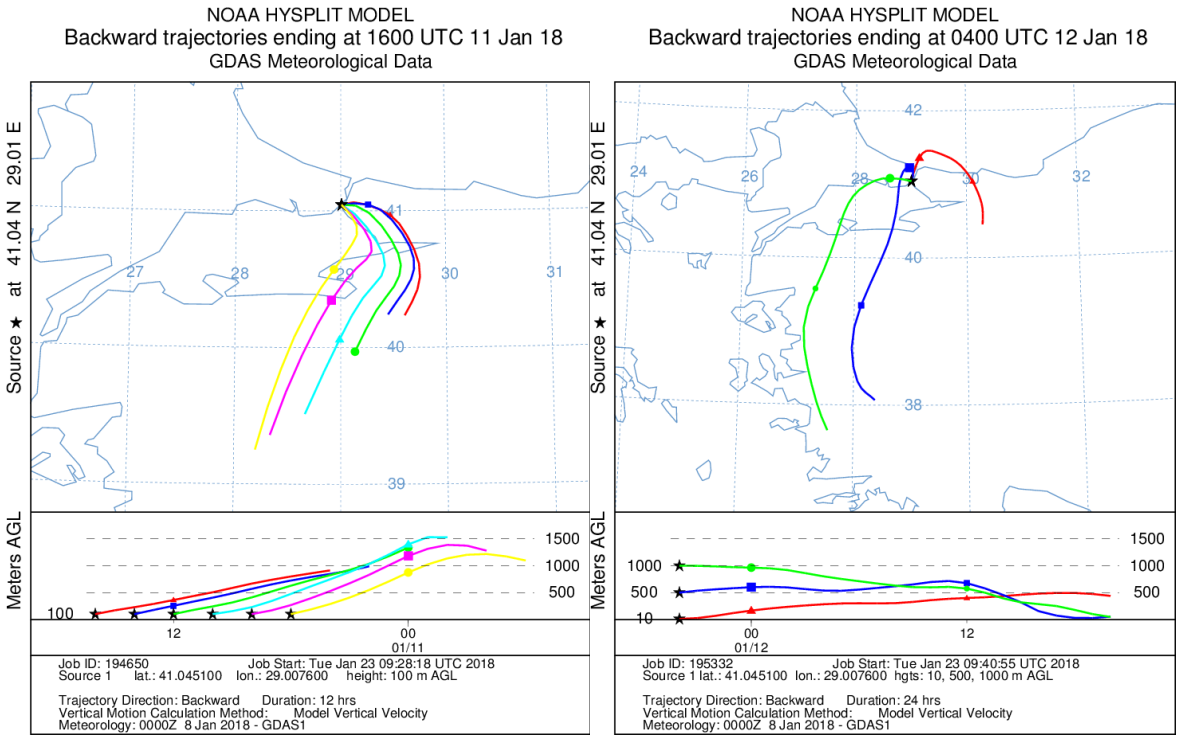


Two-hour air mass backward trajectories that correspond to daytime air samples (left) and 12-h air mass backward trajectories that correspond to nighttime air samples (right).

# *Appendix D*

## Solubilities (M) and properties of target analytes in three organic solvents

| Compound Name | Formula | MW | BP (°C) | DCM | iso-octane | Methanol |
|---|---|---|---|---|---|---|
| methyl-tert-butylether | $C_5H_{12}O$ | 88.148 | 55 | 10.748 | 2.407 | 4.223 |
| Benzene | $C_6H_6$ | 78.11 | 80.1 | 9.065 | 2.408 | 2.161 |
| Heptane | $C_7H_{16}$ | 100.2 | 98 | 9.921 | 11.946 | 1.284 |
| toluene | $C_7H_8$ | 92.138 | 110 | 14.226 | 3.834 | 2.645 |
| Octane | $C_8H_{18}$ | 114.23 | 125.7 | 13.575 | 16.834 | 1.356 |
| ethylbenzene | $C_8H_{10}$ | 106.17 | 135 | 18.523 | 5.273 | 2.758 |
| p-xylene | $C_8H_{10}$ | 106.17 | 138.4 | 16.785 | 4.541 | 2.513 |
| m-xylene | $C_8H_{10}$ | 106.17 | 139.3 | 16.825 | 4.594 | 2.532 |
| o-xylene | $C_8H_{10}$ | 106.17 | 144 | 17.083 | 4.220 | 2.502 |
| Nonane | $C_9H_{20}$ | 128.26 | 150.8 | 17.078 | 21.700 | 1.326 |
| 1,3,5-trimethylbenzene | $C_9H_{12}$ | 120.19 | 165 | 18.433 | 5.029 | 2.307 |
| 1,2,4-trimethylbenzene | $C_9H_{12}$ | 120.19 | 169 | 18.662 | 4.554 | 2.258 |
| Decane | $C_{10}H_{22}$ | 142.28 | 174 | 5,273.618 | 6,866.174 | 318.446 |
| 1,3-Diethylbenzol | $C_{10}H_{14}$ | 134.22 | 182 | 0.865 | 0.247 | 0.144 |
| Undecane | $C_{11}H_{24}$ | 156.31 | 195 | 69.469 | 92.677 | 3.262 |
| Dodecane | $C_{12}H_{26}$ | 170.33 | 216 | 127.983 | 174.918 | 4.681 |
| Naphthalene | $C_{10}H_8$ | 128.17 | 217 | 7.398 | 1.449 | 1.082 |
| naphthalene | $C_{10}H_8$ | 128.17 | 218 | 7.398 | 1.449 | 1.082 |
| Tridecane | $C_{13}H_{28}$ | 184.36 | 234 | 267.200 | 374.191 | 7.598 |
| Tetradecane | $C_{14}H_{30}$ | 198.39 | 250 | 584.145 | 838.208 | 12.916 |
| Hexacosane | $C_{26}H_{54}$ | 366.71 | 261 | 476,875,158.888 | 916,348,767.380 | 515,801.143 |
| Pentadecane | $C_{15}H_{32}$ | 212.41 | 267 | | | |
| Acenaphthene | $C_{12}H_{10}$ | 154.21 | 279.2 | 1.956 | 0.297 | 0.224 |
| Acenaphthylene | $C_{12}H_8$ | 152.19 | 280.2 | 0.452 | 0.035 | 0.04 |
| Hexadecane | $C_{16}H_{34}$ | 226.44 | 281 | 3,514.704 | 5,295.047 | 46.983 |
| Fluorene | $C_{13}H_{10}$ | 166.22 | 298.2 | 2.077 | 0.204 | 0.169 |
| Heptadecane | $C_{17}H_{36}$ | 240.47 | 302 | | | |
| Heneicosane | $C_{21}H_{44}$ | 296.57 | 306 | 783,986.709 | 1,334,027.554 | 2,978.422 |
| Octadecane | $C_{18}H_{38}$ | 254.49 | 316.3 | | | |

| Compound Name | Formula | MW | BP (°C) | DCM | iso-octane | Methanol |
|---|---|---|---|---|---|---|
| Nonadecane | $C_{19}H_{40}$ | 268.52 | 330 | | | |
| Phenanthrene | $C_{14}H_{10}$ | 178.23 | 336.2 | 1.417 | 0.098 | 0.079 |
| Anthracene | $C_{14}H_{10}$ | 178.23 | 340.2 | 0.938 | 0.051 | 0.058 |
| Eicosane | $C_{20}H_{42}$ | 282.55 | 343.2 | 231,539.291 | 384,508.372 | 1,131.299 |
| Docosane | $C_{22}H_{46}$ | 310.6 | 368.8 | 2,689,482.359 | 4,688,401.541 | 7,958.776 |
| Fluoranthene | $C_{16}H_{10}$ | 202.25 | 375 | 0.467 | 0.023 | 0.030 |
| Tricosane | $C_{23}H_{48}$ | 324.63 | 380.2 | 9,535,702.648 | 17,032,711.876 | 21,940.944 |
| Tetracosane | $C_{24}H_{50}$ | 338.65 | 391 | 34,596,861.262 | 63,320,276.117 | 61,896.245 |
| Pyrene | $C_{16}H_{10}$ | 202.25 | 393 | 0.085 | 0.006 | 0.007 |
| Pentacosane | $C_{25}H_{52}$ | 352.68 | 402.1 | 131,437,926.722 | 246,491,416.180 | 182,840.879 |
| Octacosane | $C_{28}H_{58}$ | 394.76 | 431.8 | 7,375,181,286.375 | 14,879,173,228.208 | 4,822,811.635 |
| Benz[a]anthracene | $C_{18}H_{12}$ | 228.29 | 437.8 | 0.141 | 0.005 | 0.006 |
| Nonacosane | $C_{29}H_{60}$ | 408.79 | 441 | | | |
| Chrysene | $C_{18}H_{12}$ | 228.29 | 448.2 | 0.113 | 0.004 | 0.005 |
| Triacontane | $C_{30}H_{62}$ | 422.81 | 450 | | | |
| Dotriacontane | $C_{32}H_{66}$ | 450.87 | 467.2 | 1,871,477,887,232.825 | 4,161,173,269,418.304 | 448,112,749.048 |
| Benzo[k]fluoranthene | $C_{20}H_{12}$ | 252.31 | 480.2 | 0.475 | 0.011 | 0.013 |
| Pentatriacontane | $C_{35}H_{72}$ | 492.95 | 490.2 | | | |
| Benzo[a]pyrene | $C_{20}H_{12}$ | 252.31 | 495.2 | 0.089 | 0.002 | 0.003 |
| Hexatriacontane | $C_{36}H_{74}$ | 506.97 | 497 | 490,818,247,013,165.188 | 1,202,961,698,741,938.000 | 42,955,947,211.231 |
| Benzo[ghi]perylene | $C_{22}H_{12}$ | 276.33 | 500 | 0.099 | 0.004 | 0.004 |
| Nonatriacontane | $C_{39}H_{80}$ | 549.05 | 517.5 | | | |
| Dibenz[a,h]anthracene | $C_{22}H_{14}$ | 278.35 | 524.2 | 0.216 | 0.006 | 0.006 |
| Indeno[1,2,3-cd]pyrene | $C_{22}H_{12}$ | 276.33 | 164 (Melting) | | | |
| Benzo[b]fluoranthene | $C_{20}H_{12}$ | 252.31 | 166 (Melting) | 0.267 | 0.007 | 0.009 |
| Heptacosane | $C_{27}H_{56}$ | 380.73 | 59 (Melting) | 1,853,910,226.073 | 3,650,226,385.061 | 1,559,162.210 |
| Hentriacontane | $C_{31}H_{64}$ | 436.84 | 66 (Melting) | | | |
| Tritriacontane | $C_{33}H_{68}$ | 464.89 | 72 (Melting) | | | |
| Tetratriacontane | $C_{34}H_{70}$ | 478.92 | 73 (Melting) | | | |

| Compound Name | Formula | MW | BP (°C) | DCM | iso-octane | Methanol |
|---|---|---|---|---|---|---|
| Heptatriacontane | $C_{37}H_{76}$ | 521 | 77 (Melting) | | | |
| Octatriacontane | $C_{38}H_{78}$ | 535.03 | 79 (Melting) | | | |
| Tetracontane | $C_{40}H_{82}$ | 563.08 | 81 (Melting) | | | |

# *Appendix E*

Calibration curves of PAH and n-alkanes

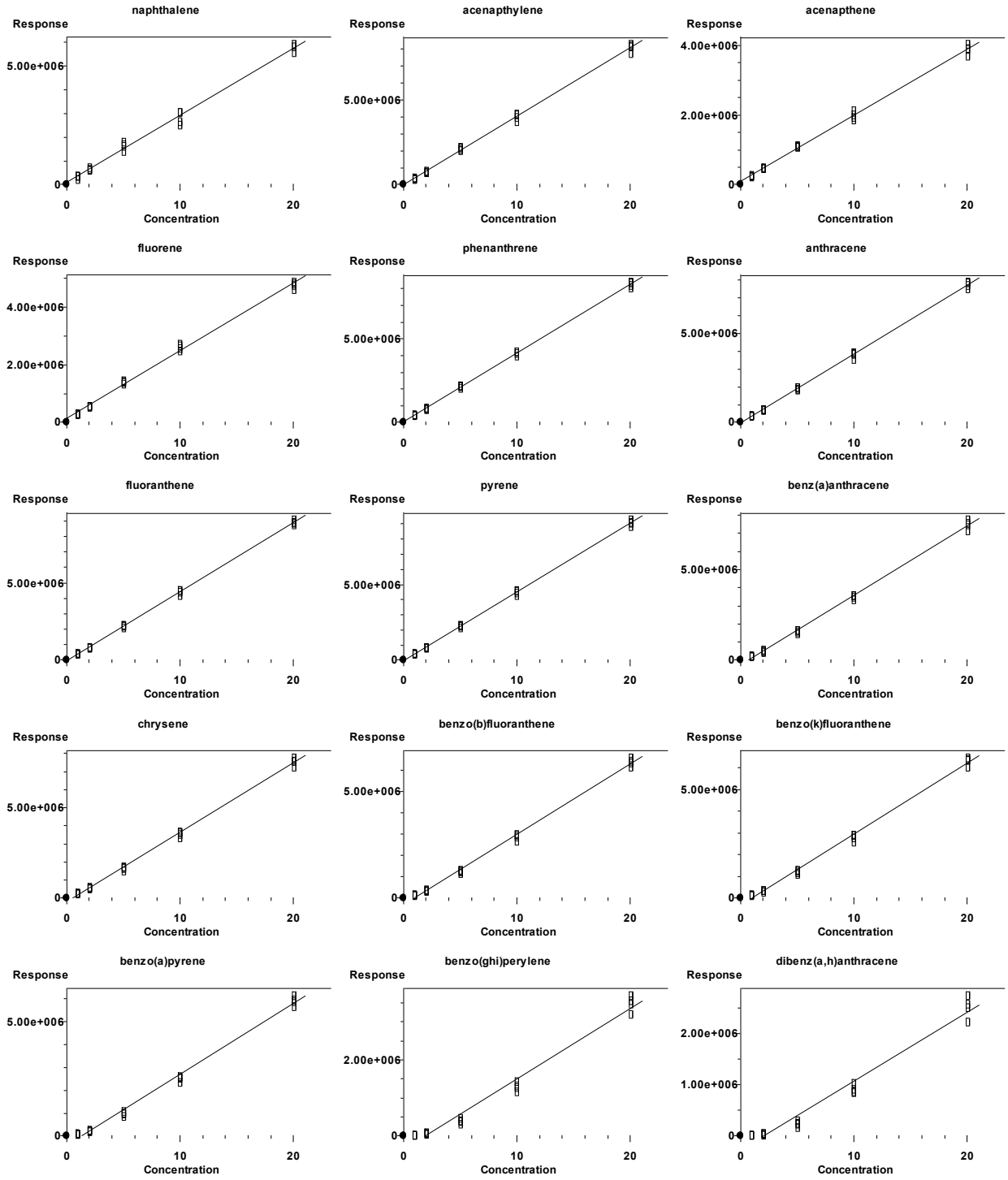

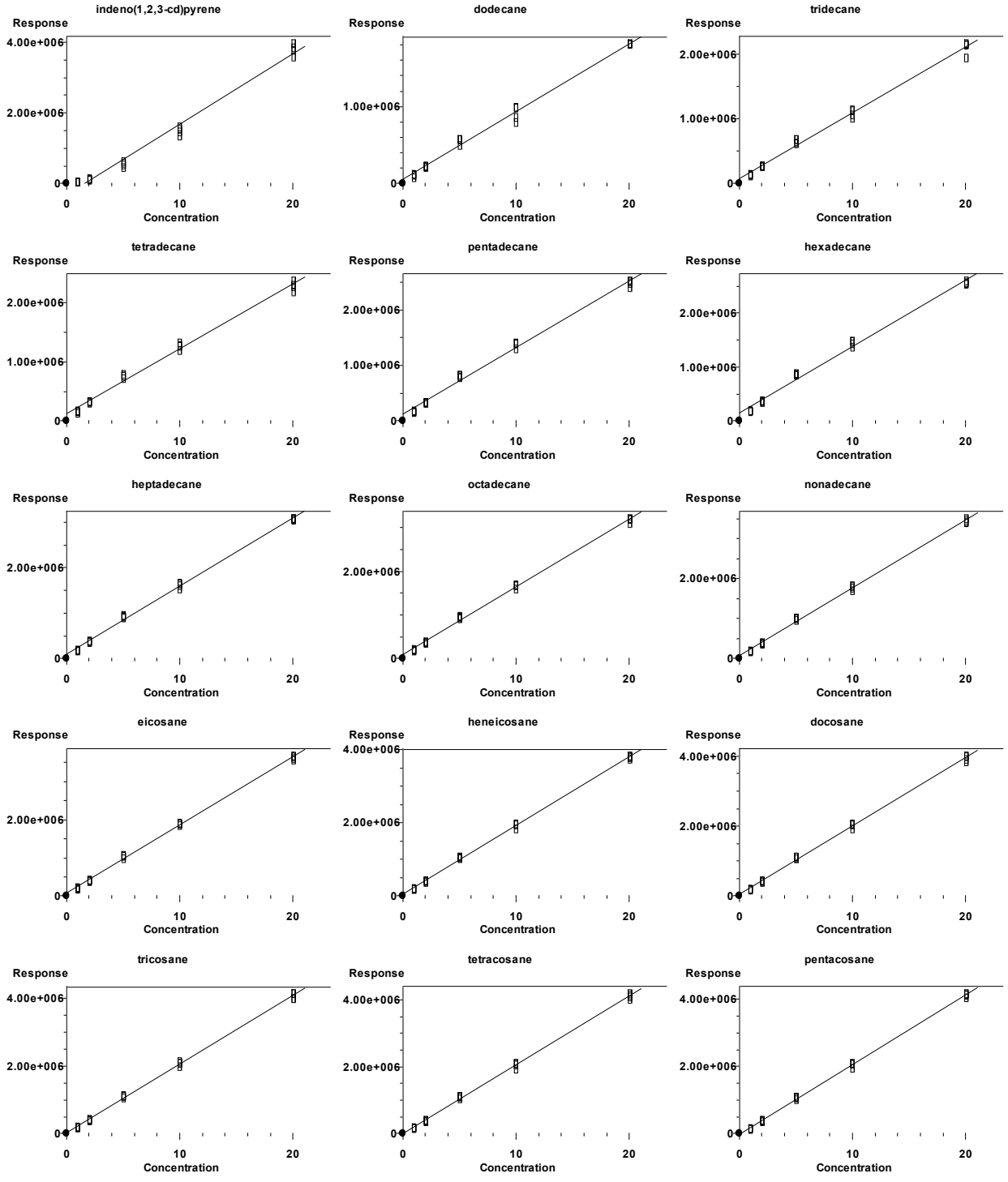
indeno(1,2,3-cd)pyrene
dodecane
tridecane
tetradecane
pentadecane
hexadecane
heptadecane
octadecane
nonadecane
eicosane
heneicosane
docosane
tricosane
tetracosane
pentacosane
Response
Concentration
0
10
20
2.00e+006
4.00e+006
1.00e+006

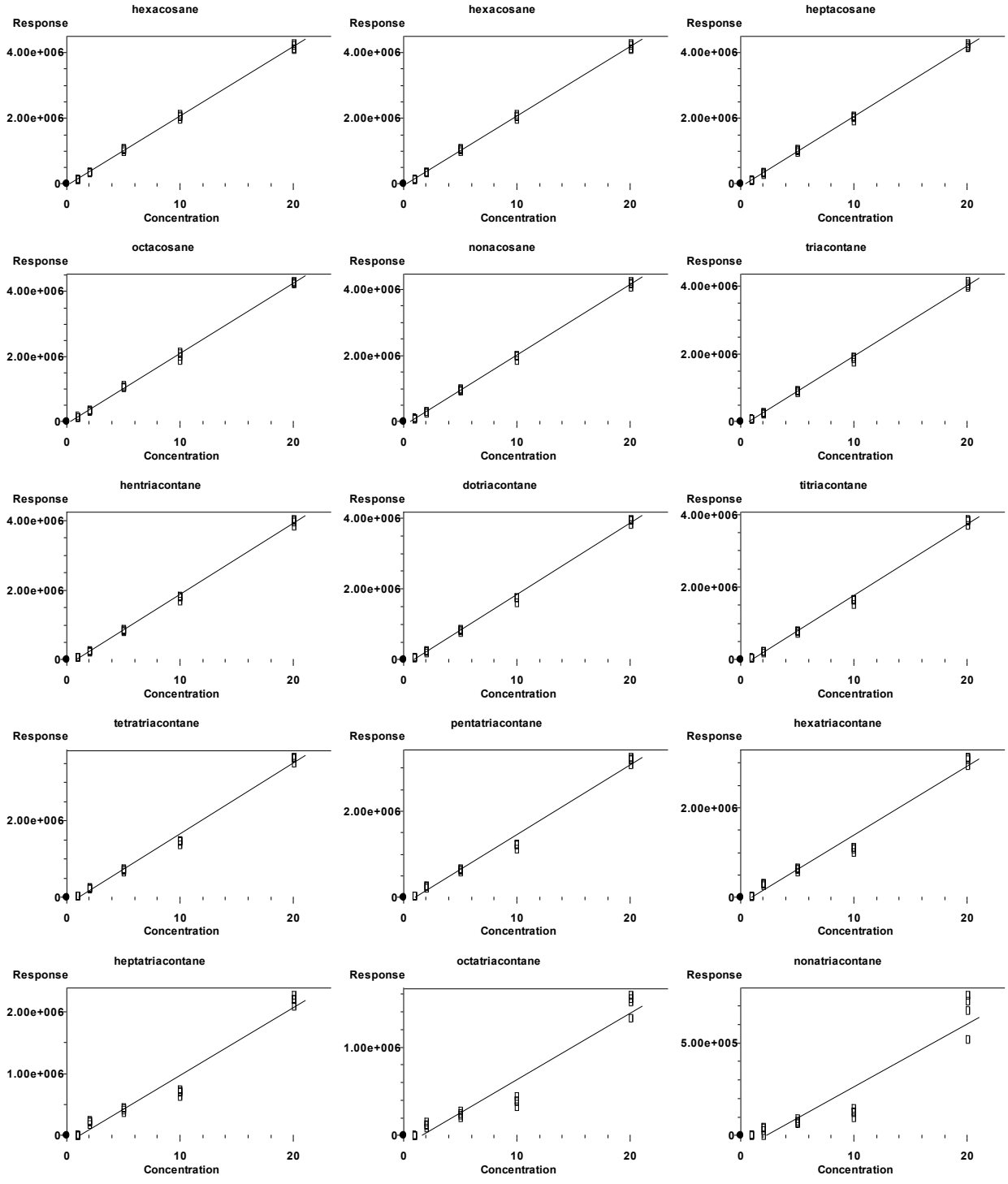
hexacosane
Response
4.00e+006
2.00e+006
0
0
10
20
Concentration
hexacosane
Response
4.00e+006
2.00e+006
0
0
10
20
Concentration
heptacosane
Response
4.00e+006
2.00e+006
0
0
10
20
Concentration
octacosane
Response
4.00e+006
2.00e+006
0
0
10
20
Concentration
nonacosane
Response
4.00e+006
2.00e+006
0
0
10
20
Concentration
triacontane
Response
4.00e+006
2.00e+006
0
0
10
20
Concentration
hentriacontane
Response
4.00e+006
2.00e+006
0
0
10
20
Concentration
dotriacontane
Response
4.00e+006
2.00e+006
0
0
10
20
Concentration
titriacontane
Response
4.00e+006
2.00e+006
0
0
10
20
Concentration
tetratriacontane
Response
2.00e+006
0
0
10
20
Concentration
pentatriacontane
Response
2.00e+006
0
0
10
20
Concentration
hexatriacontane
Response
2.00e+006
0
0
10
20
Concentration
heptatriacontane
Response
2.00e+006
1.00e+006
0
0
10
20
Concentration
octatriacontane
Response
1.00e+006
0
0
10
20
Concentration
nonatriacontane
Response
5.00e+005
0
0
10
20
Concentration

## *Appendix F*

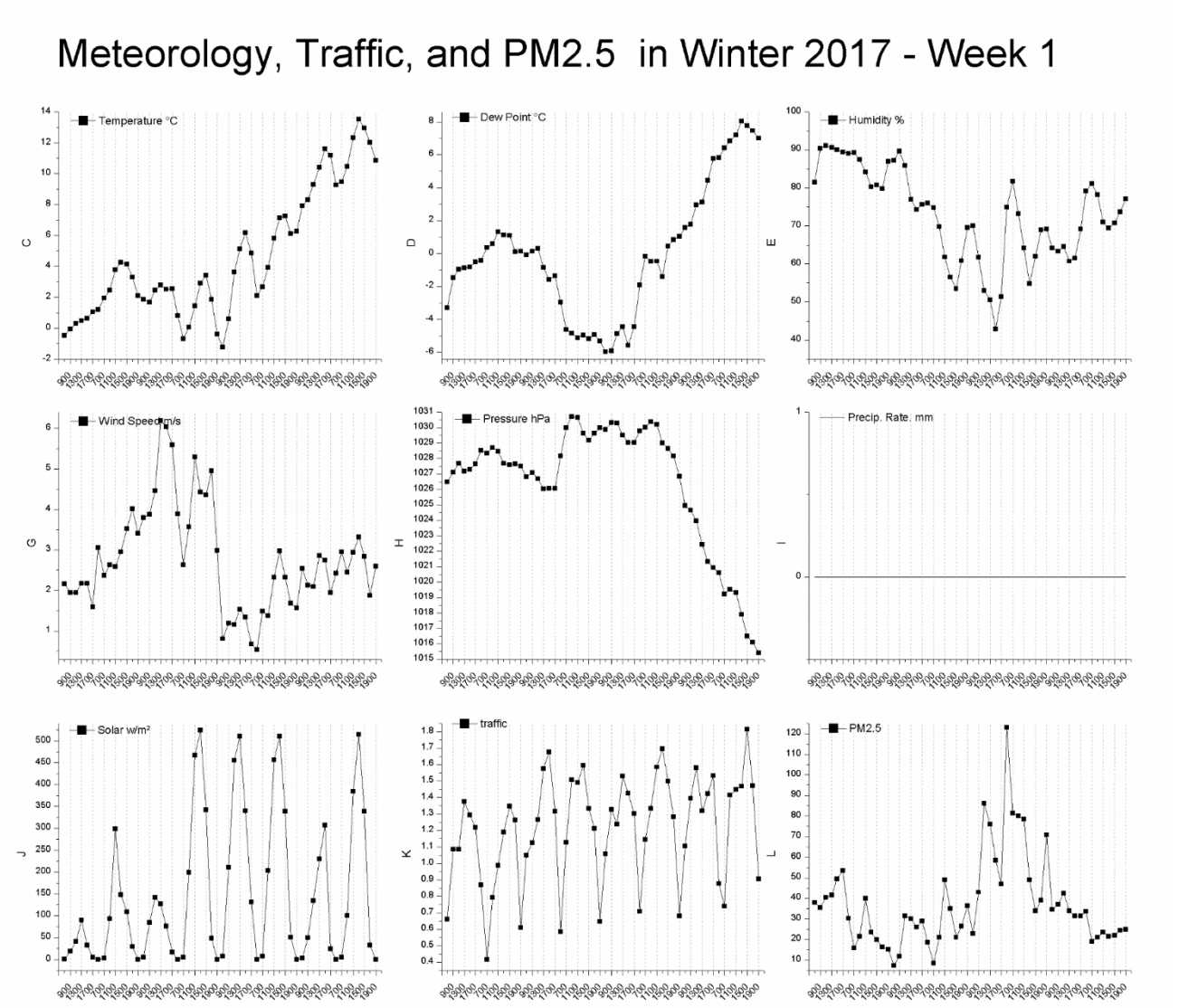
Meteorology, Traffic, and PM2.5 in Winter 2017 - Week 1
Temperature °C
Dew Point °C
Humidity %
Wind Speed m/s
Pressure hPa
Precip. Rate. mm
Solar w/m²
traffic
PM2.5

# Meteorology, Traffic, and PM2.5 in Winter 2017 - Week 2

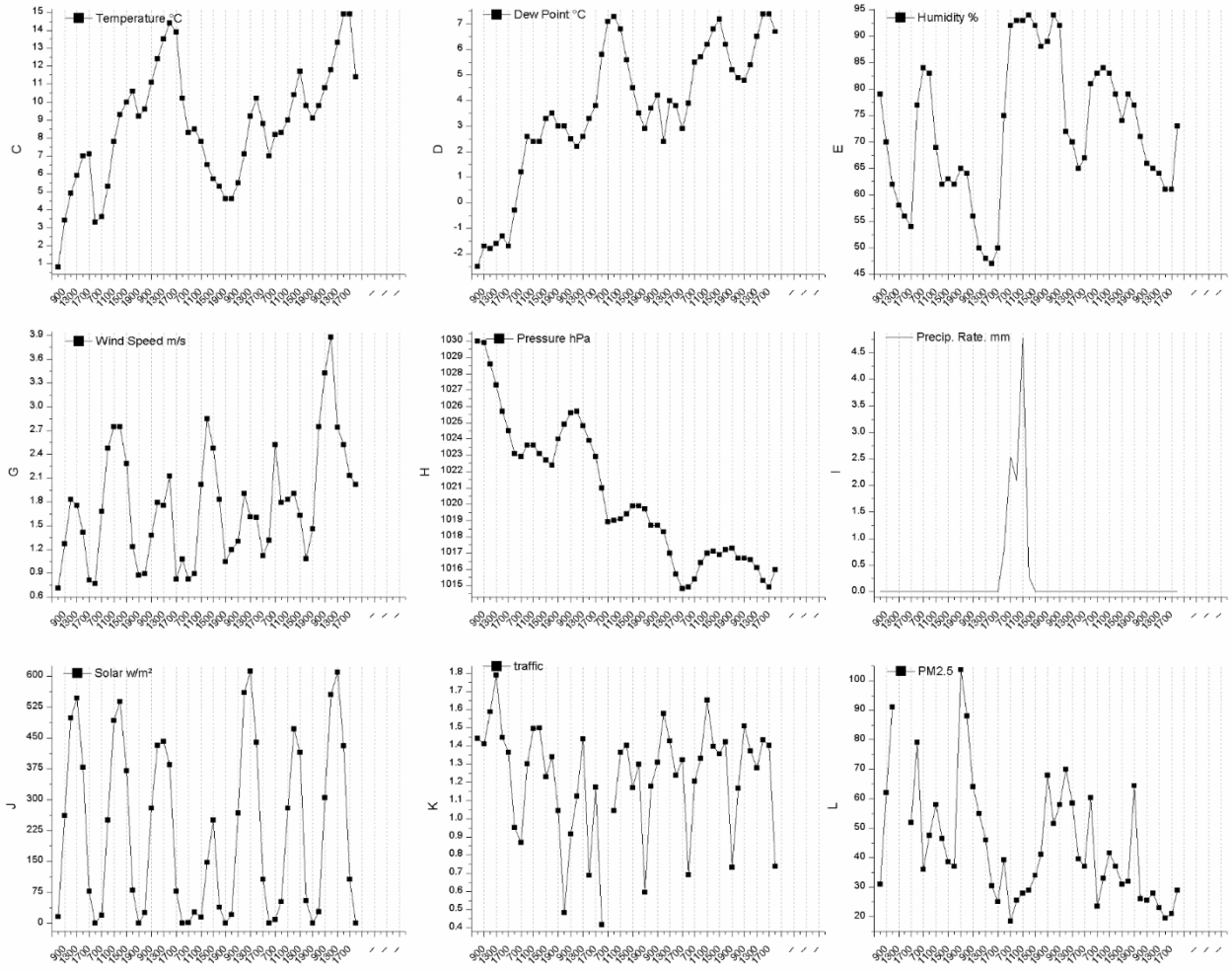

# Meteorology, Traffic, and PM2.5 in Spring 2017 - Week 3

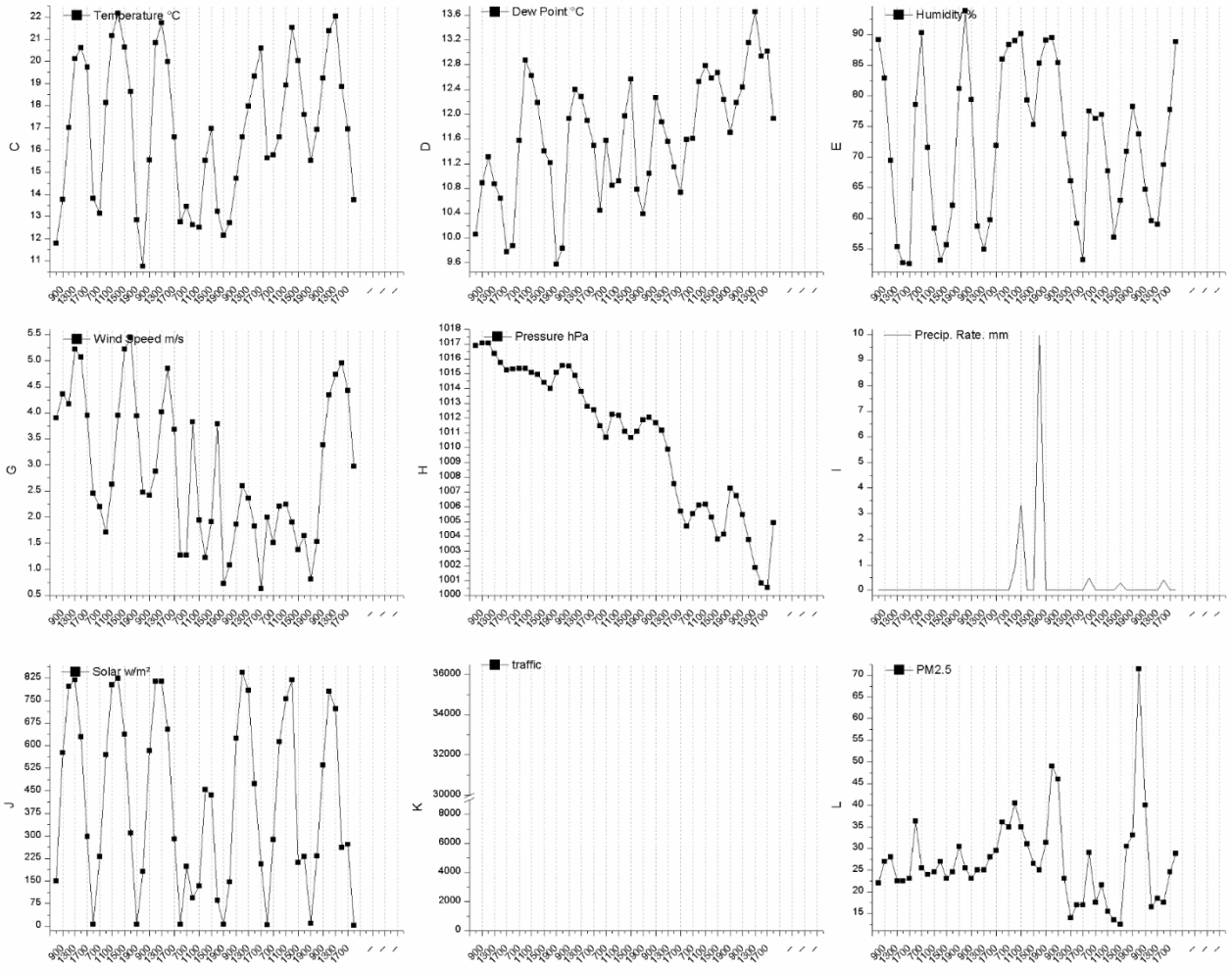

# Meteorology, Traffic, and PM2.5 in Summer 2017 - Week 4

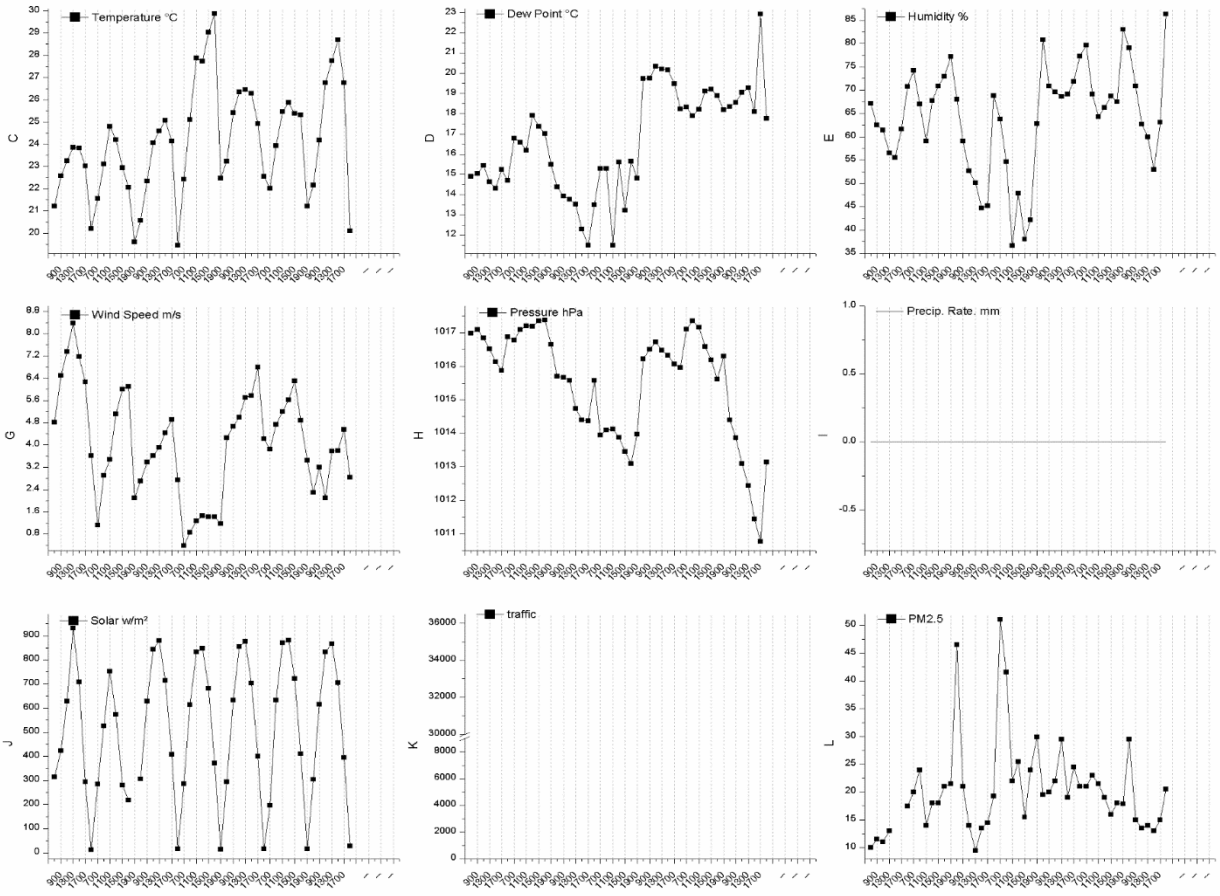

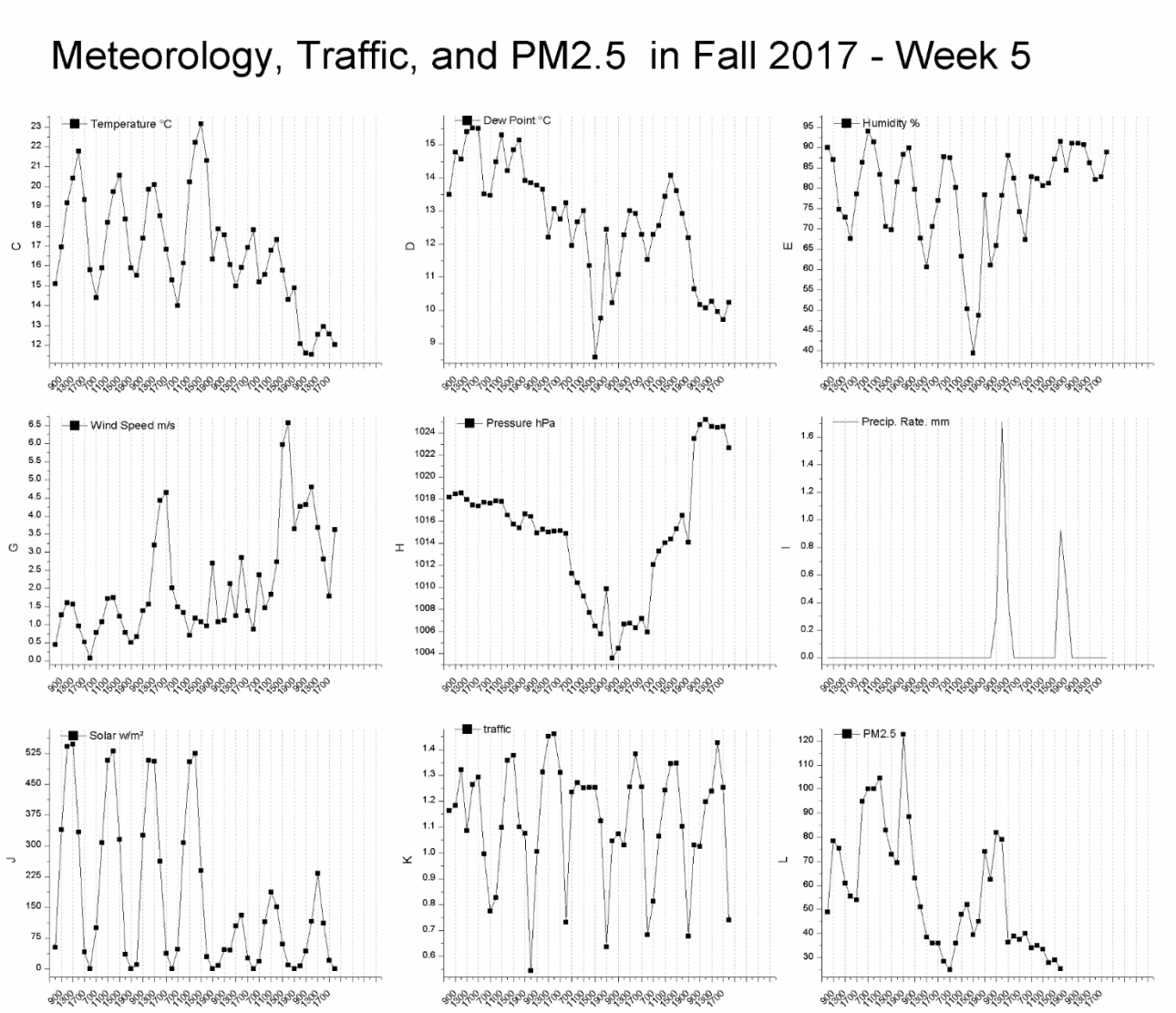
Meteorology, Traffic, and PM2.5 in Fall 2017 - Week 5
Temperature °C
Dew Point °C
Humidity %
Wind Speed m/s
Pressure hPa
Precip. Rate. mm
Solar w/m²
traffic
PM2.5

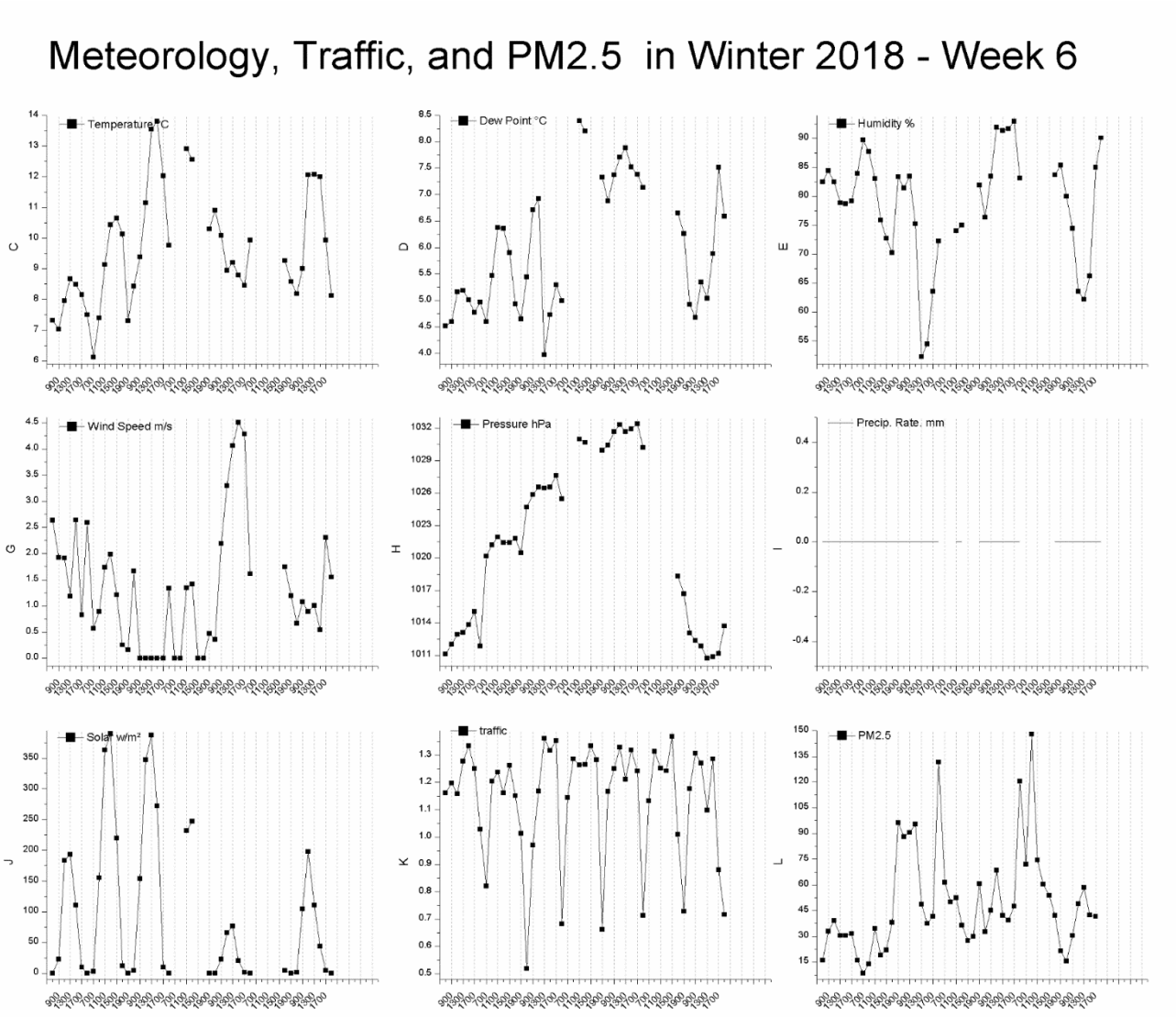
Meteorology, Traffic, and PM2.5 in Winter 2018 - Week 6
Temperature °C
Dew Point °C
Humidity %
Wind Speed m/s
Pressure hPa
Precip. Rate. mm
Solar w/m²
traffic
PM2.5

# *Appendix G*

| Daily wind roses for each sampling date in week 1 | |
|---|---|
| 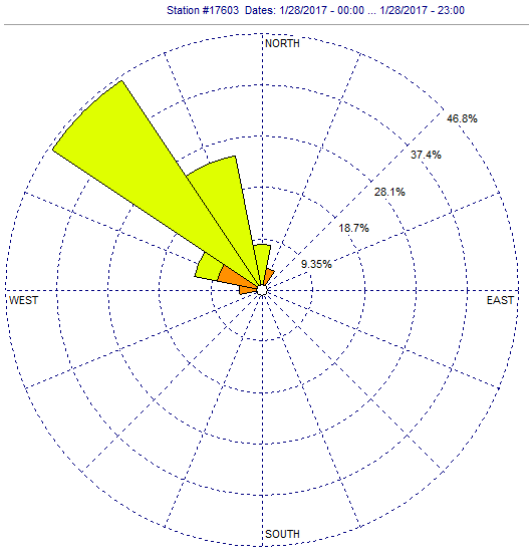 | 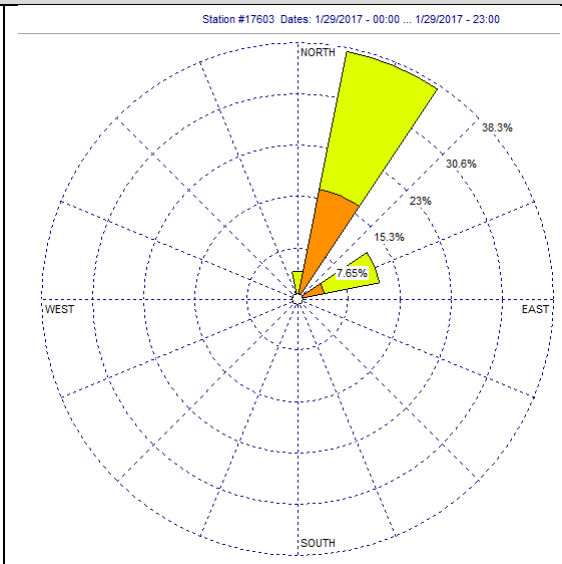 |
| 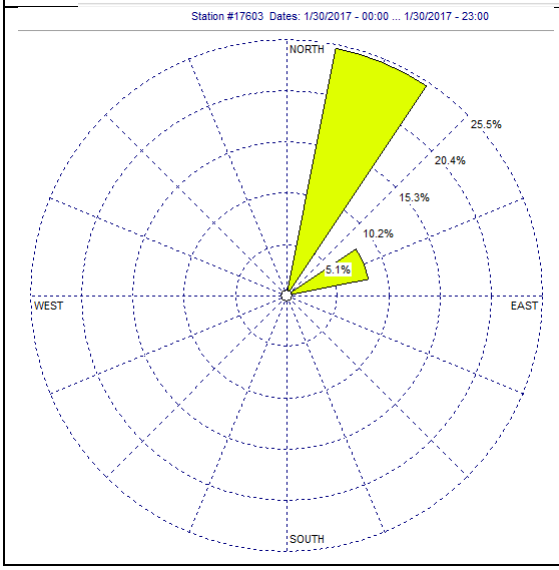 | 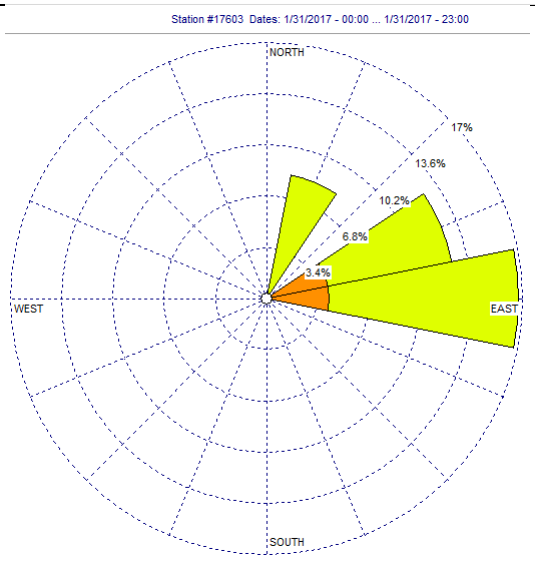 |

## Daily wind roses for each sampling date in week 1

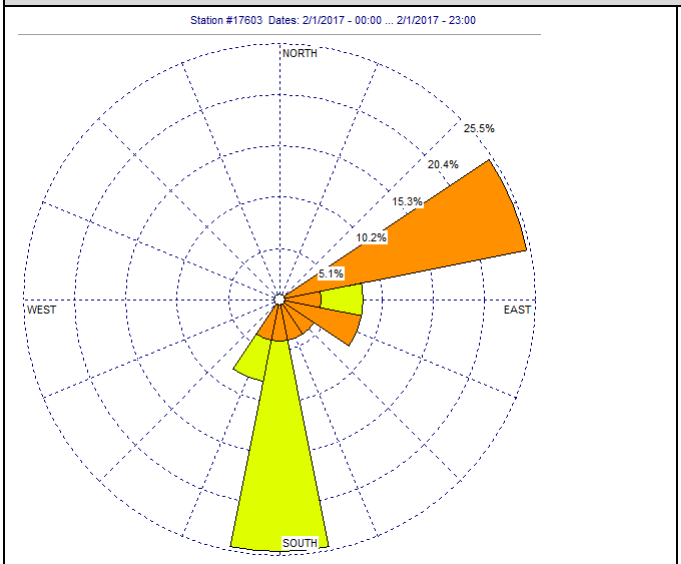


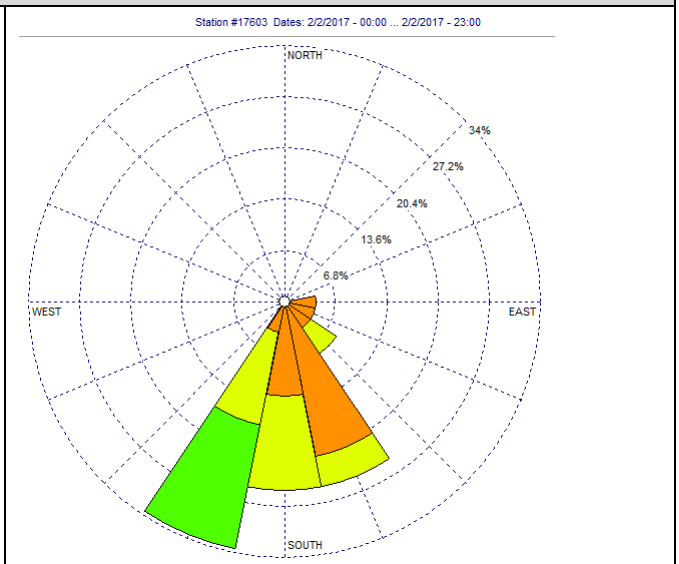


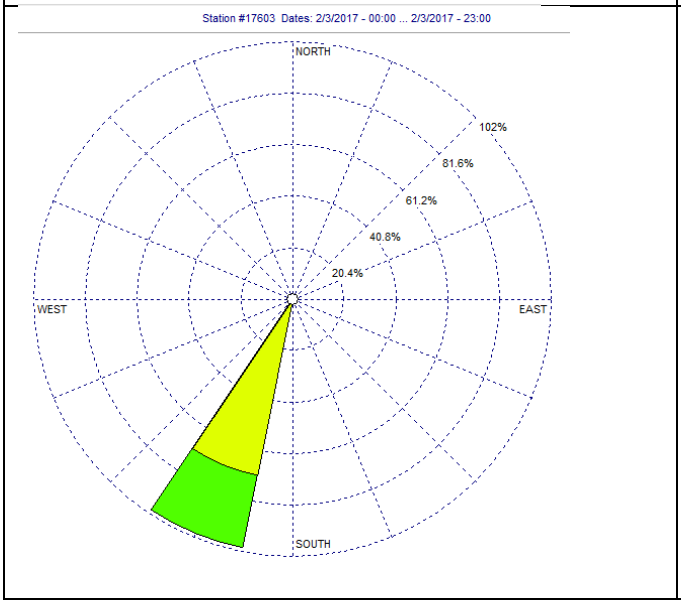


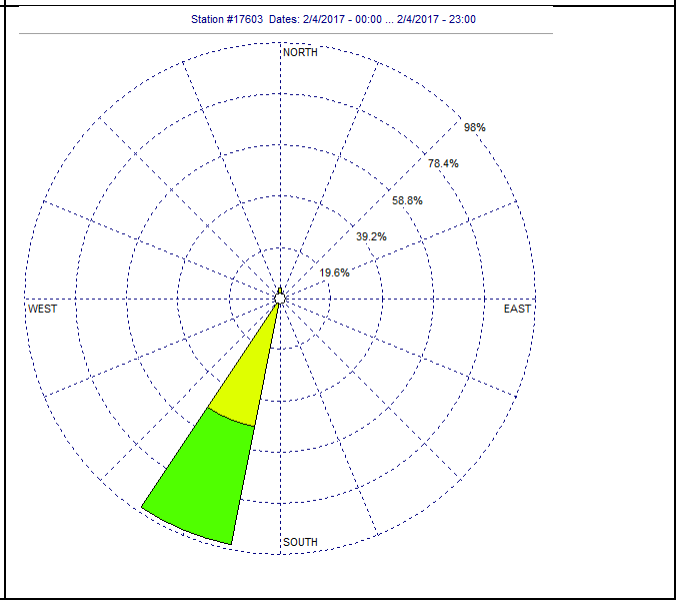

## Daily wind roses for each sampling date in week 2

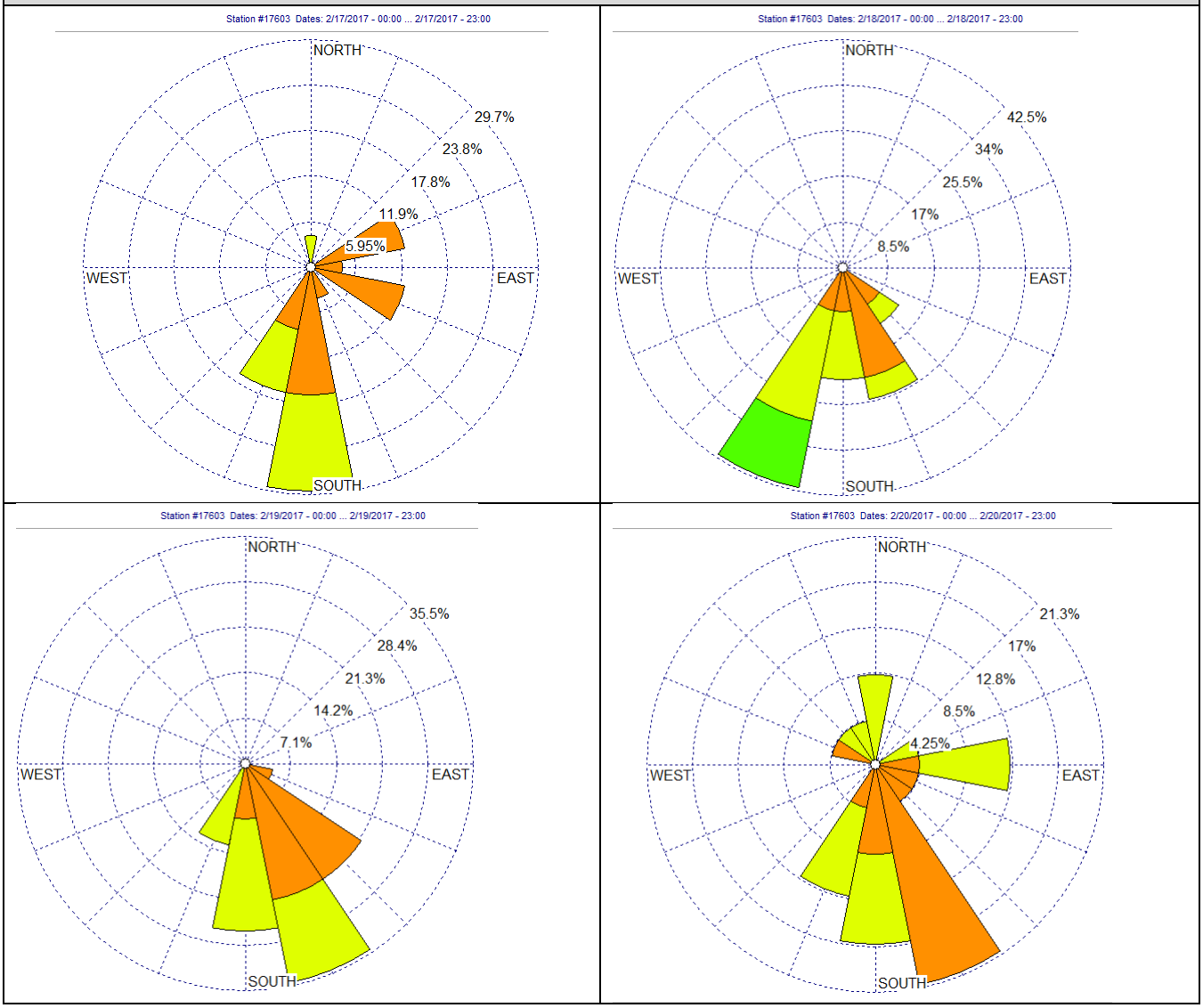

## Daily wind roses for each sampling date in week 2

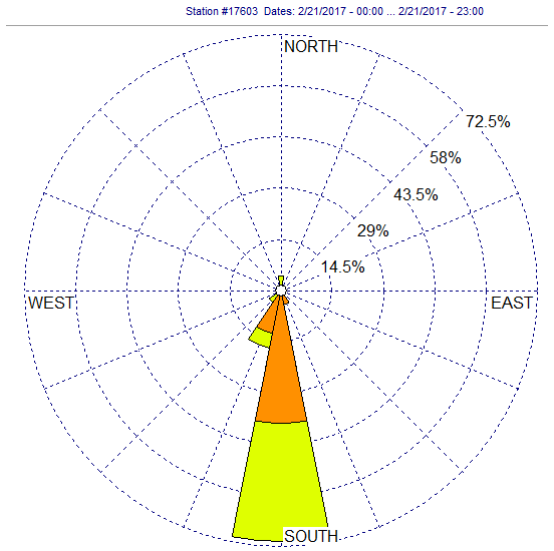


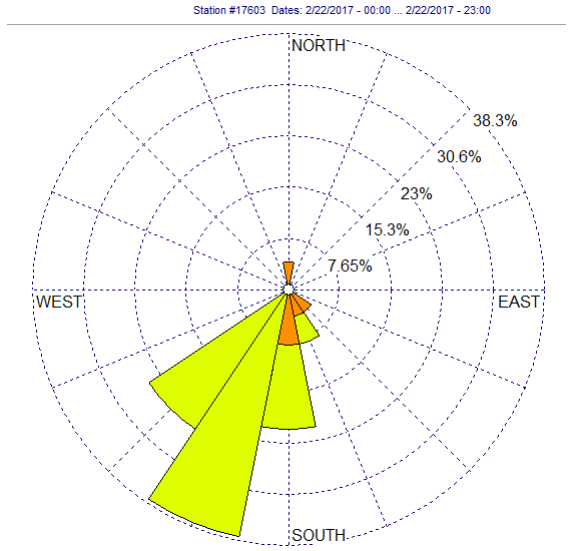


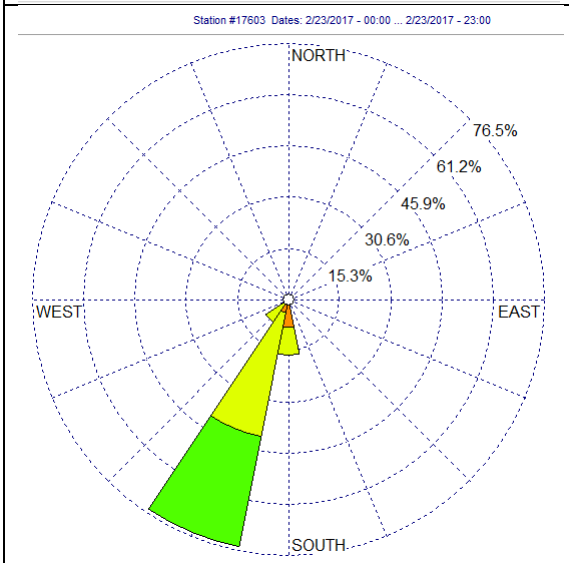

## Daily wind roses for each sampling date in week 3

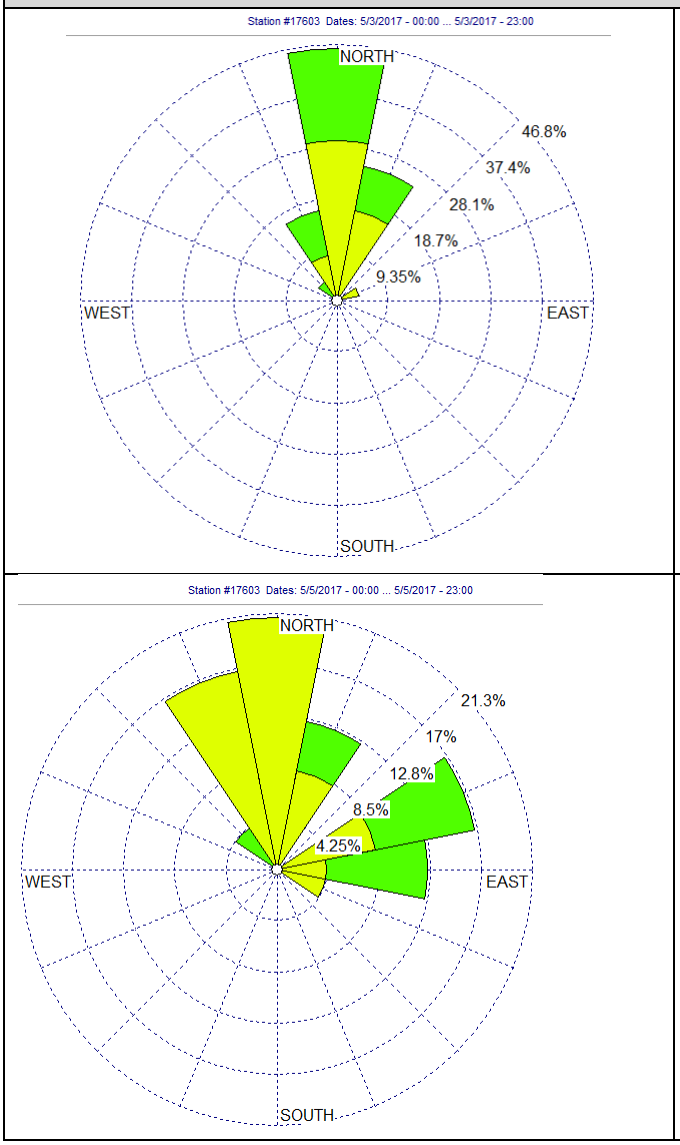


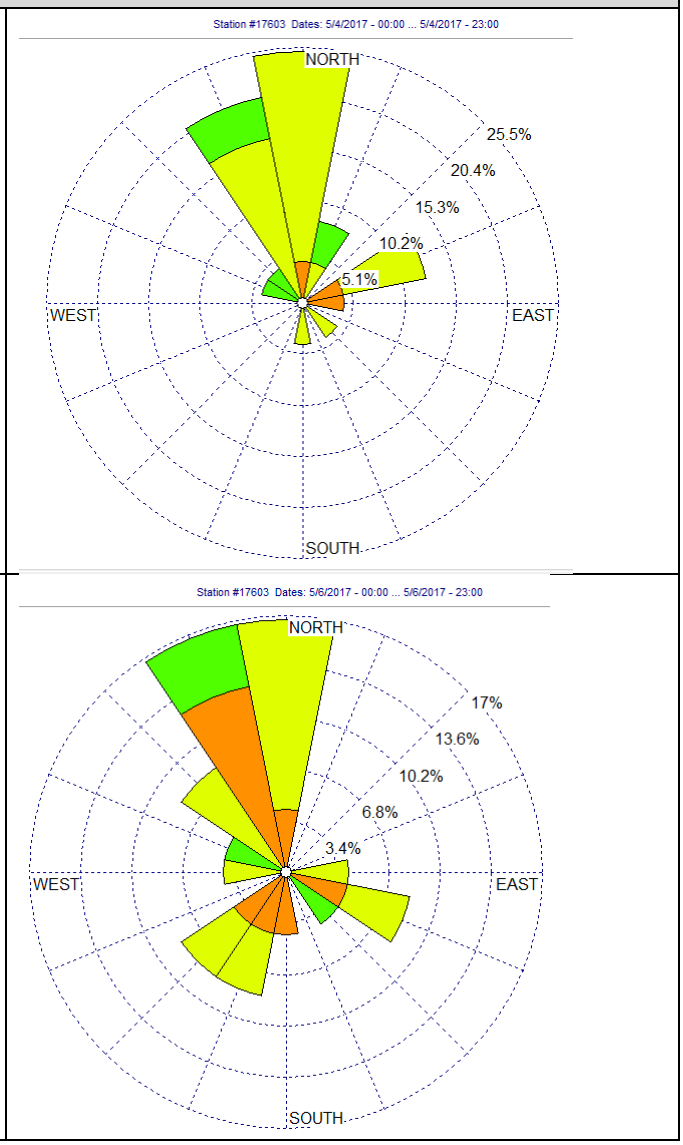

## Daily wind roses for each sampling date in week 3

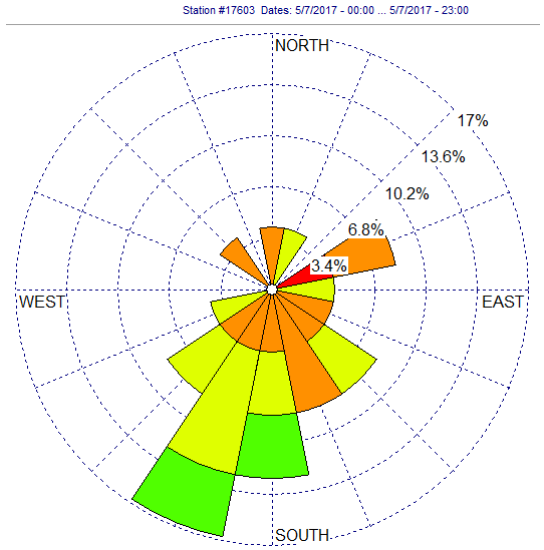


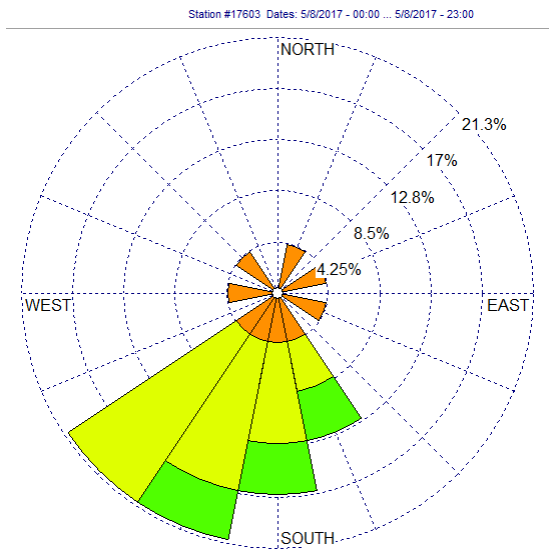


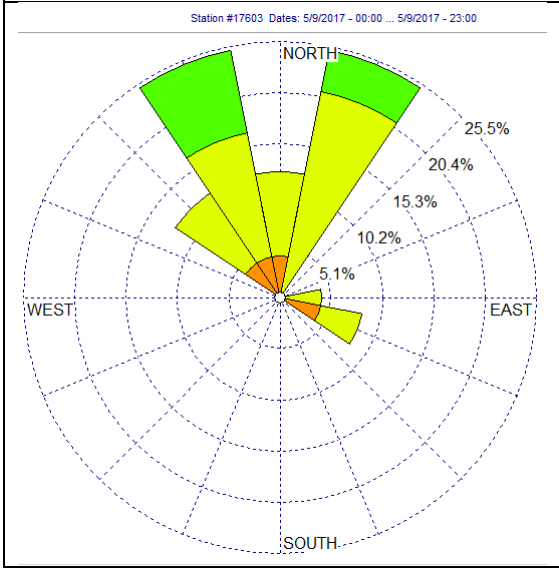

## Daily wind roses for each sampling date in week 4

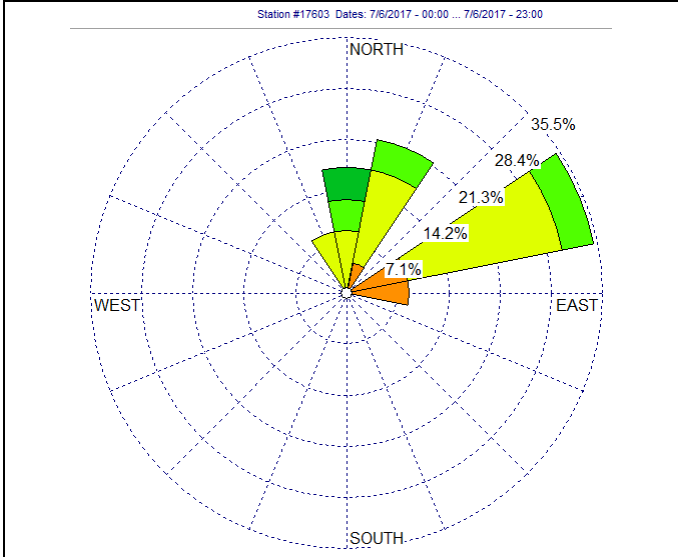


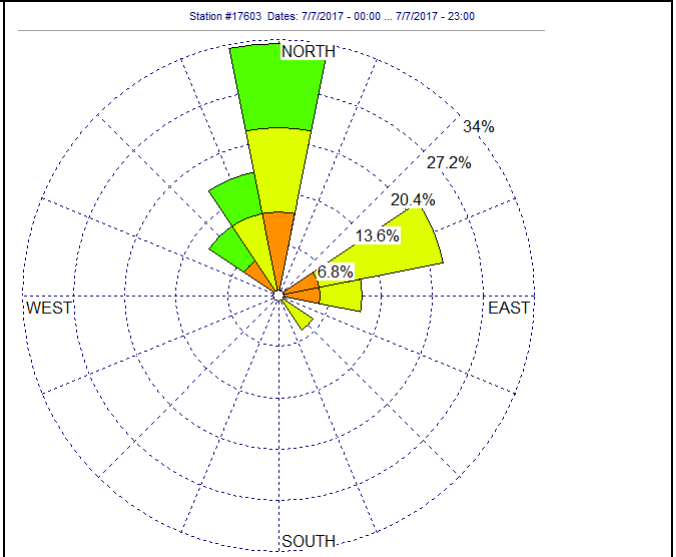


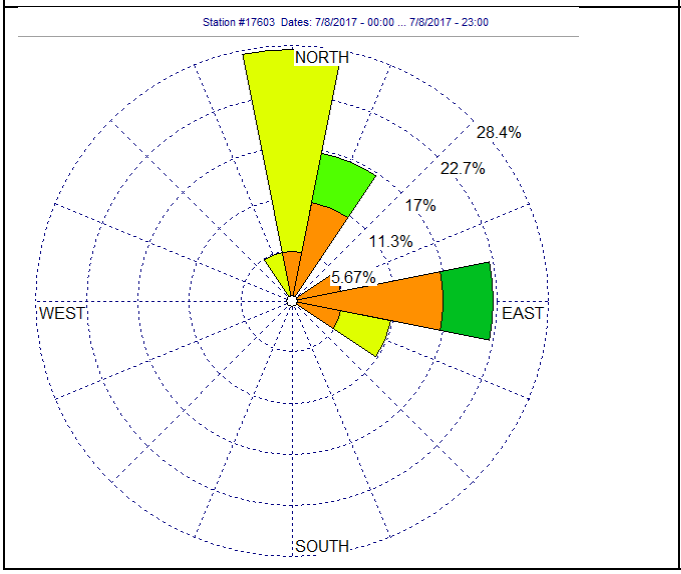


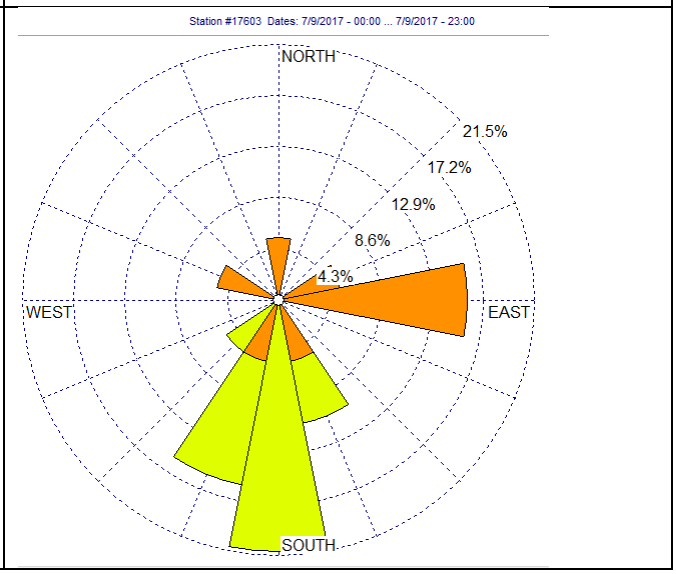

## Daily wind roses for each sampling date in week 4

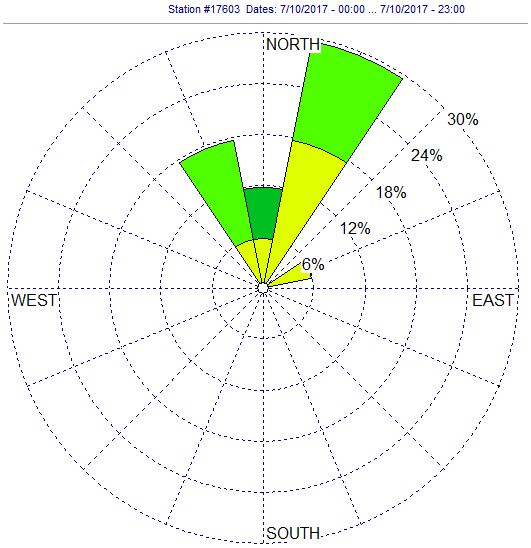


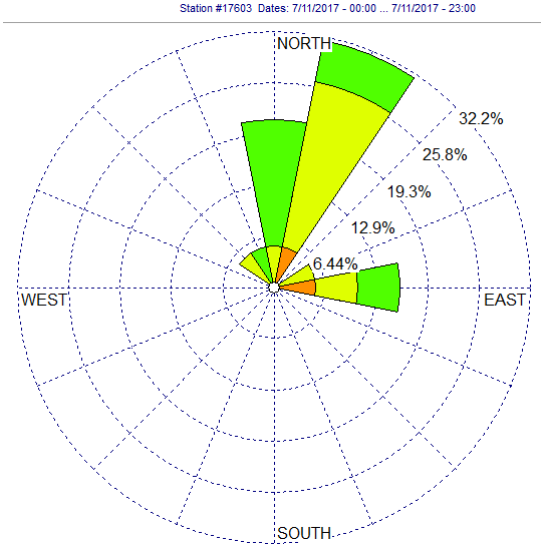


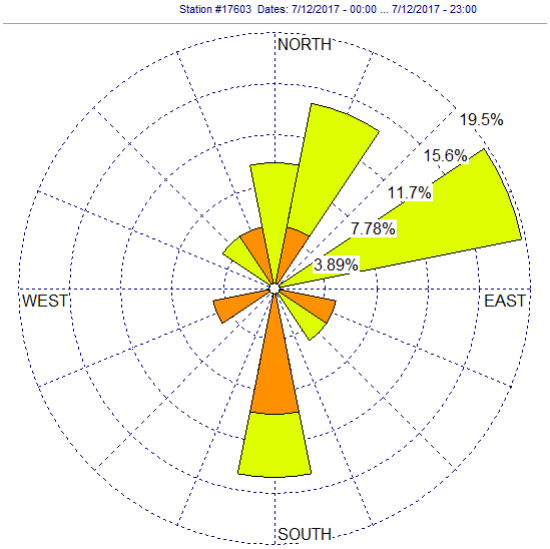

| Daily wind roses for each sampling date in week 5 | |
|---|---|
| 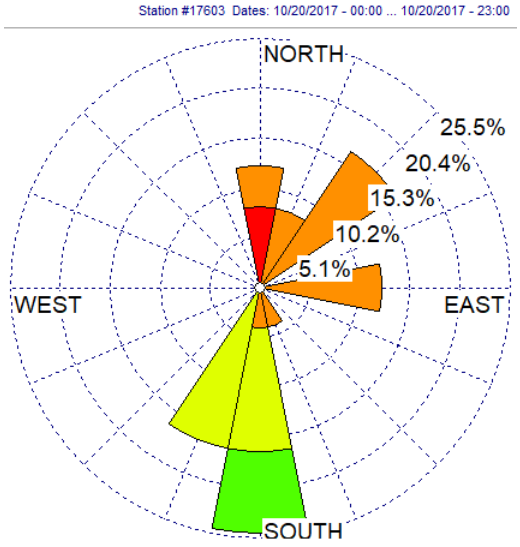 | 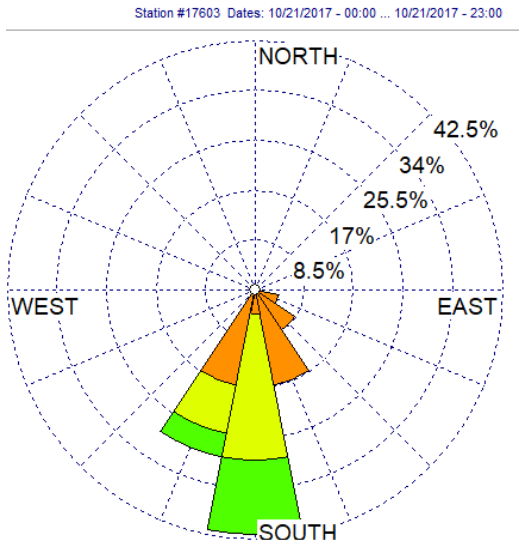 |
| 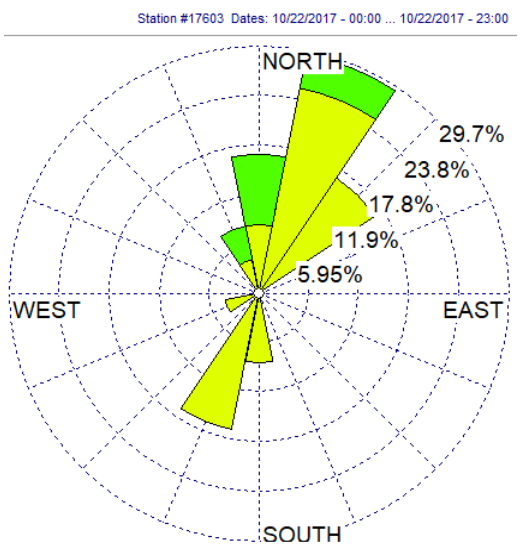 | 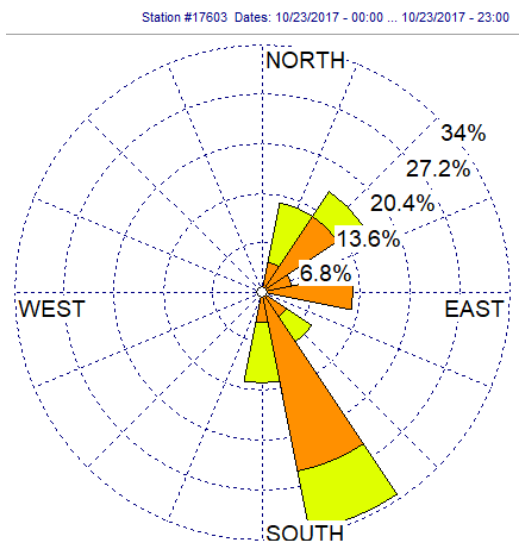 |

| Daily wind roses for each sampling date in week 5 | |
|---|---|
| 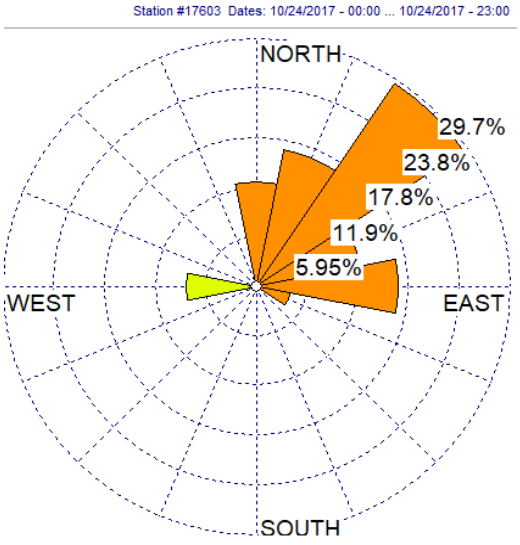 | 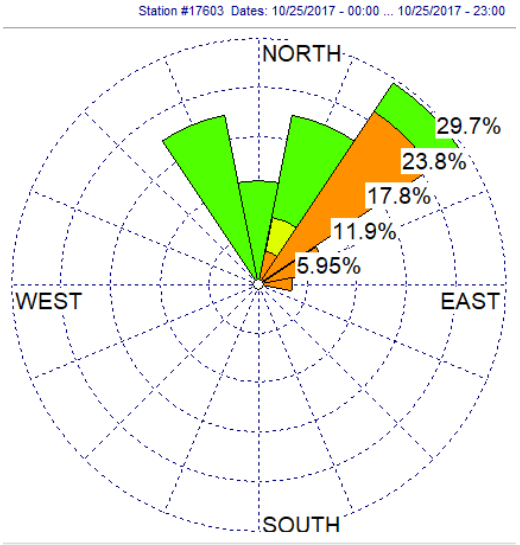 |
| 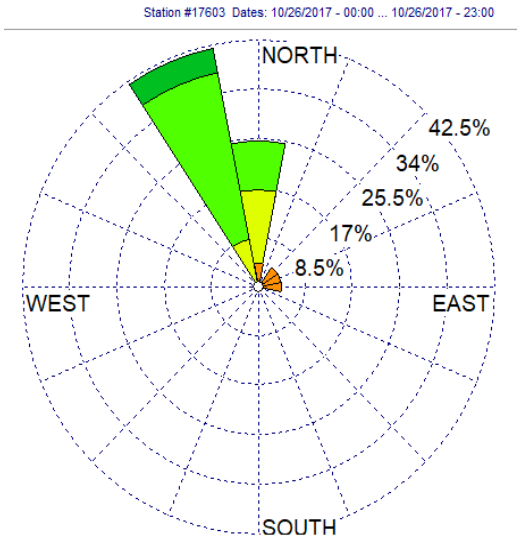 | |

Daily wind roses for each sampling date in week 6

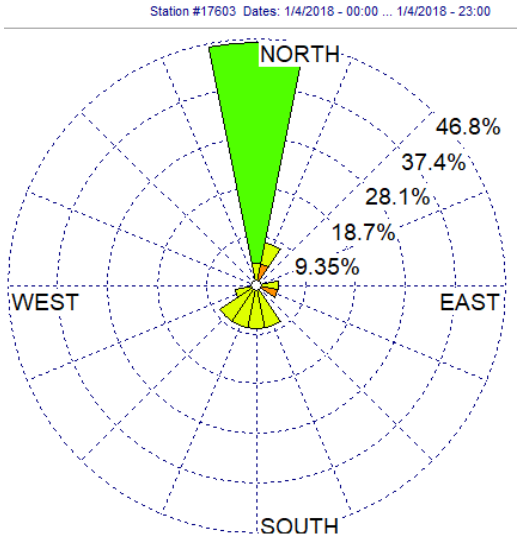


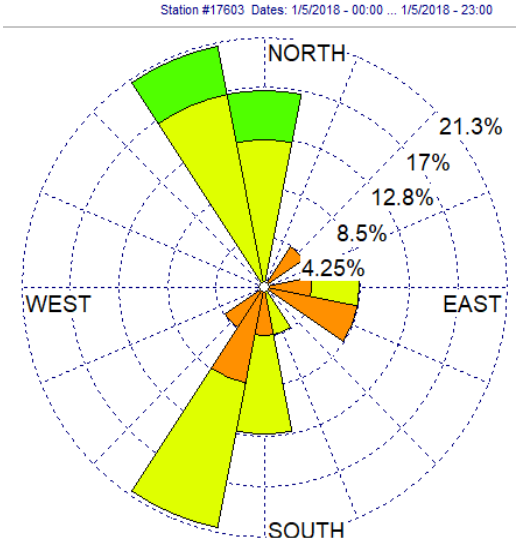


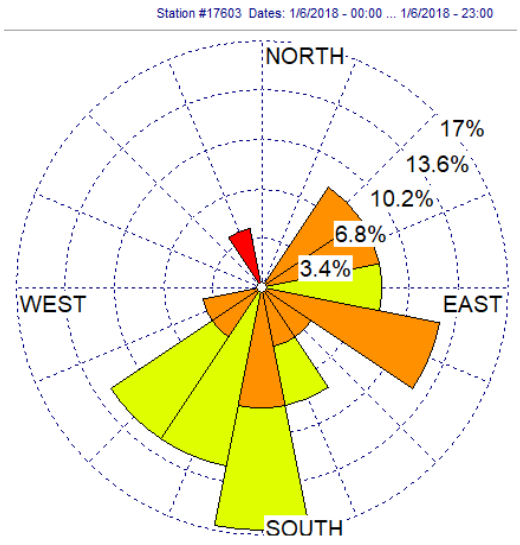


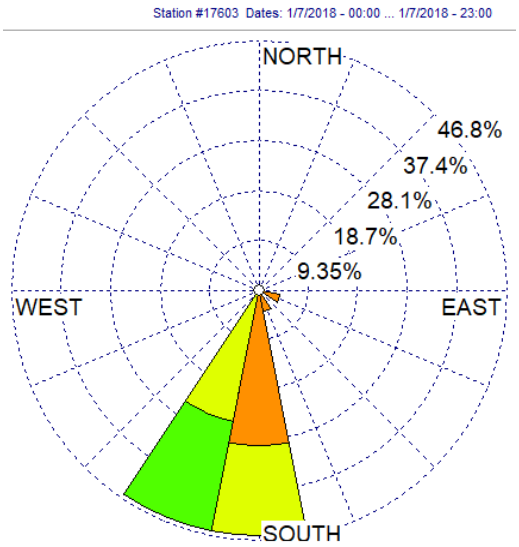

| Daily wind roses for each sampling date in week 6 | |
|---|---|
| 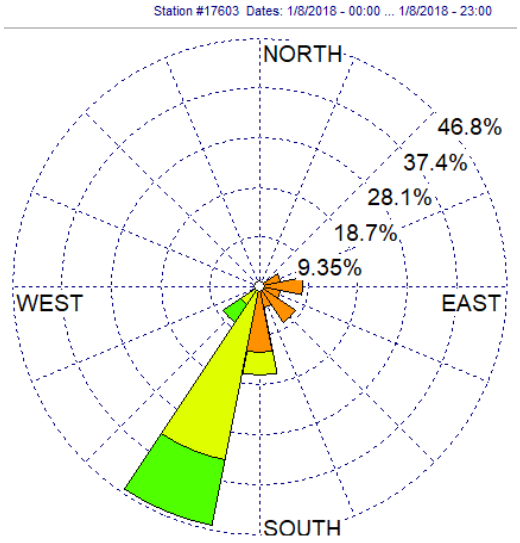 | 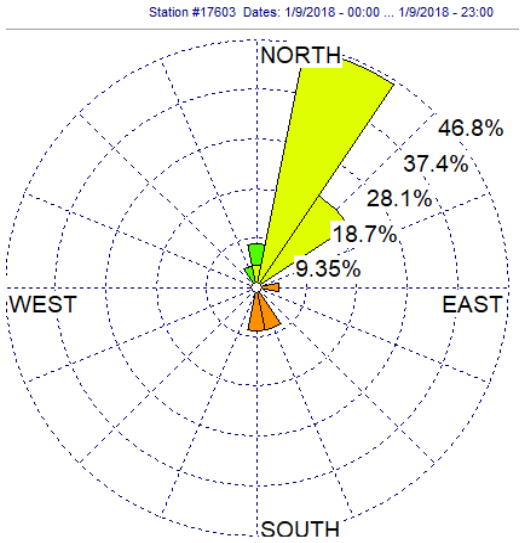 |
| 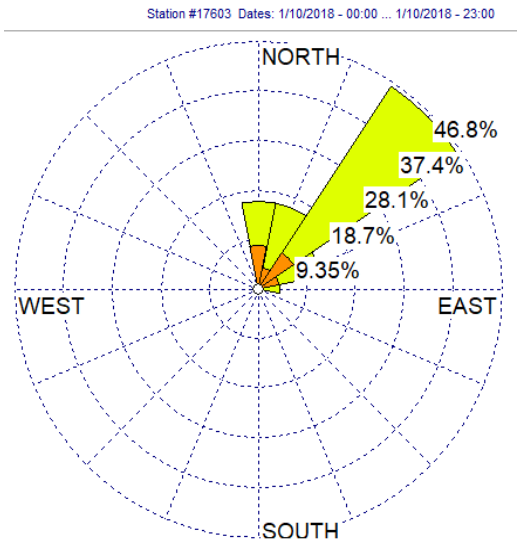 | |

# TÜBİTAK
# PROJE ÖZET BİLGİ FORMU

| | |
|---|---|
| Proje Yürütücüsü: | Dr. Öğr. Üyesi ROSA MARIA FLORES RANGEL |
| Proje No: | 115Y625 |
| Proje Başlığı: | Atmosferik Aerosollerde Pm2.5 Ve Saatlik Yarı Uçucu Organik Bileşiklerin Araştırılması |
| Proje Türü: | 1001 - Araştırma |
| Proje Süresi: | 24 |
| Araştırmacılar: | BÜLENT OKTAY AKKOYUNLU,<br>METE TAYANÇ |
| Danışmanlar: | |
| Projenin Yürütüldüğü Kuruluş ve Adresi: | MARMARA Ü. MÜHENDİSLİK F. ÇEVRE MÜHENDİSLİĞİ B.(İNGİLİZCE) |
| Projenin Başlangıç ve Bitiş Tarihleri: | 15/04/2016 - 15/10/2018 |
| Onaylanan Bütçe: | 475078.0 |
| Harcanan Bütçe: | 418091.26 |
| Öz: | Yapılan çalışmada, SVOC?ların mevsimsel ve günlük değişimlerini anlayabilmek için bir sene içinde altı hafta boyunca geceleri 12 saatte bir, gün boyu ise her iki saatte bir olmak üzere toplam 295 yüksek hacim örneği toplanmıştır. Mevsimsel değişimlerin incelenmesinde, ortalama günlük PM2.5, OC ve EC konsantrasyon değerleri kullanılmıştır. Toplanan numunelerde 15 PAH ve 28 n-alkan bileşeninin belirlenmesi ve ölçülmesi İstanbul ve Türkiye?de ilk defa yapılmıştır. Meteorolojik ve trafik verileri kullanılarak bu faktörlerin yüksek çözünürlüklü SVOC konsantrasyonlarına etkisi anlaşılmaya çalışılmıştır. Genel olarak bakıldığında, en yüksek PM2.5, OC, EC, PAH ve n-alkan konsantrasyonlarına güz ve kış döneminde rastlanılmıştır. Bunun nedeni, düşük karışma yüksekliği ve ışıma nedeniyle oluşan yetersiz atmosfer yayılımı ile evsel ısınma kaynaklı gaz salınımlarındaki artış olarak belirlenmiştir. Elde edilen OC/EC, PAH ve n-alkan konsantrasyonlarının dünya genelindeki diğer büyük şehirler ve kentsel alanlar ile karşılaştırılması da bu çalışma kapsamında yapılmıştır. Yapılan analizler sonucunda, İstanbul için elde edilen konsantrasyonların Avrupa, Amerika ve dünyadaki diğer büyük şehirlerden daha fazla olduğu gözlemlenmiştir. Buradaki iki istisna büyük şehir ise Çin?de bulunan Guanzhou ve Almanya?da bulunan Augsburg şehirleridir. Bu sonuçlar, İstanbul için özellikle kış ve güz dönemlerinde sıkı önlemlerin alınması ve uygulanmasının önemini göstermektedir. Bu önlemlerden bazıları; özel amaç için kullanılan dizel araç sayısının kısıtlanması, transatlantik ve yerel gemilerde kullanılan yakıtların kontrolü, evsel ısınmada kullanılan yakıtların kalitesinin kontrol edilmesi veya bazı yakıtların yasaklanması ve bir hafta boyunca trafikte bulunan araç sayısının kontrol edilmesi olarak verilebilir. |
| Anahtar Kelimeler: | GC-MS, yüksek zaman çözünürlüklü örnekleme, İstanbul, organik aerosol, yarı-uçucu organik bileşikler |
| Fikri Ürün Bildirim Formu Sunuldu Mu?: | Hayır |